AD NUMBER

AD490800

NEW LIMITATION CHANGE

TO

Approved for public release, distribution unlimited

FROM

Distribution authorized to U.S. Gov't. agencies and their contractors; Administrative/Operational Use; 31 DEC 1960. Other requests shall be referred to US Air Force Air Research and Development Command, Attn: Ballistic Missile Division, Inglewood, CA.

AUTHORITY

SAMSO, USAF ltr, 7 Jul 1972

490800

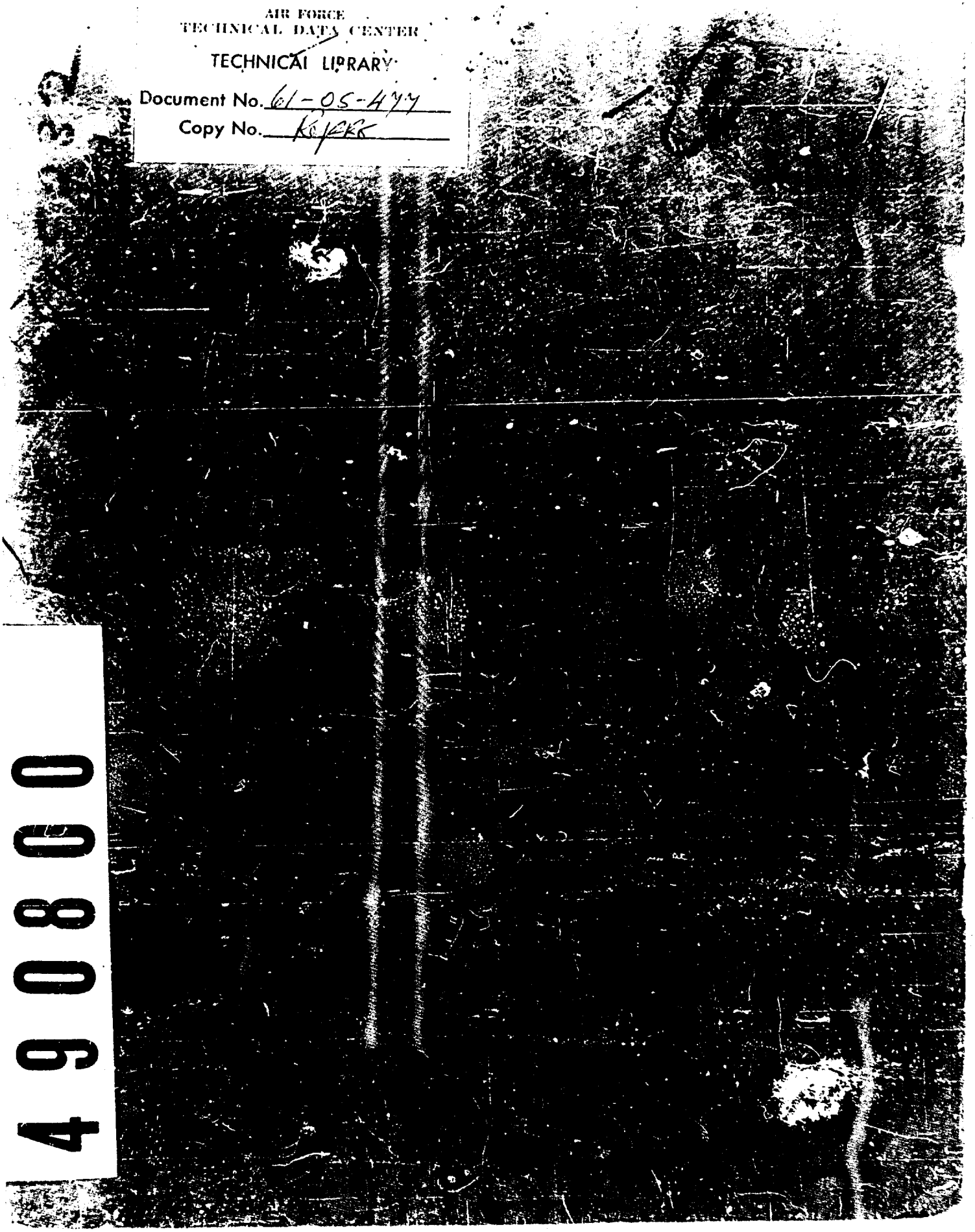

VAEST #61-05-477

AFBMD/TR-61-7

EM10-26

(9) FINAL REPORT

(6) THE DEVELOPMENT OF DESIGN CRITERIA FOR ELASTIC STABILITY OF THIN SHELL STRUCTURES

(10) by P. Seide, V. I. Weingarten and E. J. Morgan

(5) SPACE TECHNOLOGY LABORATORIES, INC.
Los Angeles 45, California

(14) Ref. no. EM10-26;
TR-60-0000-19425

(15) Contract No. AF 04(647)-619

(11) 31 December 1960

Prepared for

AIR FORCE BALLISTIC MISSILE DIVISION
AIR RESEARCH AND DEVELOPMENT COMMAND
UNITED STATES AIR FORCE
Inglewood, California

W B

Prepared for
AIR FORCE BALLISTIC MISSILE DIVISION
HEADQUARTERS AIR RESEARCH AND DEVELOPMENT COMMAND
Under Contract AF 04(647)-619

Prepared _____
P. Selde

Prepared _____
V. I. Weingarten

Prepared _____
E. J. Morgan

Approved _____
H. W. Johnson
Manager, Structures
Department

Approved _____
M. V. Barton, Director
Engineering Mechanics
Laboratory

SPACE TECHNOLOGY LABORATORIES, INC.
P.O. Box 95001
Los Angeles 45, California

ABSTRACT

The results of an extensive experimental program on the stability of cylindrical and conical shells under various loading conditions are presented and discussed. Loading conditions for both cylinders and cones include axial compression, axial compression with internal or external pressure, bending with and without internal pressure, axial compression combined with both bending and internal pressure, and a limited amount of data on torsion of conical shells. Where feasible, values suitable for design are recommended and areas needing additional theoretical and experimental study are indicated.

CONTENTS

CONTENTS (Continued)

ILLUSTRATIONS

ILLUSTRATIONS (Continued)

ILLUSTRATIONS (Continued)

ILLUSTRATIONS (Continued)

TABLES

TABLES (Continued)

I. INTRODUCTION

Although many theoretical and experimental investigations have been carried out on the buckling of cylindrical and conical shells, understanding of the phenomena is far from complete. Results which differ between investigators, insufficient numbers of specimens to obtain a measure of the validity of the experimental data, and limitations in the ranges of the parameters studied have in many instances led to inconclusive results. Over the past two years the Engineering Mechanics Department of the Space Technology Laboratories has engaged in a program to obtain a comprehensive set of experimental data under carefully controlled conditions and has attempted to correlate these data with existing theory and experimental results of other investigators. The program has also included combined loadings and specimen configurations not previously investigated. A wide range of cylindrical and conical parameters were considered, and axial compression, internal and external pressures, bending, torsion, and a number of combined load conditions were studied.

This final report under Contract AF 04(647)-619 is intended to be self-contained. Data presented in semiannual reports have been revised in the light of more recent information and supplemented with material either omitted previously or newly obtained.

It is hoped that the results of this study, many of which were unexpected, will stimulate the interest of others to engage in the many theoretical large-deflection analyses needed to explain the various phenomena and in the additional experimental work needed to complement and extend the range of parameters considered.

II. NOMENCLATURE

C, $\bar{\sigma}_{cr}$	Axial compression load coefficient $\left(\frac{P}{2\pi Et^2 \cos^2 \alpha}$ for cones or $\frac{P}{2\pi Et^2}$ for cylinders$\right)$
C^*	Axial compression buckling coefficient suggested by Kanemitsu and Nojima, including length effect.
C_b	Bending moment coefficient $\left(\frac{M}{\pi ER_1 t^2 \cos^2 \alpha}$ for cones or $\frac{M}{\pi ERt^2}$ for cylinders$\right)$
D	Flexural stiffness of shell wall $\left(\frac{Et^3}{12(1-\nu^2)}\right)$
E	Young's modulus of shell wall material
L	Axial length of cylinder or cone
ℓ	Slant length of cone
M	Critical bending moment
n	Number of circumferential waves in one buckled under external pressure
$\bar{n}$	Number of circumferential waves in equivalent cylinder buckled under external pressure
P, P_{total}	Total axial load at buckling
P_{net}	Net axial compression load for pressurized cylinders $\left(P_{total} - \pi pR^2\right)$
P_{min}	Minimum net axial compression load in buckled state
P_o	Critical axial compression load
p	Uniform internal or external hydrostatic pressure

NOMENCLATURE (Continued)

$\bar{p}$	Internal pressure parameter $\left[\frac{p}{E}\left(\frac{R_1/\cos\alpha}{t}\right)^2 \text{ for cones or } \frac{p}{E}\left(\frac{R}{t}\right)^2 \text{ for cylinders}\right]$
p_{cr}, p_o	Critical external pressure
p^*	Internal pressure parameter $\left(\sqrt{12\,(1-\nu^2)}\,\bar{p}\right)$
p_e	Critical external pressure for equivalent cylinder
$\tilde{p}$	$\frac{p}{E}\left(\frac{R}{t}\right)^{5/3}$
R	Cylinder radius
R_1	Radius of small end of cone
R_2	Radius of large end of cone
T	Critical torsion moment
t	Shell wall thickness
Z	Cylinder curvature parameter $\sqrt{3\,(1-\nu^2)}\,\frac{L^2}{Rt}$
E	$E/\sqrt{3}$
α	Semivertex angle of cone
δ_{cr}	Critical load shortening parameter $\left(\frac{\Delta L_{cr}}{L}\,\frac{R}{t}\right)$
ϵ/ϵ_{cl}	Ratio of compressive strain and classical buckling strain
ν	Poisson's ratio of wall material
ρ_1	Radius of curvature at small end of cone

NOMENCLATURE (Continued)

ρ_{av}	Average radius of curvature of cone $\left(\frac{R_1 + R_2}{2 \cos \alpha}\right)$
ρ^*	Radius of curvature of equivalent cylinder for torsion
σ, σ_{cr}	Critical average compressive stress $\left(\frac{P_{cr}}{2\pi Rt}\right)$
σ_b, σ_b'	Maximum compressive stress due to bending
σ_{c1}, σ_c	Theoretical compressive buckling stress $\left(\frac{E}{\sqrt{3(1-\nu^2)}} \frac{t}{R}\right)$
$\bar{\sigma}_{\text{prop limit}}$	Stress coefficient at proportional limit of material $\left(\frac{\sigma_{\text{prop limit}}}{E\ t/R}\right)$
σ_{max}	Maximum critical bending stress $\left(\frac{M}{\pi R^2 t}$ for cylinders or $\frac{M}{\pi R_1^2\ t \cos \alpha}$ for cones$\right)$
σ_{min}	Minimum axial compressive stress in buckled state
$\bar{\sigma}_{min}$	Minimum axial compressive stress coefficient $\left(\frac{\sigma_{min}}{E \frac{t}{R}}\right)$
τ_{max}	Critical torsion stress at small end of cone $\left(\frac{T}{2\pi R_1^2 t}\right)$
ΔL_{cr}	Total end shortening at buckling
ζ	Cone geometry parameter $\left(\sqrt{12(1-\nu^2)} \frac{R_1/\cos \alpha}{t} \cot^2 \alpha\right)$

III. PROPERTIES OF MYLAR

Most of the cylinders and conical shells used in the experimental program were constructed of Type A Dupont Mylar Polyester Film. Mylar is made by a random calendering process and, according to the manufacturer, has very nearly isotropic mechanical properties. The material has been found to have a proportional limit of about 6000 psi, a yield stress of about 11,000 psi, and a Young's Modulus in the neighborhood of 700,000 psi. What makes Mylar so attractive for investigations of this kind is the large amount of strain that it can withstand without excessive permanent set, which permits specimens to be reused many times. For instance, the yield strain for Mylar is on the order of 1.5 percent as compared to values of 0.7 percent or less for most of the structural metals. Resistance to the use of plastic models in experimental investigations of shell stability problems has been expressed in the past, but the use of Mylar for these programs appears to be increasing. Comparison of the present results for Mylar specimens with those for specimens of steel, aluminum, and brass should be convincing proof that Mylar has its place in the list of materials for shell investigations. Equally true is the fact that Mylar has its limitations in that it is too elastic to give applicable results for cases in which the stress-state prior to buckling is plastic for metal specimens or in investigations of post-buckling phenomena which would induce plastic effects in metal specimens. But then, the results for any material should be used with caution in these cases since they are undoubtedly applicable only to that particular material.

A. Thickness Variation

An investigation was made early in the course of the program to determine the variation of Mylar sheet from nominal thickness. Strips were cut from rolls of different thickness and measured at about 10 places in each strip. The normal variation of thickness was found to fall well within the limits stated by the manufacturer as shown in Table I.

Table 1. Normal Variation of Mylar Thickness.

Nominal Gage (mils)	Thickness Variation (inch)	Average Thickness (inch)
2	0.0017 - 0.0023	0.0020
3	0.0026 - 0.0034	0.0030
5	0.0043 - 0.0057	0.0050
7.5	0.0069 - 0.0085	0.0075
10	0.0089 - 0.0112	0.0101

B. Modulus of Elasticity

The modulus of elasticity of Mylar appears to vary about ±9 percent about a mean value of 735,000 psi for all thicknesses. The modulus has been found to vary from roll to roll of ostensibly identical material and from location to location in any particular roll. The approximate variation found for the different material gages used is listed in Table 2.

Table 2. Variation of Young's Modulus.

Gage (mils)	Range of Young's Modulus (ksi)
2	730 - 760
3	760 - 810
5	720 - 750
7.5	760 - 820
10	680 - 720

Investigation has shown that the Young's modulus is relatively independent of aging or working of the material, since both newly received material and material which had been tested and stored for three months yielded results within the normal range of scatter. Similarly, the moduli of material cut parallel and perpendicular to the rolling direction fell within the same scatterband. Tests also indicate that the modulus is insensitive to normal variations of strain rate.

It was decided, as the program progressed, that it would be best to measure the modulus of elasticity of each specimen. Standard tensile specimens, 6 inches in length and 1/2 inch in width, were cut from the tested cones and cylinders and clamped in a Riehle testing machine. A spring loaded 2 inch gage length extensometer was then clamped to the Mylar specimen. A continuous load-deflection output was read on the Riehle X-Y plotter. The results of these tests are given with the tabulated experimental data. A typical load-strain curve is shown in Figure 4.

C. Poisson's Ratio

It is difficult to obtain Poisson's ratio for Mylar, since strain gages do not bond readily to the material and since the stiffness of the material relative to the strain gage makes the results of dubious validity. Some attempts made using strain gages indicated a value of Poisson's ratio of approximately 0.3.

Another method yielded similar results. Small cantilevered Mylar plates measuring 0.9 by 1.8 inches were vibrated to obtain resonant frequencies. A frequency generator and amplifier were connected to a shaker using an electronic counter to give accurate frequency measurements. A sensitive microphone placed above the Mylar plate determined the frequency accurately (see Figure 2 for the test setup). The test consisted of varying the frequency input to the shaker until the second and third resonant frequencies (see Figures 3 and 4) were picked up by the microphone and recorded. The amplitude of vibration could be kept very small, thereby reducing the damping effect of the surrounding air. The equation for determining $E/(1-\nu)^2$ is given in Reference 4 as

0-0000-19425
Page 8

$$\frac{E}{1-\nu^2} = \frac{12\pi^2 f^2 \rho}{k^4} \frac{a^4}{t^2} . \qquad (1)$$

where

f = measured resonant frequency

ρ = mass density

a = length of cantilever plate

t = thickness of cantilever plate

$$k = \begin{cases} 3.472 \text{ (first mode)} \\ 21.51 \text{ (third mode)} \end{cases}$$

The average value of $E/(1-\nu^2)$, obtained from tests of all thicknesses of Mylar sheet, was 805,000 psi. Using an average value of $E = 735,000$ psi as determined from static tests, Poisson's ratio of Mylar can then be computed as

$$\nu \approx 0.3 , \qquad (2)$$

This value of Poisson's ratio for Mylar sheet was used for all calculations in this report.

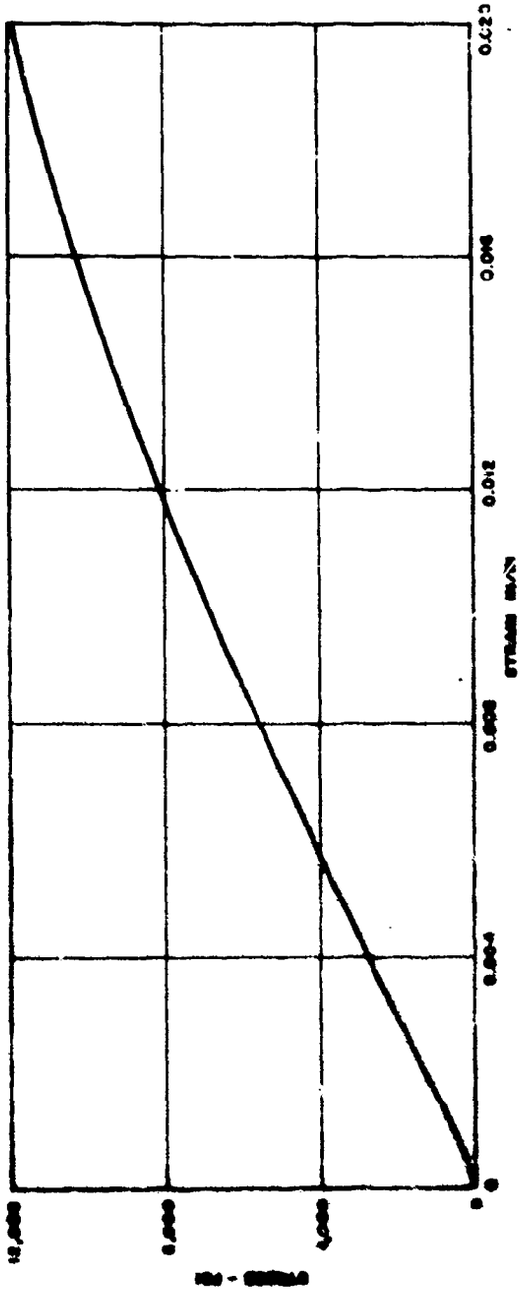

Figure 1. Typical Stress-Strain Curve for Mylar

Figure 2. Test Setup for Vibration Test of Mylar

Figure 3. First Mode of Vibration

Figure 4. Third Mode of Vibration

IV. SPECIMEN PREPARATION AND TEST EQUIPMENT

Fabrication and testing techniques and the testing equipment varied as experience was gained. The principal fabrication procedures and equipment used are outlined in the following sections. Topics of interest in the testing procedure are discussed in the sections devoted to the separate load conditions.

A. Fabrication Technique

Specimens were made by cutting accurately developed cones and cylinders from the Mylar sheet, allowing 1/2 inch on the top and a minimum of 3/4 inch on the bottom for clamping and 3/4-inch overlap (1-1/4 inch for unpressurized cones and cylinders in axial compression) for the longitudinal seam. All the cones were made with the same base radius to reduce the number of base clamping fixtures needed. The developed cone was then wrapped firmly about a conical wooden mandrel. A lap joint fastened with double-backed adhesive cellophane tape was used for the longitudinal seam. For tests involving internal pressure, the bonding material was changed to Eccobond, an epoxy cement, after experimentation with various bonding agents. This was used for cylinders and cones having a wall thickness of 0.005 inch or greater, which required the use of larger values of internal pressure than could be withstood by the cellophane tape without excessive creep. Although the thin Mylar sheet is quite flexible, the use of carefully laid out patterns and conical assembly mandrels made it possible to obtain specimens that were dimensionally accurate and relatively free of initial wrinkles or bulges. The specimens were stored on the mandrels while waiting to be tested (see Figure 5). Steel specimens, seam welded and spun, were obtained from an outside source.

B. Preparation for Testing

For the unpressurized axial compression or external pressure tests, plastic clamps were used to hold the cylinder and cone specimens. The clamping fixture for the cylinders was a cylindrical plug, or end

plate, that fitted snugly into the ends of the cylinder. The portion of the plug that extended into the cylinder was one-half inch long. To ensure that the ends of the cylinder bore uniformly against the shoulder, the ends were lapped on emery cloth, squared accurately, and fit checked when the specimen was assembled. The outer cylinder clamp shown in Figure 6 was discarded after it was found that its use induced end wrinkling which led to premature failure of the specimens. The test results were not significantly different from those obtained from more rigidly clamped specimens.

The inner and outer clamps for the conical specimens are also shown in Figure 6. Matching faces of these clamps were accurately machined to provide uniform clamping around the edges of the cone. A clamped specimen is shown in Figure 7(a).

In later tests, primarily those involving internal pressure and/or bending, the plastic clamping fixtures were replaced by machined metal end plates containing a circular trough. The end of each specimen was placed in this trough which was then filled with molten Cerrobend, a low melting point alloy. After the Cerrobend had hardened, the specimen was turned over and the other end cast into the corresponding end plate. The ends of the specimens were prevented from pulling out of the end plates at high pressures or in bending by the use of punched holes and staples around the specimen circumference. In still later tests the Cerrobend was replaced by Cerrolow, an alloy with different thermal expansion characteristics. A specimen cast into metal end plates is shown in Figure 7(b).

A procedure similar to that described above was used in preparing the steel specimens for testing. In this case a stronger casting alloy, Cerromatrix, was used.

C. **Test Equipment**

The Mylar cones and some of the cylinders tested under axial compression and internal or external pressure were loaded in the test

fixture shown in Figure 7(a). (See Section VI for test setup for pressurized cylinders in axial compression.) The specimen was loaded in axial compression by tightening the loading screw, which transmitted the load through a ball joint into the load cell and thence into the specimen through a spherical ball placed on top of the clamping fixture. Internal pressure was provided by compressed air, while external pressure was obtained by evacuating the interior of the cylinders and cones by means of a vacuum pump. For steel cones and cylinders a Baldwin Universal Testing Machine was substituted.

Mylar cones tested in bending were loaded in the test fixture shown in Figure 8. Equal and opposite loads were applied through load cells at the ends of the loading beam attached to the upper plate. The weight of both the loading beam and the end plate were counterbalanced. A cable attached to the top plate passing through the specimen was used to apply axial compression. A similar, but stiffer, test setup was used for steel cones and cylinders.

The same type of test fixture used for the bending tests was used for the steel specimen torsion tests. The only change made was to rotate the loading point 90 degrees, so that torsion could be applied instead of bending moment. The test setup for steel cones and cylinders is shown in Figure 9.

D. Instrumentation

All axial loads were determined by Statham unbonded strain-gage load cells. Five load cells were used for the tests: these covered the load ranges of 0 to 10 pounds, 0 to 25 pounds, 0 to 150 pounds, 0 to 300 pounds, and 0 to 1000 pounds. The load cell reading is accurate to within 0.1 percent of full scale reading. Internal pressure measurements were determined by Statham strain gage pressure transducers and manometers. Four pressure transducers were used for the tests; these covered the ranges of 0 to 1 psi, 0 to 5 psi, 0 to 10 psi, and 0 to 20 psi. The pressure transducer is accurate to within 0.1 percent of full scale reading.

The output of the Statham cells was read either on a Baldwin SR-4 type N strain indicator or on a Mosely X-Y plotter Model S-2. The X-Y plotter was used when load-deflection curves were desired. Deflection measurements were obtained by means of a Collins integrated differential transformer. The instrument has a ±1 inch stroke with an accuracy of 1 percent for full scale deflection.

The small critical external pressure for the Mylar specimens was measured on an alcohol-kerosene manometer shown in Figure 10. The alcohol and kerosene do not mix and can be made to have the same density by adding water to the alcohol. Food coloring was also added to the alcohol to provide a sharp dividing line between the two fluids. The pressure multiplication factor obtained with the use of this manometer is proportional to the ratio of the area of the tank and that of the manometer tube, but was obtained more accurately by calibrating the 50-inch full scale movement of the meniscus against the reading of a water manometer. For steel cones and cylinders, a water manometer was used, since the pressures involved were on the order of 40 times those for the Mylar specimens.

Figure 5. Mylar Cones Stored on Mandrels

Figure 6. Inner and Outer Plastic End Clamps for Mylar Specimens

(a) Conical Specimen Held by Plastic Clamping Fixture

(b) Conical Specimen Cast into Metal Clamping Fixture

Figure 7. Methods of Clamping

Figure 8. Test Setup for Cylinders and Cones in Bending

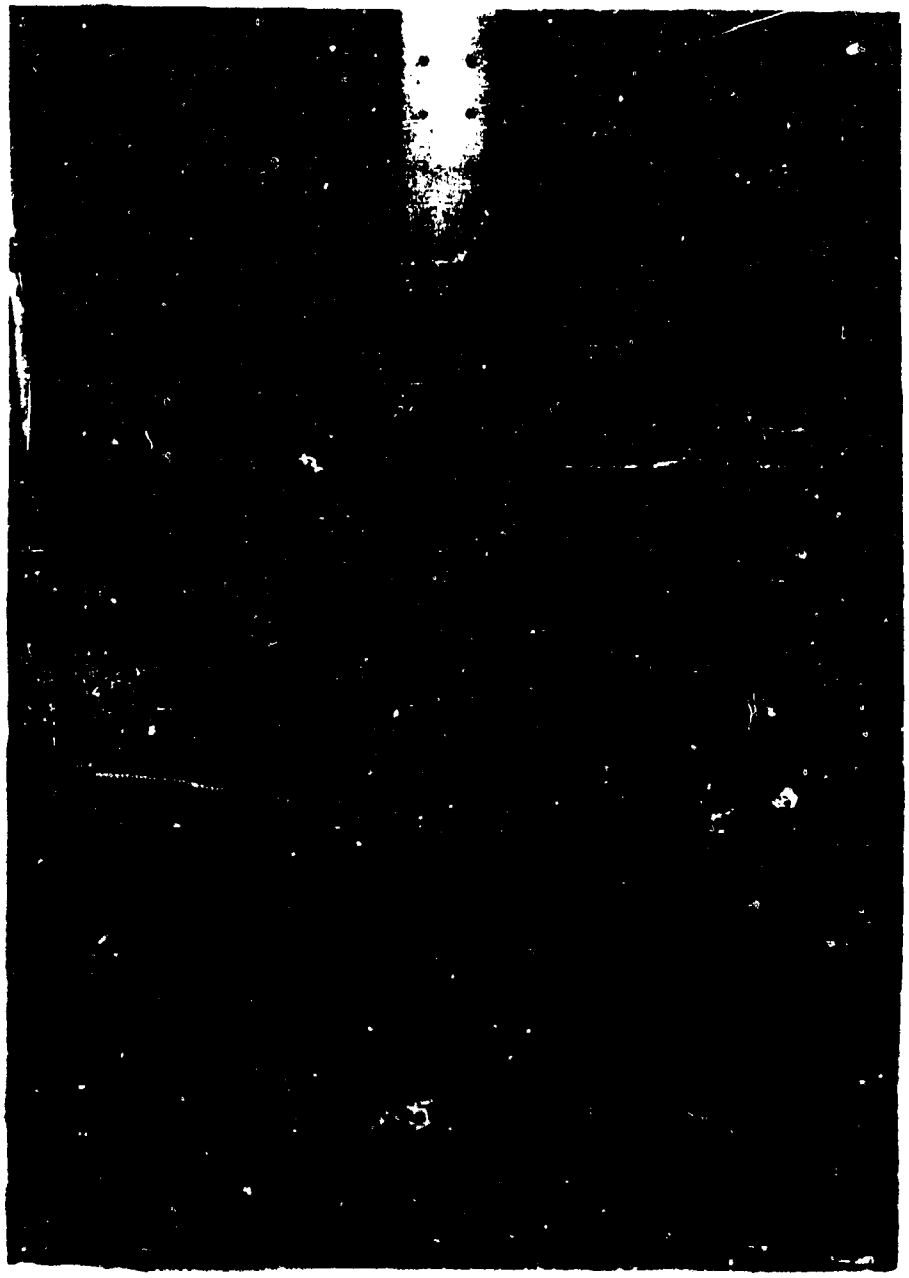

Figure 9. Test Setup for Steel Cones and Cylinders in Torsion

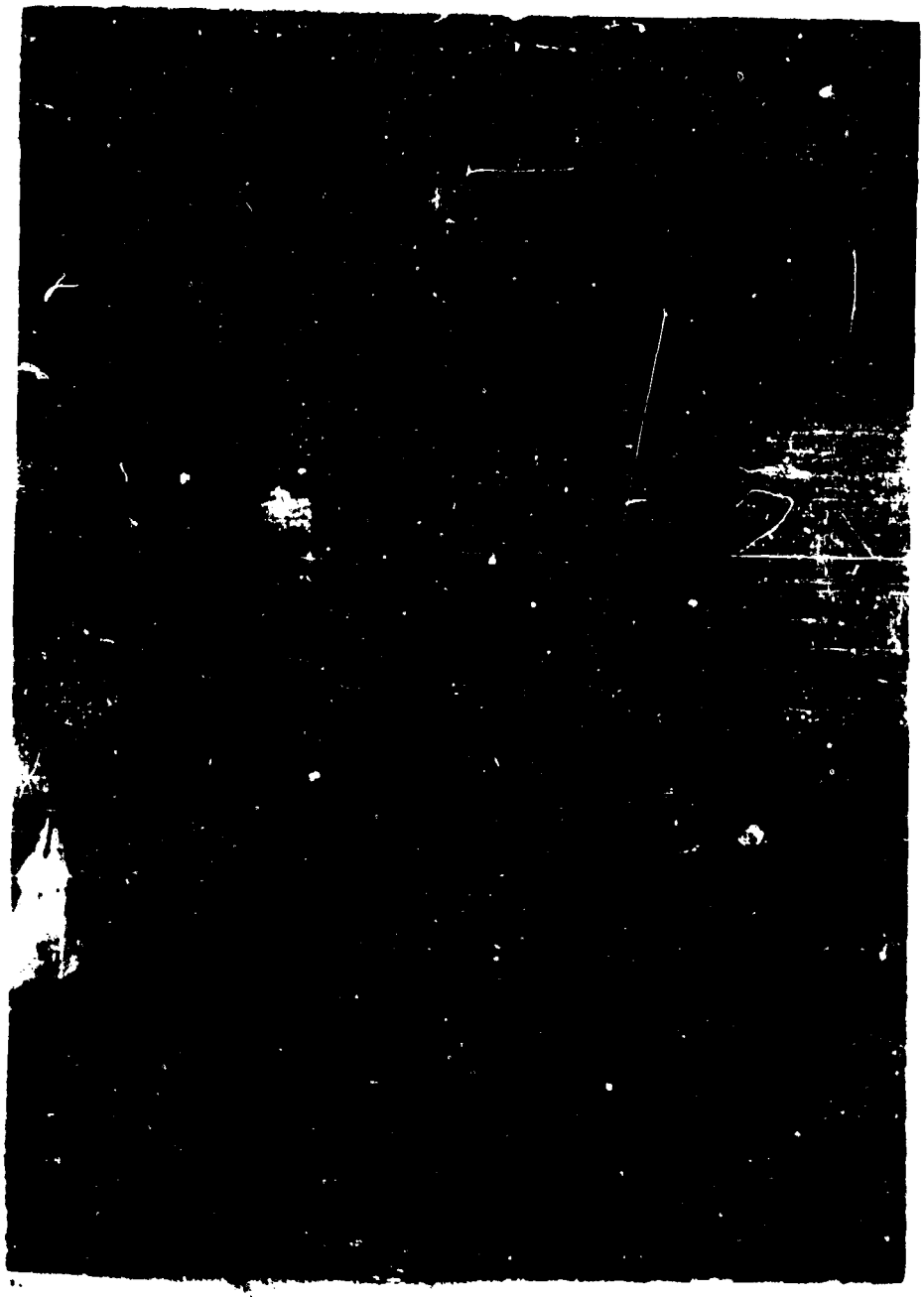

Figure 10. Alcohol-Kerosene Manometer Used to Measure Small Differences of Pressure.

V. CYLINDERS AND TRUNCATED CONES UNDER AXIAL COMPRESSION

The stability of cylinders under axial compression is a problem that has been studied both theoretically and experimentally by many investigators.* Intense interest was initially generated by serious disagreement between experimental data and the results predicted by small deflection theories of buckling, a disagreement not encountered previously with regard to columns and plates. Theoretical investigations of the post-buckling behavior of cylindrical shells (References 2, 3, and 4) revealed that the problem differed from the buckling of columns and plates in that neighboring equilibrium states were unstable, i.e., deformations could occur with a decrease in applied load. It was also found that the load carrying capacity of cylinders was extremely sensitive to initial imperfections of the order of a fraction of the wall thickness, which fact has since found acceptance as an explanation of the discrepancy between theory and experiment. More recently, additional factors, such as nonuniformity of loading around the shell circumference (Reference 5), and nuclei of plastic strain (Reference 6), have been suggested to explain the large amount of scatter in test results. The original purpose of the test program was to investigate the load carrying capacity of conical shells alone. Since the scatter of the axial compression results of other investigations was so large for cylinders, however, it was decided that a pilot program of cylinder tests would be necessary to yield comparable data as a check on the cone results and as a basis for obtaining a design criterion for conical shells postulated on the existence of an equivalent cylinder. The cylinder investigation soon outgrew the pilot program stage, however, as many factors not mentioned before in the literature intruded and demanded study. The net results of these studies, which attempt to bring some order to the study of cylindrical shells in compression, also manage to inject more unknown factors into the problem.

---

*For a much more comprehensive survey see the review paper "Instability of Thin Elastic Shells," by Y. C. Fung and E. E. Sechler in Structural Mechanics (Pergamon Press, 1960).

The controversy surrounding the design of cylindrical shells has not yet been fully extended to conical shells, since serious study of these structures began only a few years ago. In the present report, the results of the axial compression test program carried out for conical shells of various geometries are given and recommendations made for their design. It is obvious that, as the number of conical shell tests grows, the controversial aspects of design may exceed those associated with cylinders, if only because the conical shape permits another degree of freedom to the variables to be considered.

A. Test Technique

The Mylar cones and cylinders were assembled in the clamping fixtures with the bottom clamp resting on the base of the loading device. A circular plate with a hole in its center was then centrally placed on the cone with a steel ball resting in the hole. The load cell attached to the loading screw was then placed on top of the steel ball and the cone shifted until the load cell was vertical. The assembled specimen was then loaded in axial compression by turning the load screw at a relatively constant rate. The load was increased until failure occurred. Failure of the specimen was usually quite sudden, with diamond shape buckles snapping into position.

On some tests a small dimple appeared next to the seam and grew as the load was increased until the cone collapsed at a very low load. The addition of scotch tape to the seam or an increase in the seam width eliminated this type of failure and consequently increased the buckling load. After each failure the buckle dimensions, buckling load, and the extent of the buckles around the circumference of the cone were recorded. The Mylar specimens have the ability to recover completely after being buckled, presumably because the cone remains elastic in the post-buckling state. Therefore it was possible to perform several tests on one cone.

The first axial compression test on every cone was done with the steel ball and loading plate centrally located. At buckling, the location

of the first buckle was recorded. In the second compression test of the cone, the loading plate and steel ball was moved, on a line with the center of the cone, away from where the first buckle appeared. This procedure was continued until a maximum compressive load was obtained. It was felt that this procedure eliminated most of the effects of eccentricity of loading.

Steel specimens were fixed in the Cerromatrix upper and lower clamps and then placed in the Baldwin Universal Testing Machine. A swivel top plate was placed in the Baldwin Test machine so the top clamping plate and the loading plate could align themselves. A compressive load was then exerted on the specimen until buckling occurred. Failure was usually quite sudden, with diamond shape buckles snapping into position. Premature dimpling due to imperfect seams was eliminated by the addition of a 1-1/2-inch shim strap attached with an epoxy cement along the seam. After failure, the buckling load and buckle sizes were recorded. When the load was released, the buckles disappeared from the steel specimens with large R/t values. These specimens were examined closely and no evidence of plastic deformation was noticed. When the specimens were retested, however, the second buckling load was always much lower than the first. A qualitative explanation of this phenomena is given in Reference 6. During the initial compression test on the shell, failure occurred at some stress level and was initiated at that stress level by some initial imperfection of the shell. The failure took the form of a diamond shaped buckle pattern around the circumference of the shell. The shell supported a load after failure, and this load was carried in the crests of the buckles with the points of highest stress occurring at the junction of adjacent buckles. At these points the stress was above the yield stress, and microscopic plastic deformations occurred. Evidently these microscopic plastic deformations have a greater effect than the initial imperfections that were built into the shell since, in the next test, failure was initiated at these points of highest stress concentration at a lower stress level, with the points of maximum deflection of the new diamond pattern at the same location as the node points of the first.

Figure 11 shows the buckle pattern of the second test for a Mylar cone. The dots at the center of the diamonds mark the location of previous node points. The new node points are marked with an "X." It can be seen that the node points of the first test coincide with the centers of the new set of buckles. This behavior occurs in metal specimens as well as Mylar specimens. For Mylar, however, the degree of plastic deformation is less than for metals and the buckling load is not affected.

B. Results for Cylinders

The experimental data obtained during the course of the present program are listed in part (a) of Table 3 and in Table 4. These data have been collected from the results for axial compression alone and from the endpoints obtained in the investigations of axial compression combined with internal pressure, external pressure, or bending. They are therefore associated with a multiplicity of loading devices, end fixtures, and testing techniques. The results are plotted in Figure 12 (the circles) in the form of values of the buckling coefficient $P/2\pi Et^2$ or C as a function of radius-thickness ratio R/t. The buckling coefficient is another form, suitable primarily for conical shells, of the more usual $\sigma_{cr}/E\ t/r$ which is based on theoretical considerations (see Reference 7). The length-radius ratio L/R in most of the tests was either 1 or 2. There is insufficient difference between the test results for each value of L/R to warrant separate plots.

The results indicate a trend similar to that obtained by other investigators, in that the buckling coefficient appears to vary with radius-thickness ratio. A study of the data in the literature (References 8 to 23) indicated most of the experimental results fell within or near the scatterband obtained in the present program and, hence, that a discriminating choice of data might permit some conclusions to be drawn for design purposes. The choice of data was guided by several considerations. First of these was the conclusion that the effect of length could not be readily discerned if the length-radius ratio was within the range from 0.5 to approximately 5, for which most of the data applies. A length effect exists for cylinders with values of L/R less than 0.5, but there is insufficient data to finally establish design values. For values of L/R greater than 5 the few data points available indicate that there

might be a length effect, but again there is insufficient data to establish any trends. Investigations yielding buckling coefficients consistently lower than the present results were omitted entirely, on the premise that fabrication methods and testing technique were significantly inferior. Those test results in which the critical stress was greater than about 70 percent of the yield stress were likewise omitted. The resulting data are also plotted in Figure 12.

The entire group of data is reasonaby consistent, despite the large amount of scatter. The relation suggested by Kanemitsu and Nojima for long cylinders

$$C = 9 \left(\frac{t}{R}\right)^{0.6} \tag{3}$$

can be seen to be a good lower bound to the data for the range R/t greater than 500. For lower values of R/t the equation becomes increasingly unconservative. An alternate relation that appears to give a good lower bound over the entire range of R/t tested is also shown and is represented by the equation

$$C = 0.606 - 0.546 \left(1 - e^{-\frac{1}{16}\sqrt{\frac{R}{t}}}\right) \tag{4}$$

A representation of this form is later shown to yield a good lower bound to the data obtained for bending as well.

The data obtained thus far indicates that the radius-thickness ratio is a significant parameter indicative of the trend of the results. The scatter associated with any particular value of radius-thickness ratio shows, however, that the radius-thickness ratio representation disguises important factors. It has been suggested that the scatter can be explained by assuming different magnitudes of initial imperfections for various specimens. This explanation serves for the scatter obtained in the present program for ostensibly identical specimens made by a single individual and tested under similar conditions, since the initial imperfections would

be expected to occur with some statistical distribution. However, observations made in the course of testing indicate that the statistical sample can be biased.

It was observed, for instance, that many of the lower points of the scatterband are associated with earlier phases of the test program and that test results obtained at a considerably later date would yield a higher mean level. Thus the experience and competence of the fabricator and experimentalist should be taken into consideration. Another factor which evidently influences the results is the wall stiffness or size of the specimen, in that specimens attempted with Mylar gages of 0.001 inch and 0.002 inch were exceedingly hard to handle without introducing wrinkles. Additional factors were observed as well. In many of the tests of the present program, the potting material used was the low melting point alloy, Cerrobend, in others, Cerrolow was used. The main difference between these alloys is their thermal expansion characteristics. Cerrobend expands while cooling, whereas Cerrolow contracts a much smaller amount while cooling. It was found that those tests conducted with Cerrolow gave results that were consistently higher than those obtained with Cerrobend (see also Section VI). One would assume, then, that the bulging of the ends of the cylinder walls is an important parameter. Finally it was also observed, both in the present tests and from a study of the data in the literature, that results obtained when the nominal stress level was on the order of 70 percent of the yield stress or greater yielded consistently low buckling coefficients. This effect can also be traced to end conditions, since it can be shown that yielding of the restrained ends due to bending would start at about this level. (See Section VI for additional discussion.) With all of these factors influencing the results, it is interesting to note, however, that the lower bound of the various test results is reasonably consistent, indicating that there is a practical lower limit to the combined effects of all of the parameters influencing the results.

There remain several areas of importance to the designer that are yet to be explored in great detail. The effect of length given by the Kanemitsu-Nojima formula

$$C^* = 9\left(\frac{t}{R}\right)^{0.6} + 0.16\left(\frac{t}{L}\right)^{0.3} \tag{5}$$

is based on insufficient test data. There are indications that the length effect may not die out so rapidly as the formula supposes. Certainly, with long specimens it would be expected that the probability of initial imperfections would be larger than for short specimens. Another phenomenon open to investigation is the fact that results in the low range of radius-thickness ratios are undoubtedly a function of the particular material used, since plasticity effects become of importance there.

C. Results for Conical Shells*

The theoretical analysis of Reference 24 yields the critical axial load coefficient for conical shells as a modified form of the result for cylinders, namely

$$C = \frac{P}{2\pi Et^2\cos^2\alpha} = \frac{1}{\sqrt{3(1-\nu^2)}} \ . \tag{6}$$

It was also suggested in Reference 24 that the buckling load coefficient C for conical shells might be similar to that for an equivalent cylinder having the same wall thickness, a length equal to the slant length of the cone, and a radius equal to the average radius of curvature of the cone. The specimens were designed to investigate this hypothesis.

The results of the various tests are given in Tables 3 and 4 in the form of values of $P/2\pi Et^2\cos^2\alpha$. In several preliminary analyses

*Part of the experimental results of this section are presented in the paper "Buckling of Conical Shells Under Axial Compression" by Sol Litwak (M.S. Thesis, UCLA, May 1960).

of the data (References 25 and 26) attempts were made to verify the above hypothesis, with inconclusive results. The data for cones appeared to be consistently higher than those for cylinders. It has since been determined that if the equivalent cylinder is assumed to have a radius equal to the small radius of curvature of the cone, much better agreement is obtained. This conclusion was reached by a comparison of the results for both the cones and the cylinders with results predicted by the Kanemitsu-Nojima equation for C^*, Equation (5). A comparison of the values of C/C^* for cylinders and cones, given in the last column of Tables 3 and 4, indicates that the scatterband for both is similar. The experimental values for cones are compared with the lower bound curve for cylinders in Figure 13, where it can be seen that the agreement is fair. It should be noted that many of the high points correspond to cones having length small radius of curvature ratios less than 0.5.

It is surprising that the small radius of curvature should be significant, rather than the average radius of curvature, since buckle patterns of conical shells (see Figure 14) show that buckles do not particularly predominate near the top of the specimen. The answer to this problem may lie in an examination of the large deflections of conical shells, which is unavailable at present. The findings of the present paper contradict those to Reference 27, where the large radius of curvature was recommended for the equivalent cylinder. However, the edge conditions of the tests reported therein were such as to render the results invalid for conical shells attached to end plates or stiffened by end rings.

Some areas for future study can be suggested. It is likely that the acquisition of more data will suggest better parameters than l/ρ_1 and ρ_1/t and will point up possible differences in the buckling of cones and cylinders. It would be of interest in future experimental investigations to keep the small radius of the cone fixed and vary the large radius rather than vice versa, as in the present paper. Large deflection analyses are also desirable. A clue to the deformation patterns of conical shells probably can be obtained from a study of the developable surfaces that can be derived from conical shapes.

Table 3. Experimental Data for Mylar Cones and Cylinders Under Axial Compression

t (in.)	E x 10^{-3} (psi)	R/t	L/R	$P/2\pi Et^2$	C/C^*
(r) $\alpha = 0^\circ$					
0.0050	750	800	2.5	0.214	1.262
0.0050	750	800	2.0	0.187	1.088
0.0050	750	800	2.0	0.187	1.088
0.0050	750	800	2.0	0.196	1.141
0.0049	748	816	2.0	0.173	1.019
0.0050	734	800	2.0	0.213	1.240
0.0050	742	800	2.0	0.343	1.996
0.0050	742	800	2.0	0.269	1.566
0.0050	729	800	2.0	0.282	1.641
0.0050	729	800	2.0	2.286	1.665
0.0050	739	800	2.0	0.261	1.519
0.0050	739	800	2.0	0.268	1.560
0.0050	739	800	2.0	0.234	1.362
0.0050	739	800	2.0	0.238	1.385
0.0050	732	800	2.0	0.241	1.403
0.0050	732	800	2.0	0.247	1.438
0.0050	738	800	2.0	0.255	1.484
0.0050	748	800	2.0	0.340	1.978
0.0050	748	800	2.0	0.298	1.734
0.0050	729	800	2.0	0.298	1.734
0.0050	729	800	2.0	0.262	1.524
0.0050	750	800	2.0	0.166	0.966
0.0050	750	800	1.5	0.188	1.069
0.0050	750	800	1.0	0.159	0.861
0.0050	750	800	1.0	0.212	0.148
0.0050	750	800	1.0	0.196	1.061
0.0050	750	800	1.0	0.212	1.148
0.0050	750	800	1.0	0.222	1.202
0.0050	750	600	2.0	0.271	1.532
0.0050	750	600	2.0	0.276	1.357
0.0051	750	588	1.0	0.269	1.224
0.0050	750	600	1.0	0.268	1.233
0.0050	750	400	2.0	0.308	1.194
0.0050	750	400	2.0	0.283	1.097
0.0050	750	400	1.0	0.274	1.001
0.0050	750	400	1.0	0.307	1.122
0.0050	750	200	2.0	0.405	1.044
0.0050	750	200	2.0	0.361	0.931
0.0050	750	200	1.0	0.366	0.950
0.0050	750	200	1.0	0.407	0.999

Table 3. Continued

t (in.)	E x 10^{-3} (psi)	R/t	L/R	$P/2\pi Et^2$	C/C^*
(a) $\alpha = 0^\circ$					
0.0079	814	506	2	0.270	1.202
0.0075	770	533	1	0.188	0.808
0.0075	770	533	1	0.184	0.792
0.0075	770	533	1	0.258	1.110
0.0075	770	533	1	0.214	0.921
0.0079	770	506	1	0.272	1.136
0.0078	770	513	1	0.356	1.499
0.0082	725	488	1	0.385	1.575
0.0082	725	488	1	0.375	1.535
0.0078	770	385	2	0.323	1.224
0.0078	770	385	2	0.342	1.296
0.0080	725	375	2	0.348	1.299
0.0080	725	375	2	0.340	1.269
0.0080	725	375	1	0.353	1.243
0.0080	725	375	1	0.320	1.127
0.0082	725	366	1	0.359	1.247
0.0081	725	370	1	0.372	1.300
0.0075	770	267	2	0.338	1.033
0.0075	770	267	2	0.396	1.216
0.0075	770	267	2	0.420	1.284
0.0075	770	267	2	0.422	1.290
0.0078	770	256	2	0.302	0.909
0.0078	770	256	2	0.341	1.017
0.0075	770	267	1	0.360	1.044
0.0075	770	267	1	0.416	1.206
0.0075	770	267	1	0.369	1.070
0.0076	770	263	1	0.383	1.101
0.0008	725	250	1	0.367	1.024
0.0008	725	250	1	0.353	0.985
0.0075	770	133	2	0.440	0.892
0.0075	770	133	2	0.394	0.798
0.0075	770	133	1	0.432	0.838
0.0075	770	133	1	0.489	0.969

Table 3. Continued

t (in.)	$E \times 10^{-3}$ (psi)	R/t	L/R	$P/2\pi Et^2$	C/C^*
(a) $\alpha = 0^\circ$					
0.0098	690	204	2	0.352	0.918
0.0100	690	200	1	0.396	0.972
0.0100	690	200	1	0.461	1.132
0.0100	690	200	1	0.485	0.191
0.0100	690	100	2	0.361	0.618
0.0100	690	100	2	0.381	0.652
0.0100	690	100	2	0.398	0.681
0.0100	690	100	2	0.420	0.719
0.0100	690	100	1	0.418	0.687
0.0100	690	100	1	0.500	0.822
0.0100	690	100	1	0.433	0.712
0.0100	690	100	1	0.494	0.812
0.0075	770	533	2	0.218	1.000
0.0075	770	533	2	0.195	0.894
0.0075	770	533	2	0.218	1.000
0.0075	800	533	2	0.305	1.399
0.0075	800	533	2	0.253	1.161
0.0080	762	500	2	0.315	1.392
0.0080	712	500	2	0.289	1.277
0.0080	725	500	2	0.344	0.520
0.0076	770	513	2	0.264	1.184
0.0081	720	494	2	0.342	1.500
0.0081	740	494	2	0.210	0.922
0.0078	769	513	2	0.207	0.929
0.0079	775	506	2	0.219	0.974
0.0079	709	506	2	0.279	1.241
0.0079	769	506	2	0.286	1.273
0.0079	810	506	2	0.300	1.335
0.0079	810	506	2	0.300	1.335
0.0079	794	506	2	0.354	1.575
0.0079	794	506	2	0.344	1.531
0.0079	794	506	2	0.373	1.660
0.0079	794	506	2	0.331	1.473
0.0079	766	506	2	0.276	1.228
0.0079	766	506	2	0.286	1.273
0.0079	816	506	2	0.364	1.620
0.0079	816	506	2	0.395	1.758

Table 3. Continued

t (in.)	E x 10^{-3} (psi)	k/t	L/R	$P/2\pi Et^2$	C/C^*
(a) $\alpha = 0^\circ$					
0.0100	690	400	2	0.253	0.997
0.0100	690	400	2	0.320	1.241
0.0100	690	400	2	0.274	1.062
0.0100	690	400	2	0.257	0.996
0.0100	690	400	2	0.272	1.054
0.0100	690	400	2	0.356	1.380
0.0096	690	417	2	0.332	1.318
0.0100	675	400	2	0.309	1.197
0.0100	675	400	2	0.290	1.124
0.0100	680	400	2	0.308	1.194
0.0100	680	400	2	0.297	1.151
0.0100	719	400	2	0.286	1.108
0.0100	723	400	2	0.311	1.206
0.0100	723	400	2	0.298	1.155
0.0100	739	400	2	0.311	1.206
0.0100	739	400	2	0.285	1.105
0.0100	710	400	2	0.451	1.748
0.0100	710	400	2	0.415	1.609
0.0100	694	400	2	0.365	1.415
0.0100	694	400	2	0.292	1.132
0.0100	716	400	2	0.396	1.535
0.0100	716	400	2	0.332	1.287
0.0100	726	400	2	0.301	1.167
0.0100	726	400	2	0.299	1.159
0.0100	713	400	2	0.447	1.733
0.0100	713	400	2	0.409	1.586
0.0100	690	400	1	0.279	1.019
0.0100	690	400	1	0.271	0.990
0.0100	690	400	1	0.228	0.833
0.0100	690	400	1	0.246	0.899
0.0100	690	400	1	0.345	1.261
0.0100	690	400	1	0.368	1.344
0.0093	690	323	2	0.352	1.203
0.0100	690	300	2	0.326	1.167
0.0100	690	300	1	0.318	0.986
0.0100	690	300	1	0.361	1.119
0.0095	690	211	2	0.368	0.974

Table 3. Continued

t (in.)	E x 10^{-6} (psi)	ρ_1/t	ℓ/ρ_1	$P/2\pi Et^2\cos^2\phi$	C/C*
			(b) $\alpha = 10^\circ$		
0.0100	690	402	1.629	0.304	1.167
0.0100	690	402	1.629	0.309	1.186
0.0100	697	278	4.665	0.260	0.834
0.0100	690	278	4.665	0.242	0.777
0.0100	690	278	4.665	0.284	0.912
0.0100	690	278	4.665	0.287	0.921
0.0050	750	556	4.665	0.333	1.616
0.0050	750	556	4.665	0.324	1.572
0.0050	750	556	4.665	0.315	1.528
0.0050	750	556	4.665	0.341	1.654
0.0050	750	556	4.665	0.328	1.591
0.0050	750	508	5.685	0.328	1.513
0.0050	750	508	5.685	0.336	1.550
0.0030	775	1335	1.633	0.252	1.943
0.0030	775	1335	1.633	0.238	1.835
0.0030	775	925	5.194	0.198	1.304
0.0030	775	925	5.194	0.224	1.475
0.0030	775	925	4.665	0.258	1.695
0.0030	775	925	4.665	0.230	1.511
			(c) $\alpha = 20^\circ$		
0.0100	690	268	2.73	0.344	0.967
0.0100	690	268	2.73	0.332	1.030
0.0100	690	268	2.73	0.326	1.011
0.0100	690	268	2.73	0.316	0.980
0.0100	690	268	2.73	0.294	0.912
0.0100	690	160	6.40	0.379	0.869
0.0100	690	160	6.40	0.352	0.816
0.0100	690	160	6.40	0.335	0.776
0.0050	750	536	2.73	0.332	1.352
0.0050	750	536	2.73	0.366	1.711
0.0050	750	536	2.73	0.371	1.734
0.0050	750	536	2.73	0.311	1.454
0.0050	750	536	2.73	0.295	1.392
0.0050	750	320	6.40	0.337	1.192

Table 3. Continued

t (in.)	$E \times 10^{-3}$ (psi)	ρ_1/t	ℓ/ρ_1	$P/2\pi Et^2\cos^2$	C/C^*
		(c) $\alpha = 20^\circ$			
0.0050	750	320	6.40	0.350	1.228
0.0050	750	320	6.40	0.386	1.354
0.0030	775	1427	0.68	0.355	2.308
0.0030	775	1427	0.68	0.320	2.205
0.0030	775	893	2.73	0.290	1.831
0.0030	775	893	2.73	0.257	1.623
0.0020	740	1340	2.73	0.248	1.989
0.0020	740	1340	2.73	0.237	1.901
0.0020	740	800	6.40	0.293	1.776
0.0020	740	800	6.40	0.292	1.770
		(d) $\alpha = 30^\circ$			
0.0100	690	465	0.561	0.330	1.180
0.0100	690	381	1.294	0.307	1.121
0.0101	650	287	1.731	0.408	1.291
0.0100	690	233	2.571	0.326	0.929
0.0100	690	233	2.571	0.351	1.000
0.0100	690	233	2.571	0.348	0.992
0.0100	690	173	3.948	0.320	0.772
0.0081	682	357	1.737	0.284	1.021
0.0082	650	282	2.589	0.291	0.928
0.0079	725	219	4.052	0.329	0.914
0.0083	764	209	4.052	0.242	0.653
0.0050	750	927	0.563	0.265	1.375
0.0050	750	561	1.754	0.432	2.025
0.0050	750	465	2.571	0.322	1.380
0.0050	750	465	2.571	0.280	1.200
0.0050	750	465	2.571	0.270	1.157
0.0050	750	345	3.948	0.350	1.273
0.0030	775	1547	0.563	0.264	1.795
0.0030	775	1547	0.563	0.242	1.645
0.0030	775	1547	0.563	0.347	2.359
0.0030	775	1547	0.563	0.336	2.284
0.0030	775	1547	0.563	0.346	2.352
0.0030	775	1547	0.563	0.238	1.618

Table 3. Continued

t (in.)	$E \times 10^{-3}$ (psi)	ρ_1/t	ℓ/ρ_1	$P/2\pi Et^2\cos^2$	C/C^*
		(d) $\alpha = 30^\circ$			
0.0030	775	937	1.754	0.311	1.965
0.0030	775	937	1.754	0.254	1.605
0.0030	775	937	2.132	0.379	2.430
0.0030	775	937	1.754	0.238	1.504
0.0030	775	937	1.754	0.230	1.454
0.0030	775	777	2.571	0.341	1.979
0.0030	775	777	2.571	0.332	1.927
0.0020	740	1150	2.600	0.320	2.340
0.0020	740	1150	2.600	0.284	2.077
0.0020	740	860	3.971	0.282	1.766
		(e) $\alpha = 45^\circ$			
0.0100	690	211	2.351	0.394	1.055
0.0100	690	211	2.351	0.400	1.071
0.0100	690	211	2.351	0.394	1.059
0.0100	690	105	5.724	0.355	0.639
0.0100	690	105	5.724	0.383	0.689
0.0100	690	105	5.724	0.371	0.668
0.0100	690	105	5.724	0.388	0.698
0.0100	690	105	5.724	0.378	0.680
0.0050	750	1128	0.248	0.355	1.410
0.0050	750	1128	0.248	0.350	1.390
0.0050	750	1128	0.248	0.399	1.585
0.0050	750	1128	0.248	0.395	1.569
0.0050	750	424	2.340	0.381	1.541
0.0050	750	424	2.340	0.339	1.371
0.0050	750	212	5.670	0.361	0.988
0.0050	750	212	5.670	0.373	1.021
0.0050	750	212	5.670	0.356	0.975
0.0050	750	212	5.670	0.363	0.994
0.0050	750	212	5.670	0.323	0.884
0.0030	775	1172	1.009	0.319	2.146
0.0030	775	1172	1.009	0.298	2.004
0.0030	775	702	2.351	0.297	1.616
0.0030	775	702	2.351	0.291	1.584

Table 3. Concluded

t (in.)	E x 10^{-3} (psi)	ρ_1/t	ℓ/ρ_1	$P/2\pi Et^2\cos^2$	C/C^*
(e) $\alpha = 45^\circ$					
0.0030	775	348	5.757	0.236	0.858
0.0030	775	348	5.757	0.215	0.792
0.0030	775	348	5.757	0.260	0.957
0.0030	775	348	5.757	0.295	1.086
0.0030	775	348	5.757	0.266	0.979
0.0030	775	348	5.757	0.266	0.979
0.0030	775	348	5.757	0.292	1.075
0.0020	740	1702	1.767	0.226	2.020
0.0020	740	1702	1.767	0.220	1.967
(f) $\alpha = 60^\circ$					
0.0100	690	500	0.57	0.393	1.468
0.0100	690	300	1.34	0.375	1.196
0.0100	690	200	2.31	0.377	0.977
0.0100	690	200	2.31	0.405	1.050
0.0100	690	200	2.31	0.395	1.024
0.0075	770	1067	0.15	0.478	1.292
0.0075	770	1067	0.15	0.475	1.284
0.0075	770	267	2.31	0.391	1.203
0.0075	770	267	2.31	0.360	1.107
0.0050	750	1000	0.57	0.302	1.657
0.0050	750	1000	0.57	0.293	1.588
0.0050	750	1000	0.57	0.445	2.412
0.0050	750	1000	0.57	0.413	2.239
0.0050	750	600	1.34	0.417	1.987
0.0050	750	600	1.34	0.399	1.901
0.0050	750	600	1.34	0.329	1.567
0.0050	750	600	1.34	0.329	1.567
0.0050	750	600	1.34	0.381	1.816
0.0050	750	400	2.31	0.406	1.585
0.0050	750	400	2.31	0.406	1.585
0.0050	750	400	2.31	0.333	1.300
0.0050	750	400	2.31	0.365	1.415
0.0050	750	400	2.31	0.328	1.281
0.0030	775	667	2.31	0.410	2.163
0.0030	775	667	2.31	0.378	1.994

Table 4. Experimental Data for Steel Cones and Cylinders Under Axial Compression

t (in.)	E x 10^6 (psi)	R/t	L/R	$P/2\pi Et^2$	C/C*
(a) $\alpha = 0^\circ$					
0.010	30.3	800	2	0.310	1.804
0.010	30.3	800	2	0.267	1.554
0.010	30.3	800	1	0.335	1.814
0.010	30.3	800	1	0.266	1.441
0.020	30.3	400	2	0.362	1.403
0.020	30.3	400	2	0.298	1.155
0.020	30.3	400	1	0.268	0.979
0.020	30.3	400	1	0.346	1.264
0.008[1]	32.4	375	2	0.324	1.209
0.010[1]	34.4	300	2	0.273	0.895
0.010[2]	30.3	300	5	0.281	0.945
0.010[2]	30.3	300	1	0.303	0.939
0.012[1]	32.6	249	4	0.249	0.746
0.012[1]	32.6	249	2	0.257	0.753

[1] Reference 22.

[2] Reference 25.

Table 4. Concluded

t (in.)	E x 10^6 (psi)	ρ_1/t	ℓ/ρ_1	$P/2\pi Et^2\cos^2$	C/C*
(b) $\alpha = 30^\circ$					
0.010	30.3	465	2.571	0.438	1.878
0.010	30.3	465	2.571	0.410	1.758
0.010[1]	30.3	465	2.571	0.244	1.046
0.020	30.3	233	2.571	0.245	0.598
0.020[2]	30.3	233	2.571	0.267	0.760
0.020[1,2]	30.3	233	2.571	0.214	0.609
0.020[2]	30.3	233	2.571	0.267	0.760
(c) $\alpha = 60^\circ$					
0.010	30.3	1000	0.57	0.251	1.361
0.010	30.3	600	1.34	0.370	1.763
0.010	30.3	600	1.34	0.293	1.396
0.010	30.3	600	1.34	0.301	1.434
0.010	30.3	400	2.31	0.310	1.210
0.010[1]	30.3	400	2.31	0.221	0.863
(d) $\alpha = 75^\circ$					
0.010	30.3	758	1.08	0.243	1.290
0.010	30.3	758	1.08	0.337	1.790
0.010	30.3	758	1.08	0.326	1.732
0.020	30.3	570	0.635	0.288	1.185
0.020	30.3	1380	1.08	0.286	2.132

[1] Buckled adjacent to seam (seam not reinforced).

[2] Buckled near top clamping plate indicating yield condition.

Figure 11. Illustration of Shift of Buckle Pattern for Retested Mylar Cylinder. (Dots show location of buckle corners in previous test)

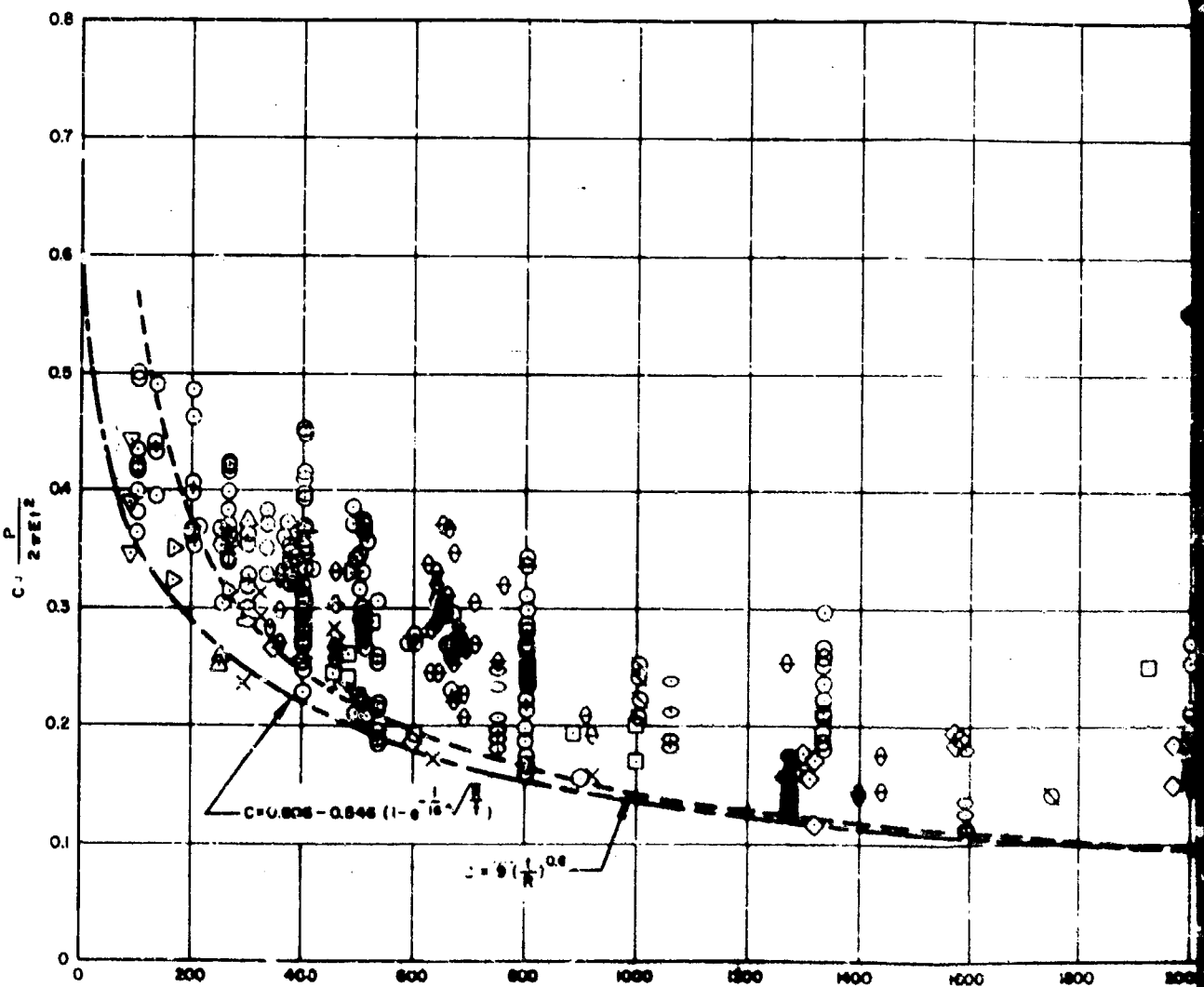

Figure 12. Comparison of Various E
in Axial Compression

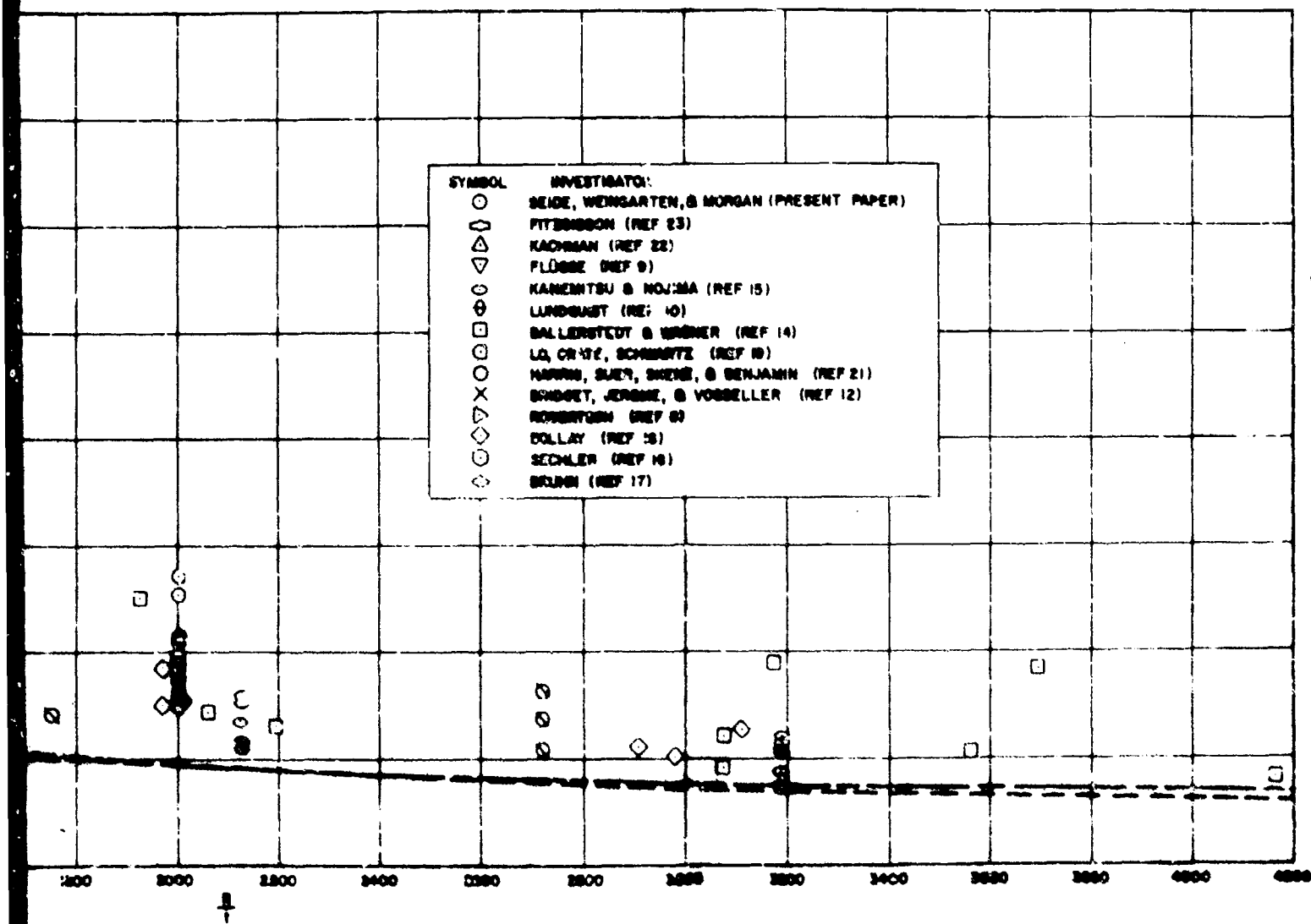

of Various Experimental Results for Cylinders
pression

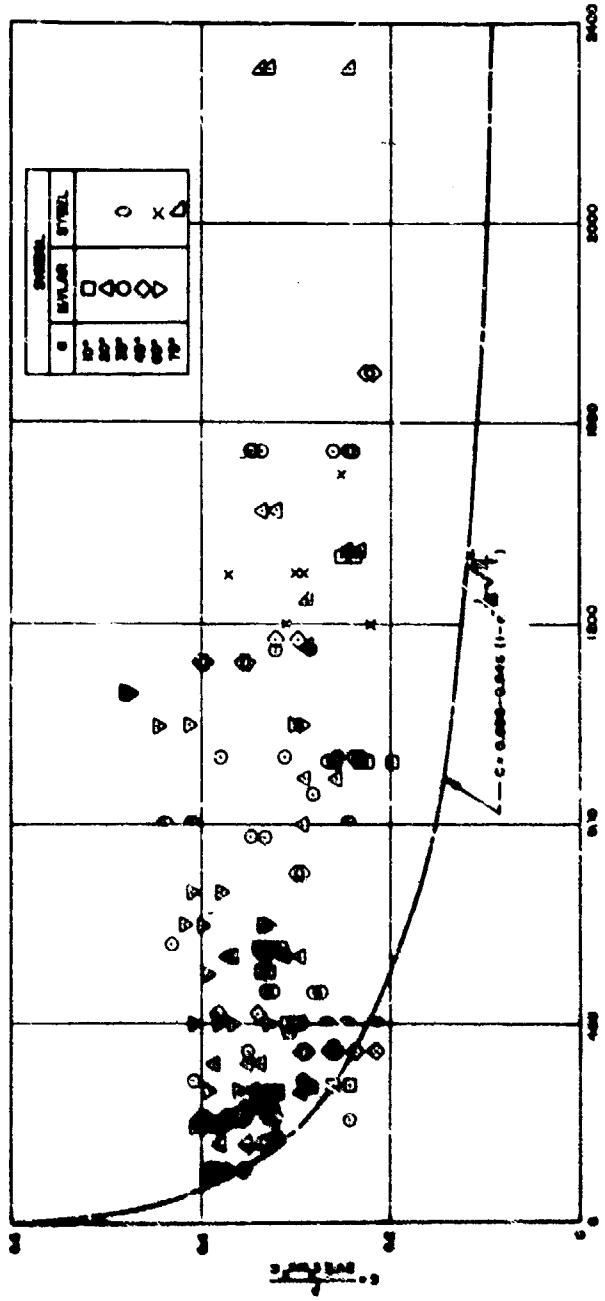

Figure 13. Comparison of Axial Compression Coefficients for Conical Shells with Lower Bound Curve for Cylinders

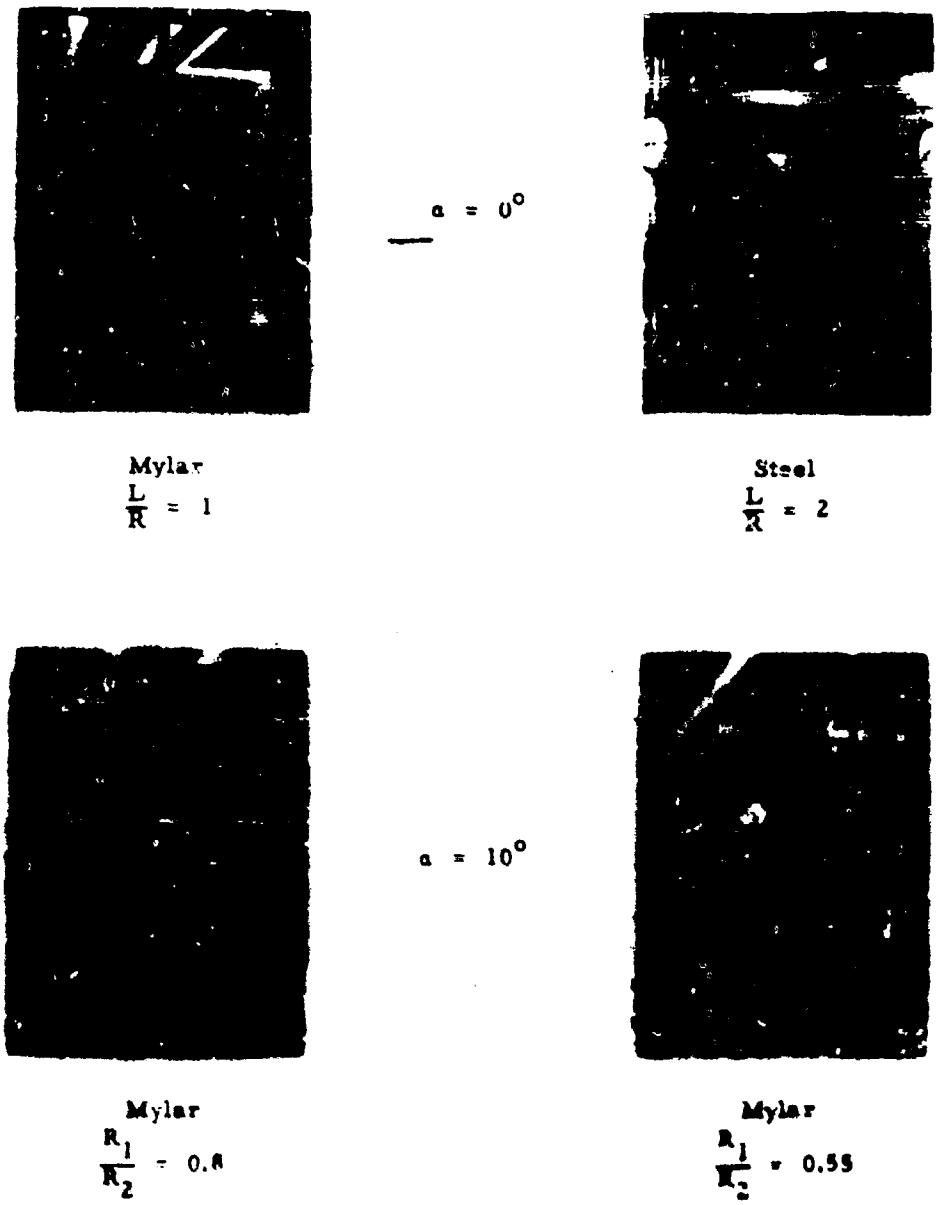

Figure 14. Experimental Buckle Patterns for Cylinders and Cones in Axial Compression

Mylar

$\frac{R_1}{R_2} = 0.8$

$\alpha = 20^\circ$

Mylar

$\frac{R_1}{R_2} = 0.5$

Mylar

$\frac{R_1}{R_2} = 0.3$

Figure 14. Continued

Mylar

$\frac{R_1}{R_2} = 0.8$

Mylar

$\frac{R_1}{R_2} = 0.5$

$\alpha = 30^\circ$

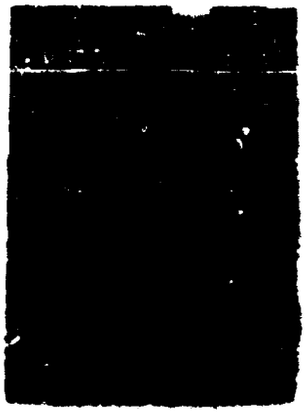

Mylar

$\frac{R_1}{R_2} = 0.4$

Steel

$\frac{R_1}{R_2} = 0.4$

Figure 14. Continued

Mylar
$\frac{R_1}{R_2} = 0.8$

Mylar
$\frac{R_1}{R_2} = 0.5$

$\alpha = 45^{\circ}$

Mylar
$\frac{R_1}{R_2} = 0.3$

Mylar
$\frac{R_1}{R_2} = 0.15$

Figure 14. Continued

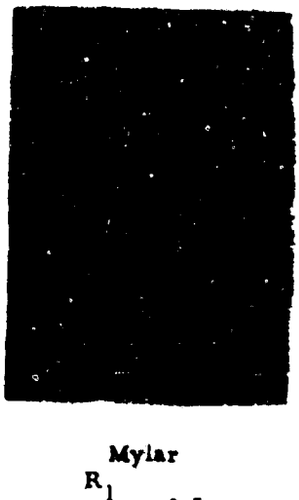

Mylar

$\frac{R_1}{R_2} = 0.5$

$\alpha = 60^\circ$

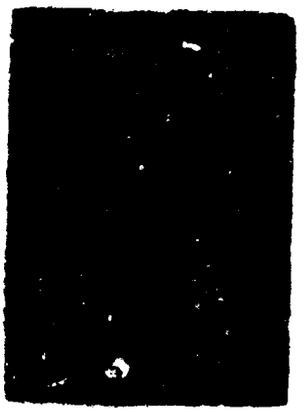

Mylar

$\frac{R_1}{R_2} = 0.3$

Mylar

$\frac{R_1}{R_2} = 0.2$

Figure 14. Concluded

VI. PRESSURIZED CYLINDERS UNDER AXIAL COMPRESSION

Increased emphasis has recently been placed upon the internally pressurized monocoque cylinder as an efficient load carrying structure for missile applications. As a result, several experimental investigations have been reported in the literature (References 5, 6, 19, 20 and 21). Practically all the results obtained to date seem inconsistent with current explanations of cylinder behavior. With the exception of the study of Reference 5, even large amounts of internal pressure did not stabilize the test cylinders to the extent that the theoretical small-deflection buckling stress was achieved. Although the discrepancy between theory and experiment is usually attributed to geometric imperfections and associated stress concentrations, large values of internal pressure should remove these initial imperfections and provide cylinders which are substantially perfect. In most cases it is suspected that the plastic yielding of the material, whether due to high buckling stresses or excessive initial damage, is the cause of the current confusion of the results.

In order to provide test data on pressurized unstiffened cylinders which would be less sensitive to plasticity effects, tests were made on 8-inch diameter and 8-inch length cylinders constructed of Mylar. The results of this investigation are reported herein.

A. Test Apparatus and Procedure

The setup for the compression tests is shown in the photograph of Figure 15. The test specimen assembly is illustrated in Figure 16. To maintain concentricity of the cylinders during casting, the grooves in the end caps were stepped to provide a locating diameter. The alignment of the two caps during assembly was provided by the center post and ball bushing assembly. The tolerance between post and bushing was adjusted to eliminate friction and to permit freedom of rotation during the tests.

It was necessary to counterbalance the top cap weight, and very careful specimen installation was required to avoid initial wrinkling of the 2-and 3-mil cylinders. The center post of the top cap also provided a mounting for a differential transformer. This displacement transducer permitted measurement of the relative movement between the caps along the axis of the cylinder. Pressurization of the cylinders was accomplished with compressed air through ports in the bottom cap. An accumulator in series with the specimen increased the control volume and assisted in stabilizing the air pressure. The compressive load was applied with a motorized screw mechanism in series with a Statham load cell, a ball bearing, and a cover plate as illustrated in Figure 16. The floating cover plate provided clearance for the transducer leads and eliminated deflections of the top cap from the transducer's measurements. Throughout the testing, the loading mechanism provided a uniform strain rate of approximately 0.4 percent/min. Load and deformation were recorded simulataneously with a Mosley X-Y recorder. The internal pressure was measured by manometers.

For each fixed pressure, the axial load was gradually increased until snap buckling occurred or until an ultimate load was reached. Then the load was decreased until the buckles disappeared. Load-deflection diagrams were recorded continuously during the loading and unloading process. The internal pressure was then increased a given amount and the process repeated. After the maximum pressure was reached, a rerun was made at zero pressure to determine the degree of deterioration of the test specimen.

B. Load-Deflection Characteristics

A set of typical load-deflection diagrams for various pressures is presented in Figure 17. The occurrence of diamond shaped buckles was unmistakable, since they appeared with a snapping noise. In the diagrams, this phenomenon is illustrated by the sharpness of the load drop-off and by the size of the unloading hysteresis loop. For increased internal pressure

buckling occurred with a smaller number of longitudinal ed diamond patterns. In the figure, this change is illustrated by a decrease in the load drop off and by a reduction in the size of the hysteresis loop.

At the higher values of initial circumferential ripples resembling the sinusoidal waves assumed in the classical small-deflection theory, appeared prior to collapse. The occurrence of these ripples is illustrated by the gradual change in the slope of the load-deformation wave.

Generally, these ring shaped deformations appeared near the end caps. For the thinner cylinders increased compressive load caused these waves to grow and to propagate from the ends, until they extended over the entire length of the cylinder. Then elongated diamonds developed in the waves near the ends and the load dropped off gradually. It is interesting to note that this behavior is in qualitative agreement with the predictions of the large-deflection theory of Reference 3. For the thicker cylinders, however, these waves were confined to the region near the ends. When the compressive load was increased, the central portion of the cylinders remained undeformed while the end waves grew until other diamond-shaped buckles developed as the cylinder ends became plastic, when the load decreased slowly.

Although the shape of the loading portion of the diagrams did not change, the onset of plasticity was readily recognised. In addition to a decrease in the net collapse load, the unloading portion of the diagrams changed. Instead of dropping to a minimum and then recovering slightly as the diamond-shaped buckles disappeared, the load dropped continuously. The diagrams for high pressures in Figure 17 illustrate this trend. The cylinder appears to have lost its ability to recover, and, as it becomes more plastic, this inability increases.

Measured load-end shortening curves for the test cylinders are illustrated in Figure 18. The test results for three values of P are compared with the theoretical curves derived by Dow and Peterson

(Reference 29) for finite cylinders with axisymmetric deformation. As indicated by the theory, the deviation from the unit slope curve of unpressurized, unrestrained cylinders increases with decreasing values of the curvature paramete. and with increasing values of the pressure parameter. For the higher values of Z (lower values of thickness), the agreement between theory and experiment is excellent, even at high values of $\bar{p}$. But for the two thicker cylinders, the deviation from the unit slope is even greater than predicted by theory. This deviation of the experimental load-shortening curves from theory is apparently associated with the difference of the radial deformation pattern previously discussed.

C. Critical Axial Stress

The experimental results for critical axial stress as a function of internal pressure for the five skin thicknesses studies are given in Table 5. Material properties of the specimens are given in Table 5(a). The results are also plotted in Figure 19 in terms of the two dimensionless parameters introduced by Lo, Crate, and Schwartz (Reference 19): $\bar{\sigma}_{cr}$ and $\bar{p}$. Solid curves representing the approximate lower bound of the scatterband are also shown. It will be noticed that the general trend of variation of $\bar{\sigma}_{cr}$ with pressure is as predicted in Reference 19, i.e., the tendency is for $\bar{\sigma}_{cr}$ to increase with increasing $\bar{p}$ and to reach a constant value at higher values of $\bar{p}$. As expected, since the influence of initial imperfections diminishes with increasing pressure, the experimental scatter is largest for very low pressures. This scatter appears to be dependent upon the end conditions, among other factors, since the two casting materials used, Cerrobend and Cerrolow, gave consistently different results. (See Table 5(a) for material used for each specimen.) Generally, higher values of $\bar{\sigma}_{cr}$ were obtained for values of $\bar{p}$ up to 0.5 when Cerrolow was used. This tendency is illustrated in Figure 20 by two series of tests on cylinders clamped in Cerrobend for the first series and in Cerrolow for the second series. The difference appears to result from the solidifying characteristics of the two allows. Upon cooling, Cerrolow contracts slightly, whereas Cerrobend expands approximately 25 times this amount of contraction. Thus the cylinders installed in Cerrobend had

more eccentricity at the ends and, consequently, gave lower values of $\bar{\sigma}_{cr}$ until the internal pressure could overcome the influence of these intial imperfections. To illustrate the generality of this difference, the unpressurized results for both clamped conditions are compared in Figure 21.

For comparison, the results for the various values of R/t curves representing the lower envelope of scatter of $\bar{\sigma}_{cr}$ versus $\bar{p}$ are shown in Figure 22. It appears that the buckling coefficients $\bar{\sigma}_{cr}$ are a function of the radius-thickness ratio for pressurized, as well as unpressurized, cylinders. However, in accordance with theory, the buckling coefficients converge to the classic value of $\bar{\sigma}_{cr}$, regardless of the values of R/t, in contrast to the results of References 19, 20, and 21.

The combined effects of axial load and internal pressure were not large enough for yielding to occur in the cylinders of smaller wall thickness, but the influence of plasticity was felt in the thicker cylinders. In Figure 19(b), plasticity near the end caps is illustrated by the drop-off of $\bar{\sigma}_{cr}$ for high values of $\bar{p}$. The cut off line illustrated in the figure,

$$\bar{\sigma}_{cr} = 0.728\bar{\sigma}_{\text{prop limit}} - 1.174\,\bar{p}\,, \tag{7}$$

was derived from a consideration of bending stresses at the ends of the cylinders and represents the combined axial stress and hoop stress which will cause the outer fibers to become plastic, based on a von Mises yield condition. The proportional limit has been used, rather than the yield condition. The proportional limit has been used, rather than the yield stress, since $\bar{\sigma}_{cr}$ appears to drop off soon after the maximum stresses exceed this limit.

D. Comparison With Other Experimental Data

The data from the current tests have been summarized in Figure 22, by curves representing the lower envelope of the experimental scatter. These curves have been used for comparison with the results from three earlier investigations. The data compiled by Dow and Peterson

(Reference 5) for cylinders of 7075-T6 aluminum are plotted in Figure 23(a) and 23(b). In general, the results for these ring-stiffened cylinders are in good agreement with those for Mylar cylinders. The 7075-T6 aluminum results in Figure 23(a) are somewhat higher since the length-radius ratio of the metal cylinders was 0.25 as compared to 2 for the Mylar cylinders. The range of pressures covered in these tests is limited. Tests covering a larger range of pressures are reported in Reference [illegible] the results of which are plotted in Figure 23(c). The cylinders used in these tests were made from 18-8 half-hard stainless steel which has a rather rounded stress-strain curve. The plasticity cut off line derived from the proportional limit is illustrated in the figure. As in the case of Mylar, the buckling coefficients drop off steadily as the biaxial state of stress is increased beyond this limit. For low pressures, however, the results are in fair agreement with the present investigation. A high strength stainless steel, 17-7 PH, was used in the investigation of Brown and Rea (Reference 6). The results of these tests are plotted in Figure 23(d). At very low pressures, the influence of imperfections is evident, but as the cylinder becomes stabilized by increased pressure, the results agree with those for Mylar. It is unfortunate that the tests were not extended to high values of $\bar{p}$, since the stresses were well below the elastic limit of the material.

One of the reasons for the discrepancy of other investigations thus appears to be the onset of plasticity resulting from clamped end bending moments. The specimens used for the study of Reference 5 differed from those of other investigations and of the present investigation in that they were ring-stiffened cylinders consisting of a test section and a buffer bay on either side of the test section. The rings helped to alleviate bending stresses due to end restraint and prevent premature buckling due to plasticity. In References 5 and 30 Peterson concluded that the short buffer bays help to distribute the load and postpone premature buckling due to irregular stress distributions in the neighborhood of the ends. However, it can be seen from the comparisons of the present section and those of Sections IV and VII that the results of References 5 and 30 are not sensibly

different from those obtained from specimens without buffer bays.

In some of the investigations, the buckling coefficients appeared to drop off prior to the predicted occurrence of plasticity (see Figure 23(c) for instance). This discrepancy is suspected to be caused by plastic yielding of the material as the result of damage incurred during the preceding tests, or, in the case of very thin specimens, during the fabrication process.

E. Critical End Shortening

Data for the axial deformation or end-shortening at which buckling occurred were also taken from the load-deflection diagrams. These results are summarized in Table 6 and are plotted in Figure 24 in terms of nondimensional parameters similar to those used previously. The magnitudes of the deformation represent a measure of the axisymmetric radial deformations which occur prior to collapse, since the difference between the total end-shortening and the compressive strain is equal to the nonlinear deformation associated with the rippling which occurs at high pressures. It was found by trial and error that plotting the strain difference $(\delta_{cr} - \bar{\sigma}_{cr})$ as a function of $p/E(R/t)^{5/3}$ (see Figure 25) eliminated the dependence upon radius-thickness ratios. It would be interesting to know if theoretical predictions bear any resemblance to the relation defined by this method of plotting.

F. Minimum Load

In addition to measurements of the critical load and end deformation, minimum load data were taken from the load-deflection diagrams. The minimum load, as used here, refers to the lowest load attained in the deformed equilibrium condition during the unloading process. The results for minimum load as a function of internal pressure for the five radius-thickness ratios are summarized in Table 7 and plotted in Figure 26. The general trend of the variation of $\bar{\sigma}_{min}$ with the pressure parameter $\bar{p}$ is in accord with the dashed curve representing the values derived in Reference 28. It is interesting to note, however, that the minimum values obtained here are less than those predicted, which would indicate that

either the currently used large-deflection theory is not accurate enough for such large strains or the current solutions are not sufficiently accurate. As predicted by the theoretical solution of Reference 4, for initially imperfect cylinders, there is little scatter in the measured values of the minimum stress coefficient which is independent of the radius-thickness ratio of the cylinders. The lower bound curve for $\overline{\sigma}_{min}$ is included in Figure 22. It is interesting to note that the lower envelope of the buckling coefficient curves appear to approach the curve for $\overline{\sigma}_{min}$ as a limit, as the radius-thickness ratio increases.

Table 5. Experimental Data for Pressurized Mylar Cylinders under Axial Compression.

Specimen No. 20.1				
P in. H_2O	P_{total} lb	P_{cr} lb	$\bar{\sigma}_{cr}$	$\bar{P}$
0.0	3.6	3.6	0.189	0.0
0.2	4.5	4.2	0.221	0.037
0.4	5.5	4.8	0.253	0.074
0.6	6.5	5.4	0.284	0.116
0.8	7.3	5.8	0.305	0.153
1.0	8.2	6.4	0.337	0.189
1.5	10.0	7.3	0.384	0.284
2.0	11.5	7.9	0.416	0.379
2.5	13.2	8.7	0.458	0.474
3.0	14.5	9.1	0.479	0.568
3.5	15.5	9.1	0.479	0.663
4.0	16.9	9.6	0.505	0.758
5.0	19.3	10.2	0.537	0.953
6.0	21.1	10.2	0.537	1.142
7.0	23.1	10.4	0.547	1.332
8.0	25.4	10.9	0.574	1.521
9.0	27.4	11.1	0.584	1.711
10.0	29.4	11.2	0.589	1.900
12.0	33.4	11.6	0.611	2.279
14.0	37.2	11.8	0.621	2.658
16.0	40.7	11.7	0.616	3.042
18.0	44.7	12.0	0.631	3.421
20.0	47.2	11.9	0.626	3.800

Specimen No. 20.2				
P in. H_2O	$P_{tot.}$ lb	P_{cr} lb	$\bar{\sigma}_{cr}$	$\bar{P}$
0.0	2.6	2.6	0.149	0.0
0.2	3.7	3.3	0.189	0.040
0.4	4.6	3.9	0.223	0.080
0.6	5.5	4.4	0.251	0.126
0.8	6.1	4.6	0.263	0.166
1.0	6.9	5.1	0.291	0.206
1.5	8.0	6.3	0.360	0.309
2.0	10.2	6.6	0.377	0.411
2.5	11.8	7.3	0.417	0.514
3.0	13.1	7.7	0.440	0.617
3.5	14.4	8.0	0.457	0.720
4.0	15.6	8.1	0.463	0.823
5.0	18.1	9.0	0.514	1.034
6.0	20.5	9.6	0.549	1.240
7.0	22.7	10.0	0.571	1.446
8.0	24.7	10.2	0.583	1.651
9.0	26.7	10.4	0.594	1.857
10.0	28.6	10.4	0.594	2.063
12.0	32.3	10.5	0.600	2.474
14.0	36.1	10.7	0.611	2.886
16.0	39.9	10.9	0.623	3.303
18.0	43.8	11.1	0.634	3.714
20.0	47.7	10.9	0.623	4.126
0.0	2.7	2.7	0.154	0.0

Specimen No. 65.1				
P in. H_2O	P_{total} lb	P_{cr} lb	$\bar{\sigma}_{cr}$	$\bar{P}$
0.0	1.0	1.0	0.162	0.0
0.2	1.1	1.9	0.310	0.039
0.4	3.1	2.6	0.268	0.078
0.6	4.2	3.1	0.279	0.118
0.8	5.1	3.6	0.384	0.157
1.0	7.7	3.9	0.318	0.196
1.5	9.6	4.7	0.382	0.295
2.0	10.9	7.3	0.394	0.394
2.5	12.2	7.7	0.415	0.490
3.0	13.4	8.0	0.431	0.588
3.5	14.8	8.4	0.453	0.686
4.0	16.1	8.8	0.479	0.784
5.0	18.6	9.5	0.502	0.980
6.0	20.6	9.7	0.514	1.176
7.0	22.6	9.9	0.534	1.372
8.0	24.7	10.2	0.550	1.567
9.0	26.8	10.5	0.567	1.763
10.0	28.8	10.8	0.575	1.959
12.0	32.9	11.1	0.599	2.351
14.0	36.7	11.3	0.610	2.743
16.0	40.4	11.4	0.615	3.135
18.0	44.2	11.9	0.621	3.527
20.0	47.8	11.9	0.621	3.919
0.0	1.2	1.2	0.177	0.0

Table 5. Continued

Specimen No. 20.4				
p In. H_2O	P_{total} lb	P_{cr} lb	γ_{cr}	$\bar{\gamma}$
0.0	4.6	4.6	0.254	0.0
0.2	6.1	5.7	0.311	0.040
0.4	6.8	6.1	0.332	0.079
0.6	7.6	6.5	0.354	0.118
0.8	8.5	7.0	0.381	0.158
1.0	9.1	7.3	0.398	0.197
1.5	10.6	7.9	0.430	0.296
2.0	11.9	8.3	0.452	0.394
2.5	13.3	8.6	0.469	0.493
3.0	14.3	8.9	0.485	0.592
3.5	15.5	9.1	0.496	0.691
4.0	16.7	9.4	0.512	0.789
5.0	19.0	9.9	0.540	0.986
6.0	20.9	10.0	0.545	1.184
7.0	23.3	10.6	0.578	1.381
8.0	25.1	10.6	0.578	1.578
9.0	27.0	10.7	0.583	1.775
10.0	29.1	10.9	0.594	1.973
12.0	32.9	11.1	0.605	2.367
14.0	36.4	11.0	0.600	2.762
16.0	40.1	11.1	0.605	3.156
18.0	43.7	11.0	0.600	3.551
20.0	47.4	11.1	0.605	3.945
0.0	4.9	4.9	0.271	0.0

Specimen No. 20.5				
p In. H_2O	P_{total} lb	P_{cr} lb	γ_{cr}	$\bar{\gamma}$
0.0	4.9	3.0	0.208	0.0
0.2	5.3	4.9	0.262	0.039
0.4	6.9	6.2	0.332	0.077
0.6	7.7	6.6	0.353	0.116
0.8	8.6	7.1	0.380	0.155
1.0	9.4	7.6	0.406	0.194
1.5	11.3	8.6	0.460	0.291
2.0	12.5	8.9	0.476	0.388
2.5	13.7	9.2	0.492	0.485
3.0	15.1	9.7	0.519	0.582
3.5	16.2	9.8	0.524	0.679
4.0	17.3	10.0	0.535	0.775
5.0	19.3	10.2	0.544	0.969
6.0	21.6	10.7	0.573	1.163
7.0	23.6	10.9	0.583	1.357
8.0	25.5	11.0	0.589	1.551
9.0	27.2	10.9	0.583	1.744
10.0	29.1	10.9	0.583	1.938
12.0	33.0	11.2	0.600	2.326
14.0	36.4	11.0	0.589	2.714
16.0	40.1	11.1	0.594	3.101
18.0	44.0	11.3	0.605	3.489
20.0	47.6	11.3	0.605	3.876
0.0	4.0	4.0	0.214	0.0

Specimen No. 20.6				
p In. H_2O	P_{total} lb	P_{cr} lb	γ_{cr}	$\bar{\gamma}$
0.0	3.6	3.6	0.195	0.0
0.2	4.9	4.5	0.244	0.039
0.4	5.8	5.1	0.276	0.078
0.6	6.2	5.1	0.276	0.118
0.8	7.0	5.5	0.298	0.158
1.0	7.8	6.0	0.326	0.197
1.5	9.6	6.9	0.374	0.295
2.0	11.0	7.4	0.401	0.394
2.5	12.5	8.0	0.434	0.492
3.0	13.8	8.4	0.455	0.590
3.5	15.0	8.6	0.466	0.689
4.0	16.2	8.9	0.482	0.787
5.0	18.6	9.5	0.515	0.984
6.0	20.9	10.0	0.542	1.180
7.0	22.8	10.1	0.548	1.377
8.0	25.2	10.7	0.580	1.574
9.0	27.3	11.0	0.596	1.771
10.0	29.2	11.0	0.596	1.967
12.0	33.0	11.2	0.607	2.361
14.0	36.8	11.4	0.618	2.754
16.0	40.2	11.2	0.607	3.148
18.0	43.9	11.2	0.607	3.541
20.0	47.6	11.3	0.613	3.935
0.0	3.3	3.3	0.179	0.0

Table 5. Continued

Specimen No. 30.1				
p In.H_2O	P_{Total} lb	P_{cr} lb	ϵ_{cr}	$\bar{p}$
0	8.5	8.5	0.212	0.0
0.5	13.2	12.3	0.306	0.046
1	14.9	13.1	0.326	0.090
2	18.5	14.9	0.371	0.180
3	21.6	16.2	0.404	0.271
4	24.8	17.5	0.436	0.361
5	27.9	18.8	0.468	0.451
6	30.3	19.4	0.483	0.541
7	32.6	19.9	0.496	0.632
8	35.1	20.6	0.513	0.722
9	37.4	21.1	0.525	0.812
10	39.3	21.2	0.528	0.902
12	43.7	21.9	0.545	1.083
14	47.6	22.2	0.553	1.263
16	51.4	22.3	0.556	1.444
20	59.6	23.3	0.580	1.804
24	67.3	23.8	0.593	2.165
28	74.9	24.1	0.600	2.526
32	82.4	24.3	0.605	2.887
0	8.4	8.4	0.209	0.0

Specimen No. 30.2				
p In.H_2O	P_{Total} lb	P_{cr} lb	ϵ_{cr}	$\bar{p}$
0	9.0	9.0	0.223	0.0
0.5	12.2	11.3	0.280	0.045
1	14.5	12.7	0.315	0.090
2	18.5	14.9	0.370	0.180
3	21.8	16.4	0.407	0.270
4	25.0	17.7	0.440	0.359
5	27.7	18.6	0.461	0.449
6	30.1	19.2	0.476	0.539
7	32.6	19.9	0.494	0.629
8	34.9	20.4	0.506	0.719
9	37.6	21.3	0.529	0.809
10	39.5	21.4	0.531	0.898
12	44.1	22.3	0.553	1.078
14	48.3	22.9	0.569	1.258
16	52.2	23.2	0.575	1.437
18	56.0	23.3	0.578	1.617
20	59.9	23.6	0.585	1.797
24	68.0	24.5	0.608	2.156
28	75.4	24.6	0.610	2.516
32	82.5	24.4	0.605	2.875
36	90.0	24.6	0.610	3.234
40	96.5	23.9	0.596	3.594
0	9.5	9.5	0.236	0.0

Specimen No. 30.3				
p In.H_2O	P_{Total} lb	P_{cr} lb	ϵ_{cr}	$\bar{p}$
0	7.6	7.6	0.184	0.0
0.5	11.8	10.9	0.264	0.044
1	14.3	12.5	0.302	0.088
2	18.5	14.9	0.361	0.175
3	21.5	16.1	0.390	0.263
4	25.0	17.7	0.428	0.350
5	27.6	18.5	0.448	0.438
6	30.4	19.5	0.472	0.526
7	32.5	19.8	0.480	0.613
8	35.1	20.6	0.499	0.701
9	36.9	20.6	0.499	0.789
10	39.8	21.6	0.523	0.876
12	43.9	22.1	0.535	1.052
14	48.8	23.4	0.566	1.227
16	53.4	24.4	0.590	1.402
18	57.3	24.6	0.595	1.577
20	60.8	24.5	0.593	1.753
22	65.2	25.3	0.612	1.928
26	72.4	25.2	0.610	2.278
30	79.2	25.3	0.612	2.629
34	86.8	25.1	0.608	2.979
38	93.6	24.6	0.600	3.330
42	101.1	24.9	0.603	3.680

Specimen No. 30.4				
p In.H_2O	P_{Total} lb	P_{cr} lb	ϵ_{cr}	$\bar{p}$
0	8.2	8.2	0.190	0.0
0.5	11.4	10.5	0.244	0.042
1	14.5	12.7	0.294	0.084
2	18.3	14.7	0.341	0.168
3	21.9	16.5	0.383	0.252
4	25.1	17.8	0.413	0.336
5	27.7	18.6	0.431	0.420
6	30.3	19.4	0.450	0.504
7	32.7	20.0	0.464	0.588
8	35.5	21.0	0.487	0.672
9	38.0	21.7	0.503	0.756
10	40.9	22.7	0.526	0.840
12	45.2	23.4	0.542	1.008
14	49.9	24.5	0.568	1.175
16	53.3	24.3	0.563	1.343
18	57.4	24.7	0.573	1.511
20	61.4	25.1	0.582	1.679
22	65.3	25.4	0.589	1.847
26	73.2	26.0	0.603	2.183
30	80.3	25.8	0.598	2.519
34	87.7	26.0	0.603	2.855
38	95.1	26.1	0.605	3.190
42	102.1	26.0	0.603	3.526

Table 5. Continued

Specimen No. 30.5				
p $In.H_2O$	P_{Total} lb	P_{cr} lb	$\bar{\sigma}_{cr}$	$\bar{\beta}$
0	11.2	11.2	0.259	0.0
0.5	15.4	14.5	0.335	0.042
1	17.5	15.7	0.363	0.084
2	20.3	16.7	0.386	0.168
3	23.0	17.6	0.407	0.252
4	25.8	18.5	0.428	0.335
5	28.7	19.6	0.453	0.419
6	31.1	20.2	0.467	0.503
7	33.7	21.0	0.486	0.587
8	36.5	22.0	0.509	0.671
9	38.7	22.4	0.518	0.755
10	41.1	22.9	0.530	0.838
12	45.1	23.3	0.539	1.006
14	49.2	23.8	0.550	1.174
16	53.6	24.6	0.569	1.342
18	57.4	24.7	0.571	1.509
20	62.0	25.7	0.594	1.677
22	65.9	26.0	0.601	1.845
26	73.8	26.6	0.615	2.180
30	80.9	26.4	0.610	2.516
34	88.2	26.5	0.612	2.860
38	95.1	26.1	0.603	3.186
42	102.1	25.9	0.599	3.522

Specimen No. 30.6				
p $In.H_2O$	P_{Total} lb	P_{cr}	$\bar{\sigma}_{cr}$	$\bar{\beta}$
0	8.6	8.6	0.194	0.0
0.5	11.9	11.0	0.249	0.041
1	14.4	12.6	0.284	0.082
2	18.3	14.7	0.332	0.164
3	22.0	16.6	0.375	0.246
4	25.2	17.9	0.405	0.328
5	29.2	20.1	0.454	0.410
6	32.4	21.5	0.486	0.492
7	34.7	22.0	0.497	0.574
8	37.2	22.7	0.513	0.655
9	39.5	23.2	0.525	0.737
10	41.8	23.6	0.534	0.819
12	46.4	24.6	0.556	0.983
14	51.0	25.6	0.579	1.147
16	55.9	26.3	0.594	1.311
18	59.4	26.6	0.603	1.475
20	63.3	27.0	0.610	1.650
22	66.6	26.7	0.603	1.803
26	74.1	26.9	0.608	2.130
30	81.6	27.1	0.612	2.458
34	88.8	27.1	0.612	2.785
38	96.1	27.1	0.612	3.113
42	103.4	27.2	0.615	3.441
0.0	8.4	8.4	0.190	0.0

Specimen No. 30.7				
p $In.H_2O$	P_{Total} lb	P_{cr} lb	$\bar{\sigma}_{cr}$	$\bar{\beta}$
0	11.1	11.1	0.252	0.0
0.5	15.1	14.2	0.322	0.042
1	16.5	14.7	0.334	0.082
2	20.3	16.7	0.379	0.164
3	23.0	17.6	0.400	0.248
4	26.1	18.8	0.427	0.329
5	29.5	20.4	0.463	0.411
6	32.5	21.6	0.490	0.493
7	34.7	22.0	0.500	0.576
8	36.9	22.4	0.509	0.658
9	39.2	22.9	0.520	0.740
10	41.2	23.0	0.522	0.822
12	45.5	23.7	0.538	0.987
14	50.0	24.6	0.559	1.151
16	54.2	25.2	0.572	1.315
18	58.3	25.6	0.581	1.480
20	62.1	25.8	0.586	1.645
22	65.9	26.0	0.590	1.809
26	73.7	26.5	0.601	2.138
30	81.3	26.8	0.608	2.467
34	88.8	27.1	0.615	2.796
38	96.2	27.2	0.618	3.125
42	103.4	27.2	0.618	3.454
0	11.4	11.4	0.259	0.0

Specimen No. 30.8				
p $In.H_2O$	P_{Total} lb	P_{cr} lb	$\bar{\sigma}_{cr}$	$\bar{\beta}$
0	13.6	13.6	0.298	0.0
0.5	16.9	16.0	0.351	0.040
1	19.1	17.3	0.379	0.079
2	22.7	19.1	0.419	0.159
3	25.4	20.0	0.438	0.238
4	27.6	20.3	0.445	0.318
5	30.0	20.9	0.458	0.397
6	32.1	21.2	0.465	0.476
7	34.1	21.4	0.469	0.556
8	36.2	21.7	0.476	0.635
9	39.0	22.7	0.498	0.714
10	41.4	23.2	0.508	0.794
12	46.0	24.2	0.530	0.953
14	50.4	25.0	0.548	1.111
16	54.6	25.6	0.561	1.270
18	58.9	26.2	0.574	1.429
20	62.4	26.1	0.572	1.588
22	66.5	26.6	0.583	1.746
26	74.1	26.9	0.590	2.064
30	81.5	27.0	0.592	2.382
34	88.7	27.0	0.592	2.699
38	96.2	27.2	0.596	3.017
42	103.6	27.4	0.600	3.334
0.0	12.2	12.2	0.267	0.0

Table 5. Continued

Specimen No. 50.1				
p In. H_2O	P_{total} lb	P_{cr} lb	$\bar{\gamma}_{cr}$	$\bar{p}$
0	28.4	28.4	0.247	0
1	38.1	36.3	0.316	0.032
2	43.0	39.4	0.343	0.063
3	47.4	42.0	0.365	0.095
4	50.7	43.4	0.378	0.126
6	57.9	47.0	0.409	0.189
8	64.7	50.2	0.436	0.252
10	71.3	53.1	0.462	0.316
15	84.1	56.8	0.494	0.473
20	95.8	59.5	0.515	0.631
25	106.9	61.5	0.535	0.789
30	118.3	63.9	0.555	0.947
40	139.7	67.1	0.584	1.262
In. Hg				
4	167.6	69.2	0.601	1.711
5	193.5	70.5	0.613	2.139
6	217.0	69.5	0.605	2.566
7	240.6	68.5	0.596	2.994
8	266.5	69.8	0.606	3.422
9	291.1	69.9	0.607	3.850
0	29.3	0	0.255	0

Specimen No. 50.2				
p In. H_2O	P_{total} lb	P_{cr} lb	$\bar{\gamma}_{cr}$	$\bar{p}$
0	27.7	27.7	0.241	0
1	37.3	35.5	0.309	0.032
2	44.1	40.5	0.352	0.063
3	47.4	42.0	0.365	0.095
4	50.0	42.7	0.375	0.126
6	56.0	45.1	0.392	0.189
8	63.8	49.3	0.429	0.252
10	69.6	51.4	0.446	0.316
15	82.8	55.5	0.483	0.473
20	95.7	59.4	0.516	0.631
25	106.1	60.7	0.528	0.789
30	117.6	63.2	0.550	0.947
40	139.1	66.5	0.578	1.262
In. Hg				
4	167.5	69.1	0.601	1.711
5	193.2	70.2	0.610	2.139
6	217.5	70.0	0.609	2.566
7	240.8	68.7	0.598	2.994
8	267.1	70.4	0.611	3.422
9	291.3	70.0	0.609	3.850
0	27.5	27.5	0.239	0

Specimen No. 50.3				
p In. H_2O	P_{total} lb	P_{cr} lb	$\bar{\gamma}_{cr}$	$\bar{p}$
0	27.1	27.1	0.234	0
1	34.4	34.6	0.298	0.031
2	42.9	39.3	0.339	0.062
3	48.3	42.9	0.370	0.094
4	53.3	46.0	0.396	0.125
6	61.9	51.0	0.440	0.188
8	69.5	55.0	0.474	0.250
10	76.1	57.9	0.499	0.313
15	89.7	62.4	0.537	0.469
20	102.1	65.8	0.566	0.625
25	112.4	67.0	0.577	0.782
30	122.9	68.5	0.590	0.938
35	132.0	68.5	0.590	1.094
40	141.5	68.9	0.593	1.251
In. Hg				
4	167.2	68.8	0.592	1.695
5	192.6	69.6	0.600	2.118
6	216.6	69.1	0.595	2.542
7	242.1	70.0	0.603	2.966
8	266.0	69.3	0.597	3.389
9	290.6	69.3	0.597	3.813
0	27.6	27.6	0.238	0

Specimen No. 50.4				
p In. H_2O	P_{total} lb	P_{cr} lb	$\bar{\gamma}_{cr}$	$\bar{p}$
0	30.3	30.3	0.261	0
1	38.3	36.5	0.314	0.031
2	43.7	40.1	0.346	0.063
3	49.7	44.3	0.382	0.094
4	55.0	47.7	0.411	0.125
6	63.4	52.5	0.452	0.188
8	70.5	56.0	0.482	0.250
10	75.4	57.2	0.493	0.313
15	86.5	59.2	0.510	0.469
20	98.1	61.8	0.532	0.625
25	108.6	63.2	0.545	0.782
30	119.8	65.4	0.563	0.938
35	130.4	66.9	0.576	1.094
40	140.0	72.6	0.580	1.251
In. Hg				
3.5	154.1	68.2	0.588	1.483
4	167.8	69.5	0.599	1.695
4.5	180.3	69.6	0.600	1.906
5	192.8	69.8	0.601	2.118
6	217.4	69.9	0.602	2.542
7	242.8	70.7	0.609	2.966
8	267.3	70.6	0.608	3.389
9	291.8	70.5	0.607	3.813
0	31.1	31.1	0.268	0

Table 5. Continued

Specimen No. 50.5				
p In. H_2O	P_{total} lb	P_{cr} lb	$\bar{\sigma}_{cr}$	$\bar{p}$
0	32.3	32.3	0.282	0
1	45.7	43.9	0.384	0.032
2	48.7	45.1	0.394	0.063
3	52.9	47.5	0.415	0.095
4	57.3	50.0	0.437	0.127
6	66.2	55.3	0.482	0.190
8	72.8	58.3	0.508	0.254
10	78.1	59.9	0.521	0.317
15	89.8	62.5	0.546	0.475
20	100.2	63.9	0.556	0.634
25	110.6	65.2	0.570	0.792
30	120.7	66.3	0.579	0.951
35	130.8	67.3	0.588	1.109
40	140.3	67.7	0.591	1.268
In. Hg				
3.5	154.6	68.7	0.600	1.503
4.0	167.6	69.3	0.605	1.718
4.5	179.3	68.6	0.599	1.933
5	191.6	68.6	0.599	2.147
6	215.5	69.4	0.606	2.577
7	241.3	69.2	0.605	3.006
8	265.6	68.9	0.602	3.436
9	290.2	68.9	0.602	3.865
0	32.7	32.7	0.286	0

Specimen No. 50.6				
p In. H_2O	P_{total} lb	P_{cr} lb	$\bar{\sigma}_{cr}$	$\bar{p}$
0	40.0	40.0	0.343	0
1	47.5	45.7	0.392	0.031
2	51.6	48.0	0.412	0.062
3	55.7	50.3	0.431	0.093
4	58.8	51.5	0.442	0.124
6	64.5	53.6	0.460	0.187
8	70.6	56.1	0.482	0.249
10	74.9	56.7	0.487	0.311
15	88.0	60.7	0.521	0.467
20	99.3	63.0	0.541	0.623
25	111.0	65.6	0.563	0.778
30	122.6	68.2	0.586	0.934
35	132.9	69.4	0.595	1.090
40	142.8	70.2	0.603	1.246
In. Hg				
3.5	155.7	69.8	0.599	1.477
4.0	168.7	70.4	0.605	1.688
4.5	180.6	69.9	0.600	1.899
5	193.4	70.4	0.605	2.110
6	217.6	70.1	0.602	2.532
7	242.0	69.9	0.600	2.954
8	267.1	70.4	0.605	3.376
9	292.2	70.9	0.609	3.798
0	31.3	31.3	0.269	0

Specimen No. 50.7				
p In. H_2O	P_{total} lb	P_{cr} lb	$\bar{\sigma}_{cr}$	$\bar{p}$
0	34.0	34.0	0.298	0
1	44.9	43.1	0.377	0.032
2	49.3	45.7	0.400	0.064
3	52.9	47.5	0.415	0.095
4	56.3	49.0	0.429	0.127
6	62.1	51.2	0.448	0.190
8	68.6	54.1	0.474	0.254
10	74.1	55.9	0.489	0.317
15	86.6	59.3	0.518	0.475
20	97.3	61.0	0.533	0.634
25	107.7	62.3	0.544	0.792
30	118.2	63.9	0.558	0.951
35	128.7	65.3	0.570	1.109
40	138.8	66.2	0.579	1.268
In. Hg				
3.5	153.7	67.8	0.593	1.503
4	166.1	67.8	0.593	1.718
4.5	179.9	69.2	0.605	1.933
5	191.9	68.9	0.603	2.147
6	217.3	69.8	0.610	2.577
7	242.8	69.9	0.611	3.006
8	266.3	69.6	0.609	3.436
9	291.2	69.9	0.611	3.865
0	29.9	29.9	0.262	0

Specimen No. 50.8				
p In. H_2O	P_{total} lb	P_{cr} lb	$\bar{\sigma}_{cr}$	$\bar{p}$
0	40.0	40.0	0.340	0
1	48.0	46.2	0.393	0.031
2	52.2	48.6	0.414	0.062
3	54.3	48.9	0.416	0.093
4	56.5	49.2	0.419	0.124
6	60.7	49.8	0.423	0.186
8	65.6	51.1	0.435	0.249
10	71.5	53.3	0.453	0.309
15	86.1	58.8	0.500	0.465
20	98.7	62.4	0.530	0.618
25	110.7	65.3	0.555	0.772
30	121.3	67.4	0.573	0.927
35	132.0	68.2	0.581	1.081
40	141.3	68.7	0.585	1.236
In. Hg				
3.5	156.1	70.2	0.597	1.453
4	168.3	70.0	0.595	1.671
4.5	182.3	71.6	0.609	1.884
5	195.2	72.2	0.614	2.098
6	217.7	70.2	0.597	2.511
7	243.0	70.9	0.603	2.939
8	268.0	71.2	0.606	3.353
9	292.4	71.1	0.605	3.767
0	35.1	35.1	0.298	0

Table 5. Continued

Specimen No. 79.1				
p In. H_2O	P_{total} lb	P_{cr} lb	$\bar{w}_{cr}$	$\bar{p}$
0	95	95	0.300	0
2	106	102	0.322	0.023
5	119	110	0.348	0.057
10	140	122	0.385	0.115
15	159	132	0.417	0.172
20	176	140	0.442	0.230
30	204	150	0.474	0.344
40	230	157	0.496	0.459
In. Hg				
4	266	168	0.530	0.622
5	295	172	0.543	0.778
6	322	174	0.550	0.934
8	377	180	0.568	1.245
10	431	185	0.584	1.556
12	487	192	0.606	1.867
14	536	192	0.606	2.178
16	582	188	0.594	2.490
18	627	186	0.588	2.801
20	673	181	0.571	3.112
22	720	179	0.565	3.423
0	95	95	0.300	0

Specimen No. 79.2				
p In. H_2O	P_{total} lb	P_{cr} lb	$\bar{w}_{cr}$	$\bar{p}$
0	84	84	0.279	0
2	106	102	0.339	0.024
5	115	106	0.352	0.060
10	140	122	0.405	0.120
15	159	132	0.439	0.181
20	177	141	0.468	0.241
30	205	151	0.501	0.362
40	230	157	0.521	0.482
In. Hg				
4	263	165	0.548	0.653
5	294	171	0.568	0.816
6	320	172	0.571	0.980
8	374	177	0.588	1.306
10	424	178	0.591	1.633
12	476	181	0.601	1.959
14	525	181	0.601	2.286
16	576	182	0.604	2.612
18	619	176	0.584	2.939
20	664	172	0.571	3.265
22	705	164	0.545	3.592
	86	86	0.286	0

Specimen 79.3-1				
p In. H_2O	P_{total} lb	P_{cr} lb	$\bar{w}_{cr}$	$\bar{p}$
0	86	86	0.270	0
2	104	100	0.314	0.029
5	125	116	0.364	0.057
10	147	129	0.405	0.114
15	164	137	0.430	0.171
20	181	145	0.456	0.228
30	211	157	0.494	0.342
40	238	165	0.519	0.456
In. Hg				
4	270	172	0.540	0.618
5	297	174	0.547	0.773
6	325	177	0.556	0.928
8	381	184	0.579	1.237
10	432	186	0.585	1.546
12	485	190	0.597	1.855
14	538	194	0.610	2.165
16	586	192	0.604	2.474
18	637	194	0.610	2.783
20	684	192	0.604	3.092
22	728	187	0.588	3.401

Specimen No. 79.3-2				
p In. H_2O	P_{total} lb	P_{cr} lb	$\bar{w}_{cr}$	$\bar{p}$
0	116	116	0.364	0
2	134	130	0.407	0.023
5	147	138	0.433	0.057
10	166	148	0.464	0.116
15	179	152	0.476	0.170
20	193	157	0.492	0.227
30	219	165	0.518	0.340
40	241	168	0.527	0.454
In. Hg				
4	273	178	0.559	0.615
5	303	180	0.564	0.769
6	328	180	0.564	0.923
8	382	188	0.590	1.231
10	434	188	0.590	1.538
12	487	192	0.602	1.846
14	538	194	0.608	2.154
16	586	192	0.602	2.461
18	633	192	0.602	2.769
20	680	188	0.590	3.077
22	722	181	0.568	3.384
0	94	94	0.295	0

Table 5. Continued

Specimen No. 79.4				
p In. H_2O	P_{total} lb	P_{cr} lb	$\bar{\sigma}_{cr}$	$\bar{p}$
0	111	111	0.370	0
2	120	116	0.386	0.024
5	131	122	0.406	0.060
10	147	129	0.430	0.121
15	162	135	0.450	0.181
20	176	140	0.466	0.241
30	202	148	0.493	0.362
40	225	152	0.506	0.482
In. Hg				
4	257	159	0.530	0.654
5	287	164	0.546	0.817
6	313	165	0.550	0.981
8	370	173	0.576	1.308
10	422	176	0.586	1.635
12	475	180	0.600	1.962
14	526	182	0.606	2.289
16	577	183	0.610	2.615
18	623	180	0.600	2.943
20	663	171	0.570	3.269
0	86	86	0.286	0

Specimen No. 79.5				
p In. H_2O	P_{total} lb	P_{cr} lb	$\bar{\sigma}_{cr}$	$\bar{p}$
0	104	104	0.346	0
2	113	109	0.363	0.024
5	122	113	0.376	0.060
10	138	120	0.400	0.121
15	153	126	0.420	0.181
20	168	132	0.440	0.241
30	195	141	0.470	0.362
40	220	147	0.490	0.482
In. Hg				
4	254	156	0.520	0.654
5	283	160	0.533	0.817
6	312	164	0.546	0.981
8	367	170	0.566	1.308
10	420	174	0.580	1.635
12	473	178	0.593	1.962
14	526	182	0.606	2.289
16	575	181	0.603	2.615
18	617	174	0.580	2.943
0	83	83	0.276	0

Specimen No. 79.6				
p In. H_2O	P_{total} lb	P_{cr} lb	$\bar{\sigma}_{cr}$	$\bar{p}$
0	116	116	0.373	0
2	127	123	0.396	0.023
5	140	131	0.421	0.058
10	157	139	0.447	0.116
15	173	146	0.470	0.175
20	188	152	0.489	0.233
30	216	162	0.521	0.350
40	239	166	0.534	0.466
In. Hg				
4	267	169	0.544	0.632
5	293	170	0.547	0.790
6	321	173	0.556	0.948
8	375	178	0.573	1.264
10	429	183	0.589	1.580
12	479	184	0.592	1.895
14	530	186	0.598	2.211
16	583	189	0.608	2.527
18	630	187	0.601	2.843
0	103	103	0.331	0

Specimen No. 79.7				
p In. H_2O	P_{total} lb	P_{cr} lb	$\bar{\sigma}_{cr}$	$\bar{p}$
0	110	110	0.354	0
2	121	117	0.376	0.023
5	134	125	0.402	0.058
10	151	135	0.428	0.116
15	168	141	0.454	0.175
20	185	149	0.479	0.233
30	211	157	0.505	0.350
40	234	161	0.518	0.466
In. Hg				
4	263	165	0.531	0.632
5	289	166	0.534	0.790
6	317	169	0.544	0.948
8	371	174	0.560	1.264
10	426	180	0.579	1.580
12	480	185	0.595	1.895
14	531	187	0.602	2.211
16	583	189	0.608	2.527
0	107	107	0.344	0

Table 5. Continued

Specimen 100.1				
p In. Hg	P_{total} lb	P_{cr} lb	$\bar{\varepsilon}_{cr}$	$\bar{\rho}$
0.0	144	144	0.311	0.0
0.5	194	182	0.393	0.053
1	234	209	0.451	0.106
2	283	234	0.505	0.212
3	320	246	0.513	0.318
4	356	258	0.556	0.424
6	415	267	0.576	0.636
8	471	275	0.593	0.847
10	525	279	0.602	1.059
12	576	281	0.606	1.271
14	624	280	0.604	1.483
16	674	280	0.604	1.695
20	773	281	0.606	2.119
24	870	280	0.604	2.542
0.0	132	132	0.285	0.0

Specimen 100.2				
p In. Hg	P_{total} lb	P_{cr} lb	$\bar{\varepsilon}_{cr}$	$\bar{\rho}$
0.0	141	141	0.311	0.0
0.5	185	173	0.382	0.054
1	215	190	0.419	0.108
2	268	219	0.483	0.217
3	312	238	0.524	0.325
4	348	250	0.551	0.433
6	410	262	0.578	0.650
8	464	268	0.591	0.866
10	515	269	0.593	1.083
12	566	271	0.597	1.299
14	616	272	0.599	1.516
16	667	273	0.602	1.732
18	718	275	0.606	1.949
20	767	275	0.606	2.165
22	816	275	0.606	2.382
24	865	275	0.606	2.598
0.0	135	135	0.298	0.0

Specimen No. 100.3-1				
p In. Hg	P_{total} lb	P_{cr} lb	$\bar{\varepsilon}_{cr}$	$\bar{\rho}$
0.0	129	129	0.286	0.0
0.5	195	183	0.406	0.055
1	216	191	0.423	0.109
2	269	220	0.488	0.218
3	310	236	0.523	0.327
4	339	241	0.534	0.435
6	404	256	0.567	0.651
8	459	263	0.583	0.871
10	512	266	0.589	1.089
12	565	270	0.598	1.306
14	616	272	0.603	1.524
16	668	274	0.607	1.742
18	718	275	0.609	1.959
20	766	274	0.607	2.177
22	813	272	0.603	2.395
24	837	267	0.592	2.613

Specimen No. 100.3-2				
p In. Hg	P_{total} lb	P_{cr} lb	$\bar{\varepsilon}_{cr}$	$\bar{\rho}$
0.0	200	200	0.447	0.0
0.5	226	214	0.478	0.055
1	247	224	0.496	0.110
2	281	232	0.518	0.220
3	317	243	0.542	0.329
4	348	250	0.558	0.439
6	404	256	0.571	0.657
8	458	262	0.585	0.878
10	509	263	0.588	1.098
12	560	265	0.592	1.317
14	611	267	0.596	1.537
16	662	268	0.598	1.756
18	710	267	0.596	1.976
20	761	269	0.601	2.196
22	810	269	0.601	2.415
24	859	269	0.601	2.635
0.0	183	183	0.409	0.0

Table 5. Concluded

Specimen No. 100.4				
p In. Hg	P_{total} lb	P_{cr} lb	$\bar{\varepsilon}_{cr}$	p
0.0	137	137	0.301	0.0
0.5	183	171	0.376	0.054
1	216	191	0.419	0.108
2	267	218	0.479	0.216
3	309	235	0.516	0.323
4	346	248	0.545	0.431
6	407	259	0.569	0.647
8	463	267	0.586	0.863
10	521	275	0.604	1.078
12	571	276	0.606	1.294
14	622	278	0.610	1.509
16	670	276	0.606	1.725
18	720	277	0.608	1.941
20	769	277	0.608	2.156
22	816	275	0.604	2.372
24	864	274	0.601	2.588
0.0	136	136	0.299	0.0

Specimen No. 100.5				
p In. Hg	P_{total} lb	P_{cr} lb	$\bar{\varepsilon}_{cr}$	p
0.0	178	178	0.396	0.0
0.5	206	194	0.431	0.055
1	228	203	0.451	0.109
2	270	221	0.491	0.219
3	309	235	0.523	0.328
4	347	249	0.554	0.437
6	405	257	0.571	0.656
8	460	264	0.587	0.874
10	512	266	0.592	1.093
12	563	268	0.596	1.312
14	613	269	0.598	1.530
16	663	269	0.598	1.749
18	714	271	0.603	1.968
20	765	273	0.607	2.186
22	813	272	0.605	2.405
24	861	271	0.603	2.624
0.0	149	149	0.332	0.0

Specimen No. 100.6				
p In. Hg	P_{total} lb	P_{cr} lb	$\bar{\varepsilon}_{cr}$	p
0.0	159	159	0.365	0.0
0.5	201	189	0.434	0.056
1	235	210	0.482	0.113
2	272	223	0.512	0.226
3	304	230	0.528	0.338
4	339	241	0.554	0.451
6	399	251	0.576	0.677
8	455	259	0.595	0.902
10	506	260	0.597	1.128
12	555	260	0.597	1.353
14	605	261	0.599	1.579
16	656	262	0.602	1.805
18	705	262	0.602	2.030
20	755	263	0.604	2.256
24	851	261	0.599	2.707
0.0	127	127	0.292	0.0

Specimen No. 100.7				
p In. Hg	P_{total} lb	P_{cr} lb	$\bar{\varepsilon}_{cr}$	p
0.0	201	201	0.451	0.0
0.5	228	216	0.485	0.055
1	247	222	0.499	0.110
2	286	237	0.532	0.220
3	319	245	0.550	0.331
4	350	252	0.566	0.441
6	406	258	0.579	0.661
8	459	263	0.590	0.882
10	511	265	0.595	1.102
12	562	267	0.599	1.323
14	612	268	0.602	1.543
16	661	267	0.599	1.764
18	712	269	0.604	1.984
20	762	270	0.606	2.205
22	811	270	0.606	2.425
24	857	267	0.599	2.646
0.0	185	185	0.415	0.0

Table 5a. Physical Characteristics of Test Specimens

Specimen Number	t(inch)	E(ksi)	Remarks
20.1	0.002	759	Cerrobend
20.2		700	Cerrobend
20.3		737	Cerrobend
20.4		732	Cerrolow
20.5		745	Cerrolow
20.6	0.002	734	Cerrolow
30.1	0.003	711	Cerrobend
30.2		714	Cerrobend
30.3		732	Cerrobend
30.4		764	Cerrobend
30.5		765	Cerrolow
30.6		783	Cerrolow
30.7		780	Cerrolow
30.8	0.003	808	Cerrolow
50.1	0.005	732	Cerrobend
50.2		732	Cerrobend
50.3		739	Cerrobend
50.4		739	Cerrobend
50.5		729	Cerrolow
50.6		742	Cerrolow
50.7		729	Cerrolow
50.8	0.005	748	Cerrolow

Table 5a. Concluded

Specimen Number	t(inch)	E(ksi)	Remarks
79.1	0.0079	810	Cerrobend
79.2		769	Cerrobend
79.3-1		814	Cerrobend
79.3-2		816	Cerrolow
79.4		766	Cerrolow
79.5		765	Cerrolow
79.6		794	Cerrolow
79.7	0.0079	794	Cerrolow
100.1	0.010	739	Cerrobend
100.2		723	Cerrobend
100.3-1		719	Cerrobend
100.3-2		713	Cerrolow
100.4		726	Cerrolow
100.5		716	Cerrolow
100.6		694	Cerrolow
100.7	0.010	710	Cerrolow

Table 6. Critical End Shortening of Pressurized Mylar Cylinders under Axial Compression.

Specimen No. 20.4				
$\bar{p}$	ΔL_{cr} 10^{-3} in.	$\bar{\delta}_{cr}$	$\bar{\delta}_{cr} - \bar{w}_{cr}$	$\tilde{p}$
0.0	1.05	0.26	0.01	0.0
0.040	1.30	0.32	0.01	0.003
0.079	1.40	0.35	0.02	0.006
0.118	1.50	0.38	0.03	0.009
0.158	1.60	0.40	0.02	0.013
0.197	1.70	0.42	0.02	0.016
0.296	1.90	0.48	0.05	0.023
0.394	2.00	0.50	0.05	0.031
0.493	2.15	0.54	0.06	0.039
0.592	2.20	0.55	0.07	0.047
0.691	2.25	0.56	0.06	0.055
0.789	2.40	0.60	0.09	0.063
0.986	2.50	0.65	0.11	0.078
1.184	2.70	0.68	0.14	0.094
1.381	3.05	0.76	0.16	0.110
1.578	3.15	0.79	0.21	0.125
1.775	3.30	0.82	0.24	0.141
1.973	3.60	0.90	0.31	0.157
2.367	4.20	1.05	0.45	0.188
2.762	4.70	1.16	0.58	0.219
3.156	5.30	1.32	0.72	0.250
3.551	6.10	1.52	0.92	0.282
3.945	6.70	1.68	1.08	0.313

Specimen No. 20.5				
$\bar{p}$	ΔL_{cr} 10^{-3} in.	$\bar{\delta}_{cr}$	$\bar{\delta}_{cr} - \bar{w}_{cr}$	$\tilde{p}$
0.0	0.85	0.21	0.0	0.0
0.039	1.20	0.30	0.04	0.003
0.077	1.35	0.34	0.01	0.006
0.116	1.40	0.35	0.0	0.009
0.155	1.55	0.39	0.01	0.012
0.194	1.65	0.41	0.0	0.015
0.291	1.90	0.47	0.01	0.023
0.388	2.00	0.50	0.02	0.031
0.485	2.10	0.52	0.03	0.039
0.582	2.25	0.56	0.04	0.046
0.679	2.30	0.58	0.06	0.054
0.775	2.40	0.60	0.06	0.062
0.969	2.50	0.62	0.07	0.077
1.163	2.75	0.69	0.12	0.092
1.357	2.85	0.71	0.13	0.108
1.551	3.00	0.75	0.16	0.123
1.744	3.25	0.81	0.23	0.138
1.938	3.45	0.86	0.28	0.154
2.326	3.90	0.98	0.38	0.185
2.714	4.45	1.11	0.52	0.215
3.101	5.10	1.28	0.69	0.246
3.489	5.75	1.44	0.84	0.277
3.876	6.55	1.64	1.04	0.308

Specimen No. 20.6				
$\bar{p}$	ΔL_{cr} 10^{-3} in.	$\bar{\delta}_{cr}$	$\bar{\delta}_{cr} - \bar{w}_{cr}$	$\tilde{p}$
0.0	0.85	0.21	0.01	0.0
0.039	1.10	0.27	0.03	0.003
0.078	1.15	0.29	0.01	0.006
0.118	1.15	0.29	0.01	0.009
0.158	1.20	0.30	0.0	0.013
0.197	1.35	0.34	0.01	0.016
0.295	1.60	0.40	0.03	0.023
0.394	1.75	0.44	0.04	0.031
0.492	1.95	0.49	0.06	0.039
0.590	2.00	0.50	0.04	0.047
0.689	2.45	0.61	0.14	0.055
0.787	2.60	0.65	0.17	0.062
0.984	2.75	0.69	0.17	0.078
1.180	2.80	0.70	0.16	0.094
1.377	2.85	0.71	0.16	0.109
1.574	3.20	0.80	0.22	0.125
1.771	3.40	0.85	0.25	0.141
1.967	3.60	0.90	0.30	0.156
2.161	4.05	1.01	0.40	0.187
2.754	4.65	1.16	0.54	0.219
3.148	5.25	1.31	0.70	0.250
3.541	5.85	1.46	0.85	0.281
3.936	6.40	1.60	0.99	0.312

Table 6. Continued

Specimen No. 30.5				
$\bar{p}$	ΔL_{cr} X10^{-3}In.	$\bar{\varepsilon}_{cr}$	$\bar{\varepsilon}_{cr} - \bar{e}_{cr}$	$\bar{\bar{p}}$
0.0	1.80	0.30	0.04	0.0
0.042	2.00	0.33	0.0	0.004
0.84	2.20	0.37	0.01	0.008
0.168	2.35	0.39	0.0	0.015
0.252	2.50	0.42	0.01	0.023
0.335	2.90	0.48	0.05	0.030
0.419	3.10	0.52	0.07	0.038
0.503	3.25	0.54	0.07	0.046
0.587	3.40	0.57	0.08	0.053
0.671	3.60	0.60	0.09	0.061
0.755	3.70	0.62	0.10	0.069
0.838	3.85	0.64	0.11	0.076
1.006	4.15	0.69	0.15	0.091
1.174	4.30	0.72	0.17	0.107
1.342	4.70	0.78	0.21	0.122
1.509	4.95	0.82	0.25	0.137
1.677	5.15	0.86	0.27	0.152
1.845	5.35	0.89	0.29	0.168
2.180	6.25	1.04	0.42	0.198
2.516	7.15	1.19	0.58	0.229
2.850	8.05	1.34	0.73	0.260
3.186	9.15	1.52	0.92	0.290
3.522	10.05	1.68	1.08	0.320

Specimen No. 30.6				
$\bar{p}$	ΔL_{cr} X10^{-3}In.	$\bar{\varepsilon}_{cr}$	$\bar{\varepsilon}_{cr} - \bar{e}_{cr}$	$\bar{\bar{p}}$
0.0	1.40	0.23	0.04	0.0
0.041	1.80	0.30	0.05	0.004
0.082	1.95	0.32	0.04	0.007
0.164	2.30	0.38	0.05	0.015
0.246	2.60	0.43	0.05	0.022
0.328	2.80	0.47	0.07	0.030
0.410	3.00	0.50	0.05	0.037
0.492	3.25	0.54	0.05	0.045
0.574	3.40	0.57	0.07	0.052
0.655	3.55	0.59	0.08	0.060
0.737	3.65	0.61	0.09	0.067
0.819	3.85	0.64	0.11	0.074
0.983	4.20	0.70	0.14	0.089
1.147	4.45	0.74	0.16	0.104
1.311	4.80	0.80	0.21	0.119
1.475	5.10	0.85	0.25	0.134
1.639	5.30	0.88	0.27	0.150
1.803	5.65	0.94	0.34	0.164
2.130	6.25	1.04	0.41	0.194
2.458	6.95	1.16	0.55	0.223
2.785	7.85	1.31	0.70	0.253
3.113	8.75	1.46	0.85	0.283
3.441	9.80	1.63	1.01	0.322

Specimen No. 30.7				
$\bar{p}$	ΔL_{cr} X10^{-3}In.	$\bar{\varepsilon}_{cr}$	$\bar{\varepsilon}_{cr} - \bar{e}_{cr}$	$\bar{\bar{p}}$
0.0	1.80	0.30	0.05	0.0
0.042	2.15	0.36	0.04	0.004
0.082	2.20	0.37	0.04	0.007
0.164	2.65	0.44	0.06	0.015
0.248	2.95	0.49	0.09	0.023
0.329	3.15	0.52	0.09	0.030
0.411	3.40	0.57	0.11	0.037
0.493	3.55	0.59	0.10	0.045
0.576	3.63	0.61	0.11	0.052
0.658	3.75	0.62	0.11	0.060
0.740	3.81	0.63	0.11	0.067
0.822	3.95	0.66	0.14	0.075
0.987	4.40	0.73	0.19	0.090
1.151	4.70	0.78	0.22	0.105
1.316	4.80	0.80	0.23	0.120
1.480	5.05	0.84	0.26	0.135
1.645	5.35	0.89	0.30	0.150
1.809	5.55	0.92	0.33	0.164
2.138	6.35	1.06	0.46	0.194
2.467	6.75	1.13	0.52	0.224
2.796	7.70	1.28	0.66	0.254
3.125	8.70	1.45	0.83	0.284
3.454	9.60	1.60	0.98	0.314

Table 6. Continued

Specimen No. 50.4				
$\bar{p}$	ΔL_{cr} 10^{-3} in.	$\bar{\delta}_{cr}$	$\bar{\delta}_{cr}-\bar{e}_{cr}$	$\bar{\bar{p}}$
0	2.75	0.28	0.02	0
0.031	3.25	0.32	0.01	0.003
0.062	3.45	0.34	0	0.007
0.094	3.75	0.38	0	0.010
0.125	4.10	0.41	0	0.013
0.188	4.55	0.46	0.01	0.020
0.250	4.95	0.50	0.02	0.027
0.313	5.15	0.52	0.03	0.034
0.469	5.80	0.58	0.07	0.051
0.625	6.30	0.63	0.10	0.067
0.782	6.85	0.68	0.14	0.084
0.938	7.25	0.72	0.15	0.101
1.094	7.60	0.76	0.18	0.118
1.251	8.20	0.82	0.24	0.135
1.483	8.75	0.88	0.29	0.160
1.695	9.60	0.96	0.36	0.183
1.906	10.30	1.03	0.43	0.205
2.118	11.05	1.10	0.50	0.228
2.542	13.35	1.34	0.74	0.274
2.966	16.50	1.65	1.04	0.320
3.389	19.35	1.94	1.33	0.365
3.813	22.60	2.26	1.65	0.411

Specimen No. 50.5				
$\bar{p}$	ΔL_{cr} 10^{-3} in.	$\bar{\delta}_{cr}$	$\bar{\delta}_{cr}-\bar{e}_{cr}$	$\bar{\bar{p}}$
0	3.00	0.30	0.02	0
0.032	3.95	0.39	0.01	0.003
0.063	4.00	0.40	0.01	0.007
0.095	4.15	0.42	0	0.010
0.127	4.40	0.44	0	0.014
0.190	4.95	0.50	0.02	0.020
0.254	5.30	0.53	0.02	0.027
0.317	5.40	0.54	0.02	0.034
0.475	5.70	0.57	0.02	0.051
0.634	5.95	0.60	0.04	0.068
0.792	6.25	0.62	0.05	0.085
0.951	6.65	0.66	0.08	0.102
1.109	7.15	0.72	0.13	0.120
1.268	7.65	0.76	0.17	0.137
1.503	8.60	0.86	0.26	0.162
1.718	9.75	0.98	0.38	0.185
1.933	10.75	1.08	0.48	0.208
2.147	11.75	1.18	0.58	0.231
2.577	13.75	1.38	0.77	0.278
3.006	17.05	1.70	1.10	0.324
3.436	20.30	2.03	1.43	0.370
3.865	23.60	2.36	1.76	0.417

Specimen No. 50.6				
$\bar{p}$	ΔL_{cr} 10^{-3} in.	$\bar{\delta}_{cr}$	$\bar{\delta}_{cr}-\bar{e}_{cr}$	$\bar{\bar{p}}$
0	3.45	0.34	0	0
0.031	4.00	0.40	0.01	0.003
0.062	4.15	0.42	0.01	0.007
0.093	4.35	0.44	0.01	0.010
0.124	4.50	0.45	0.01	0.013
0.187	4.70	0.47	0.01	0.020
0.249	4.95	0.49	0.01	0.027
0.311	5.05	0.51	0.02	0.034
0.467	5.50	0.55	0.03	0.050
0.623	5.75	0.58	0.04	0.067
0.778	6.20	0.62	0.06	0.084
0.934	6.80	0.68	0.09	0.101
1.090	7.30	0.73	0.13	0.117
1.246	8.05	0.80	0.20	0.134
1.477	8.70	0.87	0.27	0.159
1.688	9.15	0.92	0.32	0.182
1.899	9.90	0.99	0.39	0.205
2.110	10.90	1.09	0.48	0.227
2.532	13.25	1.32	0.72	0.273
2.954	16.25	1.62	1.01	0.318
3.376	19.35	1.94	1.34	0.364
3.798	22.70	2.27	1.66	0.409

Table 6. Continued

Specimen 79.3-1				
$\bar{p}$	ΔL_{cr} 10^{-3} In.	$\bar{\delta}_{cr}$	$\bar{\delta}_{cr}-\bar{\sigma}_{cr}$	$\widetilde{p}$
0	5.2	0.33	0.06	0
0.029	5.8	0.37	0.06	0.004
0.057	6.7	0.42	0.06	0.007
0.114	7.3	0.46	0.06	0.014
0.171	7.6	0.48	0.05	0.021
0.228	7.9	0.50	0.04	0.029
0.342	9.0	0.57	0.08	0.043
0.456	9.9	0.63	0.11	0.057
0.618	10.4	0.66	0.12	0.078
0.773	11.3	0.73	0.18	0.097
0.928	11.9	0.75	0.19	0.116
1.237	13.2	0.84	0.26	0.155
1.546	15.3	0.97	0.39	0.194
1.855	18.3	1.16	0.56	0.233
2.165	20.3	1.29	0.68	0.272
2.474	24.7	1.56	0.96	0.310
2.783	29.4	1.86	1.25	0.349
3.092	33.4	2.24	1.64	0.388
3.401	41.1	2.60	2.01	0.427

Specimen 79.3-2				
$\bar{p}$	$\perp_{cr}$ 10^{-3} In.	δ_{cr}	$\bar{\delta}_{cr}-\bar{\sigma}_{cr}$	$\widetilde{p}$
0	6.2	0.39	0.03	0
0.023	6.7	0.42	0.01	0.003
0.057	7.2	0.46	0.03	0.007
0.114	7.6	0.48	0.02	0.014
0.170	7.9	0.50	0.02	0.021
0.227	8.2	0.52	0.03	0.028
0.340	8.5	0.54	0.02	0.043
0.454	8.8	0.56	0.03	0.057
0.615	9.5	0.60	0.05	0.077
0.769	10.8	0.68	0.12	0.096
0.923	11.4	0.72	0.16	0.116
1.231	13.4	0.85	0.27	0.154
1.538	15.8	1.00	0.41	0.193
1.846	17.7	1.12	0.52	0.232
2.154	21.0	1.33	0.72	0.270
2.461	25.2	1.60	1.00	0.309
2.769	30.1	1.90	1.30	0.347
3.077	34.9	2.21	1.62	0.386
3.384	40.4	2.56	1.99	0.425

Specimen No. 79.4				
$\bar{p}$	ΔL_{cr} 10^{-3} In.	$\bar{\delta}_{cr}$	$\bar{\delta}_{cr}-\bar{\sigma}_{cr}$	$\widetilde{p}$
0	5.9	0.37	0	0
0.024	6.3	0.40	0.01	0.003
0.060	6.7	0.42	0.01	0.008
0.121	7.0	0.44	0.01	0.015
0.181	7.4	0.47	0.02	0.023
0.241	7.9	0.50	0.03	0.030
0.362	8.7	0.55	0.06	0.045
0.482	9.2	0.58	0.07	0.060
0.654	10.2	0.65	0.12	0.082
0.817	11.3	0.72	0.17	0.103
0.981	12.4	0.78	0.23	0.123
1.308	13.7	0.87	0.29	0.164
1.635	15.6	0.99	0.40	0.205
1.962	19.3	1.22	0.62	0.246
2.289	23.5	1.49	0.88	0.287
2.615	28.2	1.78	1.17	0.328
2.943	33.0	2.12	1.52	0.369
3.269	36.8	2.46	1.89	0.410

Table 6. Concluded

Specimen No. 100.1-2				
$\bar{p}$	ΔL_{cr} 10^{-3} in.	$\bar{\delta}_{cr}$	$\bar{\delta}_{cr} - \bar{e}_{cr}$	$\tilde{p}$
0.0	8.0	0.44	0.0	0.0
0.055	9.5	0.48	0.0	0.007
0.110	9.9	0.50	0.0	0.015
0.220	10.8	0.54	0.02	0.030
0.329	11.2	0.56	0.02	0.045
0.439	11.8	0.59	0.03	0.060
0.657	12.8	0.64	0.07	0.089
0.878	14.6	0.73	0.15	0.119
1.098	16.6	0.83	0.24	0.149
1.317	18.8	0.94	0.35	0.179
1.537	21.4	1.07	0.47	0.209
1.756	23.4	1.17	0.57	0.238
1.976	25.8	1.29	0.69	0.268
2.196	30.4	1.52	0.94	0.298
2.415	33.6	1.68	1.08	0.328
2.635	38.6	1.93	1.33	0.358

Specimen No. 100.4				
$\bar{p}$	ΔL_{cr} 10^{-3} in.	$\bar{\delta}_{cr}$	$\bar{\delta}_{cr} - \bar{e}_{cr}$	$\tilde{p}$
0.0	6.4	0.32	0.02	0.0
0.054	8.4	0.42	0.04	0.007
0.108	9.2	0.46	0.04	0.015
0.216	10.4	0.52	0.04	0.029
0.323	11.4	0.57	0.05	0.044
0.431	12.2	0.61	0.07	0.058
0.647	13.8	0.69	0.12	0.088
0.863	15.6	0.78	0.19	0.117
1.078	16.8	0.84	0.24	0.146
1.294	19.2	0.96	0.34	0.176
1.509	21.4	1.07	0.46	0.205
1.725	23.4	1.17	0.56	0.234
1.941	[illegible]	[illegible]	0.67	0.263
2.156	29.8	1.49	0.88	0.293
2.372	33.8	1.69	1.09	0.322
2.588	38.4	1.92	1.32	0.351

Specimen No. 100.5				
$\bar{p}$	ΔL_{cr} 10^{-3} in.	$\bar{\delta}_{cr}$	$\bar{\delta}_{cr} - \bar{e}_{cr}$	$\tilde{p}$
0.0	8.2	0.41	0.01	0.0
0.055	8.8	0.44	0.01	0.007
0.109	9.6	0.48	0.03	0.015
0.219	10.6	0.54	0.05	0.030
0.328	11.6	0.58	0.06	0.045
0.437	12.6	0.63	0.08	0.059
0.656	14.0	0.70	0.13	0.089
0.874	15.8	0.79	0.20	0.119
1.093	17.4	0.87	0.28	0.148
1.312	19.2	0.96	0.36	0.178
1.530	21.2	1.06	0.46	0.208
1.749	23.2	1.16	0.56	0.237
1.968	26.2	1.31	0.71	0.267
2.186	29.8	1.49	0.88	0.297
2.405	35.4	1.77	1.17	0.326
2.624	40.2	2.01	[illegible]	[illegible]

Table 7. Experimental Data for Minimum Stress Coefficient for Pressurized Mylar Cylinders in Axial Compression

Specimen No. 20.4			Specimen No. 20.5			Specimen No. 20.6		
$\bar{p}$	P_{min} lb	$\bar{\sigma}_{min}$	$\bar{p}$	P_{min} lb	$\bar{\sigma}_{min}$	$\bar{p}$	P_{min} lb	$\bar{\sigma}_{min}$
0.0	2.3	0.125	0.0	2.2	0.118	0.0	2.4	0.130
0.040	3.2	0.174	0.039	3.2	0.171	0.039	3.3	0.179
0.079	3.7	0.201	0.077	3.9	0.208	0.078	4.0	0.218
0.118	4.1	0.223	0.116	4.3	0.230	0.118	4.4	0.239
0.158	4.8	0.261	0.155	4.8	0.257	0.158	4.9	0.266
0.197	5.3	0.288	0.194	5.5	0.294	0.197	5.5	0.299
0.296	5.9	0.321	0.291	6.2	0.332	0.295	6.2	0.337
0.394	6.3	0.343	0.388	6.7	0.358	0.394	6.7	0.364
0.493	6.8	0.370	0.485	7.3	0.390	0.492	7.2	0.391
0.592	7.4	0.403	0.582	7.6	0.406	0.590	7.5	0.407
0.691	7.8	0.425	0.679	7.9	0.423	0.689	7.9	0.429
0.789	8.1	0.441	0.775	8.1	0.450	0.787	8.1	0.440
0.986	8.7	0.473	0.969	8.8	0.471	0.984	8.8	0.478
1.184	9.4	0.511	1.163	9.4	0.504	1.180	9.4	0.511
1.381	9.7	0.528	1.357	9.8	0.525	1.377	9.7	0.526
1.578	10.0	0.545	1.551	10.1	0.541	1.574	10.0	0.544
1.775	10.3	0.560	1.744	10.4	0.557	1.771	10.2	0.554
1.973	10.5	0.571	1.938	10.6	0.569	1.967	10.4	0.565
2.367	10.6	0.577	2.326	10.8	0.579	2.361	10.6	0.576
2.762	10.7	0.582	2.714	11.0	0.589	2.754	10.8	0.587
3.156	10.8	0.588	3.101	11.1	0.594	3.148	10.9	0.592
3.551	10.9	0.593	3.489	11.2	0.600	3.541	11.1	0.603
3.945	10.9	0.593	3.876	11.2	0.600	3.935	11.1	0.603

Table 7. Continued

Specimen No. 30.5			Specimen No. 30.6			Specimen No. 30.7		
$\bar{p}$	P_{min} lb	$\bar{\sigma}_{min}$	$\bar{p}$	P_{min} lb	$\bar{\sigma}_{min}$	$\bar{p}$	P_{min} lb	$\bar{\sigma}_{min}$
0.0	5.4	0.125	0.0	5.2	0.118	0.0	5.3	0.120
0.042	8.3	0.192	0.041	8.3	0.188	0.042	8.2	0.186
0.084	10.7	0.248	0.082	10.8	0.244	0.082	10.8	0.245
0.168	12.6	0.292	0.164	12.6	0.285	0.164	13.4	0.304
0.252	14.0	0.324	0.246	13.7	0.310	0.248	14.6	0.332
0.335	15.5	0.368	0.328	15.5	0.350	0.329	16.2	0.368
0.419	16.8	0.389	0.410	16.8	0.380	0.411	16.7	0.379
0.503	17.4	0.403	0.492	17.3	0.391	0.493	17.5	0.397
0.587	18.2	0.421	0.574	18.3	0.414	0.576	18.6	0.422
0.671	19.1	0.441	0.655	18.7	0.423	0.658	19.6	0.445
0.755	19.7	0.455	0.737	19.4	0.439	0.740	20.0	0.454
0.838	20.7	0.479	0.819	20.6	0.465	0.822	20.6	0.468
1.006	21.7	0.502	0.983	21.6	0.488	0.987	21.7	0.493
1.174	22.6	0.523	1.147	22.6	0.510	1.151	22.7	0.515
1.342	23.2	0.548	1.311	23.1	0.521	1.316	23.0	0.522
1.509	23.7	0.548	1.475	23.9	0.540	1.480	23.5	0.534
1.677	24.4	0.564	1.650	24.5	0.534	1.645	24.3	0.551
1.845	24.7	0.571	1.803	24.7	0.558	1.809	24.6	0.558
2.180	25.2	0.583	2.130	25.4	0.574	2.138	25.1	0.570
2.516	25.5	0.590	2.458	25.7	0.581	2.467	25.6	0.581
2.860	25.8	0.596	2.785	26.1	0.590	2.796	26.2	0.595
3.186	25.9	0.599	3.113	26.2	0.592	3.125	26.5	0.601
3.522	25.9	0.599	3.441	26.2	0.592	3.454	26.3	0.597

Table 7. Continued

Specimen No. 50.4			Specimen No. 50.5			Specimen No. 50.6		
$\bar{p}$	P_{min} lb	$\bar{\sigma}_{min}$	$\bar{p}$	P_{min} lb	$\bar{\sigma}_{min}$	$\bar{p}$	P_{min} lb	$\bar{\sigma}_{min}$
0	13.5	0.117	0	14.0	0.122	0	13.1	0.113
0.031	20.5	0.177	0.032	21.4	0.187	0.031	16.8	0.144
0.062	24.4	0.210	0.063	23.8	0.208	0.062	21.2	0.182
0.094	27.9	0.240	0.095	26.6	0.232	0.093	23.8	0.204
0.125	29.8	0.257	0.127	28.9	0.252	0.124	26.1	0.224
0.188	31.9	0.275	0.190	31.7	0.277	0.187	31.1	0.267
0.250	34.4	0.297	0.254	34.3	0.300	0.249	34.5	0.296
0.313	37.1	0.320	0.317	34.8	0.304	0.311	36.7	0.315
0.469	42.8	0.369	0.475	41.3	0.360	0.467	41.9	0.359
0.625	47.7	0.411	0.634	45.8	0.400	0.623	47.5	0.408
0.782	52.4	0.451	0.792	50.9	0.444	0.778	53.6	0.460
0.938	54.9	0.473	0.951	53.4	0.466	0.934	55.8	0.479
1.094	57.8	0.498	1.109	56.4	0.492	1.090	60.4	0.518
1.251	61.2	0.528	1.268	60.2	0.526	1.246	61.0	0.524
1.483	62.3	0.537	1.503	63.9	0.558	1.477	65.9	0.564
1.695	67.5	0.581	1.718	65.0	0.568	1.688	67.6	0.580
1.906	68.1	0.587	1.933	65.3	0.570	1.899	67.4	0.579
2.118	68.8	0.593	2.147	68.0	0.594	2.110	67.9	0.582
2.542	69.8	0.601	2.577	68.6	0.599	2.532	69.4	0.595
2.966	69.9	0.602	3.006	68.8	0.600	2.954	68.8	0.590
3.389	69.8	0.601	3.436	69.0	0.602	3.376	69.3	0.594
3.813	70.1	0.604	3.865	68.4	0.597	3.798	70.2	0.603

Table 7. Continued

Specimen No. 79.3-1			Specimen No. 79.3.2			Specimen No. 79.4		
$\bar{p}$	P_{min} lb	$\bar{\sigma}_{min}$	$\bar{p}$	P_{min} lb	$\bar{\sigma}_{min}$	$\bar{p}$	P_{min} lb	$\bar{\sigma}_{min}$
0	41	0.129	0	39	0.123	0	38	0.127
0.029	57	0.179	0.023	54	0.170	0.024	49	0.163
0.057	69	0.216	0.057	67	0.210	0.060	61	0.203
0.114	81	0.254	0.114	78	0.245	0.121	73	0.243
0.171	90	0.283	0.170	87	0.273	0.181	87	0.290
0.228	100	0.314	0.227	95	0.298	0.241	91	0.303
0.342	112	0.352	0.340	109	0.342	0.362	106	0.353
0.456	123	0.387	0.454	119	0.374	0.482	118	0.394
0.618	138	0.434	0.615	133	0.418	0.654	133	0.444
0.773	149	0.468	0.769	147	0.461	0.817	141	0.470
0.928	158	0.496	0.923	153	0.481	0.981	145	0.483
1.237	170	0.534	1.231	168	0.528	1.308	160	0.533
1.546	177	0.556	1.538	178	0.559	1.635	166	0.554
1.855	186	0.584	1.846	182	0.571	1.962	173	0.576
2.165	189	0.594	2.154	186	0.584	2.289	177	0.590
2.474	188	0.591	2.461	188	0.590	2.615	177	0.590
2.783	188	0.591	2.769	189	0.594	2.943	177	0.590
3.092			3.077			3.269		
3.401			3.384					

Table 7. Concluded

Specimen No. 100.3-2			Specimen No. 100.4			Specimen No. 100.5		
$\bar{p}$	P_{min} lb	$\bar{\sigma}_{min}$	$\bar{p}$	P_{min} lb	$\bar{\sigma}_{min}$	$\bar{p}$	P_{min} lb	$\bar{\sigma}_{min}$
0.0	58	0.130	0.0	62	0.136	0.0	59	0.131
0.055	89	0.199	0.054	99	0.217	0.055	90	0.200
0.110	104	0.232	0.108	109	0.239	0.109	109	0.242
0.220	127	0.284	0.216	131	0.288	0.219	133	0.296
0.329	143	0.320	0.323	149	0.327	0.328	154	0.342
0.439	160	0.357	0.431	171	0.375	0.437	167	0.372
0.657	186	0.416	0.647	204	0.448	0.656	196	0.436
0.878	210	0.469	0.863	221	0.485	0.874	215	0.479
1.098	221	0.494	1.078	232	0.510	1.093	228	0.508
1.317	234	0.523	1.294	243	0.533	1.312	237	0.527
1.537	247	0.551	1.509	250	0.549	1.530	247	0.550
1.756	252	0.563	1.725	255	0.560	1.749	253	0.563
1.976	255	0.570	1.941	262	0.575	1.968	256	0.570
2.196	261	0.583	2.156	265	0.582	2.186	264	0.587
2.415	261	0.583	2.372	266	0.584	2.405	268	0.596
2.635	262	0.585	2.588	268	0.588	2.624	264	0.587

Figure 15. Test Setup for Internally Pressurized Cylinders in Axial Compression

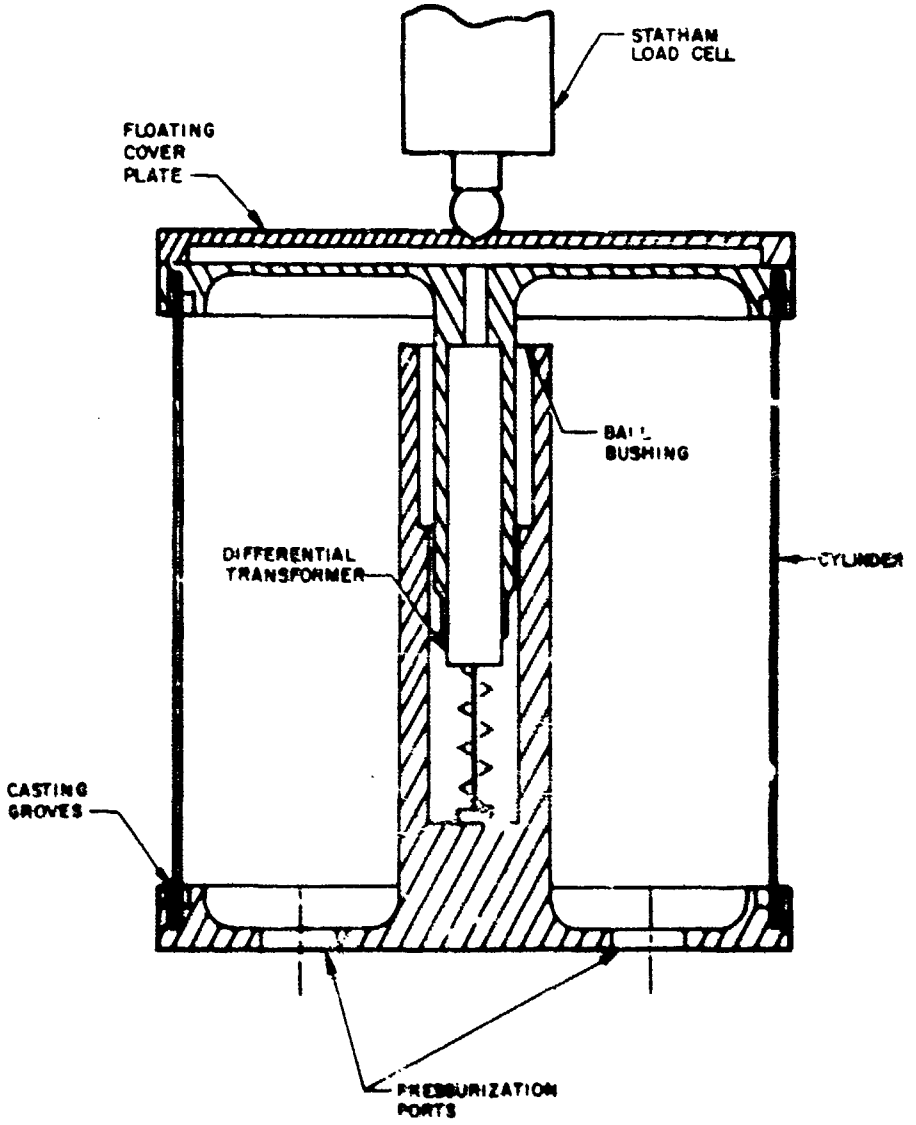

Figure 16. Test Specimen Assembly

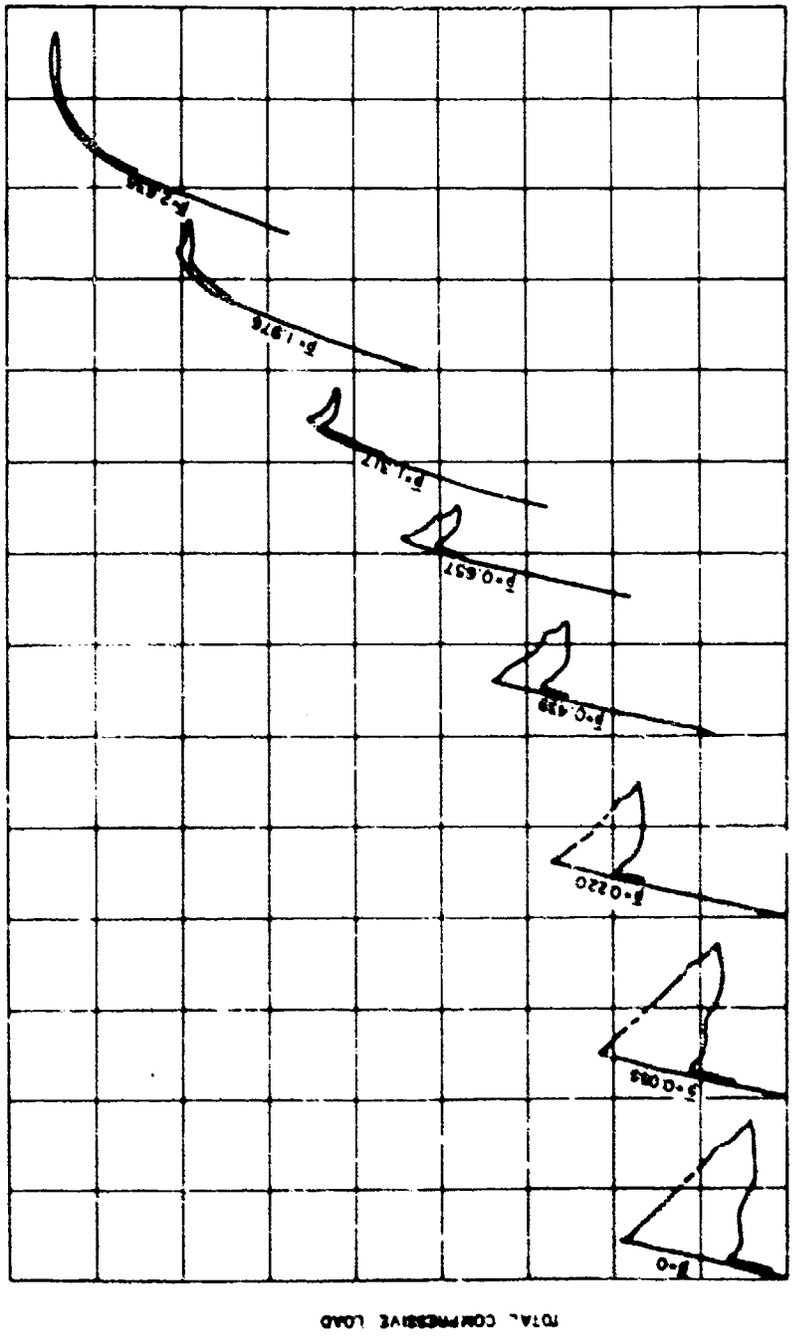

Figure 17. Typical Load Deflection Curves for Pressurized Cylinders in Axial Compression

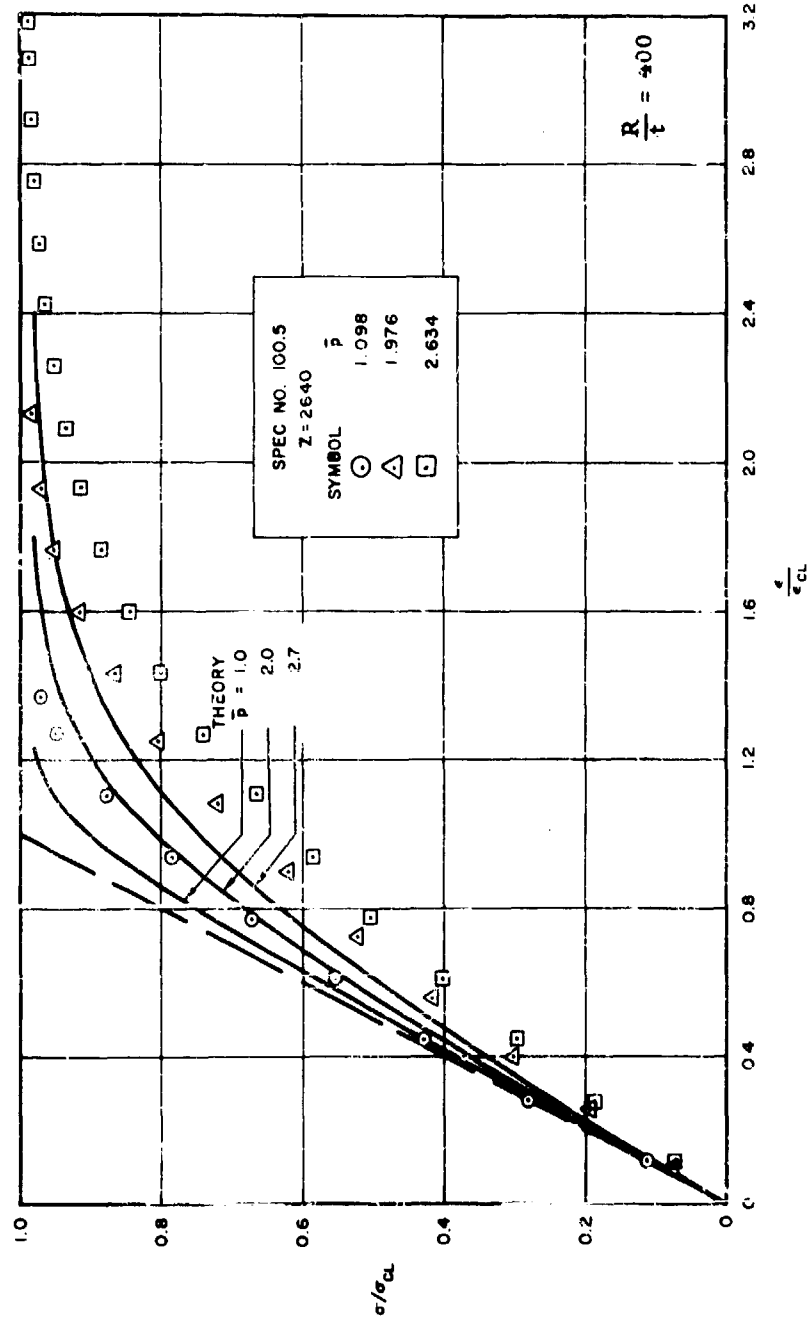

Figure 18. Comparison of Theoretical and Experimental Load-End Shortening Curves for Pressurized Cylinders

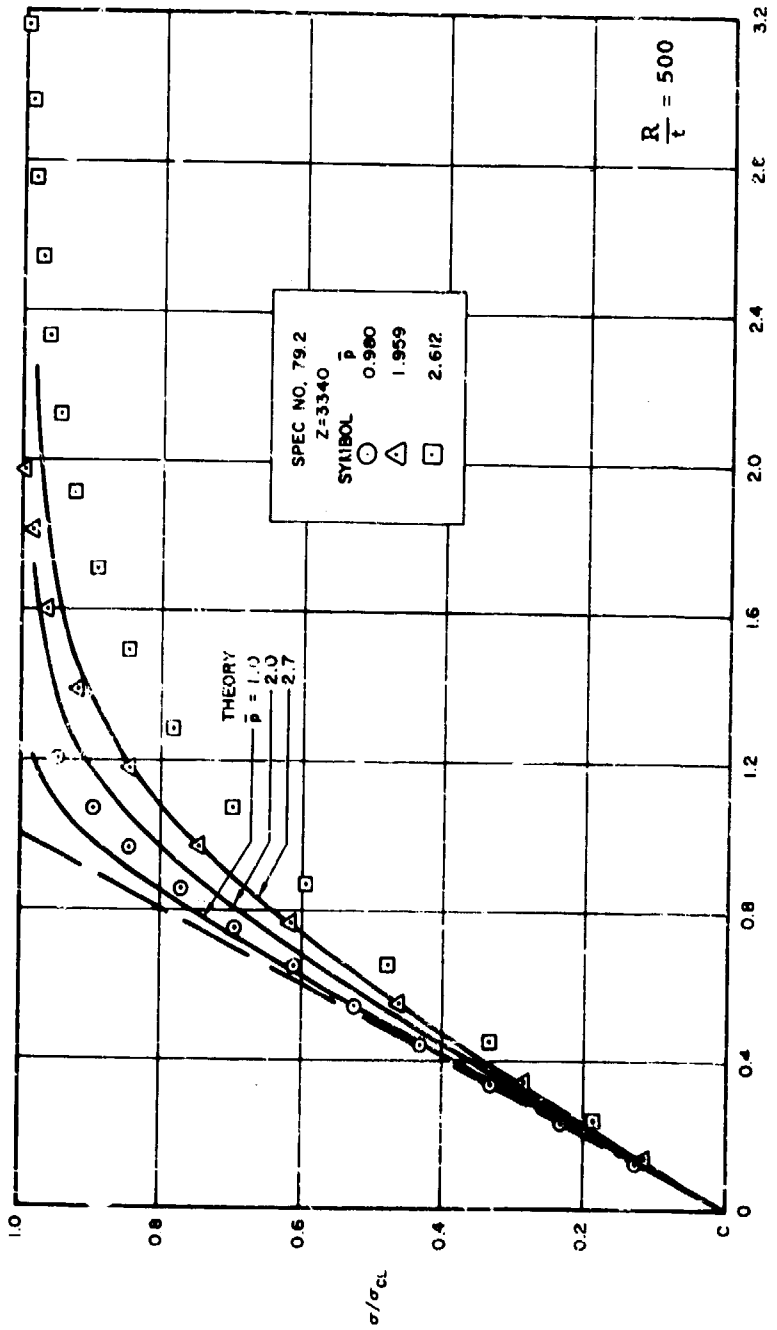

Figure 18. Continued

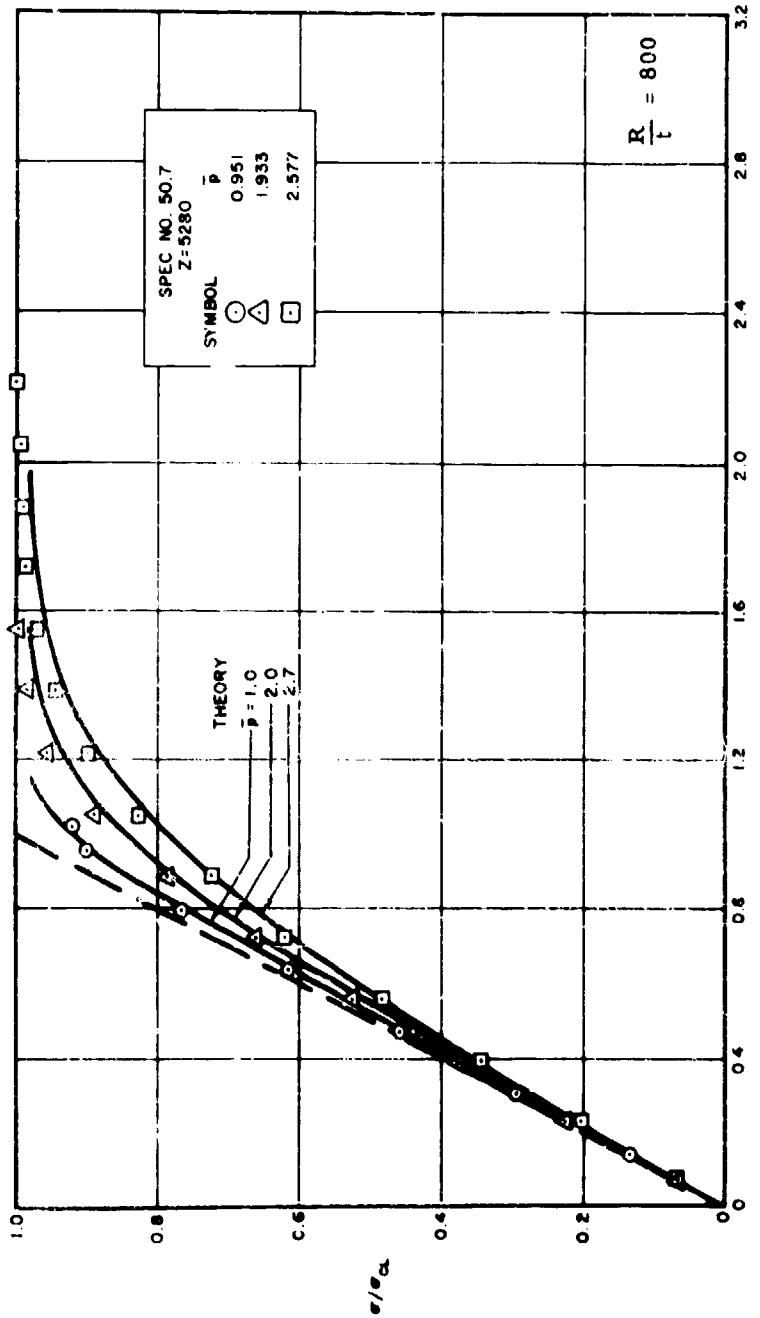

Figure 18. Continued

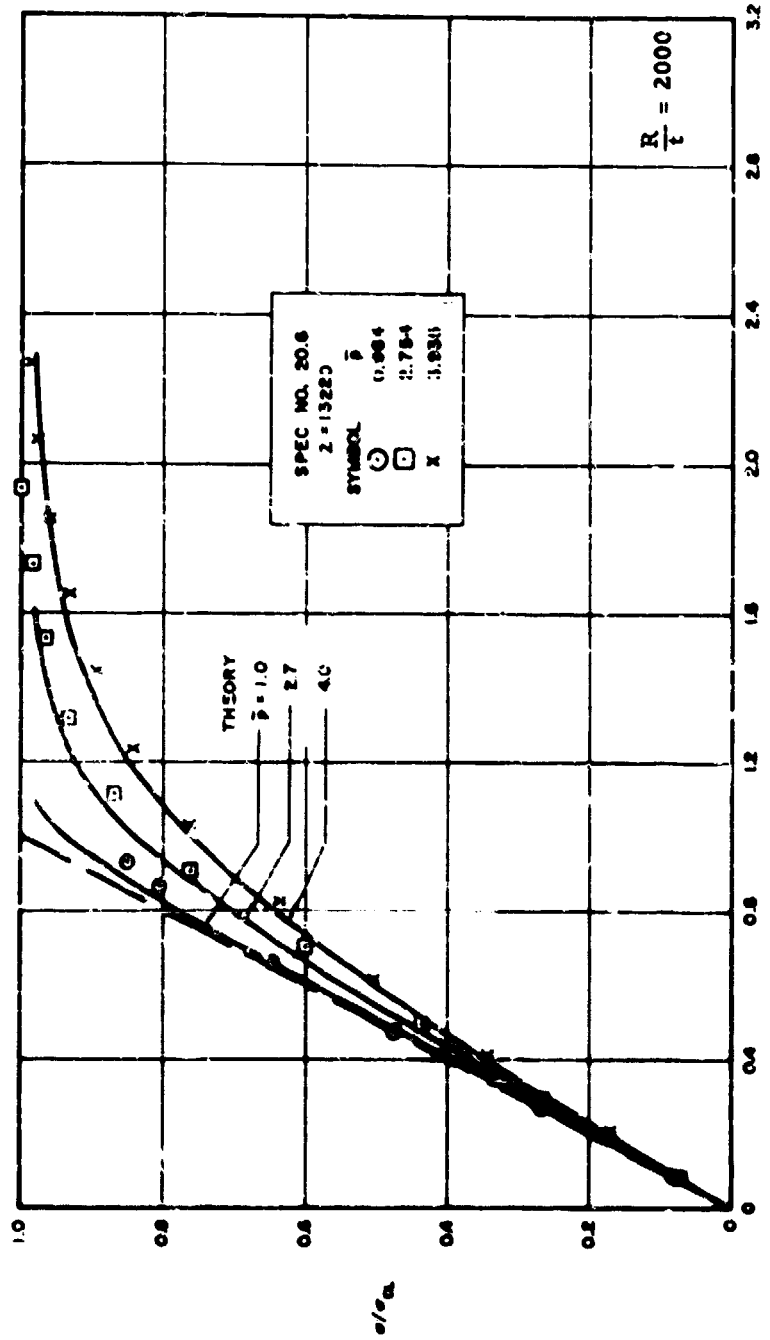

Figure 18. Concluded

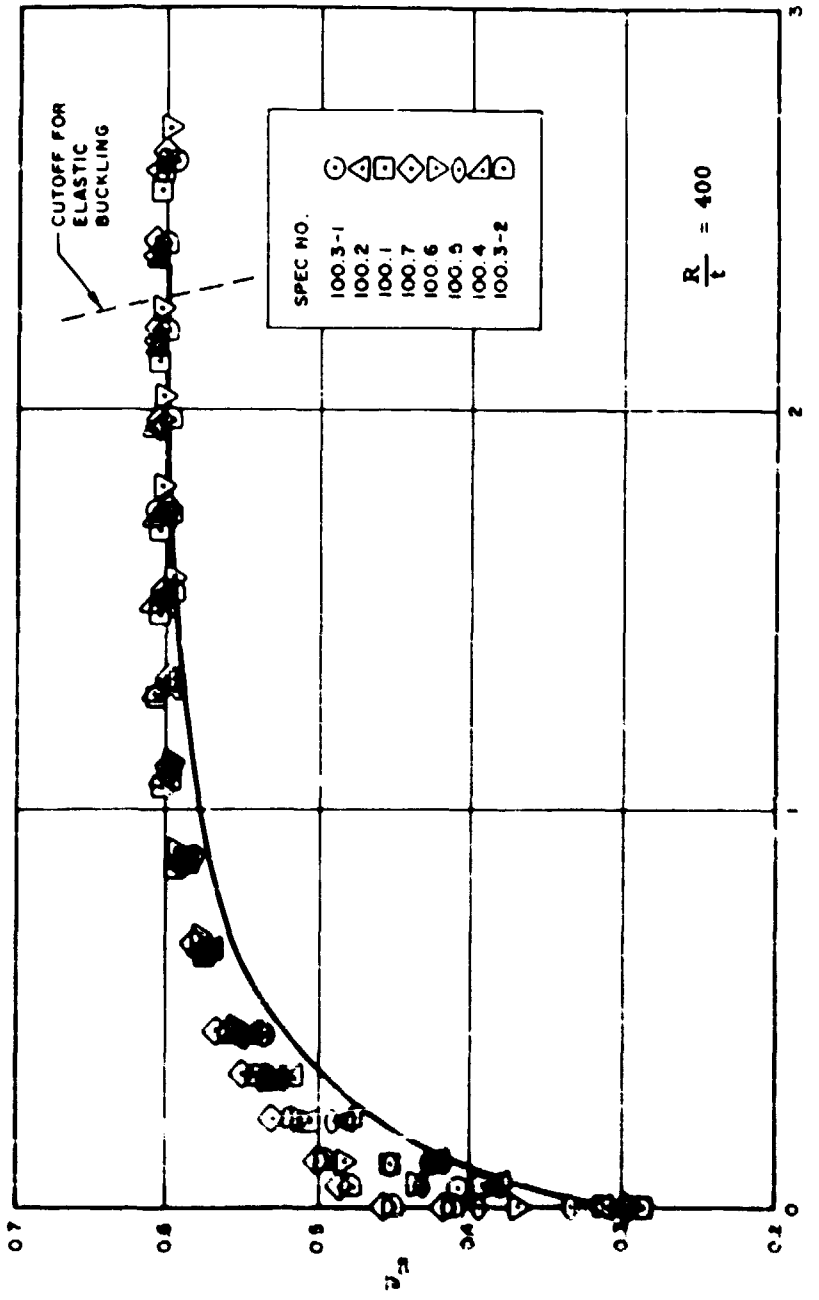

Figure 19 Variation of Axial Stress Coefficent with Internal Pressure Parameter

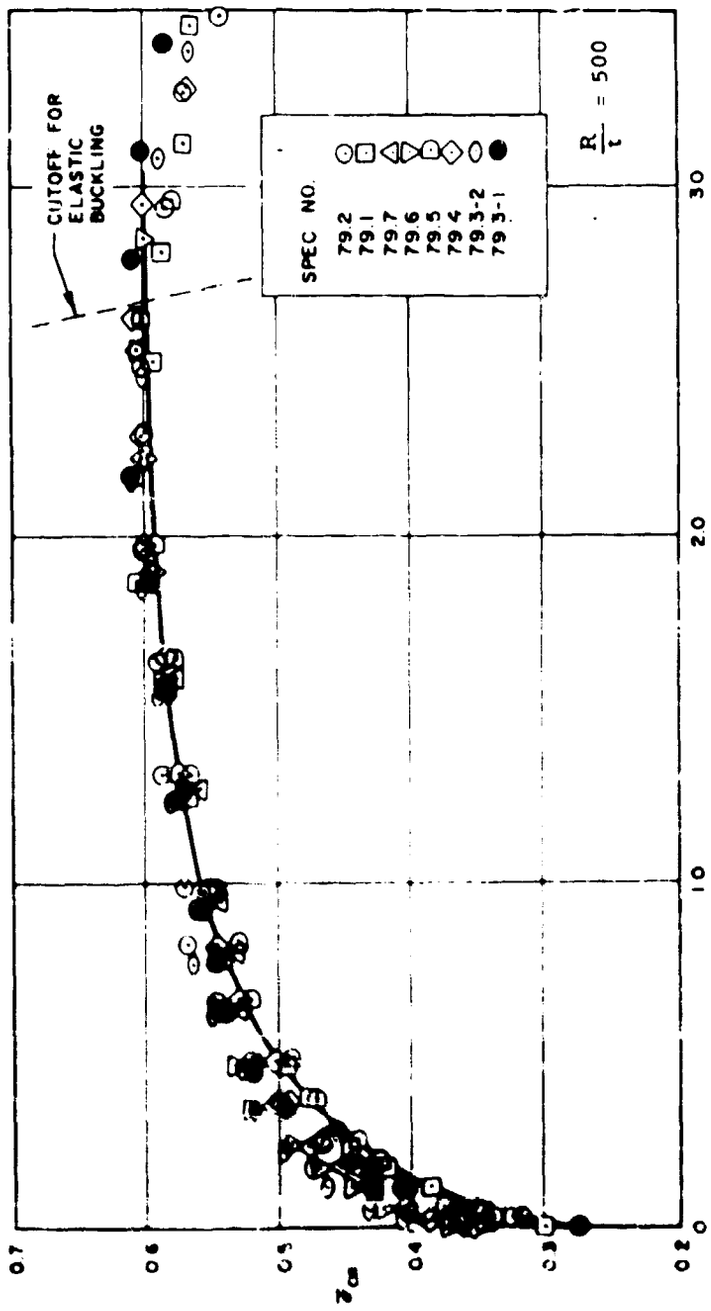

Figure 19. Continued

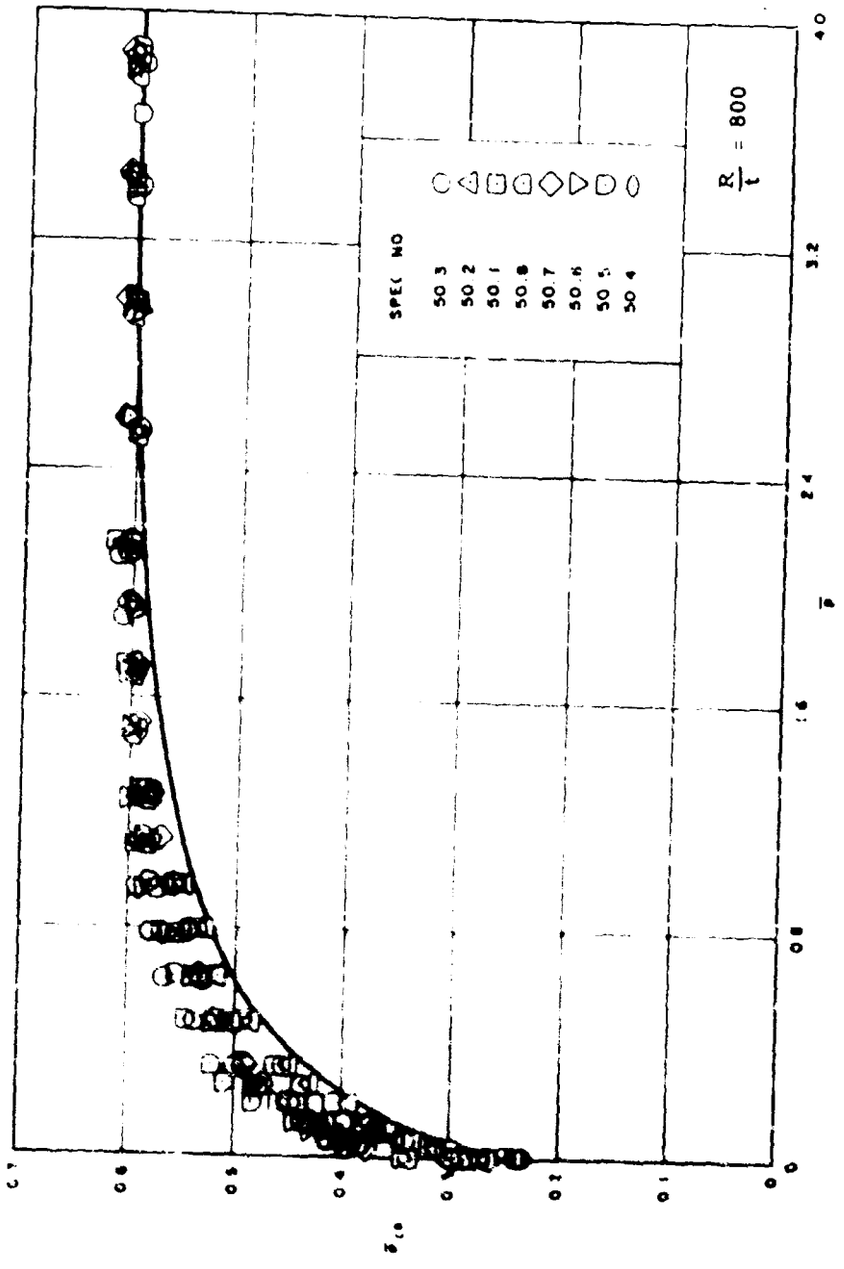

Figure 19. Continued

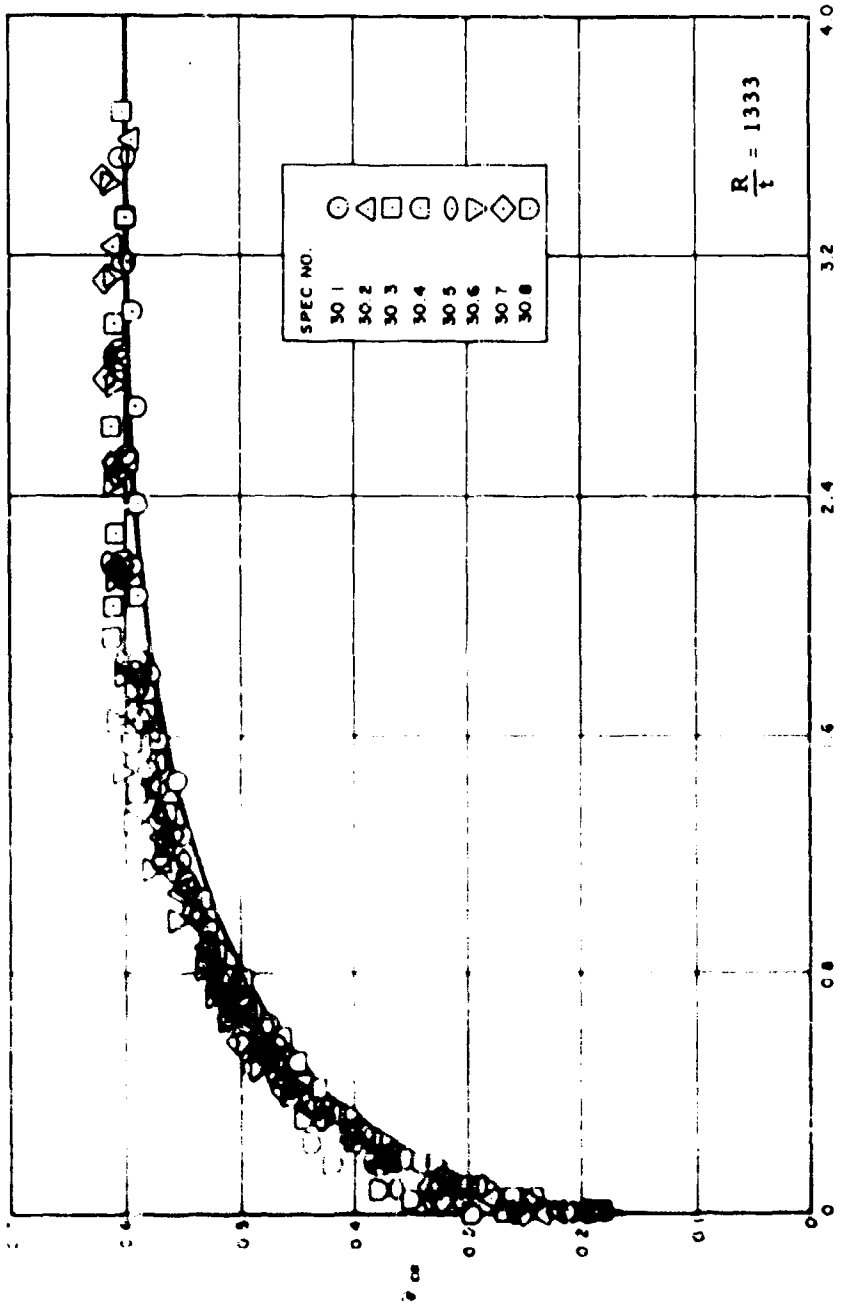

Figure 19. Continued

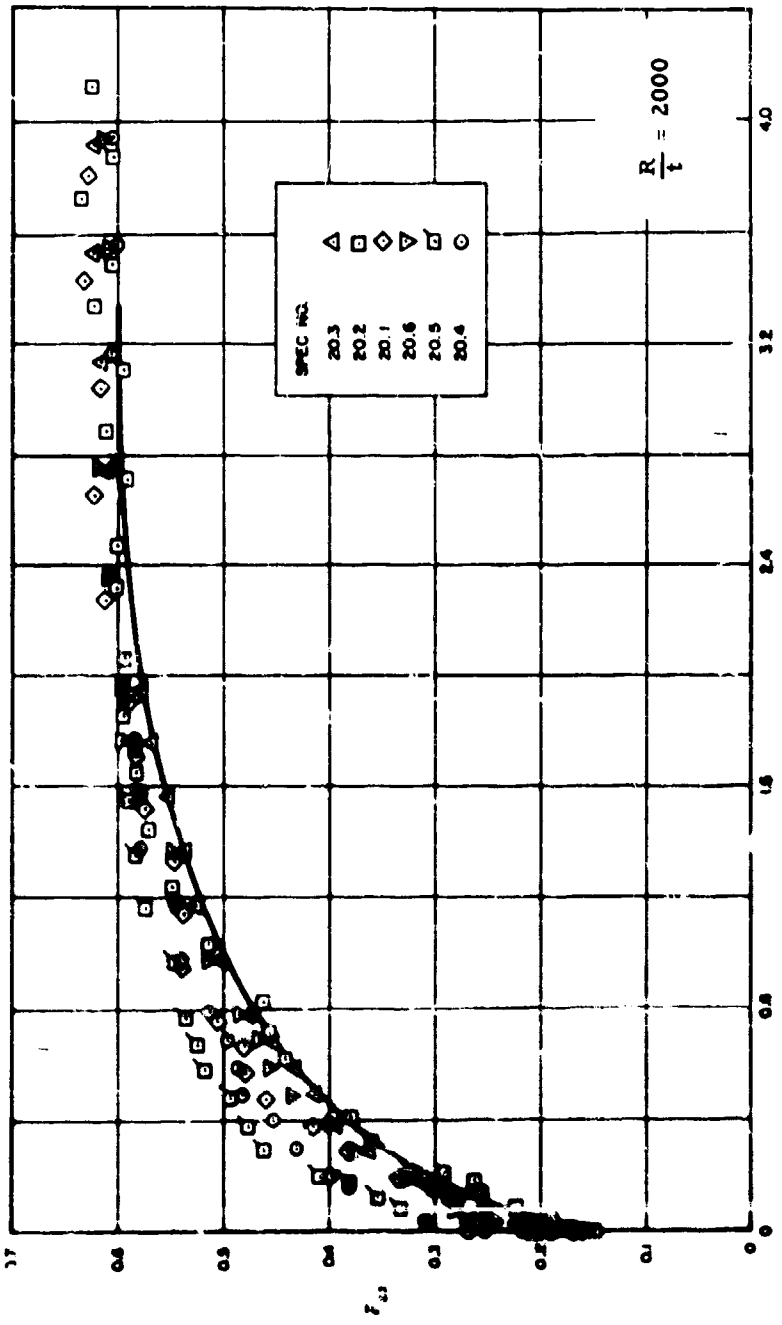

Figure 19. Concluded

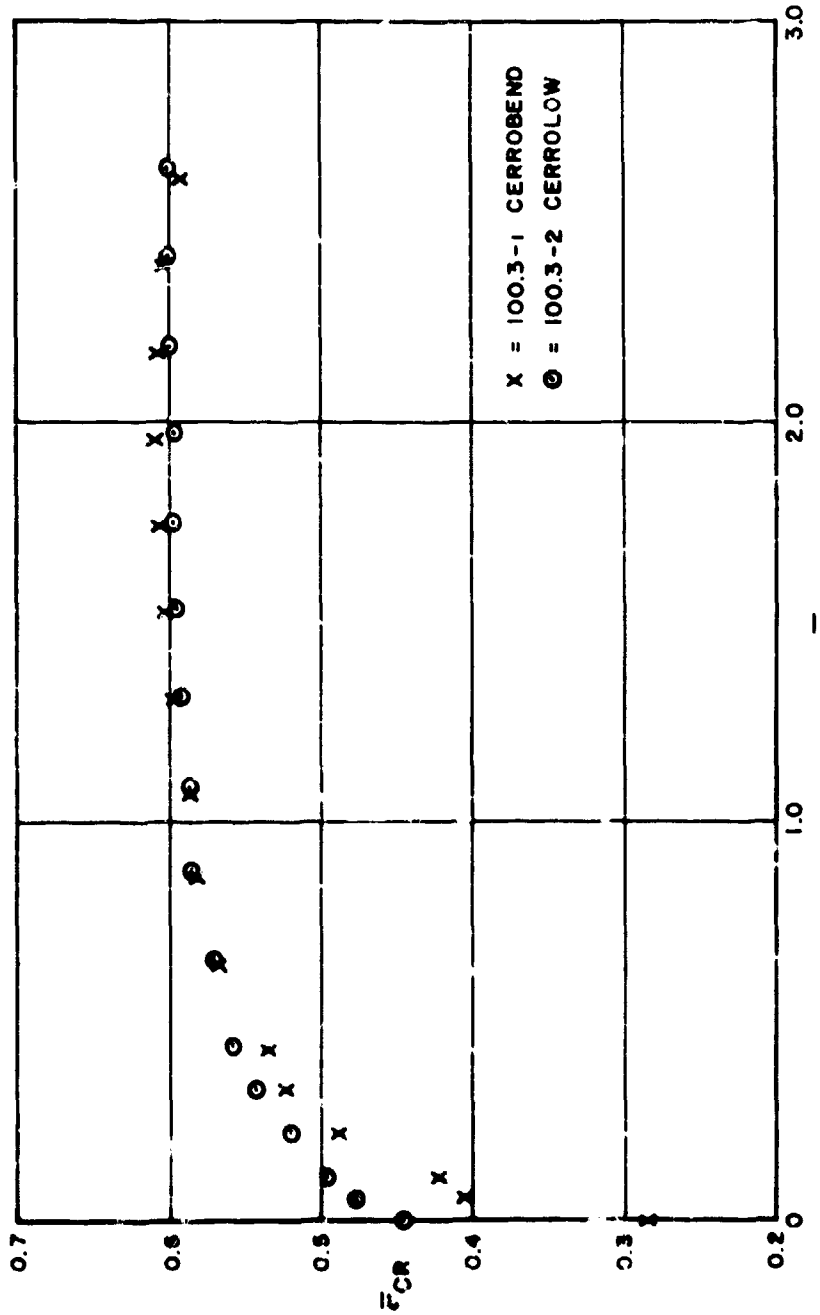

Figure 2: Effect of End Condition on Axial-Stress Coefficents for Pressurized Cylinders

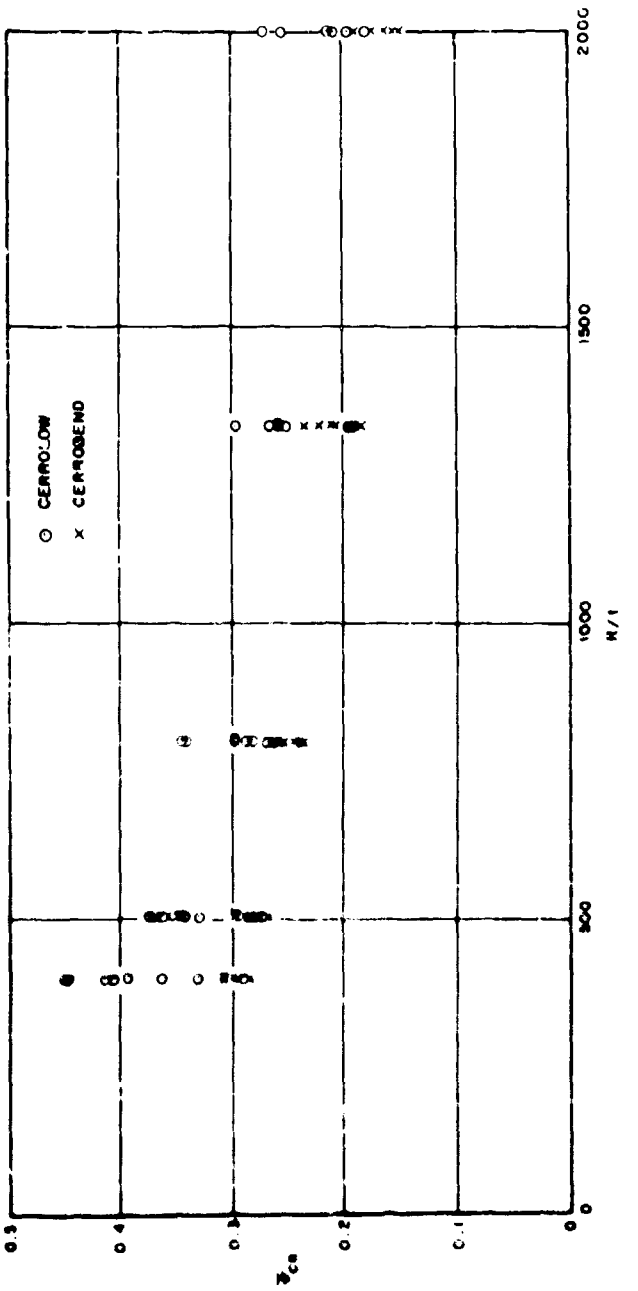

Figure 21. Effect of End Condition on Axial-Stress Coefficents for Unpressurized Cylinders

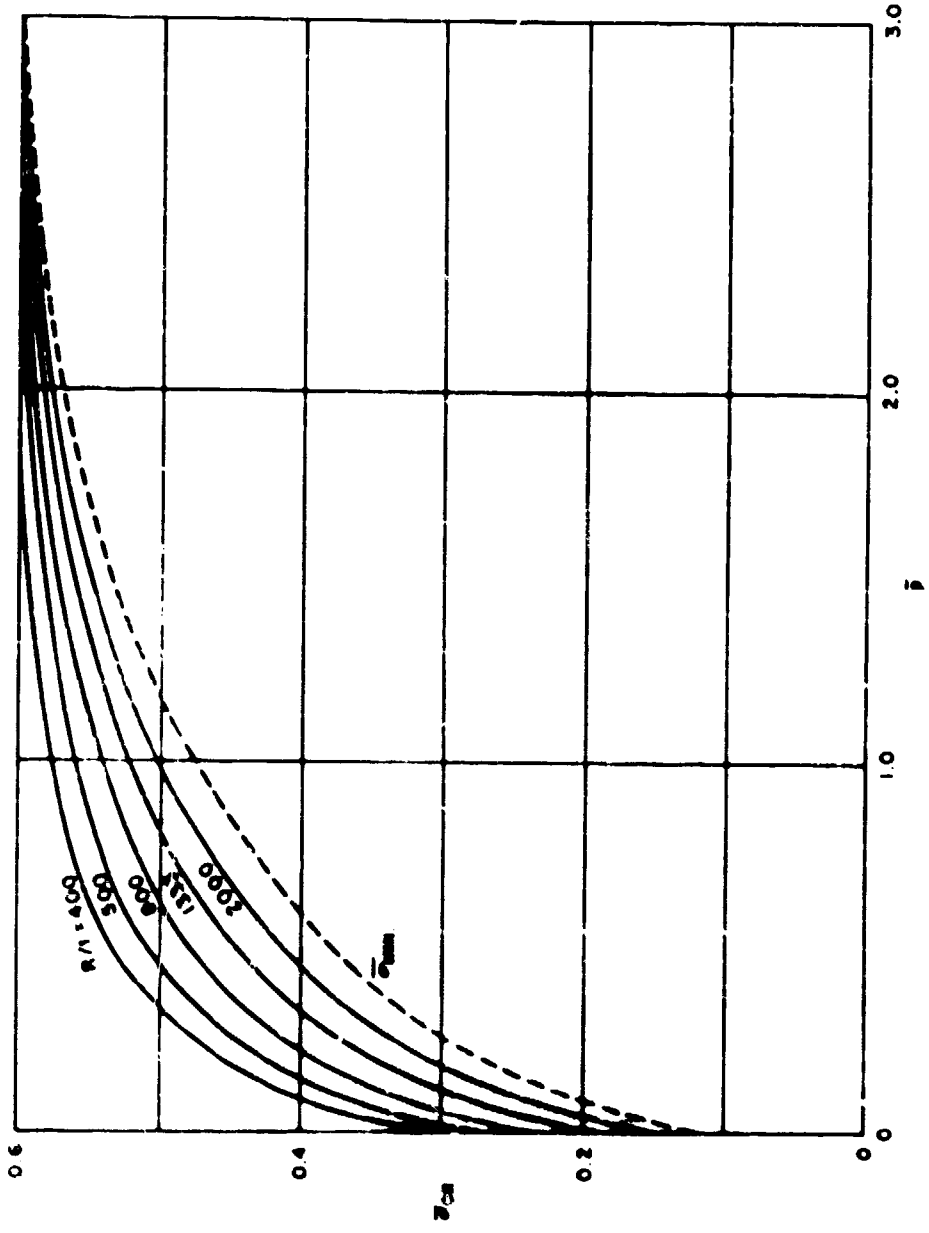

Figure 22. Lower Bounds for Variation of Axial-Stress Coefficent with Pressure Parameter

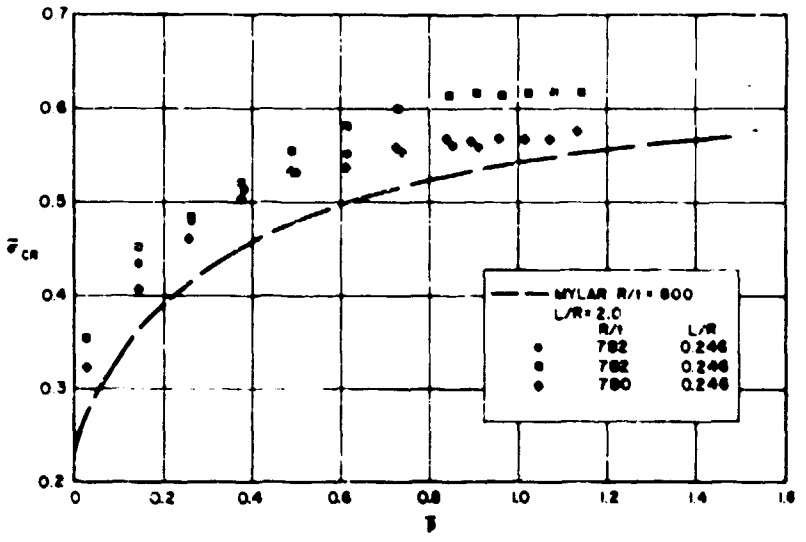

(a) 7075-T6 Aluminum (Ref 5)

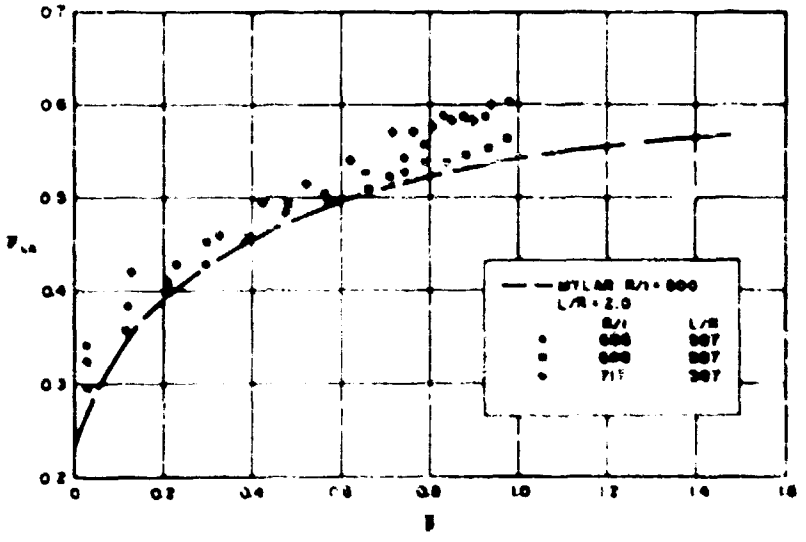

(b) 7075-T6 Aluminum (Ref 5)

Figure 23. Comparison of Mylar Result with Experimental Data for Other Material

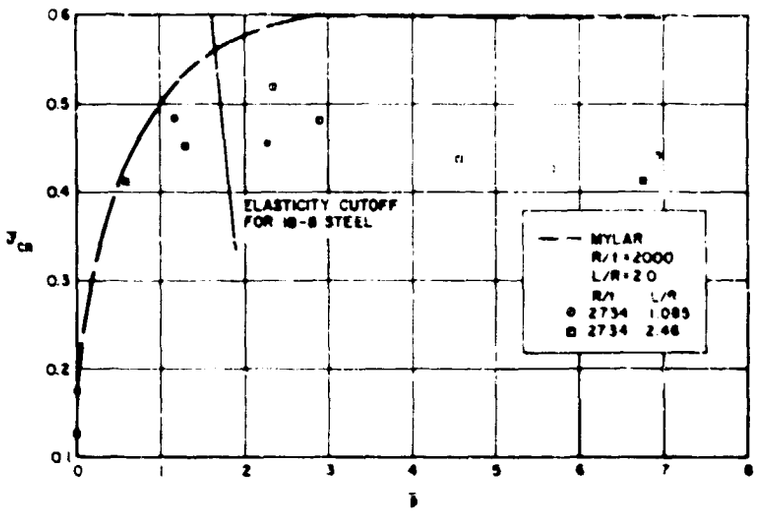

(c) 18-8 1/2 Hard Stainless Steel (Ref 21)

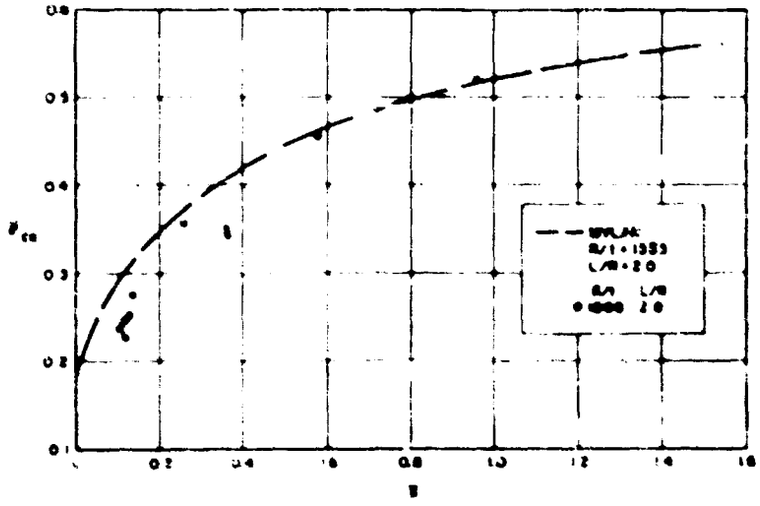

(d) 17-7 PH Stainless Steel (Ref 6)

Figure 21. Concluded

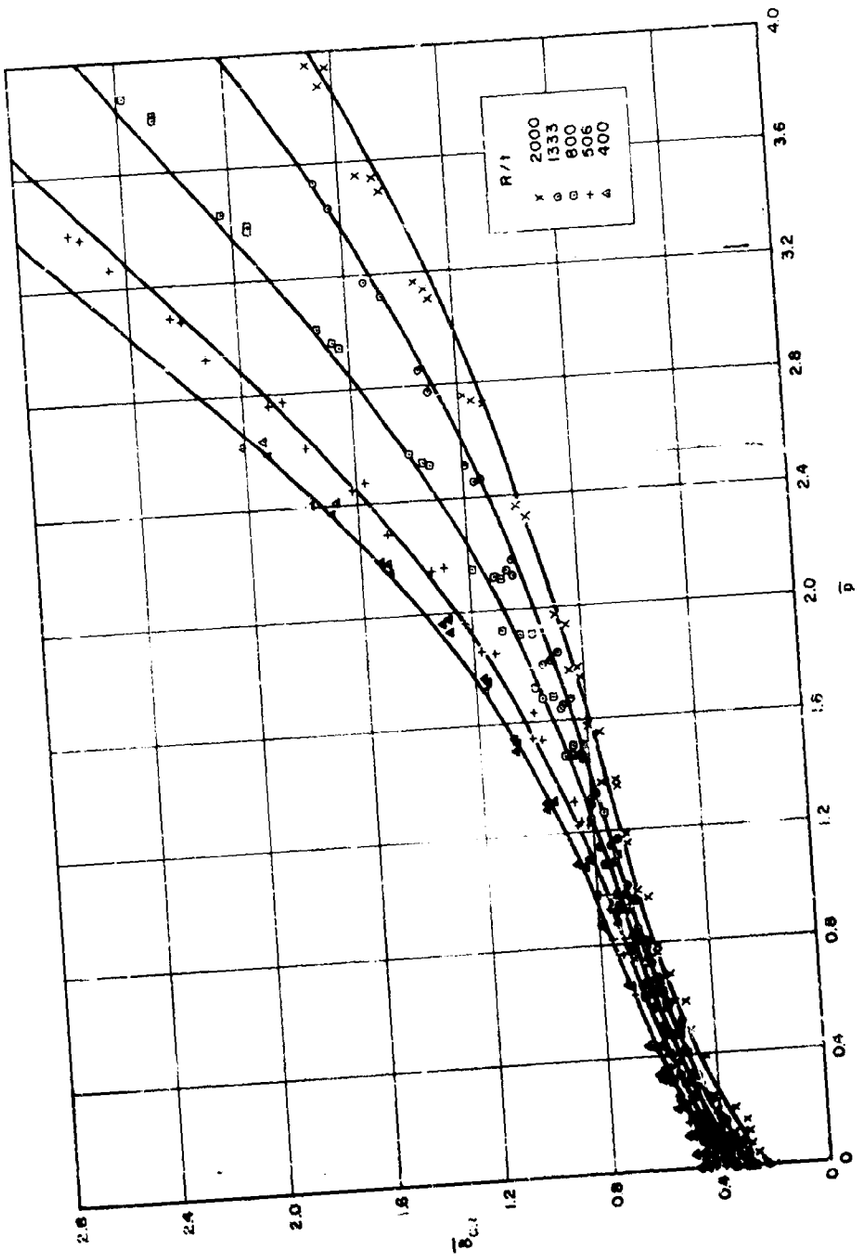

Figure 24. Variation of Critical End Shortening Parameter with Internal Pressure Parameter

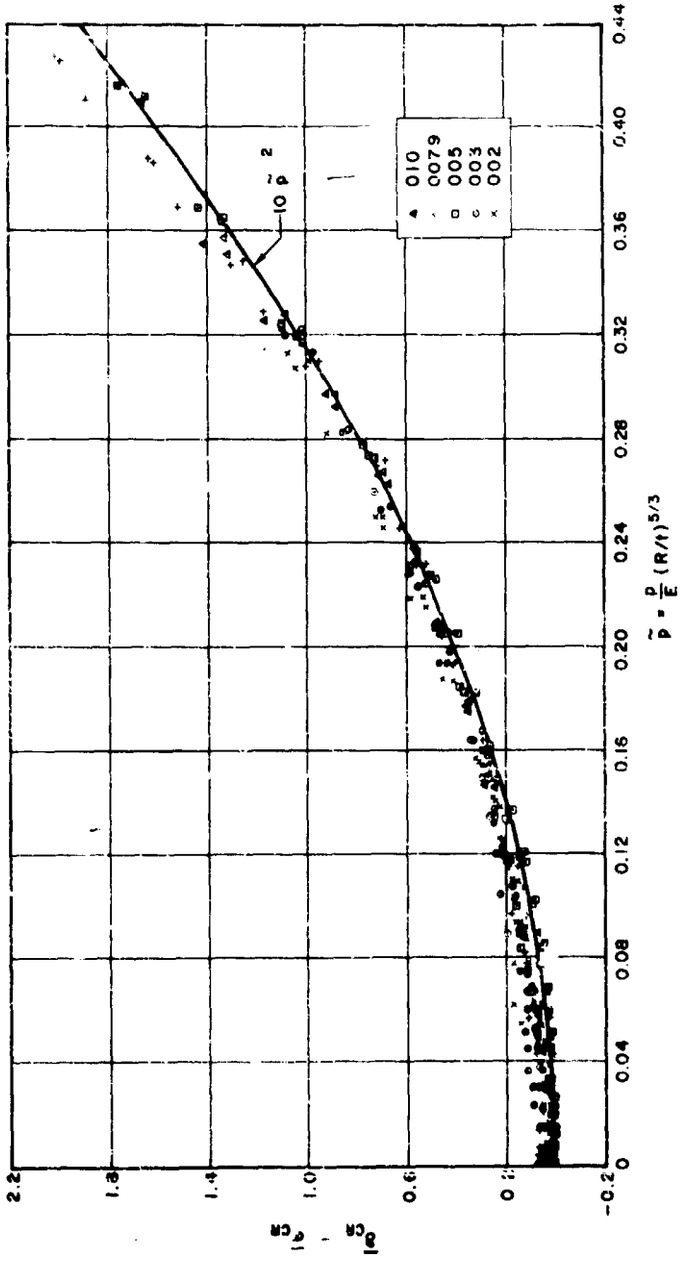

Figure 25. Transformed Data for Variation of Critical End Shortening Parameter with Internal Pressure Parameter

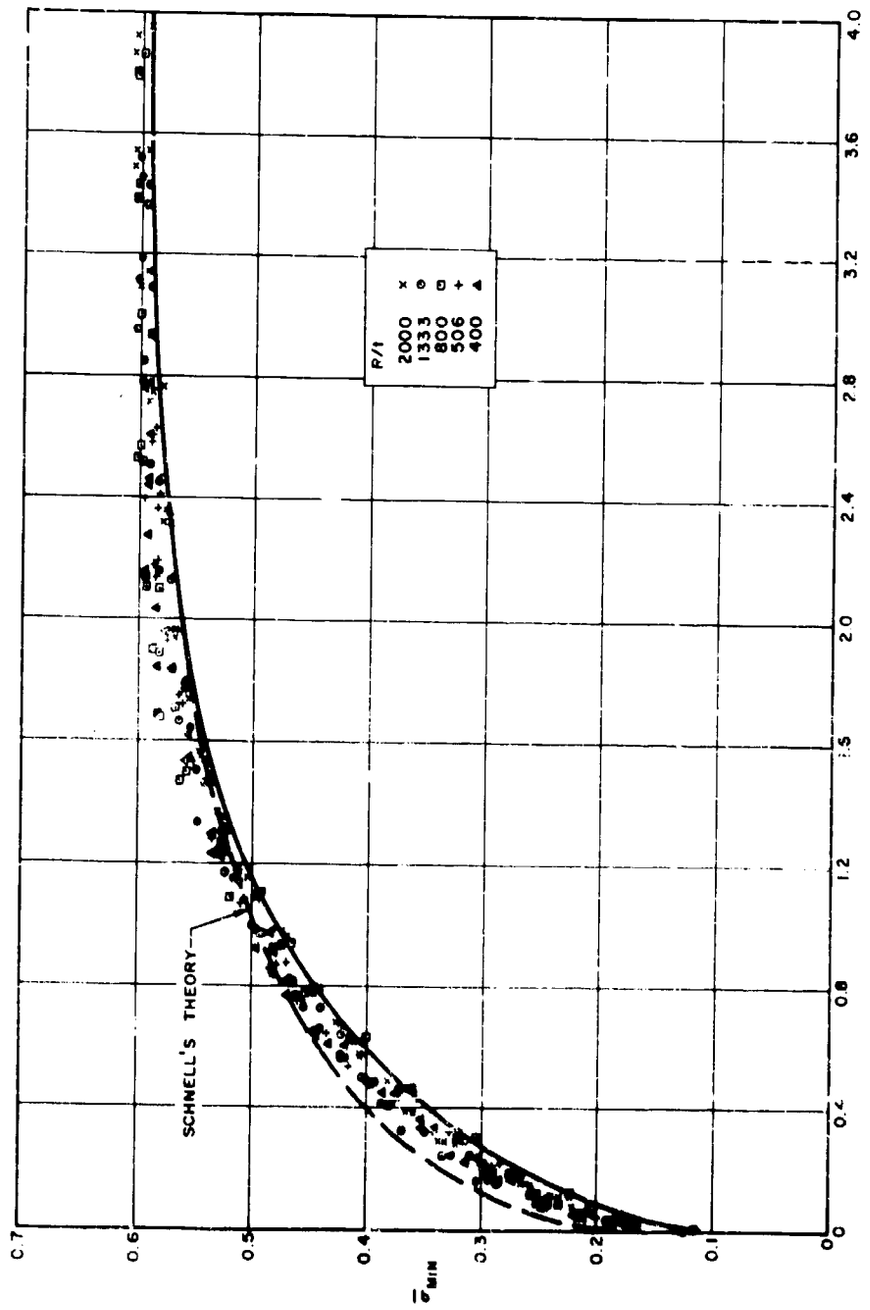

Figure 26. Variation of Minimum Load Parameter with Internal Pressure Parameter

VII. PRESSURIZED TRUNCATED CONES UNDER AXIAL COMPRESSION

Theoretical results for simply supported pressurized conical shells under axial compression (Reference 31) show that the axisymmetric buckling coefficient is a function of an internal pressure parameter and of a parameter containing the semivertex angle and the ratio of the small radius of curvature and the wall thickness. For sufficiently large pressures; i.e., for

$$\gamma = \sqrt{\frac{3(1-\nu^2)}{2}} \left(\frac{R_1/\cos\alpha}{t}\right)^2 - 1 \quad , \tag{8}$$

the total axial load carrying capacity of the conical shell is given by

$$\left[\frac{3(1-\nu^2)}{2\pi}\right]^{1/2} \frac{P}{Et^2\cos^2\alpha} = (1+\gamma)\left(1 + 1.05\zeta^{-1/3}\right) \tag{9}$$

where

$$\zeta = \left[12(1-\nu^2)\right]^{1/2} \frac{R_1/\cos\alpha}{t} \cot^2\alpha$$

Calculated buckle patterns indicate that as the pressure increases the buckle deformations become confined to the small end of the cone, since this is the only part of the cone in compression.

The experimental results obtained from a relatively small number of tests investigating the predicted increase in net load carrying capacity, based on the small cross-section of the cone, are given in Table 8 and are compared with theoretical calculations in Figure 27. It can be seen that the predictions of the small-deflection theory are qualitatively verified, in that cones with lower values of the geometry parameter ζ appear to yield larger net buckling load coefficients as a function of the pressure

parameter and, for sufficiently large pressures, the buckling load coefficients increase linearly with pressure. It will be noted that in many cases the net buckling load coefficient is larger than the theoretically predicted value. The theoretical values are suspect, however. Since the buckles occur very close to the small end of the cone, it can be expected that a rigorous analysis, taking into account the clamped end condition and the variation of the meridional stress from that given by membrane theory and experiment is not very serious, however; therefore, the present theoretical values can be used as an estimate of the load carrying capacity of conical shells for values of the pressure parameter greater than unity.

The observed buckle patterns (see Figure 28) vary with internal pressure in a manner similar to that for cylinders. It follows then that a comprehensive experimental program should include an investigation of the effect of the ratio of the small radius of curvature to the wall thickness on cones having given values of the geometry parameter ζ.

It is also obvious from the results that the stress state becomes plastic near the ends of the specimens under sufficiently high pressures, as indicated by the drop-off in net buckling load for some specimens. Thus, the benefits of pressurization are limited by the onset and effects of plasticity, which are dependent on the plastic behavior of the particular material used. The test results of Reference 6 for high strength stainless steel specimens are in good agreement with those of the present report, but do not cover a large enough range of pressure to verify the theoretical increase in net load carrying capacity over that for the cylinder for large pressures. It has been noted, however, both in the present results and in those of Reference 6, that cones appear to be relatively stronger than cylinders in the low pressure range. The results of Reference 32 appear to be considerably lower than those of the present paper. It is difficult to

effect a direct comparison since the test results tabulated in Reference 32 contradict the results given graphically. Since the load level never reached the theoretical value, even at relatively high pressure, the cones are concluded to have been of inferior construction.

Table 8. Experimental Data for Pressurized Mylar Cones under Axial Compression

t (in.)	R_1 (in.)	ζ	E (psi)	$\frac{P - \pi R_1^2 p}{2\pi E t^2 \cos^2 \alpha}$	$\frac{p}{E}\left(\frac{R_1/\cos\alpha}{t}\right)^2$	$\frac{P - \pi R_1^2 p}{2\pi E t^2 \cos^2 \alpha}$	$\frac{p}{E}\left(\frac{R_1/\cos\alpha}{t}\right)^2$
				(a) $\alpha = 20^\circ$			
0.005	2.18	11,600	693,000	0.229	0.000	0.585	0.560
				0.275	0.031	0.602	0.622
				0.310	0.062	0.615	0.684
				0.328	0.093	0.630	0.746
				0.458	0.124	0.648	0.809
				0.482	0.156	0.657	0.871
				0.475	0.187	0.675	0.933
				0.493	0.218	0.696	0.995
				0.496	0.249	0.699	1.057
				0.498	0.280	0.718	1.119
				0.505	0.311	0.728	1.182
				0.515	0.342	0.730	1.244
				0.521	0.373	0.746	1.306
				0.536	0.404	0.751	1.368
				0.550	0.435	0.754	1.431
				0.557	0.467	0.756	1.493
				0.564	0.498	0.760	1.555
0.005	2.17	11,500	704,000	0.193	0.000	0.526	0.664
				0.236	0.030	0.543	0.724
				0.261	0.060	0.560	0.785
				0.281	0.091	0.569	0.845
				0.287	0.121	0.581	0.906
				0.306	0.151	0.591	0.966
				0.322	0.181	0.595	1.026
				0.339	0.211	0.612	1.087
				0.354	0.241	0.629	1.147
				0.368	0.272	0.636	1.210
				0.378	0.302	0.647	1.268
				0.393	0.332	0.655	1.328
				0.413	0.362	0.667	1.389
				0.424	0.392	0.669	1.449
				0.436	0.422	0.685	1.509
				0.450	0.453	0.707	1.660
				0.465	0.483	0.732	1.811
				0.486	0.543	0.730	1.962
				0.507	0.603		
0.005	2.89	15,300	697,000	0.217	0.000	0.657	1.085
				0.387	0.054	0.675	1.194
				0.427	0.109	0.688	1.300
				0.410	0.162	0.701	1.411
				0.409	0.217	0.712	1.519
				0.443	0.271	0.727	1.628
				0.412	0.326	0.734	1.737
				0.399	0.380	0.746	1.845
				0.460	0.434	0.751	1.953
				0.522	0.488	0.758	2.062
				0.546	0.543	0.770	2.171
				0.562	0.597	0.784	2.279
				0.579	0.651	0.791	2.388
				0.598	0.705	0.789	2.496
				0.603	0.760	0.796	2.605
				0.616	0.814	0.794	2.713
				0.625	0.868	0.783	2.985
				0.649	0.977		

Table 8. Continued

t (in.)	R_1 (in.)	ℓ	E (psi)	$\frac{P - \pi R_1^2 p}{2\pi E t^2 \cos^2 \alpha}$	$\frac{p}{E}\left(\frac{R_1/\cos\alpha}{t}\right)^2$	$\frac{P - \pi R_1^2 p}{2\pi E t^2 \cos^2 \alpha}$	$\frac{p}{E}\left(\frac{R_1/\cos\alpha}{t}\right)^2$
(a) $\alpha = 20^\circ$							
0.005	2.93	15,600	700,000	0.276	0.000	0.645	1.001
				0.366	0.056	0.675	1.113
				0.407	0.111	0.691	1.124
				0.429	0.167	0.711	1.335
				0.466	0.223	0.714	1.446
				0.502	0.278	0.734	1.558
				0.514	0.334	0.751	1.668
				0.528	0.389	0.758	1.780
				0.550	0.445	0.769	1.891
				0.553	0.501	0.785	2.114
				0.566	0.556	0.791	2.225
				0.580	0.612	0.804	2.336
				0.594	0.667	0.805	2.448
				0.594	0.723	0.813	2.559
				0.599	0.779	0.808	2.670
				0.615	0.834	0.804	2.781
				0.626	0.890		
0.005	1.46	8,260	704,000	0.289	0.000	0.421	0.220
				0.377	0.014	0.426	0.247
				0.409	0.027	0.440	0.275
				0.410	0.041	0.451	0.302
				0.421	0.055	0.461	0.330
				0.426	0.069	0.479	0.357
				0.430	0.082	0.489	0.385
				0.438	0.096	0.506	0.412
				0.438	0.110	0.509	0.440
				0.425	0.124	0.514	0.467
				0.429	0.124	0.517	0.495
				0.434	0.137	0.554	0.522
				0.430	0.151	0.566	0.549
				0.429	0.165	0.573	0.577
				0.423	0.179	0.581	0.604
				0.413	0.192	0.574	0.632
				0.412	0.192	0.580	0.660
				0.419	0.206		
0.005	2.93	15,600	700,000	0.216	0.000	0.637	0.879
				0.451	0.055	0.653	0.989
				0.495	0.110	0.659	1.099
				0.514	0.165	0.674	1.209
				0.532	0.220	0.679	1.319
				0.557	0.275	0.691	1.428
				0.565	0.330	0.699	1.538
				0.574	0.385	0.714	1.648
				0.584	0.440	0.721	1.758
				0.594	0.494	0.727	1.867
				0.605	0.549	0.738	1.978
				0.612	0.604	0.746	2.088
				0.623	0.659	0.747	2.198
				0.621	0.714	0.753	2.307
				0.622	0.769	0.769	2.417
				0.627	0.824		

Table 8. Continued

t (in.)	R_1 (in.)	ζ	E (psi)	$\frac{P - \nu k_1^2 p}{2\pi E t^2 \cos^2 \alpha}$	$\frac{p}{E}\left(\frac{R_1/\cos\alpha}{t}\right)^2$	$\frac{P - \nu R_1^2 p}{2\pi E t^2 \cos^2 \alpha}$	$\frac{p}{E}\left(\frac{R_1/\cos\alpha}{t}\right)^2$
				(b) $\alpha = 30^0$			
0.0101	1.56	1770	690,000	−0.376 0.413 0.422 0.438 0.453 0.469 0.481 0.494	0.000 0.015 0.030 0.060 0.089 0.117 0.149 0.179	0.505 0.517 0.536 0.562 0.552 0.556 0.565	0.209 0.239 0.268 0.299 0.329 0.359 0.389
0.0101	1.56	1770	690,000	0.240 0.410 0.421 0.432 0.443 0.456 0.475 0.489 0.506 0.520	0.000 0.030 0.060 0.089 0.119 0.149 0.179 0.209 0.239 0.268	0.530 0.541 0.550 0.562 0.575 0.583 0.595 0.599 0.602	0.299 0.329 0.359 0.389 0.419 0.448 0.478 0.508 0.538
0.0100	1.56	1790	690,000	0.357 0.566 0.652 0.683	0.000 0.265 0.533 0.692	0.673 0.631 0.563	0.798 0.904 1.066
0.0100	1.56	1790	690,000	0.259 0.362 0.375 0.402 0.428 0.455 0.477 0.494 0.512 0.524 0.542	0.000 0.030 0.060 0.089 0.119 0.150 0.180 0.210 0.239 0.269 0.299	0.553 0.564 0.570 0.584 0.598 0.604 0.607 0.616 0.633 0.635	0.329 0.359 0.389 0.419 0.448 0.479 0.508 0.538 0.599 0.628
0.0095	1.57	1890	690,000	0.415 0.457 0.513 0.556 0.596 0.626 0.654 0.686 0.705	0.000 0.088 0.178 0.266 0.356 0.445 0.534 0.623 0.713	0.720 0.737 0.748 0.750 0.753 0.732 0.721 0.708 0.672	0.801 0.890 0.980 1.068 1.158 1.247 1.336 1.425 1.515
0.0075	1.32	2010	799,000	0.327 0.328 0.358 0.361 0.367 0.365 0.372 0.374 0.379 0.383 0.386 0.387 0.392 0.396 0.398 0.402 0.406	0.000 0.005 0.010 0.016 0.021 0.026 0.031 0.036 0.041 0.046 0.052 0.057 0.062 0.067 0.072 0.077 0.083	0.411 0.414 0.416 0.422 0.432 0.442 0.450 0.456 0.460 0.467 0.473 0.477 0.483 0.491 0.495 0.502 0.504	0.093 0.103 0.114 0.124 0.134 0.145 0.155 0.165 0.176 0.186 0.197 0.207 0.217 0.228 0.238 0.248 0.258
0.0075	1.39	2110	798,000	0.354 0.386 0.354 0.370 0.373 0.378 0.381 0.383 0.393 0.395 0.402 0.402 0.404 0.406 0.408 0.450 0.460	0.000 0.006 0.011 0.017 0.023 0.029 0.034 0.040 0.046 0.051 0.057 0.063 0.068 0.074 0.080 0.086 0.091	0.468 0.465 0.472 0.475 0.485 0.498 0.501 0.510 0.518 0.522 0.527 0.538 0.543 0.542 0.546 0.549 0.557	0.103 0.114 0.125 0.137 0.148 0.160 0.171 0.182 0.194 0.205 0.217 0.228 0.239 0.251 0.262 0.274 0.285
0.0075	1.57	2400	770,000	0.385 0.387 0.402 0.432 0.472 0.506 0.532 0.560	0.000 0.024 0.048 0.095 0.143 0.191 0.239 0.286	0.576 0.597 0.608 0.620 0.619 0.623 0.619	0.334 0.382 0.430 0.477 0.525 0.573 0.620

Table 8. Continued

t (in.)	R_1 (in.)	ζ	E (psi)	$\frac{P - \pi R_1^2 p}{2\pi E t^2 \cos^2 \alpha}$	$\xi\left(\frac{R_1/\cos\alpha}{t}\right)^{1/2}$	$\frac{P - \pi R_1^2 p}{2\pi E t^2 \cos^2 \alpha}$	$\xi\left(\frac{R_1/\cos\alpha}{t}\right)^{1}$
				(b) $\alpha = 30^\circ$			
0.0075	1.57	2400	770,000	0.360	0.000	0.575	0.382
				0.411	0.024	0.583	0.430
				0.413	0.048	0.601	0.477
				0.439	0.095	0.613	0.525
				0.462	0.143	0.624	0.573
				0.491	0.190	0.627	0.620
				0.515	0.239	0.612	0.668
				0.538	0.286	0.601	0.716
				0.560	0.334		
0.0075	2.07	3160	770,000	0.283	0.000	0.699	0.669
				0.410	0.083	0.712	0.753
				0.488	0.167	0.719	0.837
				0.545	0.251	0.717	0.921
				0.600	0.335	0.695	1.005
				0.631	0.418	0.732	1.089
				0.660	0.502	0.683	1.254
				0.690	0.586		
0.0075	2.07	3160	770,000	0.283	0.000	0.673	0.502
				0.425	0.083	0.693	0.586
				0.485	0.167	0.707	0.670
				0.550	0.251	0.757	0.837
				0.589	0.335	0.768	1.005
				0.636	0.418	0.697	1.172
0.0075	2.07	3160	770,000	0.274	0.000	0.579	0.502
				0.392	0.083	0.605	0.586
				0.441	0.167	0.622	0.669
				0.487	0.251	0.669	0.837
				0.525	0.335	0.683	1.005
				0.560	0.418		
0.0075	2.11	3220	793,000	0.390	0.000	0.489	0.239
				0.393	0.013	0.495	0.266
				0.404	0.027	0.510	0.293
				0.406	0.040	0.523	0.319
				0.411	0.053	0.536	0.346
				0.428	0.066	0.541	0.373
				0.435	0.080	0.561	0.399
				0.429	0.093	0.569	0.426
				0.437	0.106	0.573	0.452
				0.441	0.120	0.578	0.479
				0.449	0.133	0.594	0.505
				0.453	0.146	0.602	0.532
				0.457	0.160	0.607	0.559
				0.463	0.173	0.615	0.585
				0.468	0.186	0.623	0.611
				0.470	0.200	0.631	0.638
				0.474	0.213	0.646	0.665
0.0075	2.13	3250	799,000	0.305	0.000	0.502	0.243
				0.399	0.013	0.516	0.270
				0.415	0.027	0.527	0.297
				0.421	0.040	0.541	0.324
				0.424	0.054	0.548	0.351
				0.430	0.067	0.557	0.377
				0.436	0.081	0.565	0.404
				0.442	0.094	0.563	0.431
				0.451	0.108	0.573	0.458
				0.455	0.121	0.579	0.485
				0.461	0.135	0.587	0.512
				0.469	0.148	0.592	0.539
				0.475	0.162	0.600	0.566
				0.477	0.175	0.605	0.593
				0.482	0.188	0.613	0.620
				0.487	0.202	0.616	0.647
				0.497	0.216	0.619	0.674
0.0080	2.43	3470	725,000	0.397	0.000	0.686	0.834
				0.490	0.119	0.720	0.956
				0.541	0.238	0.734	1.076
				0.576	0.358	0.758	1.195
				0.615	0.477	0.770	1.315
				0.644	0.596	0.768	1.435
				0.678	0.717		
0.0080	2.43	3470	725,000	0.315	0.000	0.740	0.718
				0.527	0.119	0.757	0.836
				0.605	0.238	0.778	0.956
				0.642	0.358	0.781	1.076
				0.681	0.477	0.734	1.195
				0.704	0.597		
0.0075	2.86	4360	793,000	0.393	0.000	0.619	0.439
				0.421	0.024	0.629	0.488
				0.475	0.049	0.644	0.536
				0.490	0.073	0.651	0.586
				0.500	0.098	0.658	0.634
				0.510	0.122	0.667	0.683
				0.517	0.146	0.675	0.732
				0.528	0.171	0.675	0.781
				0.549	0.195	0.689	0.830
				0.556	0.220	0.694	0.878
				0.567	0.244	0.697	0.927
				0.575	0.268	0.720	0.976
				0.583	0.293	0.724	1.025
				0.592	0.317	0.729	1.074
				0.599	0.342	0.728	1.122
				0.603	0.366	0.735	1.171
				0.609	0.390	0.740	1.220

Table 8. Continued

t (in.)	R_i (in.)	ζ	E (psi)	$\frac{P - \pi R_i^2 p}{2\pi E t^2 \cos^2 \alpha}$	$\frac{P}{E}\left(\frac{R_i/\cos\alpha}{t}\right)^2$	$\frac{P - \pi R_i^2 p}{2\pi E t^2 \cos^2 \alpha}$	$\frac{P}{E}\left(\frac{R_i/\cos\alpha}{t}\right)^2$
(b) $\alpha = 30^\circ$							
0.0075	2.90	4430	793,000	0.436	0.000	0.615	0.452
				0.477	0.025	0.623	0.502
				0.502	0.050	0.637	0.552
				0.509	0.075	0.664	0.602
				0.516	0.100	0.667	0.653
				0.532	0.126	0.671	0.703
				0.542	0.151	0.674	0.753
				0.548	0.176	0.683	0.803
				0.556	0.201	0.691	0.853
				0.562	0.226	0.699	0.904
				0.573	0.251	0.702	0.954
				0.576	0.276	0.706	1.004
				0.582	0.301	0.709	1.054
				0.588	0.326	0.717	1.104
				0.599	0.351	0.716	1.155
				0.601	0.376	0.729	1.205
				0.607	0.402	0.727	1.255
0.0050	2.04	4710	750,000	0.212	0.000	0.593	0.473
				0.337	0.052	0.613	0.525
				0.337	0.104	0.633	0.577
				0.433	0.158	0.653	0.630
				0.503	0.262	0.668	0.683
				0.527	0.315	0.672	0.736
				0.553	0.367	0.676	0.788
				0.569	0.420		
0.0050	2.10	4810	662,000	0.271	0.000	0.591	0.640
				0.346	0.036	0.600	0.711
				0.439	0.071	0.611	0.782
				0.452	0.107	0.623	0.853
				0.462	0.142	0.634	0.924
				0.472	0.178	0.649	0.995
				0.478	0.213	0.692	1.066
				0.491	0.249	0.701	1.137
				0.485	0.284	0.704	1.208
				0.507	0.320	0.713	1.279
				0.512	0.355	0.720	1.350
				0.523	0.391	0.738	1.421
				0.528	0.426	0.748	1.492
				0.551	0.462	0.753	1.563
				0.559	0.497	0.748	1.634
				0.573	0.533	0.748	1.705
				0.577	0.569	0.715	1.777
0.0030	1.55	5920	775,000	0.134	0.000	0.624	0.783
				0.215	0.049	0.628	0.881
				0.345	0.098	0.641	0.979
				0.415	0.195	0.622	1.176
				0.468	0.294	0.656	1.370
				0.506	0.392	0.582	1.567
				0.546	0.489	0.691	1.762
				0.585	0.587		
				0.620	0.686		
0.0050	2.82	6450	718,000	0.225	0.000	0.656	0.767
				0.396	0.059	0.662	0.826
				0.455	0.118	0.670	0.885
				0.481	0.177	0.685	0.944
				0.497	0.236	0.703	1.062
				0.508	0.295	0.721	1.181
				0.530	0.354	0.727	1.299
				0.551	0.413	0.739	1.417
				0.570	0.472	0.743	1.535
				0.585	0.531	0.751	1.653
				0.599	0.590	0.751	1.771
				0.627	0.649	0.739	1.889
				0.640	0.708	0.721	2.007
0.0050	2.88	6590	709,000	0.295	0.000	0.693	0.870
				0.378	0.063	0.711	0.941
				0.437	0.125	0.732	1.003
				0.488	0.188	0.760	1.129
				0.522	0.251	0.769	1.254
				0.544	0.314	0.785	1.379
				0.568	0.376	0.779	1.505
				0.579	0.439	0.810	1.630
				0.591	0.502	0.830	1.756
				0.608	0.564	0.843	1.881
				0.634	0.627	0.852	2.007
				0.642	0.690	0.849	2.134
				0.653	0.752	0.819	2.257
				0.687	0.815		

Table 8. Continued

t (in.)	R_1 (in.)	ζ	K (psi)	$\frac{P \cdot \nu R_1^2 P}{2\pi E t^2 \cos^2 \alpha}$	$\frac{P}{E}\left(\frac{R_1/\cos\alpha}{t}\right)^2$	$\frac{P \cdot \nu R_1^2 P}{2\pi E t^2 \cos^2 \alpha}$	$\frac{P}{E}\left(\frac{R_1/\cos\alpha}{t}\right)^2$
				(c) α = 45°			
0.010	1.28	597	685,000	0.308	0	0.425	0.124
				0.317	0.005	0.438	0.133
				0.307	0.010	0.443	0.143
				0.312	0.014	0.456	0.152
				0.310	0.019	0.464	0.162
				0.314	0.024	0.470	0.171
				0.320	0.029	0.480	0.181
				0.322	0.033	0.485	0.191
				0.324	0.038	0.494	0.200
				0.329	0.043	0.504	0.210
				0.332	0.048	0.517	0.219
				0.338	0.052	0.527	0.229
				0.339	0.057	0.534	0.238
				0.343	0.062	0.552	0.248
				0.347	0.067	0.566	0.286
				0.352	0.071	0.582	0.310
				0.353	0.076	0.595	0.333
				0.359	0.086	0.604	0.357
				0.389	0.095	0.613	0.381
				0.404	0.105	0.623	0.405
				0.416	0.1 4		
0.010	1.29	601	685,000	0.400	0	0.534	0.125
				0.424	0.005	0.541	0.145
				0.423	0.010	0.556	0.154
				0.418	0.014	0.565	0.164
				0.434	0.019	0.559	0.174
				0.440	0.024	0.569	0.183
				0.443	0.029	0.573	0.193
				0.450	0.034	0.586	0.203
				0.459	0.039	0.589	0.212
				0.452	0.043	0.600	0.222
				0.471	0.048	0.609	0.231
				0.465	0.053	0.614	0.241
				0.467	0.058	0.637	0.265
				0.485	0.063	0.655	0.289
				0.477	0.068	0.668	0.313
				0.487	0.072	0.691	0.338
				0.491	0.077	0.707	0.362
				0.498	0.087	0.704	0.386
				0.502	0.096	0.716	0.410
				0.507	0.106	0.725	0.434
				0.518	0.116	0.730	0.458
				0.524	0.125	0.739	0.482
0.010	1.79	835	685,000	0.274	0	0.622	0.261
				0.324	0.005	0.640	0.280
				0.344	0.019	0.645	0.299
				0.351	0.028	0.664	0.317
				0.367	0.037	0.673	0.336
				0.381	0.047	0.678	0.355
				0.401	0.056	0.682	0.373
				0.417	0.065	0.696	0.39
				0.428	0.075	0.696	0.
				0.439	0.084	0.703	0.429
				0.453	0.094	0.710	0.448
				0.462	0.102	0.713	0.467
				0.474	0.112	0.728	0.514
				0.487	0.121	0.756	0.560
				0.493	0.130	0.763	0.607
				0.507	0.140	0.761	0.654
				0.514	0.149	0.772	0.700
				0.532	0.168	0.770	0.747
				0.548	0.186	0.770	0.794
				0.569	0.205	0.774	0.841
				0.585	0.224	0.774	0.887
				0.613	0.243	0.770	0.934
0.010	1.85	865	685,000	0.316	0	0.476	0.180
				0.371	0.010	0.480	0.200
				0.396	0.020	0.494	0.220
				0.417	0.030	0.502	0.240
				0.421	0.040	0.515	0.260
				0.430	0.050	0.524	0.280
				0.436	0.060	0.528	0.300
				0.439	0.070	0.539	0.320
				0.441	0.080	0.545	0.340
				0.442	0.090	0.560	0.360
				0.447	0.100	0.572	0.380
				0.451	0.110	0.584	0.400
				0.460	0.120	0.594	0.420
				0.458	0.130	0.602	0.441
				0.454	0.140	0.611	0.461
				0.464	0.150	0.619	0.481
				0.468	0.160	0.630	0.501
0.008	1.19	1110	700,000	0.236	0	0.613	0.304
				0.428	0.016	0.627	0.325
				0.455	0.032	0.648	0.350
				0.462	0.048	0.661	0.390
				0.472	0.065	0.671	0.423
				0.483	0.084	0.676	0.456
				0.494	0.097	0.691	0.488
				0.508	0.113	0.708	0.520
				0.511	0.130	0.714	0.553
				0.525	0.146	0.725	0.586
				0.532	0.162	0.734	0.618
				0.543	0.179	0.749	0.650
				0.547	0.195	0.756	0.683
				0.569	0.211	0.753	0.715
				0.571	0.227	0.763	0.748
				0.580	0.244	0.760	0.781
				0.586	0.260	0.769	0.813

Table 8. Continued

t (in.)	R_1 (in.)	ζ	E (psi)	$\frac{P \cdot \pi R_1^2 p}{2\pi E t^2 \cos^2 \alpha}$	$\frac{P}{E}\left(\frac{R_1/\cos\alpha}{t}\right)^2$	$\frac{P \cdot \pi R_1^2 p}{2\pi E t^2 \cos^2 \alpha}$	$\frac{P}{E}\left(\frac{R_1/\cos\alpha}{t}\right)^2$
				(c) α = 45°			
0.005	1.26	118	760,000	0.323	0	0.573	0.324
				0.376	0.018	0.598	0.360
				0.382	0.036	0.609	0.396
				0.387	0.054	0.696	0.432
				0.400	0.072	0.674	0.468
				0.391	0.090	0.693	0.504
				0.416	0.108	0.711	0.540
				0.420	0.126	0.711	0.576
				0.432	0.144	0.725	0.612
				0.449	0.162	0.740	0.648
				0.472	0.180	0.774	0.684
				0.489	0.198	0.773	0.720
				0.498	0.216	0.774	0.756
				0.515	0.234	0.794	0.793
				0.534	0.252	0.813	0.829
				0.536	0.270	0.811	0.865
				0.547	0.288	0.811	0.901
0.010	2.94	137	685,000	0.386	0	0.762	0.706
				0.454	0.025	0.769	0.757
				0.440	0.050	0.781	0.807
				0.520	0.075	0.789	0.858
				0.540	0.100	0.786	0.908
				0.559	0.126	0.784	0.959
				0.566	0.151	0.796	1.009
				0.581	0.176	0.781	1.060
				0.594	0.201	0.778	1.110
				0.602	0.227	0.772	1.161
				0.612	0.252	0.763	1.211
				0.623	0.277	0.777	1.262
				0.636	0.302	0.760	1.388
				0.644	0.328	0.753	1.514
				0.648	0.353	0.764	1.640
				0.658	0.378	0.734	1.767
				0.663	0.403	0.722	1.893
				0.702	0.454	0.715	2.019
				0.717	0.504	0.702	2.145
				0.726	0.555	0.691	2.271
				0.739	0.605	0.692	2.398
				0.755	0.656	0.690	2.524
0.010	2.96	1380	585,000	0.466	0	0.771	0.716
				0.521	0.025	0.792	0.767
				0.541	0.051	0.796	0.818
				0.554	0.076	0.813	0.870
				0.558	0.102	0.813	0.921
				0.578	0.127	0.822	0.972
				0.581	0.153	0.827	1.023
				0.587	0.179	0.824	1.074
				0.604	0.204	0.758	1.125
				0.615	0.230	0.824	1.177
				0.629	0.255	0.817	1.228
				0.639	0.281	0.815	1.279
				0.647	0.307	0.821	1.407
				0.659	0.332	0.817	1.535
				0.671	0.358	0.814	1.663
				0.679	0.383	0.810	1.791
				0.688	0.409	0.802	1.919
				0.707	0.460	0.796	2.047
				0.727	0.511	0.783	2.175
				0.741	0.562	0.754	2.303
				0.750	0.614	0.760	2.430
				0.762	0.665	0.754	2.558
0.005	2.08	1940	720,000	0.325	0	0.801	1.098
				0.504	0.048	0.806	1.155
				0.509	0.096	0.808	1.251
				0.525	0.144	0.808	1.347
				0.555	0.192	0.812	1.443
				0.576	0.240	0.805	1.540
				0.606	0.288	0.829	1.636
				0.626	0.336	0.826	1.732
				0.635	0.385	0.822	1.829
				0.665	0.433	0.822	1.925
				0.681	0.481	0.831	2.021
				0.704	0.529	0.836	2.117
				0.714	0.577	0.842	2.213
				0.715	0.625	0.847	2.310
				0.732	0.673	0.849	2.406
				0.739	0.721	0.836	2.502
				0.746	0.770	0.843	2.598
				0.771	0.866	0.836	2.788
				0.790	0.962	0.831	2.979
						0.826	3.169
0.005	2.91	272	720,000	0.390	0	0.781	1.686
				0.438	0.093	0.790	1.873
				0.489	0.187	0.779	2.061
				0.521	0.281	0.790	2.248
				0.555	0.374	0.796	2.436
				0.578	0.468	0.802	2.623
				0.611	0.562	0.815	2.810
				0.626	0.655	0.813	2.998
				0.649	0.748	0.817	3.185
				0.673	0.843	0.817	3.372
				0.723	0.936	0.813	3.560
				0.707	1.030	0.808	3.747
				0.730	1.124	0.820	3.935
				0.755	1.218	0.819	4.122
				0.758	1.311	0.847	4.309
				0.770	1.405	0.828	4.497
				0.772	1.499		

Table 8. Continued

t (in.)	R_1 (in.)	ζ	E (psi)	$\frac{P \cdot \pi R_1^2 p}{2\pi E t^2 \cos^2 \alpha}$	$\frac{p}{E}\left(\frac{R_1/\cos\alpha}{t}\right)^2$	$\frac{P \cdot \pi R_1^2 p}{2\pi E t^2 \cos^2 \alpha}$	$\frac{p}{E}\left(\frac{R_1/\cos\alpha}{t}\right)^2$
(c) $\alpha = 45^\circ$							
0.005	2.93	274	720,000	0.336	0	0.785	1.916
				0.435	0.096	0.790	2.108
				0.435	0.192	0.797	2.299
				0.466	0.287	0.790	2.491
				0.521	0.383	0.786	2.682
				0.562	0.479	0.794	2.874
				0.594	0.575	0.785	3.066
				0.611	0.671	0.783	3.257
				0.641	0.766	0.767	3.449
				0.666	0.862	0.769	3.640
				0.686	0.958	0.776	3.832
				0.709	1.054	0.769	4.024
				0.721	1.150	0.783	4.215
				0.737	1.245	0.779	4.407
				0.749	1.341	0.783	4.598
				0.765	1.437	0.776	4.790
				0.774	1.533	0.763	5.269
				0.772	1.724		

Table 8. Concluded

t (in.)	R_1 (in.)	ν	E psi	$\frac{P_{cr} R_1^2}{2\pi E t^2 \cos^2 \alpha}$	$\frac{p}{E}\left(\frac{R_1/\cos\alpha}{t}\right)^2$	$\frac{P_{cr} R_1^2 p}{2\pi E t^2 \cos^2 \alpha}$	$\frac{p}{E}\left(\frac{R_1/\cos\alpha}{t}\right)^2$
				(ϕ) α = 60°			
0.0075	1.74	511	770,000	0.331	0	0.749	0.403
				0.405	0.028	0.758	0.559
				0.431	0.056	0.765	0.615
				0.442	0.084	0.784	0.671
				0.460	0.112	0.792	0.727
				0.485	0.139	0.793	0.783
				0.492	0.168	0.796	0.839
				0.518	0.196	0.804	0.895
				0.539	0.224	0.830	0.951
				0.547	0.252	0.834	1.007
				0.603	0.280	0.839	1.063
				0.643	0.307	0.845	1.118
				0.666	0.336	0.853	1.174
				0.686	0.364	0.855	1.230
				0.711	0.391	0.864	1.286
				0.718	0.419	0.872	1.342
				0.734	0.447	0.874	1.398
0.010	2.33	515	700,000	0.382	0	0.750	0.421
				0.449	0.032	0.762	0.456
				0.469	0.064	0.767	0.516
				0.489	0.097	0.778	0.518
				0.498	0.129	0.779	0.583
				0.533	0.162	0.787	0.648
				0.594	0.194	0.789	0.713
				0.627	0.227	0.799	0.778
				0.655	0.259	0.799	0.842
				0.684	0.292	0.803	0.907
				0.702	0.324	0.806	0.972
				0.722	0.356	0.810	1.036
				0.733	0.388	0.809	1.100
0.0075	2.53	743	778,000	0.349	0	0.805	1.053
				0.427	0.059	0.812	1.170
				0.477	0.117	0.840	1.287
				0.501	0.175	0.843	1.404
				0.537	0.234	0.839	1.521
				0.595	0.293	0.825	1.638
				0.627	0.351	0.844	1.755
				0.654	0.410	0.853	1.872
				0.682	0.468	0.853	1.989
				0.709	0.527	0.853	2.106
				0.737	0.585	0.852	2.223
				0.756	0.644	0.846	2.340
				0.791	0.702	0.844	2.457
				0.802	0.761	0.851	2.574
				0.808	0.819	0.849	2.691
				0.812	0.878	0.843	2.808
				0.812	0.936	0.850	2.925
0.005	1.71	735	700,000	0.379	0	0.670	0.778
				0.441	0.065	0.675	1.036
				0.471	0.130	0.667	1.296
				0.487	0.194	0.714	1.426
				0.507	0.259	0.758	1.555
				0.547	0.324	0.778	1.685
				0.582	0.454	0.800	1.814
				0.597	0.583		
0.005	1.74	782	730,000	0.332	0	0.742	0.664
				0.455	0.067	0.751	0.732
				0.531	0.133	0.753	0.800
				0.651	0.200	0.764	0.865
				0.652	0.265	0.776	0.931
				0.678	0.333	0.784	1.000
				0.701	0.401	0.787	1.065
				0.709	0.449	0.800	1.190
				0.714	0.532	0.821	1.325
				0.722	0.598	0.846	1.500
0.005	2.43	1090	700,000	0.447	0.134	0.744	1.876
				0.567	0.268	0.748	2.010
				0.616	0.402	0.752	2.144
				0.658	0.536	0.771	2.412
				0.662	0.804	0.804	2.680
				0.671	0.938	0.823	2.948
				0.672	1.072	0.841	3.216
				0.678	1.206	0.852	3.484
				0.704	1.340	0.886	3.752
				0.726	1.474	0.903	4.020
				0.732	1.608	0.914	4.288
				0.737	1.742		
0.005	2.43	1090	700,000	0.492	0	0.507	1.742
				0.574	0.134	0.810	1.876
				0.636	0.268	0.817	2.010
				0.675	0.402	0.818	2.144
				0.711	0.536	0.872	2.412
				0.746	0.670	0.895	2.948
				0.767	0.938	0.906	3.216
				0.775	1.206	0.906	3.484
				0.798	1.340	0.923	3.752
				0.807	1.474	0.948	4.020
				0.798	1.608	0.944	4.288

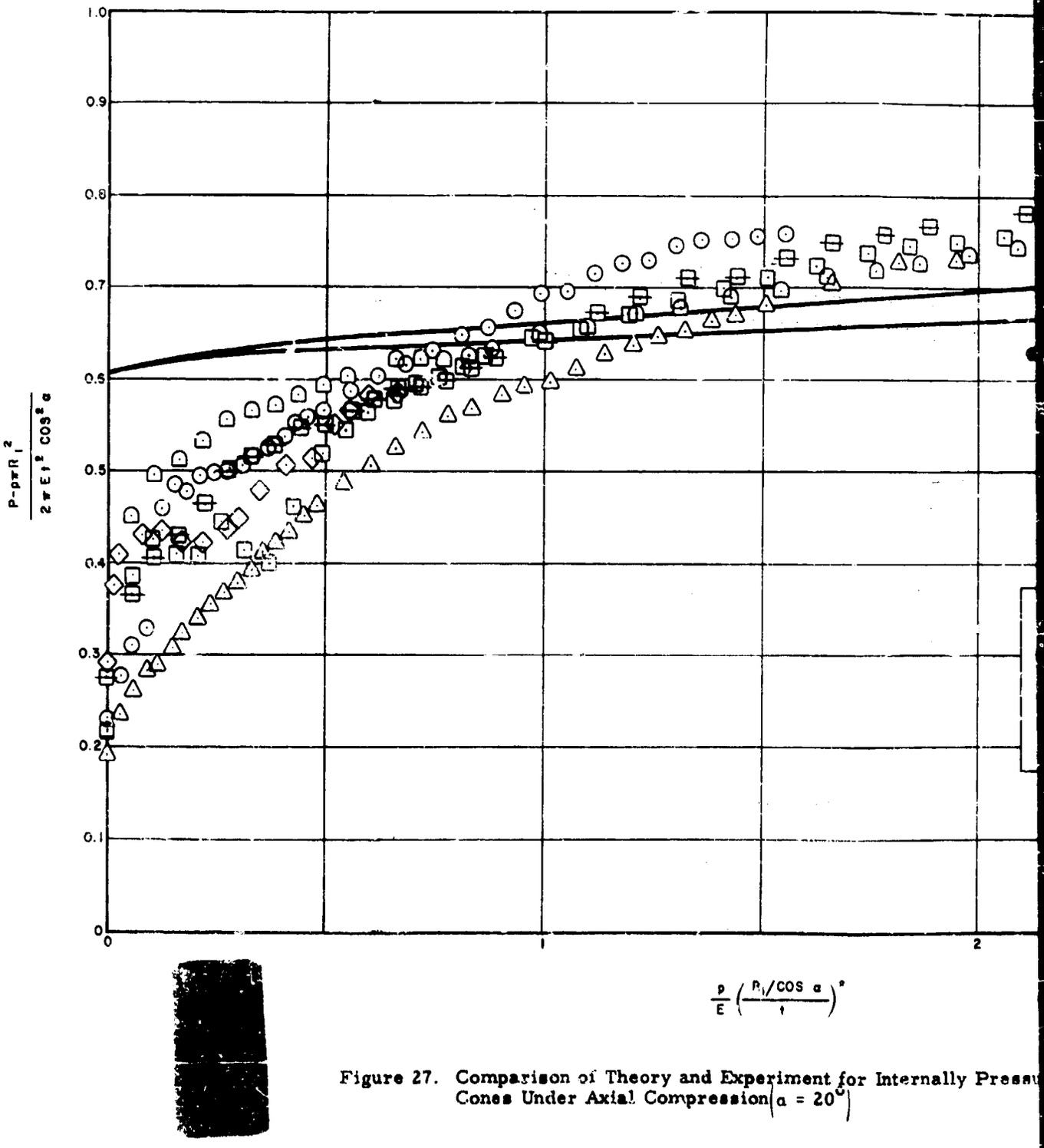

Figure 27. Comparison of Theory and Experiment for Internally Pressu
Cones Under Axial Compression ($\alpha = 20^\circ$)

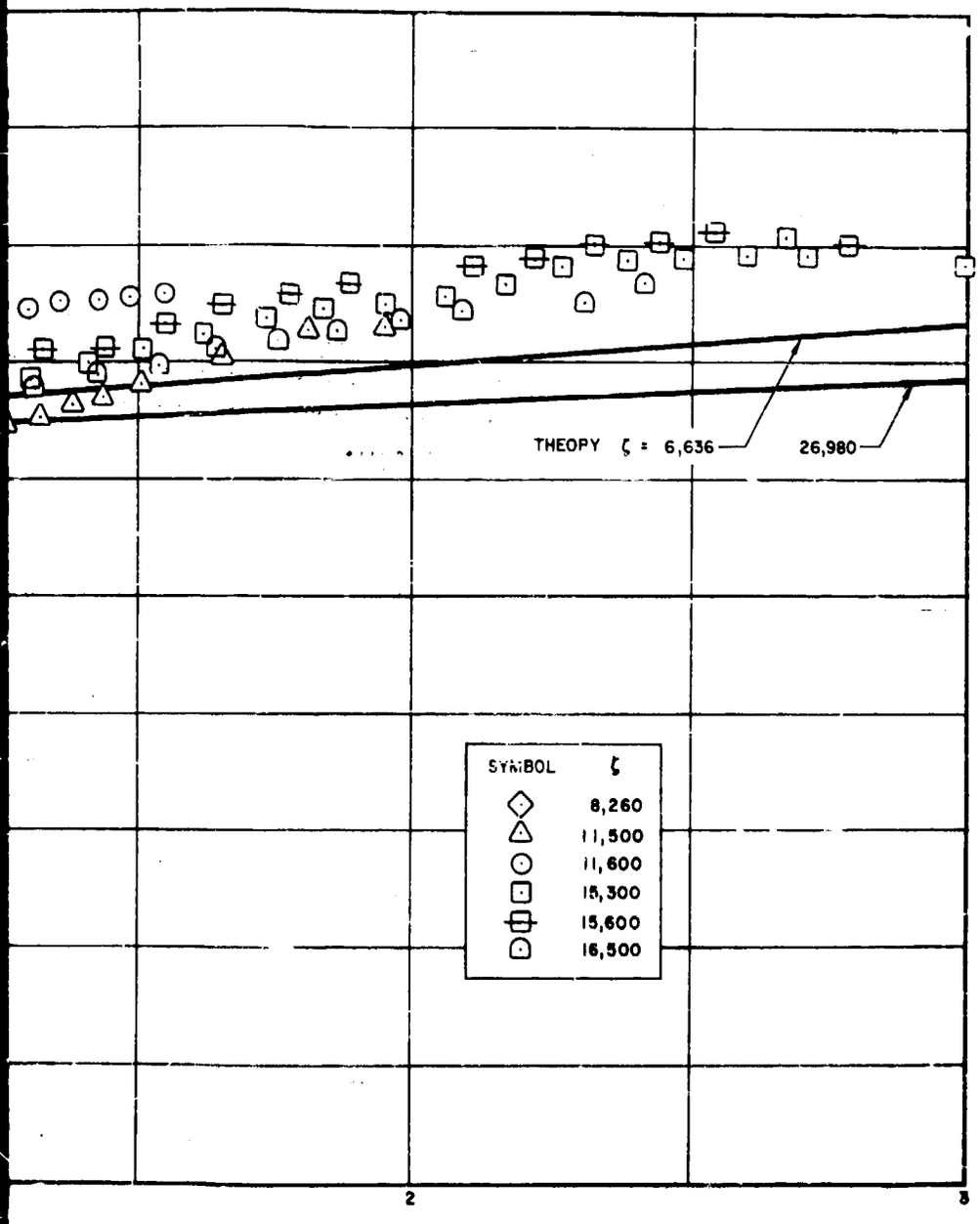

$$\frac{p}{E}\left(\frac{R_1/\cos\alpha}{t}\right)^2$$

y and Experiment for Internally Pressured
ompression ($\alpha = 20^\circ$)

2

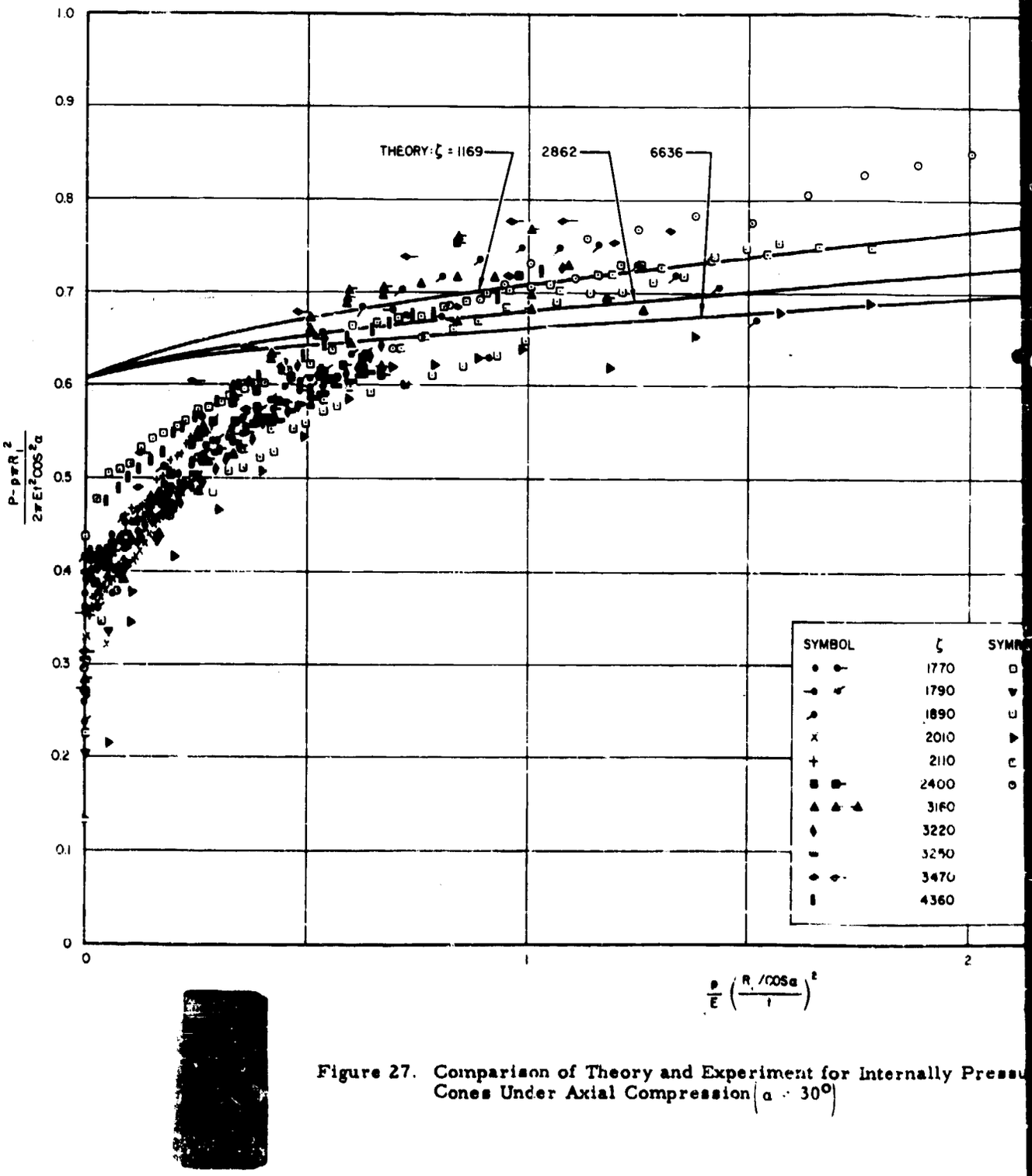

Figure 27. Comparison of Theory and Experiment for Internally Pressu
Cones Under Axial Compression ($\alpha = 30^\circ$)

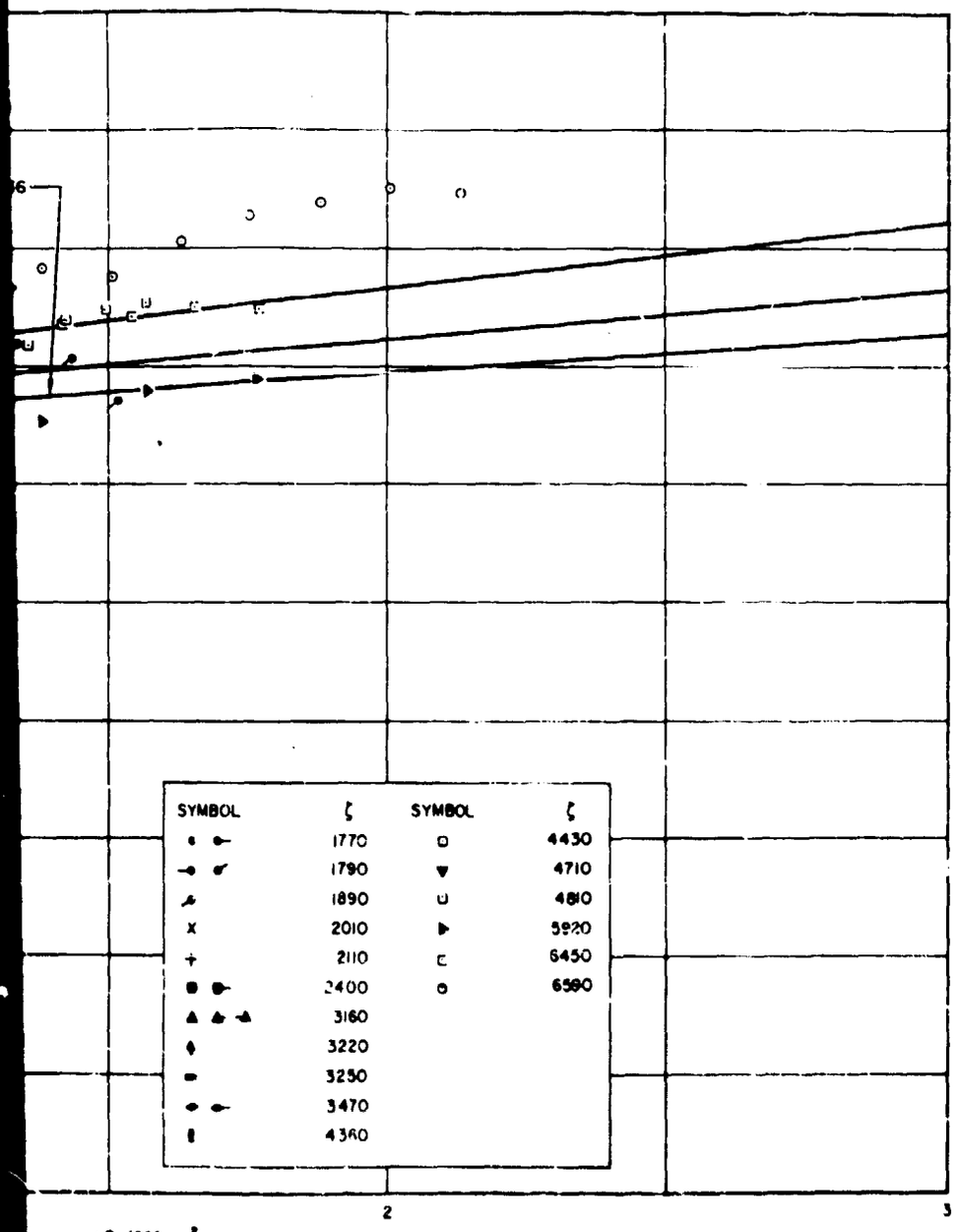

$\frac{p}{E}\left(\frac{R_i/\cos\alpha}{t}\right)^2$

d Experiment for L ernally Pressured
ression $(\alpha = 30^\circ)$

2

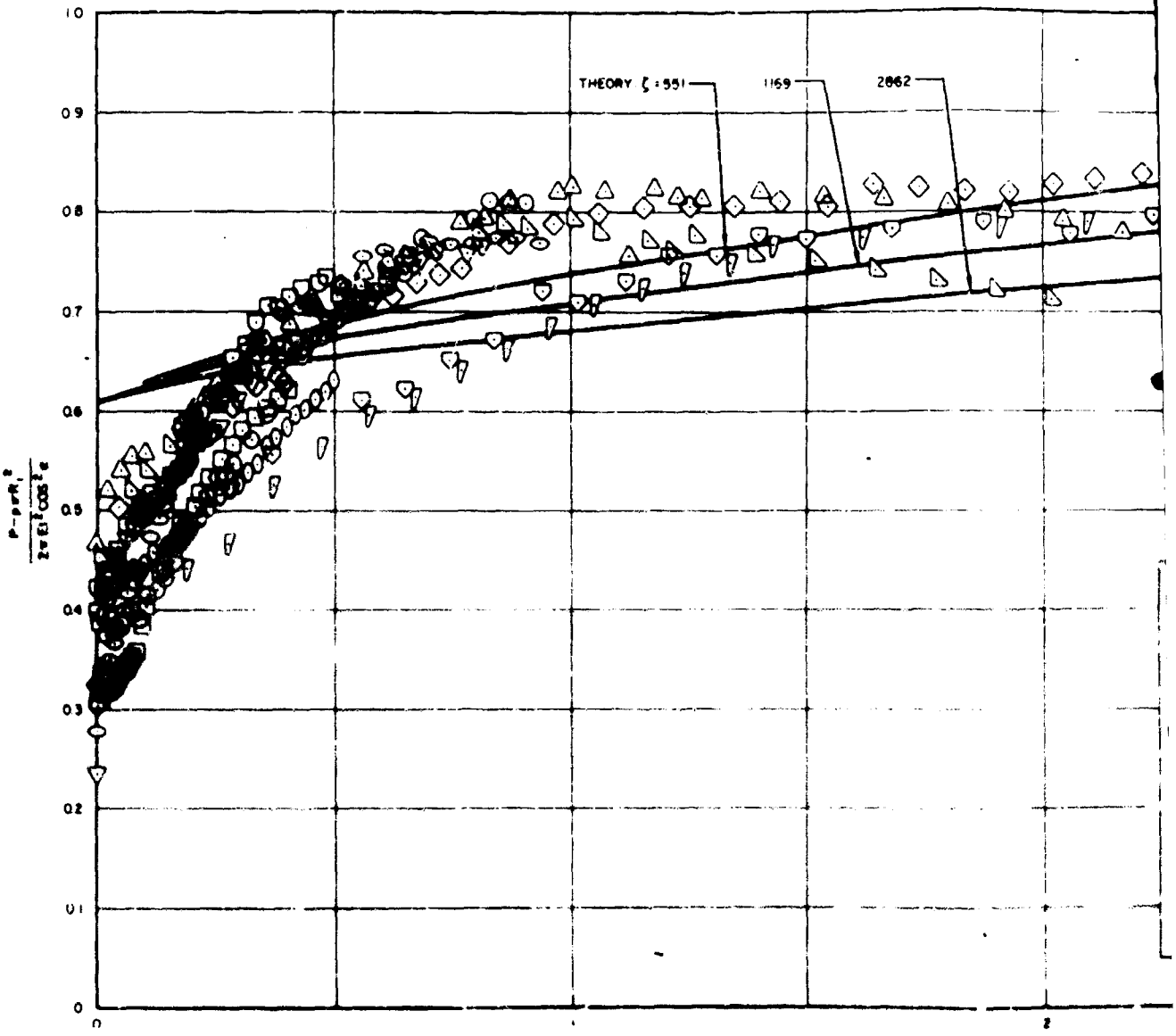

Figure 27. Comparison of Theory
Cones Under Axial Co

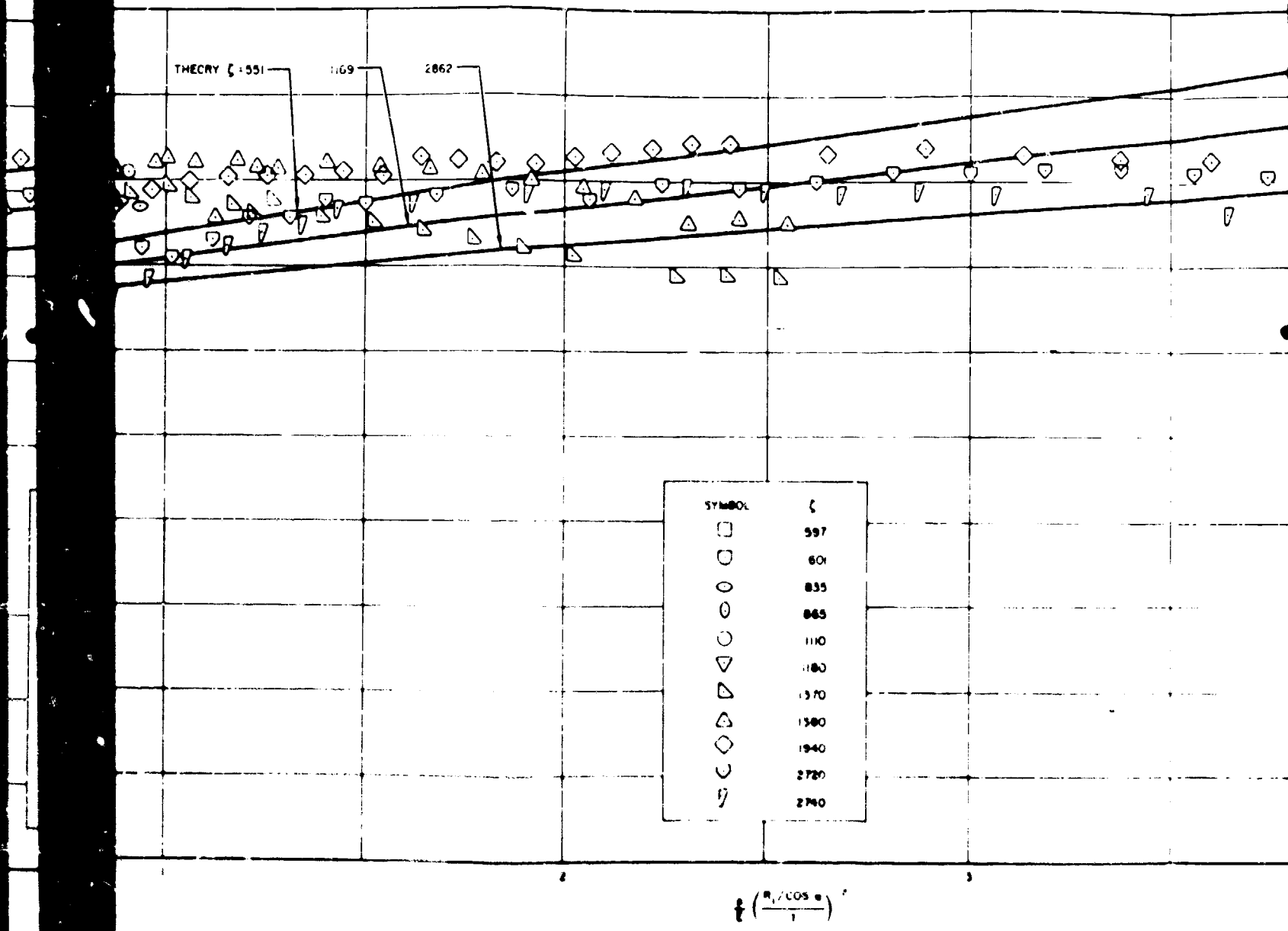

Figure 27. Comparison of Theory and Experimental for Internally Pressured Cones Under Axial Compression ($\alpha = 45^\circ$)

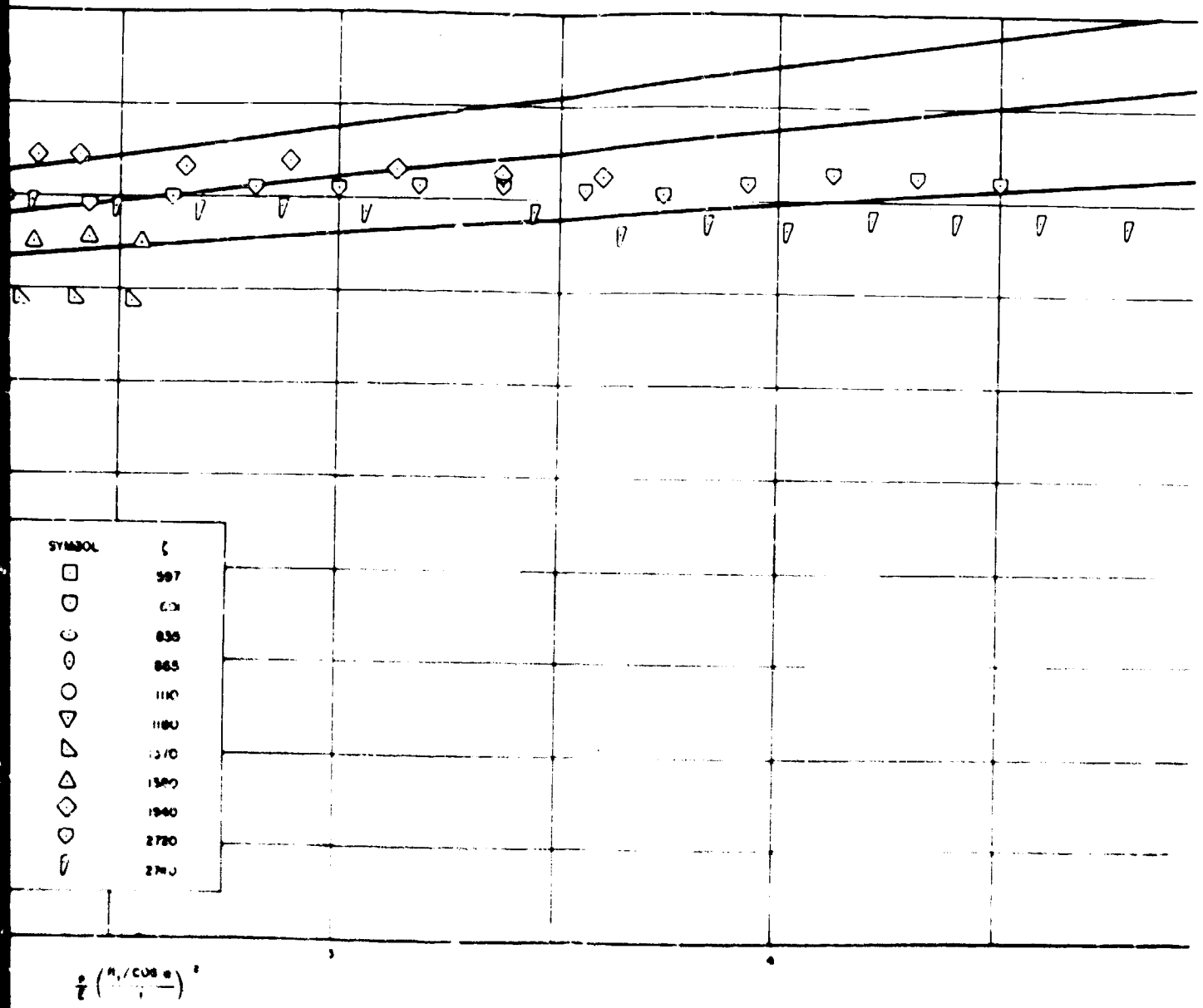

and Experimental for Internally Pressured
mpression ($\alpha = 45^{0}$)

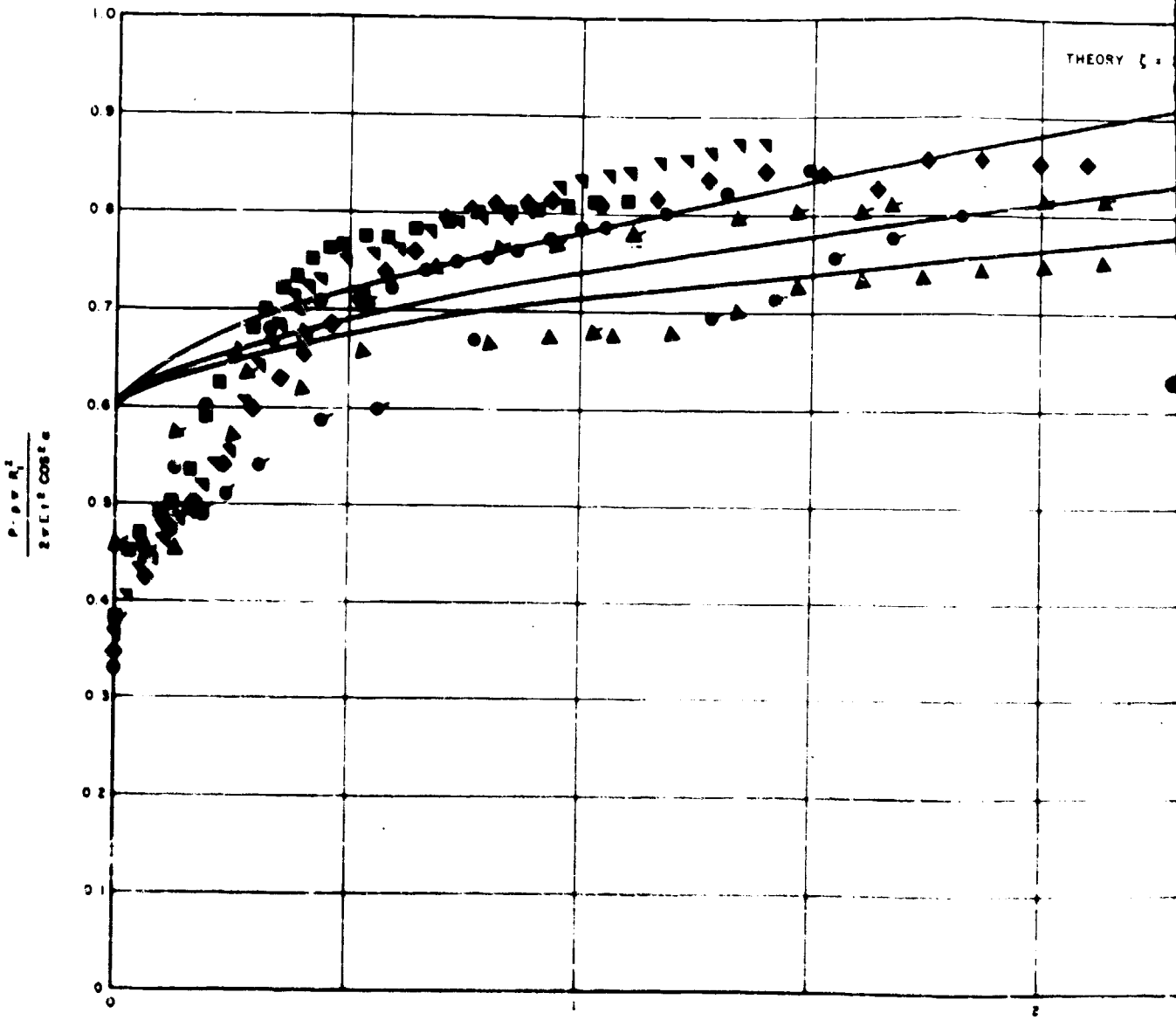

Figure 27. Comparison of Theory and
Cones Under Axial Compr

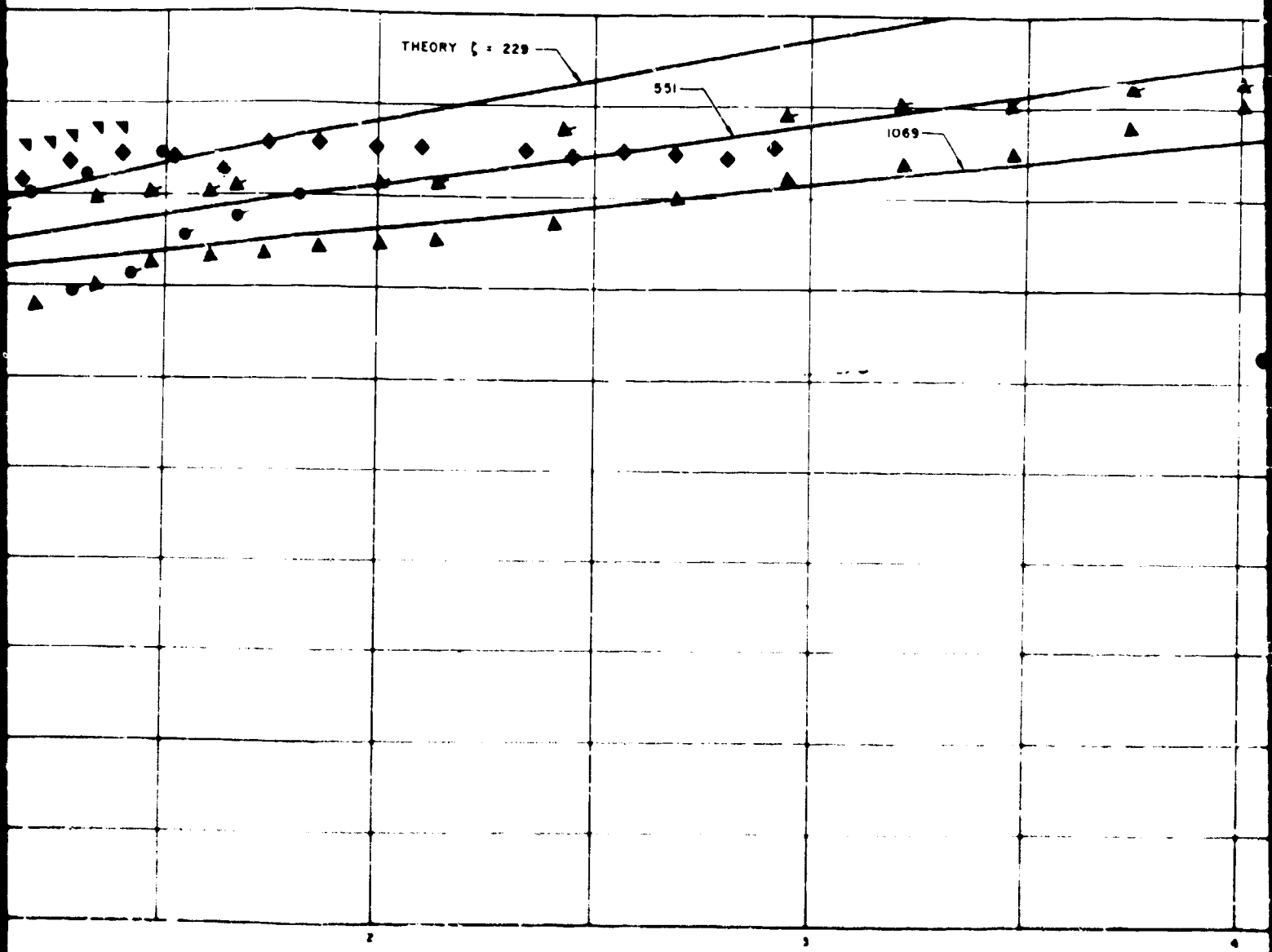

Figure 27. Comparison of Theory and Experiment for Internally Pressured Cones Under Axial Compression ($\alpha = 60^\circ$)

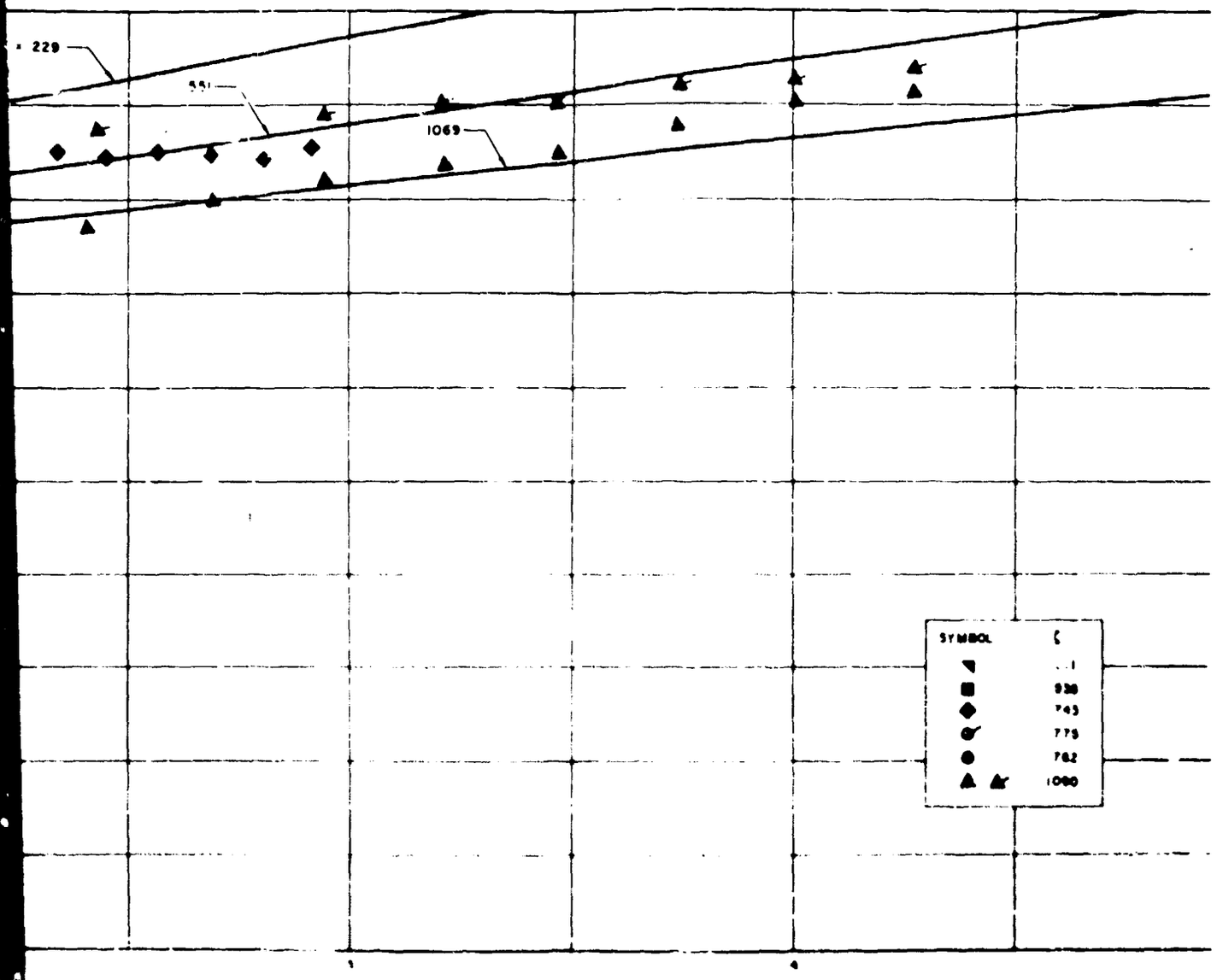

$$\frac{\sigma}{\gamma}\left(\cdot\frac{\theta_1/\cos\theta}{1}\right)^2$$

nd Experiment for Internally Pressured
ression ($\alpha = 60^\circ$)

(a) $\bar{p} = 0$

(b) $\bar{p} = 0.27$

(c) $\bar{p} = 1.09$

Figure 28. Typical Variation of Axial Compression Buckle Pattern with Increasing Internal Pressure for Conical Shells

(d) $\bar{p}$ = 1.63

(e) $\bar{p}$ = 2.17

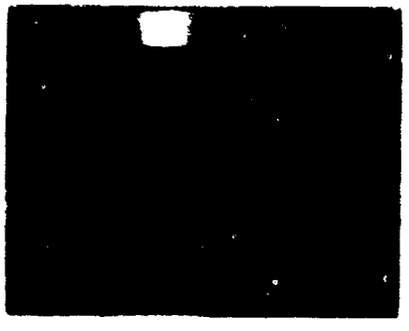

(f) $\bar{p}$ = 2.71

Figure 28. Concluded

VIII. CYLINDERS AND TRUNCATED CONES UNDER PURE BENDING

The design of cylindrical shells in bending, like that of cylinders in compression, is in an inconclusive state at the present time. It is only recently (see Reference 33) that small-deflection theory for this loading condition has been fully solved, reliance having been previously placed on an incomplete result due to Flugge (Reference 9). According to small-deflection theory the critical maximum compressive stress due to bending is approximately equal to that for axial compression, or

$$C_b = \frac{M}{\pi E R t^2} \approx \frac{1}{\sqrt{3(1-\nu^2)}} \quad . \tag{10}$$

Experimental results obtained to date are lower than this classic value, but higher than results for the case of axial compression. No large-deflection analysis exists to show whether the increase in stress is or is not an inherent characteristic of cylinders in bending, but certain conjectures have been made to explain both the large scatter of bending results and the increase over axial compression results.

The experimental buckle patterns for cylinders in bending (Figure 29) are very much like those obtained in axial compression. It therefore appears reasonable to assume that the theoretical post-buckling behavior under both loading conditions is similar and that initial imperfections and other factors discussed in Section V are significant for both. (See, however, Section XIII.) The stress distribution varies circumferentially in the case of bending, however, so that the shells have a preferred region of buckling. The lower probability of imperfections occurring within this region would lead one to expect stress coefficients in bending that, on the average, are higher than those for compression.*

*This explanation was suggested by Prof. B. Budiansky in commenting on Reference 33.

For conical shells, bending represents a completely unexplored loading condition. Since no theoretical solution exists, investigations must be guided primarily by the facts known about cylinders and cones in compression and about cylinders in bending. The bending test program reported in this section was intended to provide additional data for cylinders in bending and to provide data for at least establishing a tentative method for the design of conical shells in bending.

A. Results for Cylinders

The experimental data for cylinders are given in part (a) of Tables 9 and 10. It can be seen that the magnitudes of the critical bending moment coefficients are considerably higher than those for axial compression. The data are plotted in Figure 30 together with experimental results obtained by other investigators (Reference 5, 30, 34, 35, and 36). Some of the data in the literature, namely that of References 13 and 17, have been omitted, since the results were not in agreement with either those of the present program or with those of the other investigations. It is suspected that the cylinder wall thicknesses reported in Reference 13 were too small to permit easy handling and resulted in significantly inferior specimens. The data of Reference 17 are suspect since the specimens were subjected to plastic damage in previous tests of the same specimens. The various test results cover the range of radius-thickness ratios less than 2000. The only available data for a larger radius-thickness ratio (Reference 35) are not plotted since they were obtained from very thin-walled specimens and are not in accord with the trend established by the other data.

It can be seen that the remaining data are in relatively good agreement and define a smooth, consistent lower bound curve. A good representation of this lower bound, interestingly enough, can be obtained by a slight modification of the lower bound curve defined for axial compression as

$$C_b = \frac{M}{\pi E R t^2} = 0.606 - 0.443 \left(1 - e^{-\frac{1}{16}\sqrt{\frac{R}{t}}}\right) \qquad (11)$$

which is shown in Figure 33. Also shown is the coefficient given by Equation (4) multiplied by a factor of 1.3, which has been suggested in the literature. The agreement of this curve with the test data is poor.

B. Results for Cones

Before presenting the experimental data for conical shells in bending, it is necessary to discuss the parameter used as a critical bending moment coefficient. The theoretical results of Reference 33 for cylinders in bending indicate that the predicted buckle wavelength is small and that the maximum compressive bending stress should be approximately equal to the critical axial compressive stress. The results of Reference 24, for conical shells in axial compression, indicate that the critical local meridional stress is equal to the critical compressive stress of a cylinder having the same wall thickness and the same local radius of curvature. It is also known that stresses in cones under bending decrease in the longitudinal direction at a rate much faster than do the corresponding stresses in axially compressed cones. It appears reasonable, therefore to hypothesize that small-deflection theory for conical shells in bending would predict that buckling occurs when the maximum meridional compressive stress, at or near the small cross section of the cone, is equal to the critical compressive stress of a cylinder having the same wall thickness and the same local radius of curvature. Thus utilizing the membrane theory of shells, we predict that the classic buckling moment coefficient is given by

$$C_b = \frac{\sigma_{max}}{Et/\rho_i} = \frac{M}{\pi E t^2 R_1 \cos^2\alpha} \cdot \frac{1}{3(1-\nu^2)} \qquad (12)$$

It may very well be that the theoretical buckling coefficient is a function of the parameter ζ suggested by the work on cones under axial compression and internal pressure, since the theoretical buckled shape can be

expected to be concentrated in the vicinity of the small radius because of the rapid drop-off in stress, and of the semivertex angle α itself since the membrane stress state also consists of a shearing stress distribution which increases in importance as the semivertex angle increases. Actual buckle patterns for conical shells (Figure 29) are not very much different from those for cylinders, however. In the absence of an analytical solution of this problem, it is difficult to ascertain the important parameters in view of the large number of tests that would be required. Thus, about all that can be done at the present time is to see if experimental values of C_b, defined by Equation (12) and plotted against ρ_1/t for the conical shells, fall within the scatterbands defined by the cylinder results.

The experimental data are presented in Table 9 and 10 and are plotted in terms of the parameters C_b and ρ_1/t in Figure 31. Also shown is the lower bound curve suggested by the cylinder results. It is evident that most of the cone data lie above the lower bound curve and reasonably well within the scatterband established by the cylinder results. A study of the data indicates that the length of the conical shell may be a significant parameter, but there is insufficient data to firmly establish this trend. It would be helpful in future test programs to construct specimens with a fixed small radius, rather than the large radius, and to comprehensively study the effects of variations of length, wall thickness, and semivertex angle within the framework of the discussion given above.

Table 9. Experimental Data for Mylar Cones and Cylinders in Pure Bending

t (in)	$E \times 10^{-3}$ (psi)	$\frac{\rho_1}{t}$	$\frac{\ell}{\rho_1}$	$\frac{M}{\pi E t^2 R_1 \cos^2 \alpha}$
(a) $\alpha = 0^\circ$				
0.0100	690	400	0.875	0.331
0.0100	690	100	12.0	0.404
0.0100	690	100	12.0	0.395
0.0100	690	100	10.0	0.448
0.0100	690	100	6.0	0.476
0.0100	690	100	6.0	0.500
0.0100	690	100	6.0	0.480
0.0100	690	100	4.0	0.504
0.0100	690	100	4.0	0.536
0.0100	690	100	2.0	0.468
0.0100	690	100	2.0	0.456
0.0100	690	100	1.0	0.487
0.0100	690	100	1.0	0.512
0.0100	690	100	1.0	0.545
0.0080	725	125	1.0	0.528
0.0080	725	125	1.0	0.523
0.0080	725	125	1.0	0.508
0.0050	750	800	2.0	0.320
0.0050	750	800	2.0	0.416
0.0050	750	800	2.0	0 373
0.0050	750	800	2.0	0.343
0.0050	750	800	0.875	0.379
0.0050	750	800	0.875	0.392
0.0050	800	200	1.0	0.511
0.0050	800	200	1.0	0.423
0.0050	800	200	1.0	0.393
0.0050	800	200	1.0	0.417
0.0030	775	1333	2.0	0.327
0.0030	775	1333	2.0	0.321
0.0030	775	1333	2.0	0.285
0.0030	775	1333	2.0	0.290
0.0030	775	1333	0.875	0.388
0.0030	775	1333	0.875	0.307
0.0030	775	1333	0.875	0.335
0.0030	775	333	1.0	0.366
0.0030	775	333	1.0	0.408
0.0030	775	333	1.0	0.429
0.0020	740	2000	2.0	0.219
0.0020	740	2000	2.0	0.190
0.0020	740	2000	2.0	0.192

Table 9. Continued

t (in)	$E \times 10^{-3}$ (psi)	$\frac{\rho_1}{t}$	$\frac{\ell}{\rho_1}$	$\frac{M}{\pi E t^2 R_1 \cos^2 \alpha}$
0.0020	740	2000	0.875	0.212
0.0020	740	2000	0.875	0.271
0.0020	740	500	1.0	0.345
0.0020	740	500	1.0	0.366
(b) $\alpha = 20^\circ$				
0.0050	704	321	6.35	0.505
0.0050	704	321	6.35	0.439
0.0050	693	321	6.35	0.466
0.0050	693	321	6.35	0.540
0.0050	693	620	1.97	0.429
0.0050	693	620	1.97	0.505
0.0050	693	472	3.44	0.449
0.0050	693	472	3.44	0.416
(c) $\alpha = 30^\circ$				
0.0100	700	333	1.275	0.429
0.0100	700	333	1.275	0.451
0.0100	680	332	1.265	0.443
0.0100	680	332	1.265	0.468
0.0100	680	330	1.285	0.438
0.0100	680	330	1.285	0.438
0.0100	700	330	1.296	0.430
0.0100	700	330	1.296	0.432
0.0100	690	252	2.241	0.449
0.0100	690	252	2.241	0.456
0.0100	690	248	2.296	0.480
0.0100	690	248	2.296	0.486
0.0100	690	169	4.200	0.519
0.0100	690	169	4.200	0.512
0.0100	690	166	4.282	0.492
0.0100	690	166	4.282	0.510
0.0100	690	163	4.410	0.457
0.0100	690	163	4.410	0.464
0.0100	720	161	4.454	0.423
0.0100	720	161	4.454	0.400
0.0075	797	445	1.265	0.398
0.0075	797	445	1.265	0.421
0.0075	797	443	1.275	0.412
0.0075	797	443	1.275	0.418

Table 9. Continued

t (in)	$E \times 10^{-3}$ (psi)	$\frac{\rho_1}{t}$	$\frac{\ell}{\rho_1}$	$\frac{M}{\pi E t^2 R_1 \cos^2 \alpha}$
0.0075	797	335	2.241	0.423
0.0075	797	335	2.241	0.434
0.0075	778	335	2.241	0.425
0.0075	778	335	2.241	0.466
0.0075	778	225	4.200	0.452
0.0075	778	225	4.200	0.458
0.0075	778	223	4.241	0.471
0.0075	778	223	4.241	0.490
0.0050	708	680	1.224	0.360
0.0050	708	680	1.224	0.370
0.0050	708	679	1.234	0.346
0.0050	708	679	1.234	0.373
0.0050	787	505	2.259	0.365
0.0050	787	505	2.259	0.331
0.0050	787	502	2.277	0.352
0.0050	787	502	2.277	0.346
0.0050	668	335	4.282	0.378
0.0050	668	335	4.282	0.421
0.0050	668	333	4.324	0.409
0.0050	668	333	4.324	0.396
0.0050	668	328	4.410	0.479
0.0050	668	328	4.410	0.435
(d) $\alpha = 45^\circ$				
0.0100	690	417	0.695	0.459
0.0100	690	417	0.695	0.452
0.0100	776	412	0.718	0.418
0.0100	776	412	0.718	0.421
0.0100	776	410	0.724	0.399
0.0100	776	410	0.724	0.402
0.0100	677	304	1.326	0.433
0.0100	677	304	1.326	0.421
0.0100	678	304	1.326	0.363
0.0100	678	304	1.326	0.399
0.0100	776	303	1.336	0.399
0.0100	776	303	1.336	0.402
0.0100	690	303	1.336	0.420
0.0100	690	303	1.336	0.451
0.0100	677	207	2.425	0.431
0.0100	677	207	2.425	0.488
0.0100	677	205	2.448	0.477

Table 9. Continued

t (in)	$E \times 10^{-3}$ (psi)	$\frac{\rho_1}{t}$	$\frac{l}{\rho_1}$	$\frac{M}{\pi E t^2 R_1 \cos^2 \alpha}$
0.0100	677	205	2.448	0.506
0.0100	690	199	2.546	0.480
0.0100	690	199	2.546	0.503
0.0075	691	411	1.304	0.492
0.0075	691	411	1.304	0.508
0.0075	691	400	1.358	0.513
0.0075	691	400	1.358	0.458
0.0075	691	277	2.401	0.485
0.0075	691	277	2.401	0.479
0.0075	691	270	2.497	0.533
0.0075	691	270	2.497	0.481
0.0050	731	833	0.695	0.376
0.0050	731	833	0.695	0.407
0.0050	731	825	0.712	0.374
0.0050	731	825	0.712	0.380
0.0050	690	608	1.326	0.465
0.0050	690	608	1.326	0.464
0.0050	731	600	1.358	0.367
0.0050	731	600	1.358	0.400
0.0050	678	408	2.472	0.415
0.0050	678	408	2.472	0.344
0.0050	679	398	2.546	0.423
0.0050	679	398	2.546	0.431
(e) $\alpha = 60^\circ$				
0.0100	683	542	0.486	0.557
0.0100	683	542	0.488	0.540
0.0100	683	538	0.496	0.520
0.0100	683	538	0.496	0.520
0.0100	690	394	0.888	0.516
0.0100	690	394	0.888	0.493
0.0100	690	386	0.918	0.520
0.0100	690	386	0.918	0.494
0.0100	686	384	0.926	0.533
0.0100	686	384	0.926	0.434
0.0100	690	382	0.934	0.527
0.0100	690	382	0.934	0.527
0.0100	690	382	0.934	0.523
0.0100	690	382	0.934	0.535
0.0100	650	380	0.942	0.486
0.0100	650	380	0.942	0.451

Table 9. Concluded

t (in)	$E \times 10^{-3}$ (psi)	$\frac{\rho_1}{t}$	$\frac{f}{\rho_1}$	$\frac{M}{\pi E t^2 R_t \cos^2 \alpha}$
0.0100	700	278	1.499	0.481
0.0100	700	278	1.499	0.497
0.0100	700	278	1.499	0.583
0.0100	700	278	1.499	0.485
0.0100	700	264	1.610	0.564
0.0100	700	264	1.610	0.537
0.0100	650	240	1.789	0.527
0.0100	650	240	1.789	0.527
0.0100	650	238	1.848	0.529
0.0100	650	238	1.848	0.534
0.0075	778	744	0.457	0.508
0.0075	778	744	0.457	0.482
0.0075	778	717	0.496	0.484
0.0075	778	717	0.496	0.472
0.0075	760	557	0.804	0.495
0.0075	760	557	0.804	0.517
0.0075	760	515	0.918	0.514
0.0075	760	515	0.918	0.539
0.0075	772	379	1.456	0.526
0.0075	772	379	1.456	0.455
0.0075	772	363	1.545	0.502
0.0075	772	363	1.545	0.457
0.0050	720	1096	0.476	0.373
0.0050	720	1096	0.476	0.361
0.0050	685	1096	0.476	0.415
0.0050	685	1096	0.476	0.399
0.0050	685	1092	0.480	0.389
0.0050	685	1092	0.480	0.363
0.0050	685	1088	0.484	0.369
0.0050	685	1088	0.484	0.353
0.0050	676	778	0.903	0.370
0.0050	676	778	0.903	0.356
0.0050	676	764	0.934	0.445
0.0050	676	764	0.934	0.406
0.0050	676	764	0.934	0.449
0.0050	676	764	0.934	0.425
0.0050	730	528	1.610	0.505
0.0050	730	528	1.610	0.492
0.0050	730	528	1.610	0.447
0.0050	730	528	1.610	0.447
0.0050	783	516	1.660	0.345
0.0050	783	516	1.660	0.383

Table 10. Experimental Data for Steel Cones and Cylinders in Pure Bending

t (in)	$E \times 10^{-6}$ (psi)	$\frac{\rho_1}{t}$	$\frac{\ell}{\rho_1}$	$\frac{M}{\pi E t^2 R_1 \cos \alpha}$
(a) $\alpha = 0^\circ$				
0.020	30	400	2	0.314
0.020	30	400	2	0.361
0.020	30	400	1	0.318
0.020	30	400	1	0.322
0.020	30	400	1	0.318
0.020	30	400	1	0.385
0.010	30	800	2	0.442
0.010	30	800	2	0.421
0.010	30	800	1	0.411
0.010	30	800	1	0.433
0.010	30	800	1	0.455
0.010	30	800	1	0.320
0.010	30	800	1	0.421
0.010	30	800	1	0.319
0.010	30	800	1	0.388
(b) $\alpha = 30^\circ$				
0.020	30	231	2.598	0.354
0.020	30	231	2.598	0.362
0.020	30	231	2.598	0.272
0.020	30	231	2.598	0.357
0.010	30	462	2.598	0.365
0.010	30	462	2.598	0.351
0.010	30	462	2.598	0.326
(c) $\alpha = 60^\circ$				
0.020	30	300	1.347	0.336
0.020	30	300	1.347	0.313
0.020	30	300	1.347	0.322
0.020	30	300	1.347	0.304
0.010	30	1000	0.577	0.361
0.010	30	600	1.347	0.340
0.010	30	600	1.347	0.301
0.010	30	600	1.347	0.402
0.010	30	600	1.347	0.415
0.010	30	400	2.310	0.302

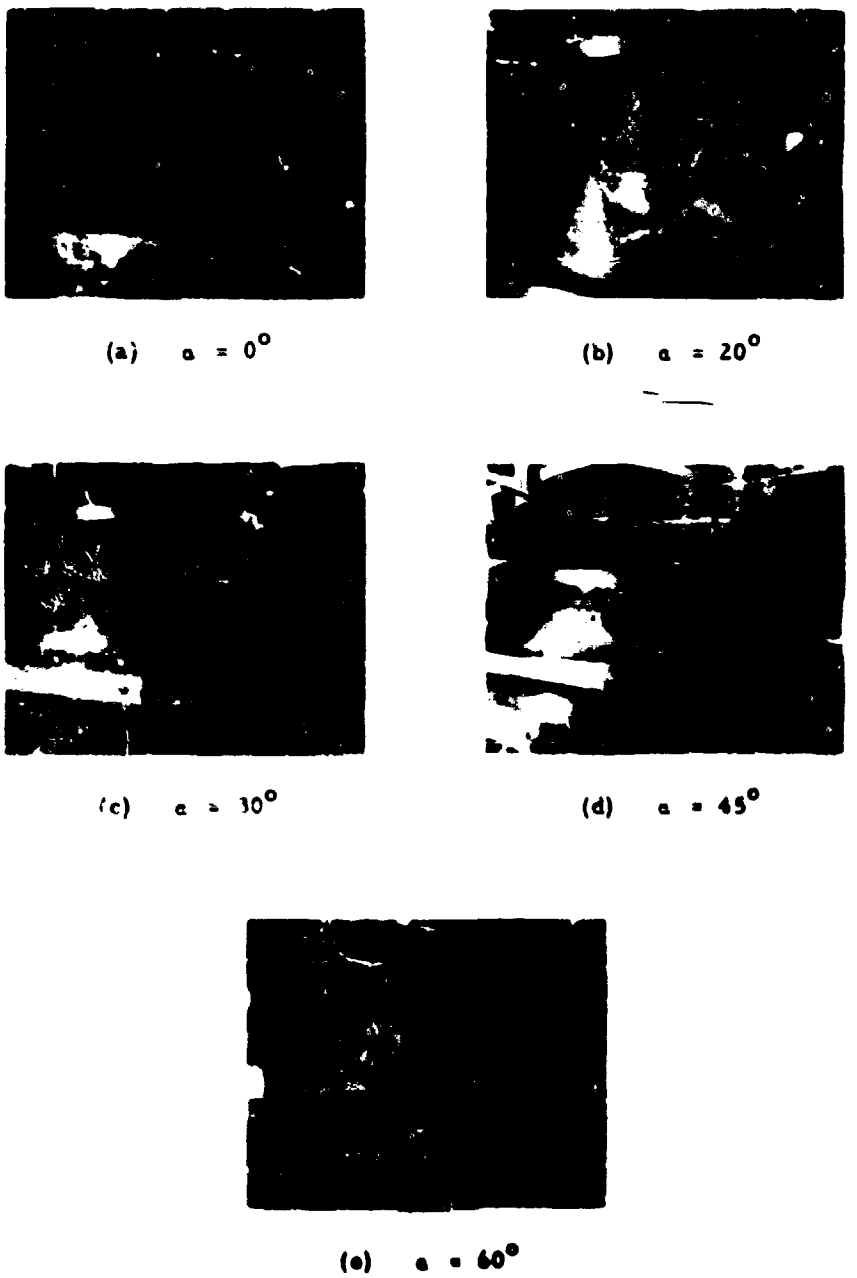

(a) $\alpha = 0^{\circ}$ (b) $\alpha = 20^{\circ}$

(c) $\alpha = 30^{\circ}$ (d) $\alpha = 45^{\circ}$

(e) $\alpha = 60^{\circ}$

Figure 29. Typical Buckle Patterns for Cylindrical and Conical Shells Under Pure Bending

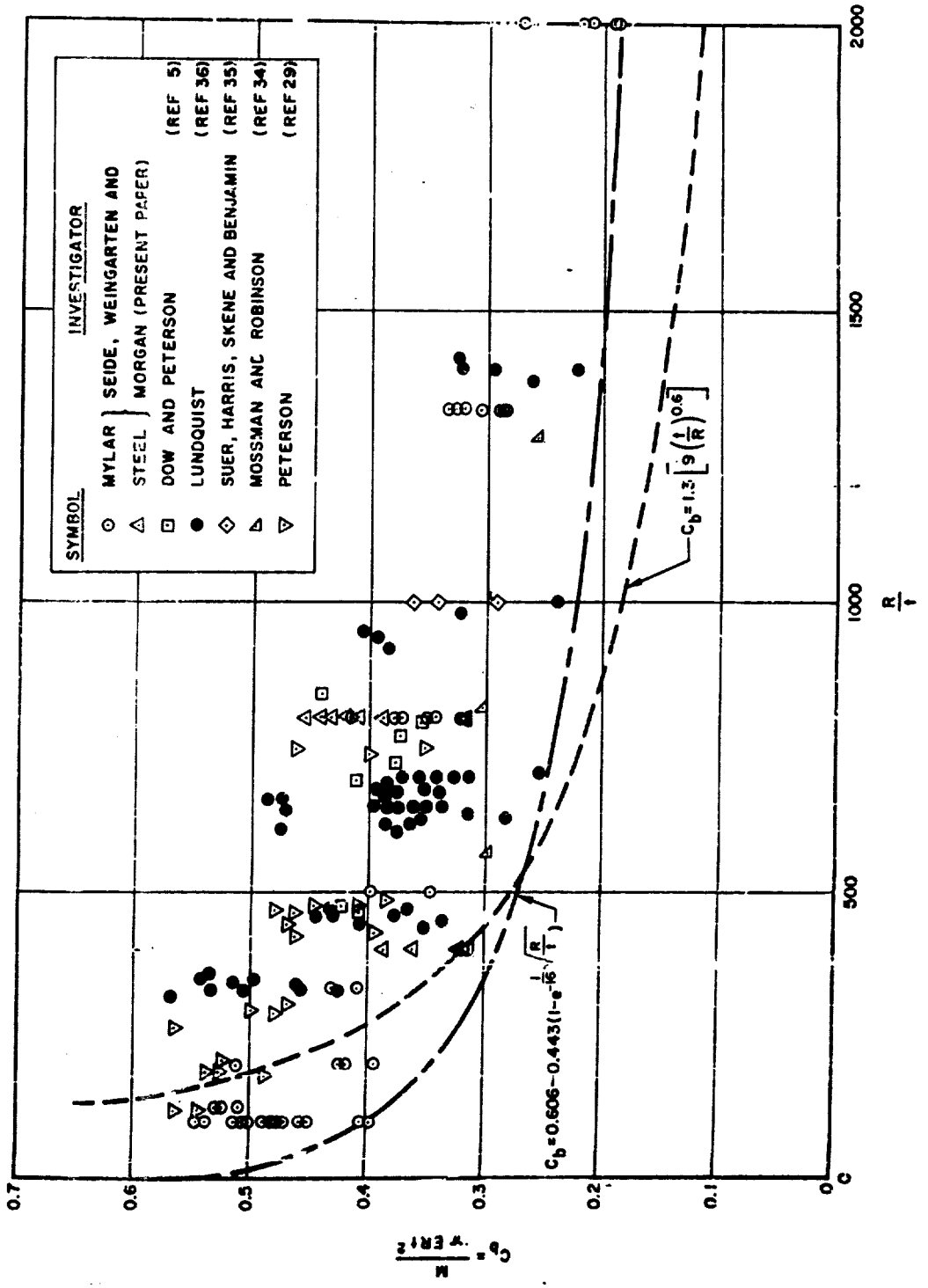

Figure 30. Comparison of Various Experimental Results for Cylinders in Bending

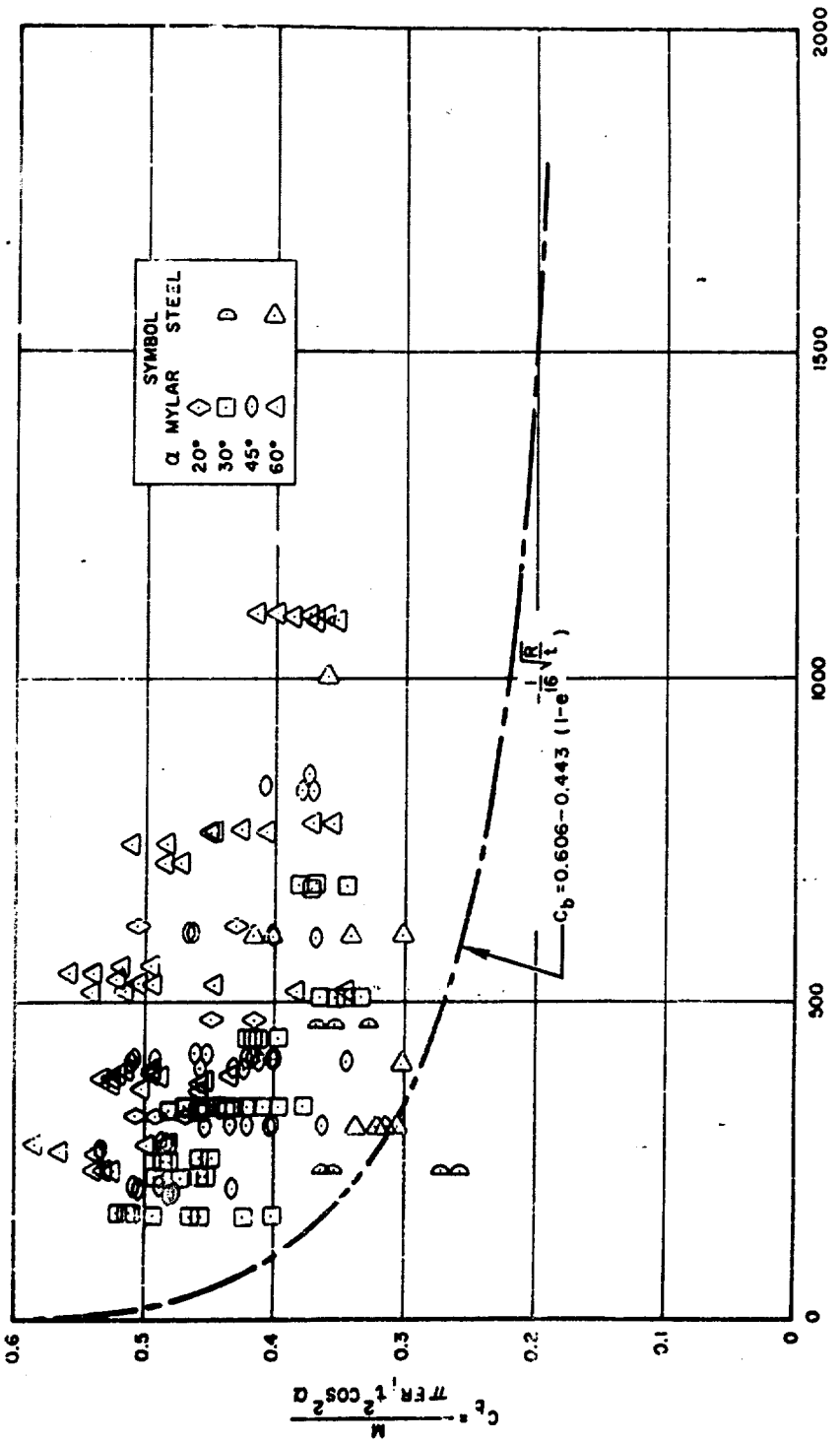

Figure 31. Comparison of Bending Moment Coefficent for Conical Shells with Lower Bound Curve for Cylinders

IX. PRESSURIZED CYLINDERS AND TRUNCATED CONES UNDER BENDING AND AXIAL LOADS

Of the loading conditions studied in the present report, the interaction between bending, axial load, and internal pressure is the least investigated in the literature. It is known that there is a straight line interaction curve between bending and axial compression for unpressurized cylinders (Reference 17 and 33). Further, it has been supposed, on the basis of theoretical results for pressurized cylinders in axial compression, that the maximum nominal compressive stress for pressurized cylinders in bending should approach the classic value for axial compression. Experimental evidence to disprove this assumption has recently appeared in References 5 and 35, where it is shown that, for pressurized cylinders in bending, maximum compressive stress coefficients that are greater than the classic value for axial compression can be obtained. The experimental data are insufficient, however, to yield any clear picture of what critical loads can be expected, since they are available only for relatively low values of internal pressure.

A small-deflection analysis of the stability of pressurized cylinders in bending (Reference 37) reveals that lateral pressure slightly increases the critical compressive stress of cylinders in bending, with the increase varying with the lateral pressure and with the radius-thickness ratio of the cylinder. When axial tension is added, as in the case of hydrostatic pressure for instance, the net compressive stress at buckling is larger than for lateral pressure alone and continues to increase as the axial tension increases. Small-deflection theory is inadequate, however, and, since large-deflection analysis is not available at this time, the true behavior of pressurized cylinders in bending must be revealed by experiment.

The experimental results presented herein represent an indication of what can be expected of elastic pressurized cones and cylinders in bending. However, establishing design criteria from the available data would appear to be premature.

A. Load-Deformation Curves

Load-deformation curves for pressurized cylinders and cones in bending were obtained by continuously recording the force in the loading cable and the downward movement of the end plate at the compression side of the shell. Typical sets of curves for cylinders with varying pressures are shown in Figures 32 and 33. The X mark on each curve is the critical load calculated from linear theory. Each curve of Figure 32 was obtained by keeping the internal pressure constant, applying an end compressive load equal to the calculated pressure force on the end plate, and varying the bending moment until a maximum value was obtained. This corresponds to a cylinder under lateral pressure alone. The curves of Figure 33 correspond to a cylinder under uniform hydrostatic pressure since the pressure force on the end plate was not counterbalanced. Values of the pressure parameter p^*, which is about 3.3 times the usual parameter $\bar{p}$, and the corresponding critical load predicted by the small-deflection solution of Reference 37 are shown for each curve.

The implications of Figures 32 and 33 are quite unexpected, since there are few hints of the phenomena in the literature. We note, first of all, that the maximum loads recorded are considerably larger than those predicted by small-deflection theory for sufficiently high pressure. The present results indicate that the nominal compressive stress due to bending increases with increasing internal pressure. Similar results were obtained in Reference 5 for aluminum cylinders with a maximum value for p^* of about 3.

It was observed, as the bending moment was increased, that approximately radial deformations, similar to those observed in tests of pressurized cylinders under axial compression, first appeared near the cylinder ends and grew in magnitude. The level of load at which this occurred was near the critical value predicted by small-deformation theory. The only effect these large ripples appeared to have on the overall load-deformation behavior, however, was to slightly decrease the cylinder stiffness. As the moment was increased beyond this level, diamond-shaped deformations appeared and spread around the circumference.

The depth of these buckles at the "collapse" load was so large that the buckles could lead to fracture of the metal shells. The problem is what to define as a critical load. If large deformations are the criterion, then the predictions of small-deflection theory are reasonably correct. On the other hand, these large deformations on the compression side of the shell only bring about a redistribution of stress within the shell which continues to carry increasing load until the deformations of a much larger magnitude occur. This behavior would appear to be similar to the Brazier type of failure of cylinders in bending (References 38-40) and would possibly be predictable by a Brazier-type of theory; but the values obtained in Reference 40, for instance, are found to be considerably higher than experimental results for pressurized cylinders.

It will also be noticed that the effect of pressure on the shape of the load-deformation curves for cylinders is entirely different for the cases of lateral and hydrostatic pressure. While lateral pressure has the effect of sharpening the peak of the curve, hydrostatic pressure serves to make the load-deformation curve slope gently to a plateau in the manner of pressurized cylinders under axial compression. In the latter case, the variation of the shape of the curves indicates that the deformation modes prior to collapse vary with internal pressure. For low pressures the curve is linear until collapse occurs. As the pressure increases, the linear portion of the curve breaks sharply prior to buckling and proceeds linearly to collapse at another slope. With still higher pressures the sharp break rounds off and collapse is apparently initiated by still another large deformation mode. The comparison indicates that the rounding-off effect is due to the axial tensile force induced by the pressure, a conjecture that is strengthened by the results of some preliminary bending tests which applied axial tension in addition to hydrostatic pressure. For sufficiently large tension loads it was impossible to define a collapse load since the load-deformation curve did not level off even for extremely large amount of deformation. A similar result was observed for very large values of internal hydrostatic pressure.

B. Collapse Loads for Cylinders

Net compressive stress coefficients for the cylinders tested are given in Table II and are shown in Figures 34 and 35. The results are given in the form of the ratio of the nominal maximum compressive stress at collapse and the theoretical critical stress for axial compression as a function of the internal pressure parameter. For the case of lateral pressure, the stress ratio is,

$$\frac{\sigma_b}{\sigma_c} = \frac{\sqrt{3(1-\nu^2)}}{\pi} \quad \frac{M}{ERt^2} \tag{13}$$

while for hydrostatic pressure

$$\frac{\sigma_b}{\sigma_c} = \frac{\sqrt{3(1-\nu^2)}}{\pi} \quad \frac{M}{ERt^2} - \frac{1}{4} \quad p^* \tag{14}$$

A comparison of Figures 34 and 35 shows that the net compressive stress coefficient rises more rapidly for the case of internal uniform hydrostatic pressure than for lateral pressure. For hydrostatic pressure, it would take a value of p^* on the order of 1 to 1.5 for the compressive stress to attain the small deflection value whereas the value of p^* required for lateral pressure is about 2. For sufficiently high pressures, results of both types of pressurization indicate a linear increase of the critical net compressive stress with internal pressure. The results for hydrostatic pressure rise at a rate about 4 times as great as those for lateral pressure. Preliminary tests indicate that even greater increases in the net compressive stress coefficient for the same value of internal pressure can be obtained with additional tension load proportional to the internal pressure.

The number of tests is insufficient to show whether or not the collapse moments depend to any great extent on the radius-thickness ratio of the cylinders. There is some indication that this is true, but a great deal of additional experimentation is required to firmly establish any trends. It is obvious that experimentation is required for less elastic materials to determine where plasticity effects bring about deviations from the results for Mylar.

C. Collapse Loads for Cones

A few bending tests were performed on internally pressurized cones having semivertex angles of 30 degrees and 60 degrees, the results of which are given in Table 12 and in Figure 36 and 37. Because no axial compressive load was applied, the results pertain to the case of internal uniform hydrostatic pressure and bending. The data is given in the form of the net maximum compressive stress coefficient as a function of the pressure parameter p^*, all based on the small end of the conical shell. Thus

$$\frac{\sigma_b'}{\sigma_c} = \frac{\sqrt{3(1-\nu^2)}}{\pi} \frac{M}{ER_1 t^2 \cos^2 \alpha} - \frac{1}{4} p^*. \tag{16}$$

We note that there appears to be considerably more scattor of the results than for cylinders. Some scatter is to be expected since initially the region of compressive stress is concentrated near the small end of the cylinder, where any irregularities such as dimpling or ovalization of the cross section would affect the results. This might persist even at high internal pressure since the combination of edge restraint and pressure would create irregularities in the region of concern. It is interesting that all of the lower values in Figure 36 are associated with those cones made of 0.003 inch Mylar, which were difficult to assemble satisfactorily. The fact that some of the 0.003 inch cone results agreed with the results obtained for the 0.005 inch and 0.010 inch cones tends to support the theory of inferior fabrication and scatter.

The net compressive stress coefficients for conical shells appear, then, to be larger than those for cylinders having the same value of p^*. It will be noticed, also, that the results for 60 degree cones are larger than those for 30 degree cones. This might have been expected since the parameter ζ, found to be significant for axial compression and internal pressure, is very likely an important parameter for bending and internal pressure as well and is considerably smaller for the 60 degree cones than for the 30 degree cones. There is some indication in the results for 30 degree cones alone that there is an increase in the net compressive stress coefficient with decreasing values of ζ, but this conclusion is masked by the scatter in the data.

D. Interaction Between Axial Compression and Bending

Tests were performed on a single cylinder and a single 30 degree cone to determine the effect of pressure on the interaction curve for bending moment and axial compression. The interaction curve was first obtained for the unpressurized shell. A constant amount of pressure was then added and data again obtained for bending and axial compression, axial compression and no moment, and for several points in between these two limits. The procedure was repeated once more for an additional increment of internal pressure.

The data obtained are given in Tables 13 and 14. The pressure loading on the end plate (the small end of the cone) was subtracted from the total compression load coefficient C. The nominal maximum compressive stress due to the bending moment was used to determine the bending moment coefficient C_b. The data was then put into the form of a stress ratio by dividing the axial compression load coefficient C by its value for the case of no bending moment, and the bending moment coefficient C_b by its value for the case of no net axial stress (C_b at C = 0). The determination of the value of C_{b_o} required interpolation of the data.

The interaction curves for the cylinder are given in Figure 38. It can be seen, that, for the values of pressure considered, the interaction curve between bending moment and net axial force is very well approximated by a straight line. When the curve is extended into the axial tension region there is a definite departure from the straight line, such that the addition of tension is more beneficial to the moment carrying capacity. A study of the experimental data for bending and internal lateral or hydrostatic pressure indicates that at higher pressures the interaction curve in the axial tension region should be merely a continuation of the straight line for the axial compression region. The nonlinear interaction curve in the tension region might persist, however, for values of p^* less than about 10.

The bending-axial compression interaction curve for the conical shell having a semivertex angle of 30 degrees, shown in Figure 39, is different from the cylinder interaction curve. The curves for the three values of the pressure parameter coincide remarkably well and lie above a straight line connecting the end points. In the tension region the interaction curve lies below the straight line. Similar results, for somewhat lower values of the pressure parameter, are given in Reference 6 for 17-7 PH stainless steel cones.

It appears reasonable to conclude, despite the small amount of data, that a straight line interaction curve is adequate for pressurized cylinders in bending and axial compression. The corresponding curve for pressurized cones lies above the straight line and is probably a function of one or more cone geometry parameters. The use of a straight-line interaction curve for conical shells would be conservative, but adequate for design purposes.

Table 11. Experimental Data for Pressurized Mylar Cylinders in Bendi_g

t	$\frac{L}{W}$	$\frac{R}{t}$	E (psi)	$\frac{\sigma_b}{\sigma_c}$	p*	$\frac{\sigma_h}{\sigma_c}$	p*
Lateral Pressure							
0.003	2	1333	721,000	0.774	0.81	1.330	6.50
				0.843	1.63	1.405	7.30
				1.036	2.43	1.455	8.12
				1.079	3.25	1.495	8.94
				1.210	4.06	1.995	10.55
				1.245	4.88	1.940	11.36
				1.275	5.70	1.735	13.00
0.010	2	400	680,000	0.574	0.00	1.091	2.26
				0.766	0.38	1.138	2.64
				0.861	0.75	1.188	3.01
				0.924	1.13	1.215	3.37
				0.964	1.51	1.180	3.77
				0.1002	1.89	1.188	4.12
Hydrostatic Pressure							
0.003	2	1333	700,000	0.300	0.00	3.947	12.58
				1.068	1.68	4.078	13.42
				1.538	3.36	4.306	15.10
				2.010	5.03	4.761	16.78
				2.442	6.71	5.116	18.46
				2.855	8.39	5.469	20.14
				3.330	10.07		
0.005	2	800	700,000	0.705	0.60	2.307	6.04
				0.919	1.21	2.642	7.55
				1.122	1.81	2.926	9.07
				1.266	2.47	3.384	10.58
				1.455	3.02	3.719	12.09
				1.599	3.63	4.020	13.60
				1.828	4.53		
0.010	2	400	700,000	0.584	0.00	1.714	2.64
				0.658	0.08	1.862	3.02
				0.828	0.38	1.958	3.40
				0.984	0.76	1.962	3.78
				1.143	1.13	2.046	4.16
				1.307	1.51	2.147	4.53
				1.453	1.89	2.285	4.91
				1.591	2.27		
0.005	2	800	750,000	0.366	0.00	2.825	8.46
				0.830	0.56	3.257	9.87
				1.009	1.13	3.505	11.28
				1.214	1.69	3.685	12.69
				1.380	2.26	4.132	14.10
				1.531	2.82	4.297	15.51
				2.238	5.64	4.492	16.92
				2.532	7.05	4.805	18.33
0.003	2	1333	723,000	0.670	0.00	2.644	7.31
				0.932	0.81	2.845	8.12
				1.187	1.63	2.983	8.94
				1.348	2.44	3.224	9.75
				1.642	3.25	3.496	10.56
				1.845	4.06	3.523	11.37
				2.015	4.88	3.705	12.19
				2.224	5.69	3.850	13.00
				2.406	6.50	4.112	14.62
						4.455	16.25
0.0075	2	533	754,000	0.558	0.00	1.774	3.73
				0.644	0.12	1.906	4.35
				0.886	0.52	1.979	4.97
				1.142	1.24	2.126	5.60
				1.338	1.87	2.246	6.22
				1.500	2.49	2.370	6.84
				1.629	3.11	2.508	7.46
0.010	2	400	700,000	0.532	0.00	1.59	3.04
				0.568	0.38	1.647	3.40
				0.833	0.76	1.721	3.78
				0.926	1.13	1.785	4.16
				1.064	1.51	1.841	4.53
				1.183	1.89	1.929	4.91
				1.292	2.27	1.932	4.91
				1.413	2.64	1.977	5.29
				1.505			
0.0075	2	533	756,000	0.528	0.00	2.155	5.60
				0.884	0.62	2.278	6.22
				1.045	1.24	2.411	6.84
				1.318	1.86	2.531	7.46
				1.434	2.49	2.647	8.08
				1.617	3.11	2.798	8.70
				1.718	3.73	2.893	9.33
				1.893	4.35	3.025	9.95
				2.020	4.97		
0.005	2	800	750,000	0.863	0.96	2.718	7.05
				1.050	1.13	2.947	8.46
				1.254	1.69	3.153	9.87
				1.469	2.26	3.474	11.28
				1.571	2.82	3.619	12.69
				1.765	3.38	3.798	14.10
				1.939	4.23	4.111	16.21
				2.266	5.64	4.492	18.32
0.005	2	800	750,000	0.373	0.00	2.678	8.45
				1.050	1.13	2.866	9.87
				1.408	2.26	3.198	11.28
				1.492	2.82	3.498	12.69
				1.871	4.23	3.825	14.10
				2.119	5.64	4.128	15.51

Table 12. Experimental Data for Pressurized Mylar Cones in Bending (Hydrostatic Pressure)

t	R_1	E (psi)	$\frac{\sigma_b^1}{\sigma_c}$	p*	$\frac{\sigma_b^1}{\sigma_c}$	p*
			(a) $\alpha = 30^\circ$			
0.001	2.90	700,000	0.584 0.687 0.815 0.934 1.059 1.170 1.314 1.451 1.495	0.42 0.85 1.27 1.70 2.12 2.54 2.96 3.39 3.82	1.571 1.692 1.897 2.090 2.386 2.668 2.902 2.936	4.24 4.70 5.87 7.04 8.22 9.39 10.56 11.74
0.003	2.96	720,000	0.476 0.578 0.697 0.811 0.927 1.102 1.219	0.43 0.86 1.29 1.72 2.15 2.57 3.00	1.335 1.428 1.522 1.675 2.455 2.963	3.43 3.86 4.29 4.76 9.51 10.70
0.003	1.44	700,000	0.296 0.317 0.319 0.446 0.476 0.525 0.573 0.633 0.673 0.706	0.10 0.21 0.32 0.42 0.52 0.63 0.73 0.84 0.94 1.05	0.770 0.851 0.948 1.026 1.011 1.105 1.222 1.314 1.363	1.16 1.45 1.74 2.03 2.32 2.61 2.90 3.19 3.481
0.003	1.45	700,000	0.663 0.805 0.872 0.940	0.21 0.32 0.42 0.53	1.026 1.038 1.011 1.036	0.64 0.74 0.96 1.06
0.003	1.45	720,000	0.563 0.585 0.621 0.669 0.727 0.775 0.793	0.41 0.52 0.62 0.72 0.83 0.93 1.03	0.848 0.942 1.033 1.163 1.294 1.408 1.479	1.14 1.43 1.72 2.00 2.29 2.57 2.86
0.003	1.45	720,000	0.553 0.593 0.631 0.669 0.707	0.41 0.52 0.62 0.72 0.83	0.757 0.831 0.884 0.978 1.041	0.92 1.03 1.14 1.43 1.72
0.003	2.16	700,000	0.446 0.539 0.646 0.726 0.856 0.884	0.26 0.47 0.71 0.94 1.18 1.41	0.952 1.033 1.079 1.138 1.241	1.66 1.88 2.12 2.36 2.61
0.003	2.16	700,000	0.482 0.524 0.620 0.692 0.770 0.848 0.919 1.023 1.198	0.92 1.15 1.37 1.60 1.83 2.06 2.49 2.54 3.17	1.380 1.405 1.467 1.585 1.702 1.819 1.938 2.068	1.81 4.12 4.46 5.00 5.71 6.35 6.90 7.61
0.003	3.00	725,000	0.594 0.819 0.949 1.144 1.386 1.561 1.698 1.827	0.32 0.63 0.95 1.27 1.59 1.91 2.22 2.54	1.990 2.024 2.214 2.393 2.549 2.706 2.772 2.928	2.86 3.18 3.52 4.40 4.86 5.20 5.72 6.16
0.010	2.14	680,000	0.694 0.774 0.798	0.08 0.02 0.04	0.829 0.868 0.889	0.06 0.09 0.11
0.005	3.00	725,000	0.396 0.769 0.946 1.098 1.223 1.327	0.00 0.16 0.32 0.48 0.63 0.79	1.428 1.560 1.814 1.904 1.780	0.95 1.11 1.27 1.43 1.59
0.008	2.18	720,000	0.540 0.648 0.784 0.749 0.772 0.839 0.900 0.968 0.998 1.041 1.098 1.173 1.231 1.312 1.371	0 0.08 0.17 0.25 0.34 0.42 0.50 0.59 0.67 0.75 0.84 0.93 1.00 1.15 1.67	1.419 1.667 1.884 1.981 1.888 1.673 1.788 1.883 1.927 2.012 2.064 2.148 2.211 2.282	1.59 1.81 1.88 1.76 1.88 2.08 2.32 2.90 2.76 3.04 3.26 3.47 3.71 3.94

Table 12. Concluded

t	R_1	E (psi)	$\frac{\sigma_h^i}{\sigma_i}$	p^*	$\frac{\sigma_h^l}{\sigma_i}$	p^*
(a) α = 30°						
0.005	2.16	720,000	0.486	0	1.397	1.14
			0.609	0.08	1.490	1.37
			0.688	0.17	1.609	1.60
			0.733	0.25	1.636	1.72
			0.779	0.33	1.662	1.83
			0.846	0.41	1.738	2.06
			0.914	0.50	1.813	2.29
			0.971	0.58	1.877	2.52
			1.027	0.66	1.963	2.75
			1.073	0.74	2.050	2.98
			1.163	0.83	2.114	3.20
			1.240	0.92	2.169	3.43
			1.322	1.03	2.176	3.66
0.005	2.90	720,000	0.575	0.00	0.861	0.30
			0.808	0.157	0.889	0.44
0.005	1.467	720,000	0.494	0	0.990	0.47
			0.446	0.04	1.036	0.53
			0.479	0.08	1.059	0.58
			0.590	0.11	1.088	0.63
			0.635	0.15	1.114	0.69
			0.684	0.19	1.136	0.74
			0.734	0.23	1.195	0.79
			0.763	0.27	1.224	0.84
			0.819	0.30	1.285	0.95
			0.851	0.34	1.337	1.05
			0.884	0.38	1.405	1.16
			0.952	0.42		
0.005	1.450	720,000	0.585	0	0.983	0.41
			0.687	0.04	1.019	0.46
			0.732	0.07	1.056	0.52
			0.752	0.11	1.114	0.62
			0.758	0.15	1.186	0.72
			0.777	0.19	1.224	0.82
			0.833	0.22	1.315	0.93
			0.867	0.26	1.371	1.03
			0.894	0.30	1.413	1.13
			0.924	0.34	1.459	1.24
			0.950	0.37	1.570	1.75
0.005	1.442	720,000	0.302	0	0.926	0.51
			0.491	0.04	0.961	0.56
			0.547	0.07	0.998	0.61
			0.561	0.11	1.071	0.71
			0.571	0.15	1.138	0.82
			0.694	0.18	1.191	0.92
			0.727	0.22	1.252	1.02
			0.745	0.29	1.298	1.12
			0.755	0.33	1.305	1.22
			0.779	0.37	1.346	1.32
			0.851	0.41		
(b) α = 60°						
0.005	2.035	720,000	0.528	0	1.711	1.32
			0.930	0.22	1.797	1.54
			1.157	0.44	2.024	1.76
			1.348	0.66	2.065	2.43
			1.539	0.88	2.170	3.04
			1.660	1.10	2.289	3.65
0.005	2.677	720,000	0.642	0	1.997	2.28
			1.109	0.38	2.143	2.66
			1.308	0.76	2.289	3.04
			1.506	1.14	2.434	3.42
			1.652	1.52	2.633	3.80
			1.825	1.90		
0.005	1.930	720,000	0.668	0	1.529	1.19
			0.947	0.20	1.583	1.38
			1.029	0.39	1.645	1.58
			1.209	0.59	1.707	1.78
			1.345	0.79	1.776	1.98
			1.444	0.99		
0.005	1.345	720,000	0.499	0.13	1.391	1.46
			0.657	0.27	1.464	1.59
			0.837	0.40	1.484	1.73
			0.964	0.53	1.504	1.86
			1.111	0.66	1.503	1.99
			1.110	0.80	1.512	2.13
			1.173	0.93	1.628	2.39
			1.203	1.06	1.731	2.66
			1.255	1.20	1.824	2.92
			1.318	1.33		

Table 13. Experimental Data for a Pressurized Mylar Cylinder under Bending and Axial Compression

p lbs	$p - \pi R^2 p$ lbs	C	$\frac{C}{C_o}$	M in-lbs	C_b	$\frac{C_b}{C_{b_o}}$
(a) p = 0 psi, $\hat{p}$ = 0.00						
53.2		0.201	1.000	0.0	0.000	0.000
47.3		0.178	0.886	9.2	0.017	0.076
41.4		0.156	0.776	25.7	0.048	0.214
35.5		0.134	0.667	39.0	0.073	0.326
29.6		0.112	0.557	55.6	0.105	0.469
23.7		0.089	0.443	63.2	0.119	0.531
17.7		0.067	0.333	82.4	0.155	0.692
11.8		0.045	0.224	98.8	0.186	0.830
5.9		0.022	0.109	112.1	0.211	0.942
0.0		0.000	0.000	118.8	0.224	1.000
(b) p = 0.5 psi, $\hat{p}$ = 0.63						†
128.9	103.8	0.392	1.000	0.0	0.000	0.000
116.3	93.2	0.352	0.898	19.0	0.036	0.087
94.6	69.5	0.262	0.668	68.4	0.129	0.311
71.0	45.9	0.173	0.441	122.6	0.231	0.556
47.3	22.2	0.084	0.215	171.0	0.323	0.778
23.7	-1.4	-0.005	-0.013	245.1	0.462	1.113
0.0	-25.1	-0.095	-0.242	295.5	0.557	1.342
(c) p = 1.0 psi, $\hat{p}$ = 1.25						††
174.5	124.2	0.469	1.000	0.0	0.000	0.000
147.9	97.6	0.368	0.785	68.4	0.129	0.240
113.3	68.0	0.257	0.548	133.0	0.251	0.468
88.7	38.4	0.145	0.309	197.6	0.373	0.694
59.2	8.9	0.033	0.070	260.3	0.491	0.914
29.6	-20.7	-0.078	-0.166	342.0	0.645	1.200
0.0	-50.3	-0.190	-0.405	397.9	0.805	1.500

(a) t = 0.0075 in., R = 4 in., L = 8 in., E = 750,000 psi

† $C_{b_o} \approx 0.415$

†† $C_{b_o} \approx 0.538$

Table 14. Experimental Data for a Pressurized Mylar Cone under Bending and Axial Compression

p lbs	$p - \pi R_2^2 p$ lbs	C	$\frac{C}{C_o}$	M in - lbs	C_b	$\frac{C_b}{C_{b_o}}$
(a) p = 0 psi, $p^* = 0.00$						
0.0		0.000	0.000	43.2	0.360	1.000
2.9		0.035	0.136	39.2	0.327	0.908
5.8		0.070	0.272	33.7	0.281	0.781
8.7		0.105	0.409	29.2	0.244	0.678
11.6		0.141	0.549	24.5	0.205	0.569
14.5		0.176	0.685	18.9	0.158	0.439
17.4		0.210	0.817	11.8	0.098	0.272
21.2		0.257	1.000	0.0	0.000	0.000
(b) p = 0.5 psi, $p^* = 1.06$						†
0.0	-13.2	-0.161	-0.301	107.2	0.896	1.203
5.8	-7.4	-0.090	-0.168	100.5	0.840	1.127
11.6	-1.6	-0.020	-0.037	91.9	0.768	1.031
17.4	4.2	0.050	0.093	82.0	0.685	0.919
23.2	10.0	0.121	0.226	73.9	0.617	0.828
29.0	15.8	0.191	0.357	64.9	0.542	0.728
34.8	21.6	0.261	0.488	54.8	0.457	0.613
40.6	27.4	0.332	0.621	44.2	0.369	0.495
46.4	33.2	0.402	0.75[illegible]	33.4	0.275	0.369
52.2	39.0	0.472	0.882	21.0	0.175	0.235
57.4	44.2	0.535	1.000	0.0	0.000	0.000
(c) p = 1.0 psi, $p^* = 2.11$						††
0.0	-26.5	-0.321	-0.[illegible]	162.9	1.361	1.444
2.9	-23.6	-0.285	-0.443	151.9	1.269	1.347
8.7	-17.8	-0.215	-0.334	142.1	1.187	1.266
14.5	-12.0	-0.145	-0.225	134.8	1.126	1.195
20.3	-6.2	-0.075	-0.116	122.5	1.023	1.086
26.1	-0.4	-0.005	-0.008	113.3	0.947	1.005
31.9	5.4	0.066	0.102	102.9	0.860	0.913
37.7	11.2	0.136	0.211	93.1	0.778	0.826
43.5	17.0	0.206	0.320	82.1	0.686	0.728
49.3	22.8	0.277	0.430	71.7	0.599	0.636
55.1	28.6	0.347	0.539	61.3	0.512	0.544
60.9	34.4	0.417	0.648	50.0	0.418	0.444
66.7	40.2	0.487	0.756	37.5	0.313	0.332
72.5	46.0	0.558	0.866	25.7	0.215	0.228
79.6	53.1	0.644	1.000	0.0	0.000	0.000

(a) $\alpha = 30°$, t = 0.005 in., R_1 = 2.90 in., R_2 = 5.00 in., E = 700,000 psi

† $C_{b_o} \approx 0.745$

†† $C_{b_o} \approx 0.942$

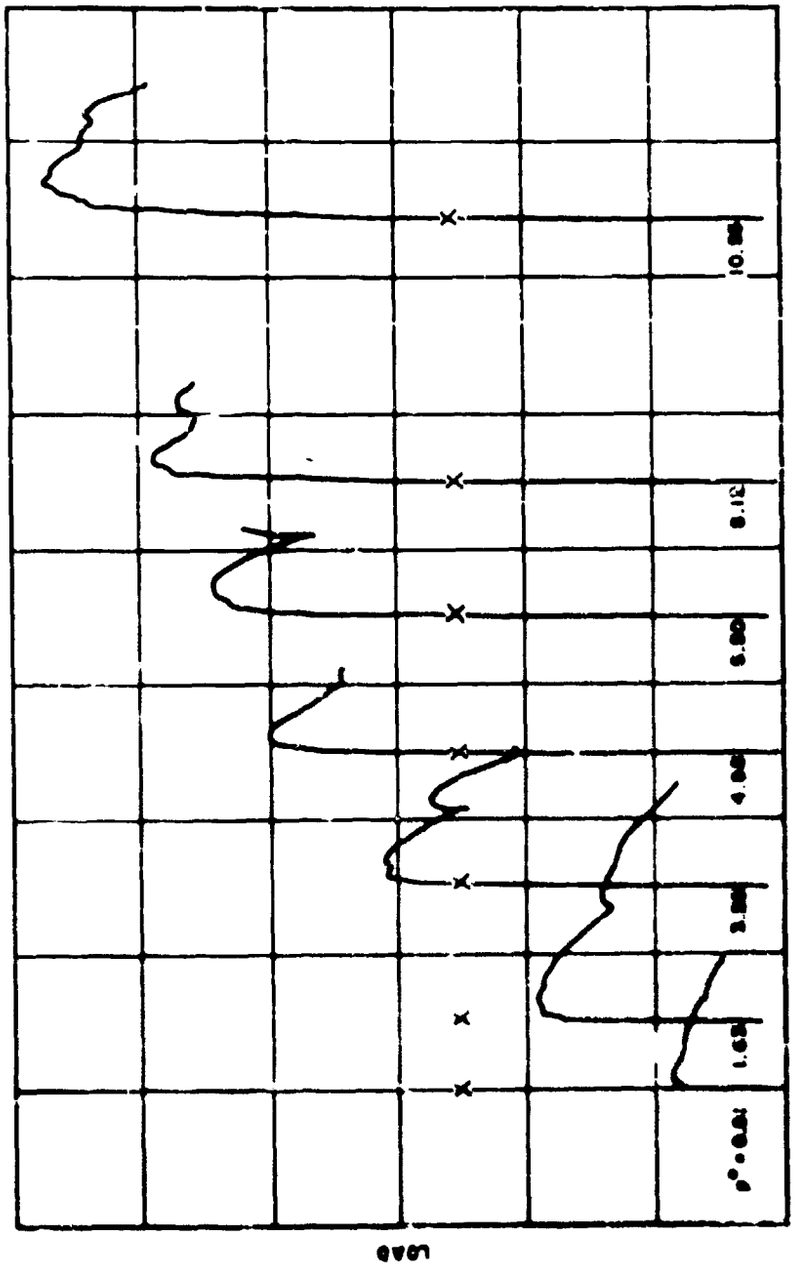

Figure 32. Typical Variation with Internal Lateral Pressure of Load Deformation Curves for a Cylinder in Bending

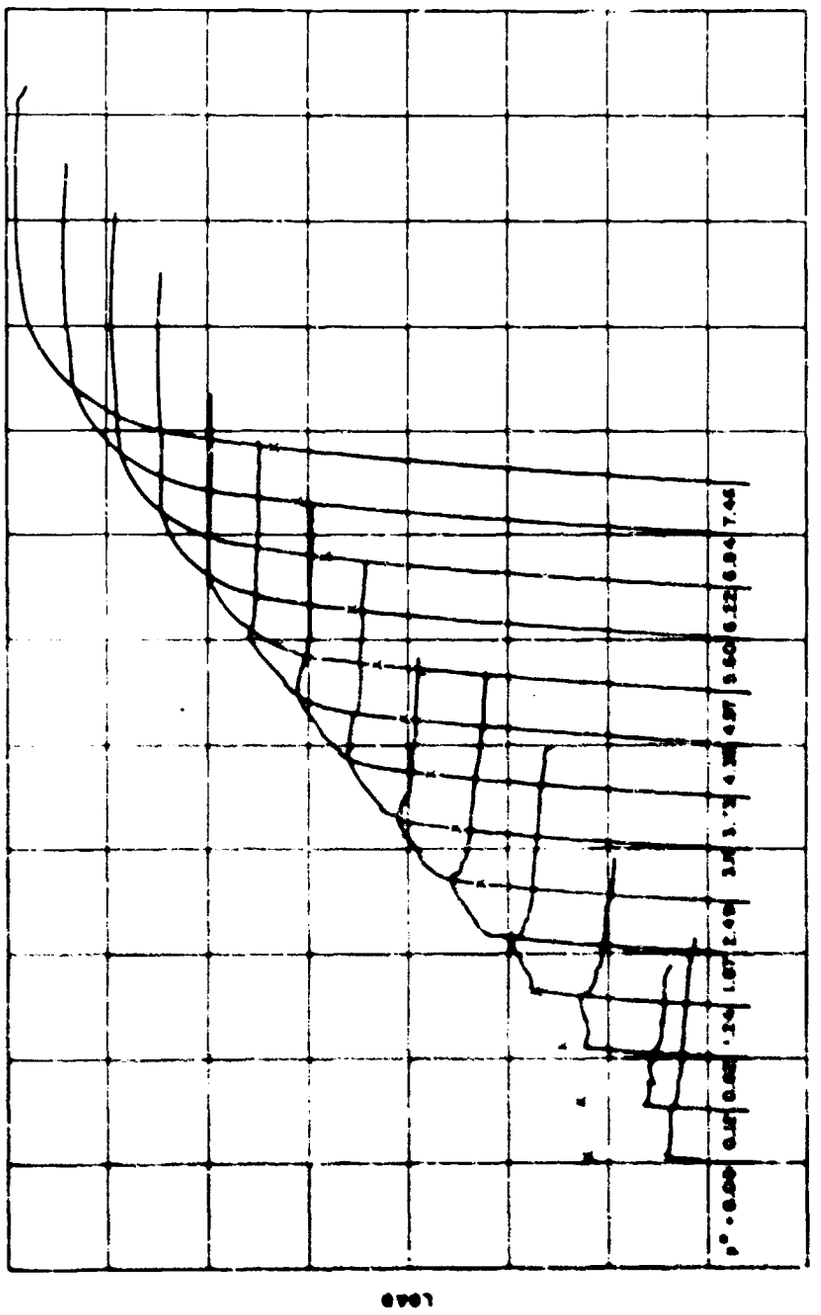

Figure 3.. Typical Variation with Interna' Hydrostatic Pressure of Load Deformation Curves for Cylinders in Bending

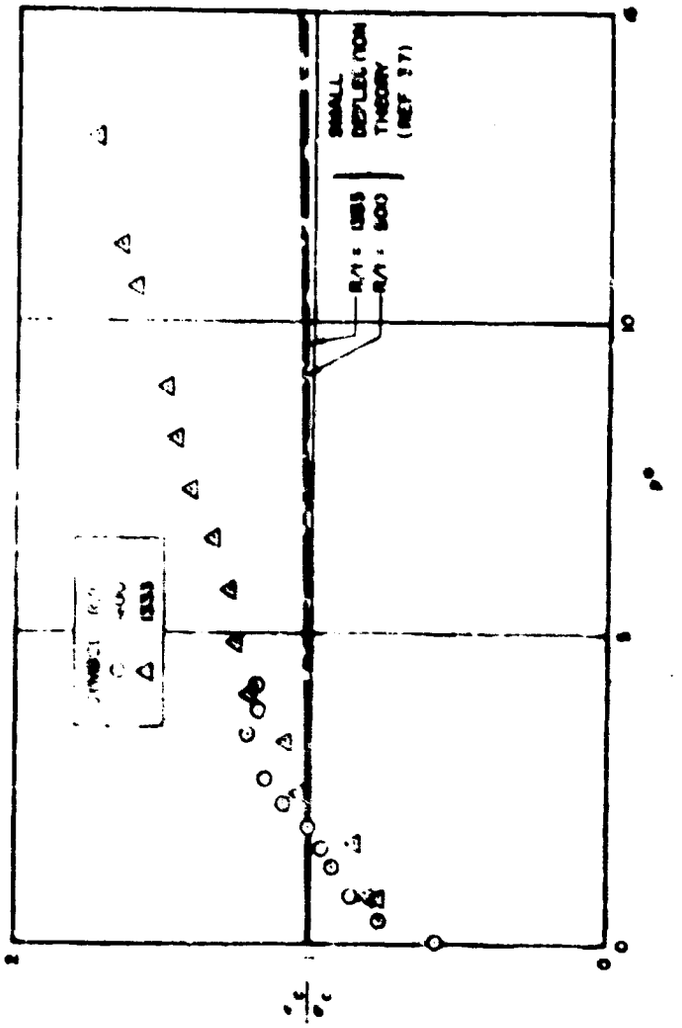

Figure 34 Variation with Internal Pressure Parameter of Collapse Bending Stress Ratios for Cylinders Under Lateral Pressure

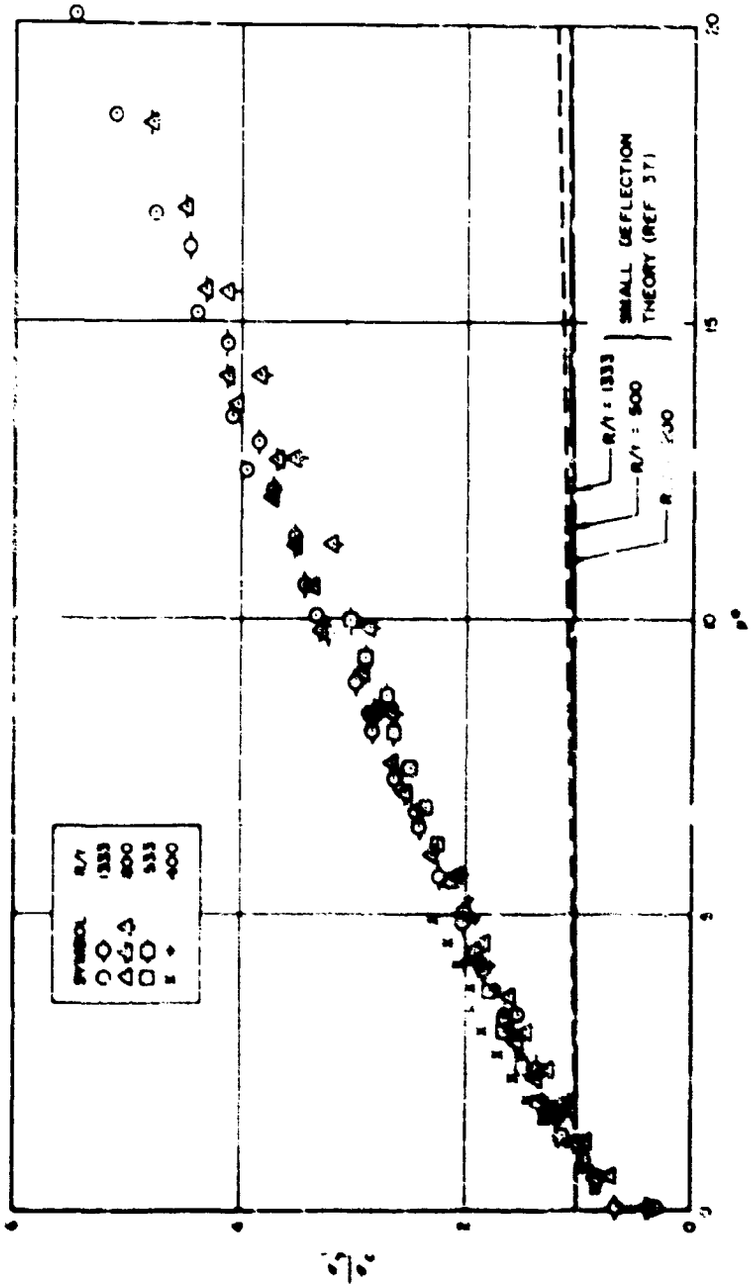

Figure 35. Variation with Internal Pressure Parameter of Net Bending Stress Ratios for Cylinders Under Uniform Hydrostatic Pressure

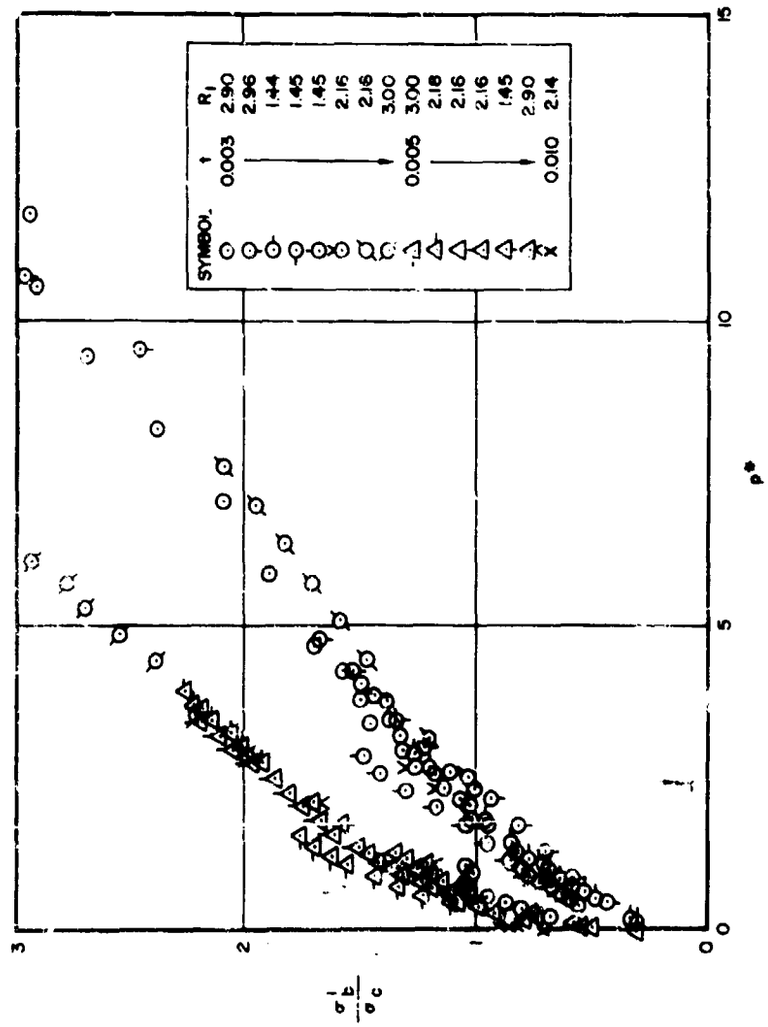

Figure 36. Variation with Internal Pressure Parameter of Net Bending Stress Ratios for 30° Cone Under Uniform Hydrostatic Pressure

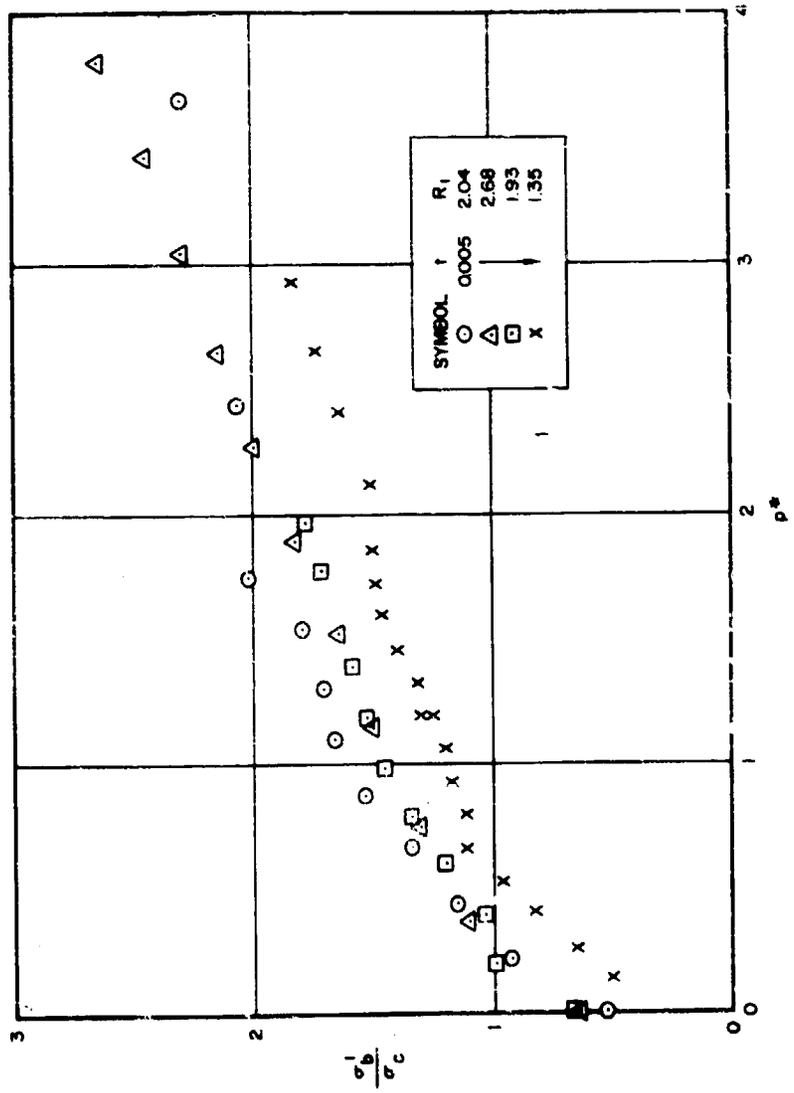

Figure 37. Variation with Internal Pressure Parameter of Net Bending Stress Ratios for 60° Cones Under Uniform Hydrostatic Pressure

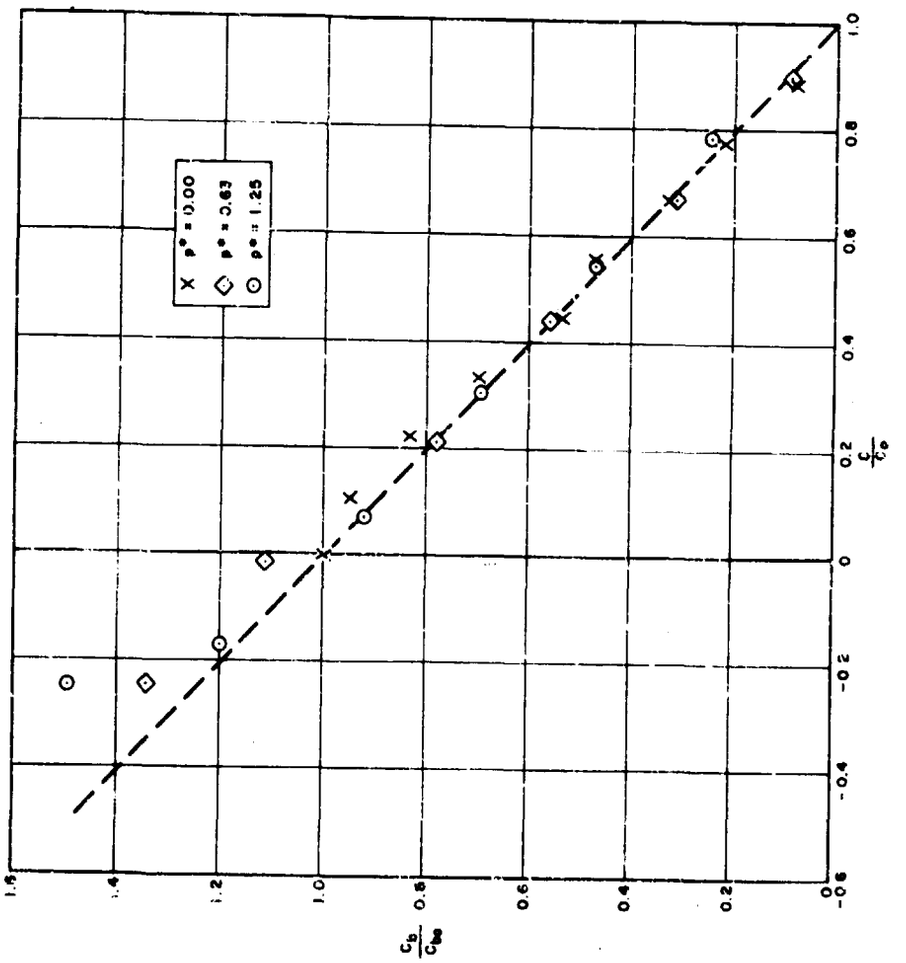

Figure 38. Interaction Curves for Pressurized Cylinder Under Bending and Axial Compression $\left(\frac{R}{t} = 533\right)$

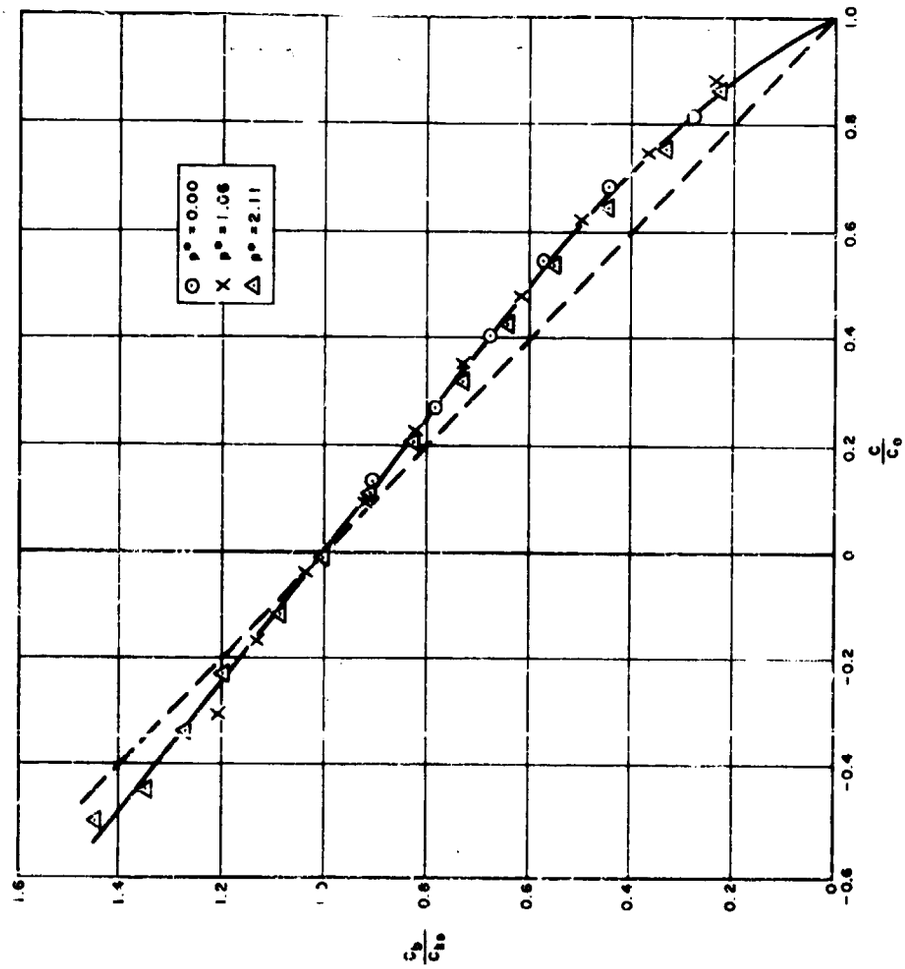

Figure 39. Interaction Curve for a Pressurized Cone Under Bending and Axial Compression $\left(\alpha = 30^\circ, \frac{p}{E}\frac{l}{t} = 670\right)$

X. CYLINDERS AND TRUNCATED CONES UNDER UNIFORM EXTERNAL HYDROSTATIC PRESSURE

The problem of the buckling of conical shells under external uniform hydrostatic pressure has been studied theoretically by many investigators. The various investigations are summarized in Reference 41, which also presents the results of a more accurate independent analysis. The conclusion reached in Reference 41 is that the critical external pressure of a conical frustum is approximately equal to a factor times the critical external pressure of a cylinder having the same wall thickness, a radius equal to the average radius of curvature of the cone, and a length equal to the slant length of the frustum. The factor is a function only of the ratio of the end radii of the cone and increases from 1.00 for the cylinder ($1 - R_1/R_2 = 0$) to 1.22 for a cone with $1 - R_1/R_2$ equal to 0.8 and then decreases to about 1.17 for a complete cone ($1 - R_1/R_2 = 1.0$). Lower values of the factor are implied by the studies of Niordson in Reference 42 and Bijlaard in Reference 43, but these cannot be regarded as theoretically accurate since Niordson makes many approximations of unknown effect in his analysis, while Bijlaard's values are based on intuition.

A. Test Technique

The tests reported in the present section were designed to explore the conclusions of Reference 41. The Mylar specimens were first fixed in the upper clamping fixture (see Figure 6) and then placed on the inner portion of the lower clamping fixture which was raised approximately two inches above the base of the loading fixture by two parallel rectangular blocks. This prevented the bottom of the cone from pressing on the base of the loading fixture. The outer portion of the clamp was then placed over the cone and brought down loosely on the top of the inner lower clamp, since it was discovered that if the lower clamps were fastened by screws, dimples appeared and produced premature buckling as the cones were loaded. The equivalent of external pressure was supplied by evacuating the interior of the specimen by means of a vacuum pump until buckles appeared.

A number of thin-gage and thick-gage cones of various semi-vertex angles were tested with the outer portion of the bottom clamp removed. It was discovered that as long as the cone was dimple free, the buckling pressure was the same for the 10, 20, and 30 degrees whether or not the outer bottom clamp was placed over the cone. For the 45 and 60 degree cones appreciably higher buckling pressures were obtained with the outer portion of the bottom clamp placed over the cones.

B. Results and Discussion

The data for the various tests are given in Tables 15 and 16 in the form of corresponding values of p_{cr}/p_e and $1 - R_1/R_2$. Values of p_e for the average cylinder were obtained from the analysis of Batdorf in Reference 44. In the notation of the present paper

$$p_e = \frac{E}{\sqrt{12(1-\nu^2)}} \left(\frac{t}{\rho_{av}}\right)^2 \frac{1}{\frac{1}{2} + \left(\frac{\bar{n}\ell}{\pi\rho_{av}}\right)^2} \left\{ \frac{\left[1 + \left(\frac{\bar{n}}{\pi\rho_{av}}\right)^2\right]^2}{\frac{\sqrt{12(1-\nu)}}{\pi^2}\left(\frac{\ell}{\rho_{av}}\right)^2 \frac{\rho_{av}}{t}} + \frac{\frac{\sqrt{12(1-\nu^2)}}{\pi^2}\left(\frac{\ell}{\rho_{av}}\right)^2 \frac{\rho_{av}}{t}}{\left[1 + \left(\frac{\bar{n}\ell}{\pi\rho_{av}}\right)^2\right]^2} \right\} . \tag{18}$$

The number of circumferential waves $\bar{n}$ was varied until a minimum value of p_e was obtained.

Let us first consider the cylindrical specimens. In Part (a) of Table 15 corresponding values of Z and C_p are given for the specimens and are compared with the theoretical curve of Reference 44 in Figure 40. Also shown in Figure 44 are the experimental results of Windenberg and

Trilling (Reference 45) and of Sturm (Reference 46). It can be seen that the scatter of the present Mylar and steel results is of the same order as that obtained previously for aluminum and steel specimens. Part of the scatter for the results may be attributed to uncertainty in the modulus of elasticity, for which an average value was used for each thickness. However, there are at least two additional sources of scatter which should be noted. One factor is the effect of initial imperfections, which has only recently been explored in some detail. While initial imperfections of the shape of the buckle pattern have been found to have only a small effect on the critical pressure, Kempner* has noted that asymmetric imperfections may result in significant increases or decreases in buckling pressure. The data available is insufficient, but a grouping of the Mylar data indicates a possible dependence on radius-thickness ratio. A second source of error is the difficulty in some cases of defining a buckling pressure. For the thicker cylinders and cones, buckling was well defined, with many buckles appearing suddenly at some critical pressure. With the thinner cones however, buckling occurred in a progressive fashion, with an isolated buckle appearing at a low pressure, a few more at a somewhat higher pressure, and still more at a higher pressure. The definition of buckling pressure for these cases was, as can be seen, a matter of individual judgement which may have varied from specimen to specimen.

The results for conical shells are shown in Figure 41, together with values obtained by other investigators (References 47-54), which theoretical results of References 41, 42, and 43. We see from Figure 41 that the scatter of the data is too large to verify the trends indicated by the theory of Reference 41. The results do indicate that Niordson's approximation yields a fairly good average fit to the data since the scatter about the line $p_{cr}/p_e = 1$ is relatively uniform for both cones and cylinders of many materials over most of the range of $1 - R_1/R_2$. Since most of the results fall within 80 percent of the line $p/\bar{p} = 1$, it is recommended that both conical shells and cylinders be designed by the formula

*Unpublished paper by J. Kempner, presented at the 10th International Congress of Theoretical and Applied Mechanics, Stresa, Italy, 31 August-8 September 1960.

$$P_{cr} = 0.8\, p_e \tag{19}$$

where p_e can be obtained from Equation (18) or from the approximate relation

$$p_e = \frac{0.92\ E}{\left(\frac{\ell}{\rho_{av}}\right)\left(\frac{\rho_{av}}{t}\right)^{5/2}} \tag{20}$$

The similar buckled shapes of various cylinders and cones are shown in Figure 42. It can be seen that the point of maximum deflection has a tendency to shift toward the large radius of the cone as the small radius decreases, as predicted in Reference 41. The number of circumferential waves obtained experimentally is given in Tables 15 and 16. The computed value of n shown is the number n, which yields the lowest value between the number of buckles given in the two columns is fair, the experimental result being somewhat lower in most cases. It is interesting to note that, while the theory of Reference 41 predicts an increase in the wave number n from that given by $\bar{n}$ cos α for values of $\alpha - R_1/R_2$ greater than 0.6, the experimental results do not indicate any such phenomenon.

Table 15. Experimental Data for Mylar Cylinders and Cones under External Uniform Hydrostatic Pressure.

t (inch)	$E \times 10^{-3}$ (psi)	R/t*	L/R*	P_{cr}/P_e	n (experimental)	n (computed)	$\bar{Z}$	C_p
(a) $\alpha = 0^\circ$								
0.010	690	400	1	0.895	10	12	382	18.2
0.010	690	400	1	1.087	9	12	382	22.1
0.0075	770	533	1	0.983	11	13	508	23.1
0.0075	770	533	1	1.079	11	13	508	25.4
0.005	750	800	1	0.882	11	14	762	25.4
0.005	750	800	1	0.941	12	14	763	27.1
0.005	750	800	1	0.740	--	14	763	21.3
0.005	750	800	1	1.161	--	14	763	33.5
0.003	775	1333	1	0.967	13	16	1272	36.0
0.003	775	1333	1	0.901	13	16	1272	33.5
0.003	775	1333	1	0.901	13	16	1272	33.5
0.003	775	1333	1	0.882	13	16	1272	32.8
0.003	775	1333	1	0.844	13	16	1272	31.4
0.003	775	1333	1	0.948	13	16	1272	35.3
0.005	750	800	1.5	1.078	--	--	1717	46.6
0.010	690	400	2	0.991	6	9	1526	39.5
0.010	690	400	2	0.969	6	9	1526	37.3
0.010	675	400	2	1.227	8	9	1526	50.0
0.010	675	400	2	1.340	8	9	1526	54.6
0.0080	762	500	2	1.094	8	9	1908	49.8
0.0080	712	500	2	1.232	9	9	1908	56.1
0.0075	800	533	2	1.220	9	9	2034	57.4
0.0075	800	533	2	1.253	8	9	2034	58.9
0.0075	770	533	2	0.983	7	9	2034	46.2
0.0075	770	533	2	0.811	7	9	2034	38.1
0.0050	750	800	2	1.029	8	10	3053	59.3
0.0050	750	800	2	0.951	8	10	3053	54.8
0.0050	750	800	2	0.787	--	10	3053	45.3
0.0030	775	1333	2	1.043	9	12	5086	77.6
0.0030	775	1333	2	0.977	9	12	5086	72.7
0.0100	690	400	3	1.354	--	--	3434	82.7

*R = 4 inches in all cases.

Table 15. Continued

(inch)	$E \times 10^{-3}$ (psi)	ρ_{av}/t	t/ρ_{av}	$1 - R_1/R_2$*	P_{cr}/P_e	n (experimental)	n (computed)
(b) $\phi = 10^{\circ}$							
0.010	690	455	1.44	0.20	1.386	--	--
0.010	690	455	1.44	0.20	1.227	--	--
0.003	775	1515	1.44	0.20	1.043	13	13 - 14
0.003	775	1515	1.44	0.20	1.081	12	13 - 14
0.010	690	393	3.3	0.45	1.150	5	6 - 7
0.010	690	393	3.3	0.45	1.097	5	6 - 7
0.010	690	393	3.3	0.45	1.149	--	6 - 7
0.010	690	393	3.3	0.45	1.208	--	6 - 7
0.005	750	786	3.3	0.45	0.960	6	7 - 8
0.005	750	786	3.3	0.45	1.029	6	7 - 8
0.005	750	786	3.3	0.45	0.927	--	7 - 8
0.005	750	786	3.3	0.45	0.943	--	7 - 8
0.005	750	786	3.3	0.45	1.064	--	7 - 8
0.003	775	1310	3.3	0.45	0.996	7	8 - 9
0.003	775	1310	3.3	0.45	0.977	7	8 - 9
0.002	740	1970	3.3	0.45	0.884	7	9 - 10
0.002	740	1970	3.3	0.45	0.864	7	9 - 10
0.005	750	762	3.79	0.50	1.205	--	--
0.005	750	762	3.79	0.50	1.181	--	--
0.003	775	1270	3.79	0.50	1.110	7	7 - 8
0.003	775	1270	3.79	0.50	1.015	7	7 - 8
0.002	740	1650	6.13	0.70	0.884	5	6 - 7
0.002	740	1650	6.13	0.70	0.884	5	6 - 7

*R_2 = 5 inches in all cases.

Table 15. Continued

t (inch)	E x 10^{-3} (psi)	P_{av} t	f = P_{av}	1 - $R_1 P_2^*$	P_{cr} = P_e	n (experimental)	n (predicted)
			ϕ = 20°				
0.003	775	1600	0.61	0.20	0.977	16	20 - 21
0.003	775	1600	0.61	0.20	0.873	16	20 - 21
0.010	690	400	1.83	0.50	1.094	--	8 - 9
0.010	690	400	1.83	0.50	1.227	--	8 - 9
0.010	690	400	1.83	0.50	1.227	--	8 - 9
0.010	690	400	1.83	0.50	1.129	7	8 - 9
0.010	690	400	1.83	0.50	1.023	7	8 - 9
0.005	750	800	1.83	0.50	0.844	9	10 - 11
0.005	750	800	1.83	0.50	0.960	9	10 - 11
0.005	750	800	1.83	0.50	1.055	--	10 - 11
0.005	750	800	1.83	0.50	1.103	--	10 - 11
0.005	750	800	1.83	0.50	1.007	--	10 - 11
0.003	775	1333	1.83	0.50	0.910	10	11 - 12
0.003	775	1333	1.83	0.50	0.929	10	11 - 12
0.002	740	2000	1.83	0.50	0.805	11	12 - 13
0.002	740	2000	1.83	0.50	1.013	11	12 - 13
0.010	690	346	2.96	0.70	1.148	--	--
0.010	690	346	2.96	0.70	1.148	--	--
0.010	690	346	2.96	0.70	1.148	--	--
0.005	750	692	2.96	0.70	1.203	--	--
0.005	750	692	2.96	0.70	1.362	--	--
0.005	750	692	2.96	0.70	1.245	--	--
0.002	740	1730	2.96	0.70	0.983	7	9 - 10
0.002	740	1730	2.96	0.70	1.045	7	9 - 10

* R_2 = 5 inches in all cases.

Table 15. Continued

t (inch)	$\Sigma \times 10^{-3}$ (psi)	ρ_{av}/t	ℓ/ρ_{av}	$1 - R_1/R_2$*	P_{cr}/P_e	n (experimental)	n (predicted)
(d) α = 30°							
0.003	775	1735	0.50	0.20	1.166	21	20 - 21
0.003	775	1735	0.50	0.20	1.195	21	20 - 21
0.005	750	1041	0.50	0.20	0.980	--	--
0.010	690	521	0.50	0.20	1.349	--	--
0.003	775	1430	1.15	0.50	0.929	11	13 - 14
0.003	775	1430	1.15	0.50	0.948	11	13 - 14
0.005	750	858	1.15	0.50	0.917	--	--
0.010	690	429	1.15	0.50	1.008	--	--
0.002	740	2020	1.48	0.60	0.844	11	13
0.003	740	2020	1.48	0.60	0.913	11	13
0.003	775	1350	1.48	0.60	0.966	8	12 - 13
0.004	775	1350	1.48	0.60	0.939	8	12 - 13
0.005	750	810	1.48	0.60	0.921	8	10 - 11
0.005	750	810	1.48	0.60	0.872	8	10 - 11
0.005	750	810	1.48	0.60	0.882	8	10 - 11
0.005	750	810	1.48	0.60	0.950		
0.010	690	405	1.48	0.60	1.033	7	8 - 9
0.010	690	405	1.48	0.60	1.172	7	8 - 9
0.010	690	405	1.48	0.60	0.980	7	8 - 9
0.010	690	405	1.48	0.60	1.118	7	8 - 9
0.010	690	405	1.48	0.60	1.102	--	8 - 9
0.005	750	750	1.92	0.70	0.950	--	--
0.010	690	375	1.92	0.70	1.065	--	--

* R_2 = 5 inches in all cases

Table 15. Continued

t (inch)	$E \times 10^{-3}$ (psi)	ρ_{av}/t	ℓ/ρ_{av}	$1 - R_1/R_2$*	p_{cr}/p_e	n (experimental)	n (predicted)
(e) $\alpha = 45^{\circ}$							
0.005	750	1270	0.22	0.20	0.843	20	22 - 23
0.005	750	1270	0.22	0.20	0.784	21	22 - 23
0.003	775	1765	0.67	0.50	0.854	13	14 - 15
0.003	775	1765	0.67	0.50	0.910	12	14 - 15
0.002	740	1875	1.82	0.70	0.954	8	11 - 12
0.002	740	1875	1.82	0.70	0.954	8	11 - 12
0.003	775	1530	1.08	0.70	1.034	9	11 - 12
0.003	775	1530	1.08	0.70	1.015	9	11 - 12
0.005	750	918	1.08	0.70	1.002	--	--
0.005	750	918	1.08	0.70	0.978	--	--
0.010	690	459	1.08	0.70	1.142	--	--
0.010	690	459	1.08	0.70	1.215	--	--
0.010	690	459	1.08	0.70	1.134	--	--
0.002	740	2030	1.48	0.85	0.993	9	10 - 11
0.002	740	2030	1.48	0.85	1.053	10	10 - 11
0.003	775	1353	1.48	0.85	0.863	10	9 - 10
0.003	775	1353	1.48	0.85	0.910	10	9 - 10
0.005	750	812	1.48	0.85	1.029	8	8 - 9
0.005	750	812	1.48	0.85	0.951	8	8 - 9
0.005	750	812	1.48	0.85	0.932	--	8 - 9
0.005	750	812	1.48	0.85	0.928	--	8 - 9
0.005	750	812	1.48	0.85	0.900	--	8 - 9
0.010	690	406	1.48	0.85	1.044	6	7
0.010	690	406	1.48	0.85	1.065	6	7
0.010	690	406	1.48	0.85	1.181	--	7
0.010	690	406	1.48	0.85	1.181	--	7
0.010	690	406	1.48	0.85	1.251	--	7

*R_2 = 5 inches in all cases

Table 15. Concluded

t (inch)	$E \times 10^{-3}$ (psi)	p_{av}/t	t/p_{av}	$1 - R_1/R_2$*	p_{cr}/p_e	n (experimental)	n (predicted)
			(f) α = 60°				
0.005	750	1500	0.38	0.50	0.892	10	13 - 14
0.005	750	1500	0.38	0.50	0.813	10	13 - 14
0.010	690	750	0.38	0.50	0.786	--	--
0.005	750	1300	0.62	0.70	0.787	--	--
0.005	750	1300	0.62	0.70	0.862	8	10
0.005	750	1300	0.62	0.70	0.882	9	10
0.010	690	650	0.62	0.70	1.534	--	--
0.005	750	2000	0.77	0.80	0.863	10	10 - 11
0.005	750	2000	0.77	0.80	0.996	10	10 - 11
0.005	750	1200	0.77	0.80	0.941	8	9
0.005	750	1200	0.77	0.80	0.960	9	9
0.005	750	1200	0.77	0.80	0.823	--	--
0.0075	720	800	0.77	0.80	0.926	8	8
0.0075	720	800	0.77	0.80	0.935	8	8
0.010	690	600	0.77	0.80	0.969	7	7 - 8
0.010	690	600	0.77	0.80	0.969	7	7 - 8
0.010	690	600	0.77	0.80	1.020	--	7 - 8

*R_2 = 5 inches in all cases.

Table 16. Experimental Data for Steel Cylinders and Cones under External Uniform Hydrostatic Pressure

t (inch)	E x 10^{-6} (psi)	ρ_{av}/t	t/ρ_{av}	$1 - R_1/R_2$*	P_{cr}/P_e	n (experimental)	n (predicted)
			$\alpha = 0^\circ$				
0.010	30.3	800	1	0	0.928	12	14
0.010	30.3	800	2	0	0.930	8	10
0.010	30.3	800	2	0	1.015	8	10
0.010	30.3	800	1	0	0.970	12	14
			$\alpha = 30^\circ$				
0.010	30.3	810	1.48	0.60	1.270	9	10 - 11
0.010	30.3	810	1.48	0.60	1.250	10	10 - 11
0.020	30.3	405	1.48	0.60	1.108	9	8 - 9
0.020	30.3	405	1.48	0.60	0.982	9	8 - 9
			$\alpha = 60^\circ$				
0.010	30.3	1500	0.38	0.50	0.937	11	13 - 14
0.010	30.3	1500	0.38	0.50	0.904	11	13 - 14
0.010	30.3	1300	0.62	0.70	0.959	8	10
0.010	30.3	1300	0.62	0.70	1.105	9	10
0.010	30.3	1200	0.77	0.80	0.970	7	9
0.010	30.3	1200	0.77	0.80	1.200	8	9
0.020	30.3	600	0.77	0.80	1.045	6	7 - 8
			$\alpha = 75^\circ$				
0.020	30.3	1255	0.29	0.70	0.989	--	7 - 8
0.010	30.3	2318	0.36	0.80	0.941	8	8 - 9
0.010	30.3	2318	0.36	0.80	0.973	9	8 - 9
0.010	30.3	2318	0.36	0.80	0.971	9	8 - 9
0.020	30.3	1159	0.36	0.80	1.130	8	6 - 7

*R_2 = 8 inches for cylinders and 10 inches for cones.

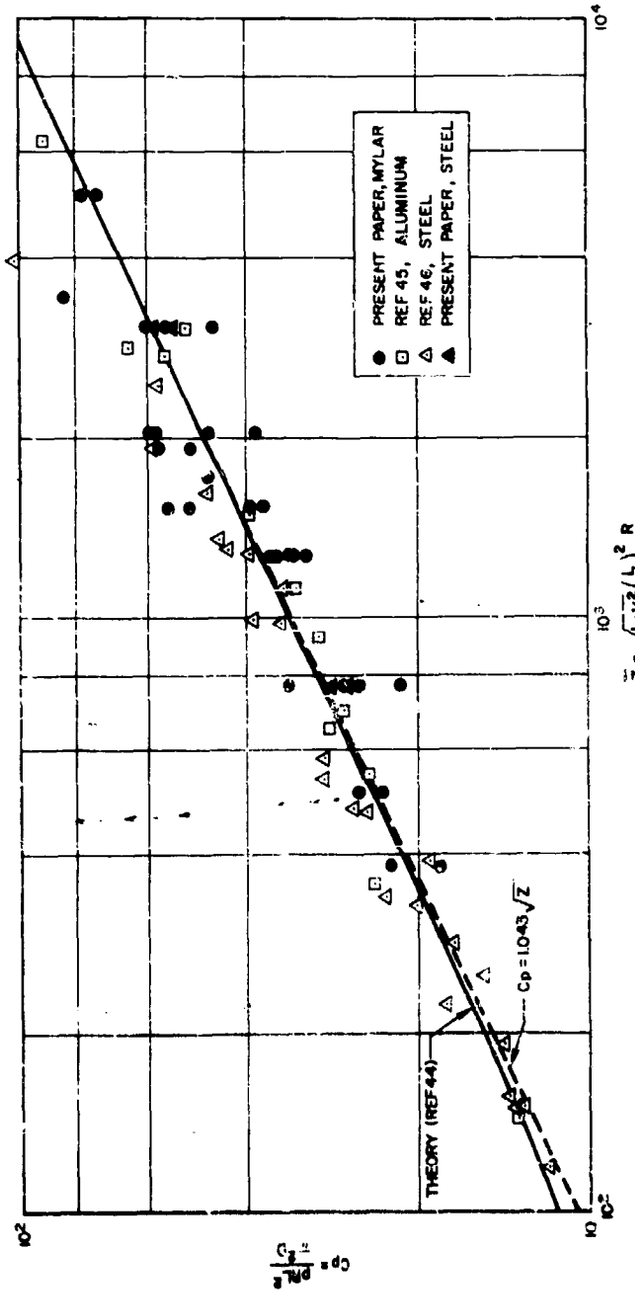

Figure 40. Comparison with Theory of Various External Hydrostatic Pressure Test Results for Cylinders

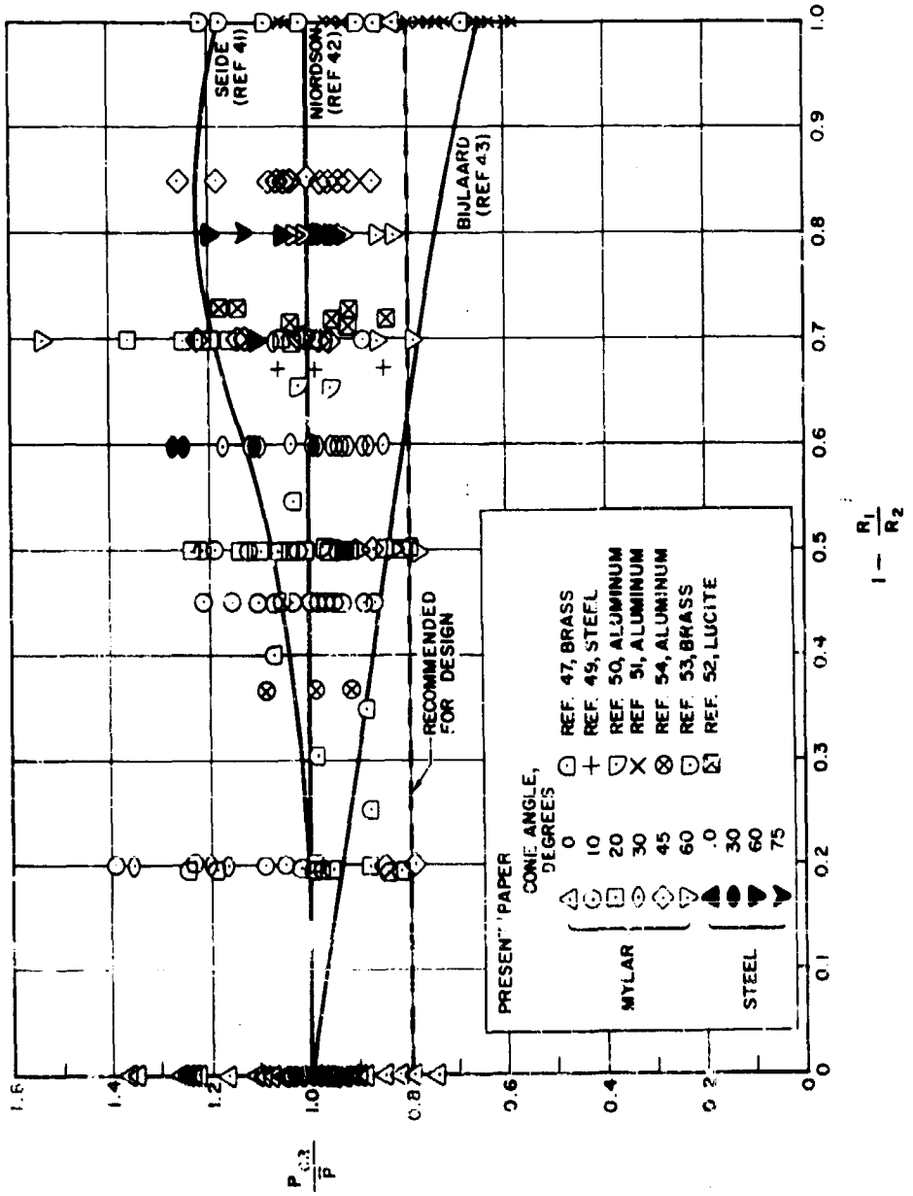

Figure 41. Comparison with Various Theoretical Results of External Pressure Test Data for Conical Shells

$1 - \frac{R_1}{R_2} = 0$ $\alpha = 0^\circ$ $1 - \frac{R_1}{R_2} = 0$

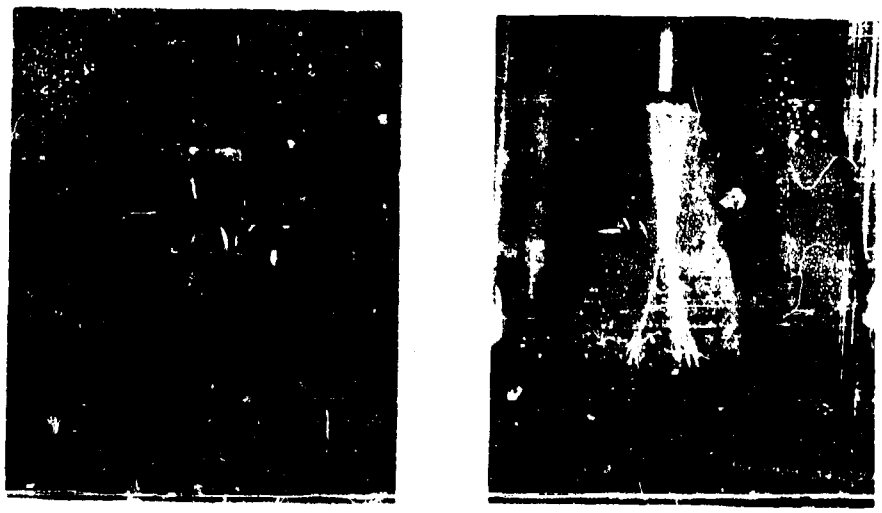

$1 - \frac{R_1}{R_2} = 0.2$ $\alpha = 10^\circ$ $1 - \frac{R_1}{R_2} = 0.45$

Figure 42. Experimental Buckle Patterns for Cylinders and Cones Under External Uniform Hydrostatic Pressure

Mylar

$1 - \frac{R_1}{R_2} = 0.6$

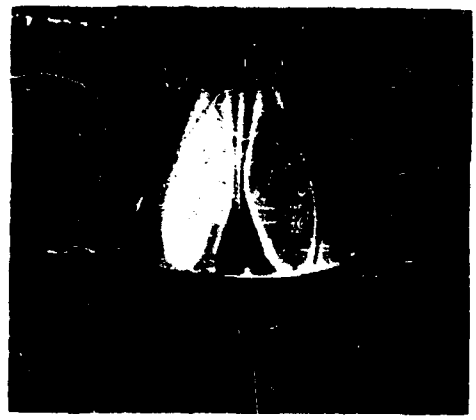

$\alpha = 30^\circ$

Steel

$1 - \frac{R_1}{R_2} = 0.6$

$1 - \frac{R_1}{R_2} = 0.50$

$\alpha = 45^\circ$

$1 - \frac{R_1}{R_2} = 0.85$

Figure 42. Continued

$$1 - \frac{R_1}{R_2} = 0.7$$

$\alpha = 60^\circ$

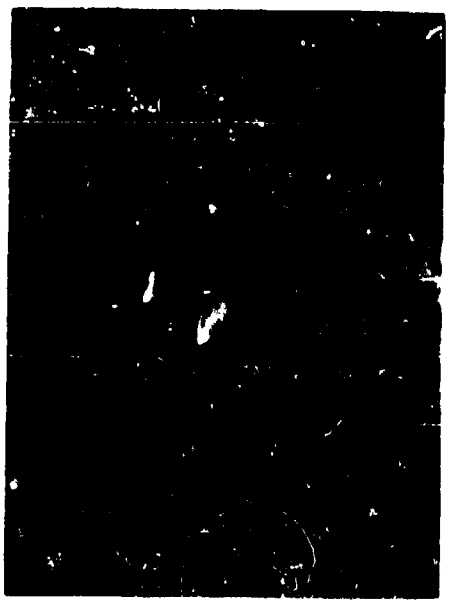

$$1 - \frac{R_1}{R_2} = 0.8$$

Figure 42. Concluded

XI. CYLINDERS AND TRUNCATED CONES UNDER AXIAL COMPRESSION AND EXTERNAL PRESSURE

The theoretical small-deflection behavior of cylinders under axial compression and external uniform hydrostatic pressure is discussed in References 7 and 9 and is more thoroughly investigated for both cylinders and cones in Reference 31. The results indicate that the interaction curve is nearly a straight line for cylinders and becomes more concave downward as the taper ratio $(1 - R_1/R_2)$ increases for conical shells. No experimental data have appeared in the literature to deny or confirm these results.

The experimental program discussed herein is very limited, comprising 10 cylinders, 5 cones having a 30 degree semivertex angle, and 3 cones having a 60 degree semivertex angle. The results for cylinders are given in part (a) of Table 17 in several different ways. For the purpose of constructing interaction curves, corresponding values of P/P_o and p/p_o are tabulated. These are shown in Figure 43. It is apparent that the spread of the data is so great that no single interaction curve can be drawn. The reason for this spread of data is more readily seen from the values of $P/2\pi Et^2$ plotted as a function of p/p_o^* in Figure 44. Also shown is the theoretical interaction curve obtained in Reference 31. It can be seen that, for values of external pressure near the critical value, the data follow the theoretical interaction curve reasonably well. Those cylinders which yield lower axial buckling coefficients depart from the theoretical interaction curve much sooner than do those which yield higher values of the axial buckling coefficient. Thus the interaction curves for cylinders undoubtedly depend on the radius-thickness ratio of the cylinder and would require many more tests for their detailed establishment. However, from the limited data we may conclude that the use of a straight line interaction curve, or the theoretical curve, is conservative

---

*p/p_e could also have been used, but with somewhat more scatter.

and, considering the wide range of values that might be expected for cylinders having a given radius-thickness ratio, adequate for design.

The behavior of the few cones tested was quite different in that an unexpected phenomenon was encountered. Although the load carrying capacity of cylinders always decreased when buckling occurred (with the buckle mode remaining the same), such is not the case for conical shells. It was found that for low values of external pressure, two distinct equilibrium shapes could be obtained for approximately the same axial compressive load. For larger values of the external pressure, the mode associated with buckling was first obtained as the axial load was increased. When buckling occurred, the load carrying capacity would drop slightly but then would continue to increase beyond the buckling load until the second mode, called the collapse mode, was obtained. In addition, the cones continued to carry some load when the pressure was increased beyond the critical value for external pressure alone, decreasing finally to zero when the external pressure that would yield the collapse mode was reached.

An illustration of the buckle and collapse modes of conical shells for various external pressures is shown in Figure 45. It is interesting to note that, except for the case of axial compression alone, the buckle mode shape does not vary much with external pressure and that the collapse mode can be considered to be independent of load. The buckling behavior differs somewhat from that associated with cylinders, for which the buckled shapes are illustrated in Figure 46.

The experimental data for the conical shells is given in parts (b) and (c) of Table 17. In addition to parameters involving the buckling load P, other parameters for the collapse load P^1 are given. The curves for P/P_o and P^1P_o as a function of p/p_o are shown in Figure 47 for the 30 degree cones and in Figure 48 for the 60 degree cones. It can be seen that the different physical behavior of conical shells is associated with interaction curves that differ from those for cylinders. The buckling data

for the various cones are in fairly good agreement with the theoretically predicted interaction curves. The collapse data indicates that the phenomenon is a function of the semivertex angle since the collapse loads for the 30 degree cones differ from the buckling loads at pressures greater than about 60 percent of the critical value for pressure alone, compared to pressures greater than about 20 percent of the critical value for pressure alone for the 60 degree cones. The 60 degree cones are also seen to have collapse load ratios larger than those for 30 degree cones, as well as a larger collapse pressure ratio.

When the values of $P/2\pi Et^2\cos^2\alpha$ are plotted as a function of p/p_o (Figure 49) it can be seen that even though the axial load coefficient for axial load alone is of the same order as those for the smaller radius-thickness ratio cylinders, the shapes of the curves are quite different. The cone data indicates a percentage reduction in the axial load parameter which is almost independent of the pressure ratio (hence, yielding almost a straight line interaction curve), whereas the cylinder data (Figure 44) indicates agreement between theory and experiment for pressure ratios near unity and an insensitivity to pressure for pressure ratios near zero.

It is evident that considerable theoretical and experimental work remains to be done to explain the differences between cone and cylinder behavior under combined axial compression and external pressure. The limited results do indicate, however, that a straight line interaction curve is safe for design purpose.

Table 17. Experimental Data for Mylar Cylinders and Cones under Axial Compression and External Uniform Hydrostatic Pressure.

t (in.)	E (psi)	ρ_{av}/t	t/ρ_{av}	P/P_o	p/p_o	$P/2\pi Et^2 \cos^2 \alpha$	p/p_e
(a) $\alpha = 0^\circ$							
0.010	690,000	400	3.0	1.000	0.000	0.269	0.000
				0.992	0.161	0.267	0.217
				0.943	0.323	0.255	0.437
				0.856	0.484	0.231	0.655
				0.769	0.646	0.208	0.875
				0.610	0.807	0.164	1.092
				0.396	0.887	0.108	1.202
				0.107	0.968	0.029	1.310
				0.000	1.000	0.000	1.354
0.010	675,000	400	2.0	0.000	1.000	0.000	1.340
				1.000	0.000	0.290	0.000
				0.982	0.139	0.285	0.186
				0.971	0.279	0.282	0.372
				0.967	0.416	0.281	0.558
				0.952	0.554	0.276	0.744
				0.849	0.695	0.246	0.930
				0.537	0.834	0.156	1.116
				0.179	0.972	0.052	1.303
				0.154	1.110	0.045	1.488
0.005	750,000	800	2.0	1.000	0.000	0.163	0.000
				0.958	0.169	0.156	0.132
				0.942	0.337	0.153	0.265
				0.848	0.505	0.137	0.398
				0.791	0.673	0.128	0.529
				0.644	0.720	0.105	0.566
				0.592	0.773	0.096	0.609
				0.494	0.820	0.080	0.646
				0.410	0.867	0.067	0.682
				0.334	0.913	0.054	0.719
				0.258	0.960	0.042	0.756
				0.000	1.000	0.000	0.787
0.005	750,000	800	1.5	1.000	0.000	0.184	0.000
				0.989	0.132	0.182	0.142
				0.906	0.264	0.168	0.284
				0.828	0.394	0.153	0.425
				0.722	0.526	0.133	0.566
				0.547	0.661	0.101	0.712
				0.506	0.726	0.093	0.783
				0.453	0.792	0.084	0.855
				0.387	0.858	0.071	0.925
				0.320	0.923	0.059	0.995
				0.253	0.949	0.047	1.025
				0.000	1.000	0.000	1.078
0.005	750,000	800	1.0	1.000	0.000	0.156	0.000
				0.858	0.166	0.133	0.123
				0.743	0.333	0.116	0.246
				0.634	0.500	0.099	0.370
				0.499	0.667	0.078	0.493
				0.317	0.833	0.049	0.616
				0.254	0.897	0.039	0.663
				0.222	0.922	0.034	0.682
				0.190	0.947	0.030	0.700
				0.000	1.000	0.000	0.740

Table 17. Continued

t (in.)	E (psi)	ρ_{av}/t	t/ρ_{av}	P/P_o	p/p_o	$P/2\pi Et^2 \cos^2 \alpha$	p/p_e
(a) $\alpha = 0^o$							
0.005	750,000	500	2.0	1.000	0.000	0.210	0.000
				0.872	0.204	0.182	0.237
				0.730	0.408	0.153	0.473
				0.625	0.610	0.130	0.709
				0.365	0.814	0.076	0.945
				0.200	0.915	0.042	1.062
				0.129	0.960	0.027	1.115
				0.000	1.000	0.000	1.161
0.0075	800,000	533	2.0	0.000	1.000	0.000	1.220
				1.000	0.000	0.305	0.000
				0.993	0.131	0.302	0.161
				0.966	0.263	0.294	0.321
				0.949	0.395	0.289	0.482
				0.906	0.526	0.276	0.643
				0.815	0.659	0.248	0.803
				0.535	0.790	0.163	0.964
				0.343	0.922	0.105	1.125
0.0075	800,000	533	2.0	1.000	0.000	0.253	0.000
				0.000	1.000	0.000	1.253
				0.939	0.129	0.238	0.161
				0.850	0.257	0.215	0.321
				0.757	0.384	0.192	0.482
				0.737	0.513	0.187	0.643
				0.716	0.643	0.181	0.803
				0.534	0.770	0.135	0.964
				0.270	0.898	0.069	1.125
				0.210	1.025	0.053	1.285
0.0080	712,000	500	2.0	0.000	1.000	0.000	1.232
				1.000	0.000	0.289	0.000
				0.963	0.125	0.278	0.154
				0.909	0.250	0.263	0.308
				0.888	0.375	0.257	0.462
				0.874	0.500	0.253	0.616
				0.819	0.626	0.237	0.771
				0.742	0.750	0.215	0.924
				0.375	0.875	0.108	1.078
				0.182	1.000	0.053	1.232
0.008	762,000	500	2.0	0.000	1.000	0.000	1.094
				1.000	0.000	0.315	0.000
				0.988	0.131	0.311	0.144
				0.959	0.263	0.302	0.288
				0.937	0.394	0.295	0.432
				0.880	0.527	0.277	0.576
				0.622	0.659	0.196	0.721
				0.261	0.923	0.082	1.008
				0.141	1.051	0.044	1.151
				0.111	1.185	0.0349	1.295

Table 17. Continued

t (in.)	E (psi)	ρ_{av}/t	t/ρ_{av}	P/P_o	P'/P_o	p/p_o	$P/2\pi Et^2\cos^2\alpha$	$P'/2\pi Et^2\cos^2\alpha$	p/p_o
					(b) $\alpha = 30^\circ$				
0.0081	682,000	535	1.16	1.000	1.000	0.000	0.284	0.284	0.000
				0.000	--	1.000	0.000	--	1.185
				0.879	0.879	0.148	0.250	0.250	0.175
				0.758	0.758	0.296	0.216	0.216	0.351
				0.637	0.637	0.407	0.181	0.181	0.483
				0.517	0.517	0.555	0.147	0.147	0.658
				0.396	0.396	0.667	0.113	0.113	0.790
				0.275	0.304	0.778	0.078	0.086	0.922
				0.154	0.289	0.889	0.044	0.082	1.053
				0.082	0.284	0.925	0.023	0.081	1.097
				--	0.231	1.111	-	0.066	1.317
				--	0.149	1.296		0.042	1.536
				--	0.111	1.482	--	0.031	1.756
0.0082	650,000	493	1.49	1.000	1.000	0.000	0.291	0.291	0.000
				0.000	--	1.000	0.000	--	1.063
				0.879	0.879	0.227	0.256	0.256	0.241
				0.758	0.758	0.454	0.221	0.221	0.241
				0.637	0.637	0.591	0.186	0.186	0.628
				0.516	0.516	0.727	0.151	0.151	0.771
				0.396	0.396	0.841	0.115	0.115	0.894
				0.275	0.314	0.909	0.080	0.091	0.966
				0.154	0.279	0.954	0.045	0.082	1.015
				--	0.251	1.000	--	0.073	1.063
				--	0.181	1.136	--	0.052	1.208
				--	0.101	1.364	--	0.029	1.450
				--	0.079	1.591	--	0.023	1.691
0.0082	682,000	493	1.49	1.000	1.000	0.000	0.332	0.332	0.000
				0.000	--	1.000	0.000	--	1.138
				0.879	0.879	0.058	0.291	0.291	0.066
				0.757	0.757	0.231	0.251	0.251	0.263
				0.636	0.636	0.423	0.211	0.211	0.481
				0.514	0.514	0.616	0.170	0.170	0.701
				0.393	0.393	0.731	0.130	0.130	0.832
				0.271	0.271	0.807	0.090	0.090	0.919
				0.149	0.190	0.922	0.049	0.063	1.050
				0.109	0.190	0.922	0.036	0.063	1.050
				0.068	0.194	0.922	0.023	0.064	1.050
				--	0.198	0.922	--	0.066	1.050
				--	0.154	1.153	--	0.051	1.313
				--	0.089	1.385	--	0.029	1.576
0.0181	700,000	372	1.87	1.000	1.000	0.000	0.254	0.254	0.000
				0.000	--	1.000	0.000	--	1.113
				0.871	0.871	0.188	0.221	0.221	0.20
				0.769	0.769	0.255	0.196	0.196	0.25
				0.668	0.668	0.300	0.170	0.170	0.334
				0.543	0.543	0.525	0.138	0.138	0.584
				0.440	0.468	0.600	0.112	0.119	0.668
				0.363	0.403	0.688	0.092	0.103	0.765
				0.261	0.371	0.775	0.066	0.094	0.863
				0.159	0.329	0.850	0.040	0.084	0.946
				0.091	0.312	0.888	0.023	0.079	0.988
				0.057	0.234	0.913	0.014	0.059	1.016
				--	0.175	0.975	--	0.044	1.085
				--	0.186	1.125	--	0.047	1.253
				--	0.171	1.250	--	0.043	1.391
				--	0.122	1.375	--	0.031	1.531
				--	0.083	1.500	--	0.021	1.670
				--	0.064	1.625	--	0.016	1.809
				--	0.000	1.750	--	0.000	1.948

Table 17. Concluded

t (in.)	E (psi)	ρ_{av}/t	t/ρ_{av}	P/P_o	P'/P_o	p/p_o	$P/2\pi Et^2 \cos^2 \alpha$	$P'/2\pi Et^2 \cos^2 \alpha$	p'/p_o
					(b) α = 30°				
0.0100	700,000	375	1.87	1.000	1.000	0.000	0.230	0.230	0.000
				0.000	--	1.000	0.000	--	1.141
				0.899	0.899	0.125	0.207	0 207	0.143
				0.792	0.792	0.250	0.182	0.182	0.285
				0.665	0.665	0.500	0.153	0.153	0.570
				0.535	0.535	0.600	0.123	0.123	0.684
				0.397	0.397	0.750	0.091	0.091	0.856
				0 264	0.294	0.875	0.061	0.068	0.999
				0.099	0.244	0.938	0.023	0.056	1.070
				--	0.212	1.000	--	0.048	1.141
				--	0.191	1.125	--	0.044	1.284
				--	0.160	1.250	--	0.037	1.426
				--	0.149	1.375	--	0.039	1.569
				--	0.114	1.500	--	0.026	1.711
				--	0.000	1.625	--	0.000	1.854
0.0104	673,000	389	1.49	1.000	1.000	0.000	0.280	0.280	0.000
				0.000	--	1.000	0.000	--	1.132
				0.866	0.866	0.184	0.243	0.243	0.208
				0.745	0.745	0.395	0.209	0.209	0.447
				0.624	0.624	0.579	0.175	0.175	0.655
				0.504	0.504	0.711	0.141	0.141	0.805
				0.383	0.383	0.841	0.107	0.107	0.903
				0.262	0.280	0.921	0.073	0.079	1.042
				0.142	0.274	0.948	0.040	0.077	1.071
				0.081	0.268	0.974	0.019	0.075	1.101
				--	0.256	1.000	--	0.072	1.132
				--	0.235	1.053	--	0.066	1.193
				--	0.178	1.184	--	0.050	1.341
				--	0.142	1.316	--	0.040	1.490
				--	0.108	1 448	--	0.030	1.640
				--	0.057	1.579	--	0.014	1.788
					(c) α = 60°				
0.0075	776,000	867	0.62	1.000	1.000	0.000	0.283	0.283	0.000
				0.000	--	1.000	0.000	--	0.973
				0.639	0.804	0.214	0.181	0.228	0.208
				0.600	0.701	0.430	0.170	0.199	0.418
				0.402	0.613	0.715	0.114	0.174	0.696
				--	0.552	1.073	--	0.156	1.044
				--	0.459	1.430	--	0.130	1.391
				--	0.356	1.788	--	0.101	1.740
				--	0.300	2.145	--	0.085	2.087
				--	0.000	2.500	--	0.000	2.433
0.0075	778,000	800	0.77	1.000	1.000	0.000	0.253	0.253	0.000
				0.000	--	1.000	0.000	--	0.984
				0.783	0.783	0.214	0.198	0.198	0 410
				0.533	0.700	0.430	0.135	0.177	0 823
				0.366	0.566	0.644	0.093	0.143	0.533
				0.299	0.449	0.857	0.076	0.114	0.843
				--	0.341	1.232	--	0.086	1.231
				--	0.257	1.430	--	0.065	1.406
				--	0.232	1.789	--	0.059	1 758
				--	0.141	2.145	--	0.035	2.109
0.0100	700,000	650	0.62		1.000	0.000		0.308	0.000
					--	1.000		--	1.124
					0.847	0.168		0.261	0.188
					0.708	0.334		0.218	0.376
					0.599	0.502		0.185	0.564
					0.522	0.569		0.161	0.751
					0.504	0.752		0.156	0.845
					0.463	0.836		0.143	0.939
					0 410	0.856		0.126	0.96[illegible]
					0.383	1.003		0.118	1.127
					0.351	1.086		0.108	1.220
					0.307	1.170		0.095	1.315
					0.289	1.253		0.089	2.657
					0.239	1.332		0.074	1.502
					0.189	1.504		0.058	1.690
					0.189	1.671		0.058	1.878
					0.162	1.755		0.050	1.972

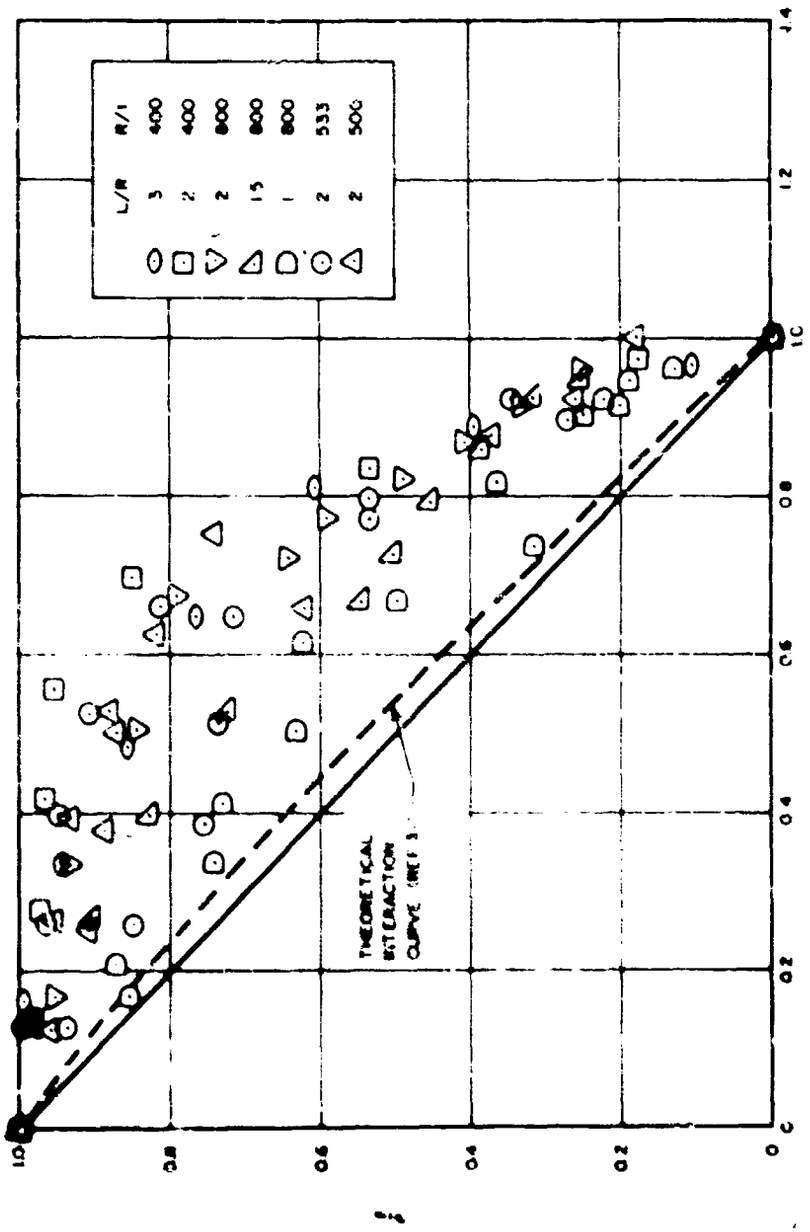

Figure 41. Interaction Curves for Cylinders Under Axial Compression and Uniform External Hydrostatic Pressure

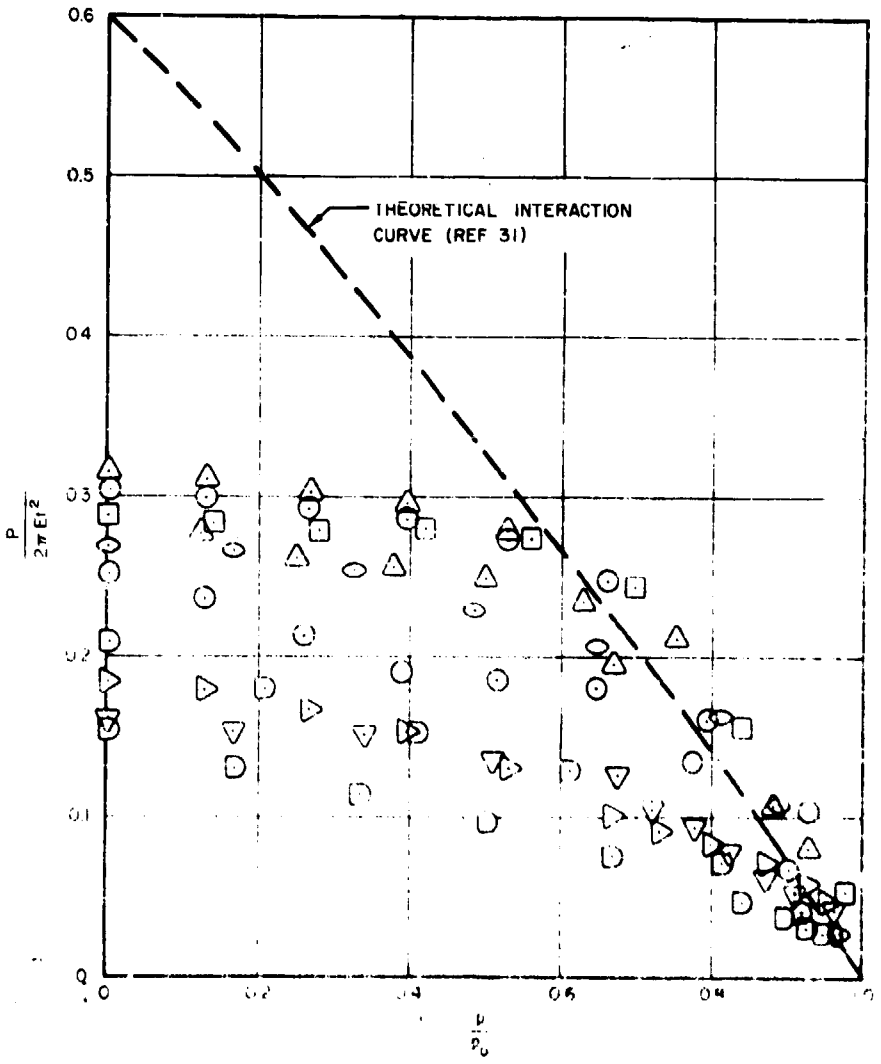

Figure 44. Variation of Axial Compression Coefficient with External Pressure Ratios

a. Buckling and Collapse
p = 0 psi
P = 1220 lb

b. Buckling
p = 1.2 psi
P = 800 lb

c. Collapse
p = 1.2 psi
P = 800 lb

Figure 45. Variation of Buckle and Collapse Patterns for a Conical Shell with Different Combinations of Axial Compression and External Pressure.

d. Buckling
p = 1.8 psi
P = 400 lb

e. Collapse
p = 1.8 psi
P = 400 lb

f. Buckling
p = 2.0 psi
P = 200 lb

Figure 45. Continued

g. Collapse
p = 2.0 psi
P = 255 lb

h. Buckling
p = 2.3 psi
P = 0.0 lb

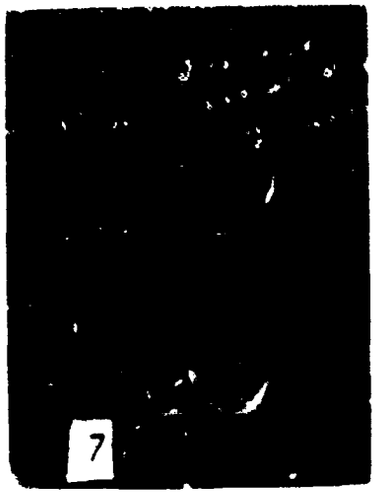

i. Collapse
p = 4.0 psi
P = 0.0 lb

Figure 45. Concluded

(a) $\frac{P}{P_o} = 1, \quad \frac{p}{p_o} = 0$

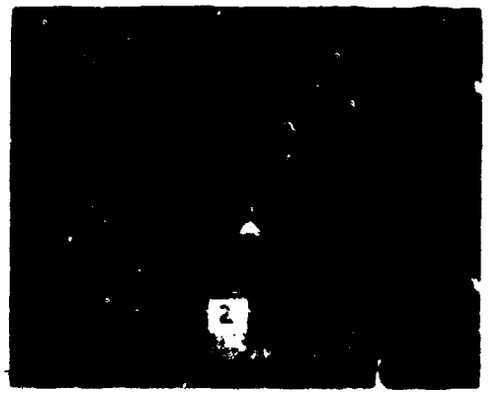

(b) $\frac{P}{P_c} = 0.74, \quad \frac{p}{p_o} = 0.2$

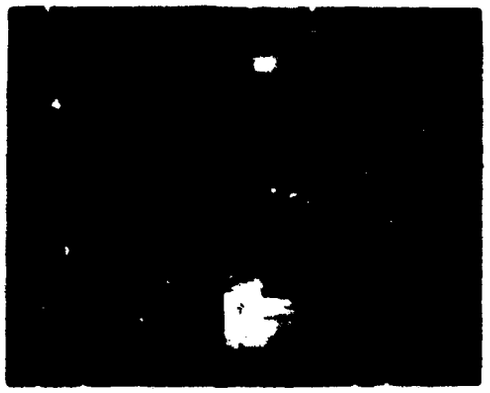

(c) $\frac{P}{P_o} = 0.54, \quad \frac{p}{p_o} = 0.4$

Figure 46. Variation of Buckle Pattern for Cylinders with Different Combinations of Axial Compression and External Pressure

(d) $\frac{P}{P_o} = 0.46, \frac{p}{p_o} = 0.6$

(e) $\frac{P}{P_o} = 0.30, \frac{p}{p_o} = 0.7$

(f) $\frac{P}{P_o} = 0, \frac{p}{p_o} = 1$

Figure 46. Concluded

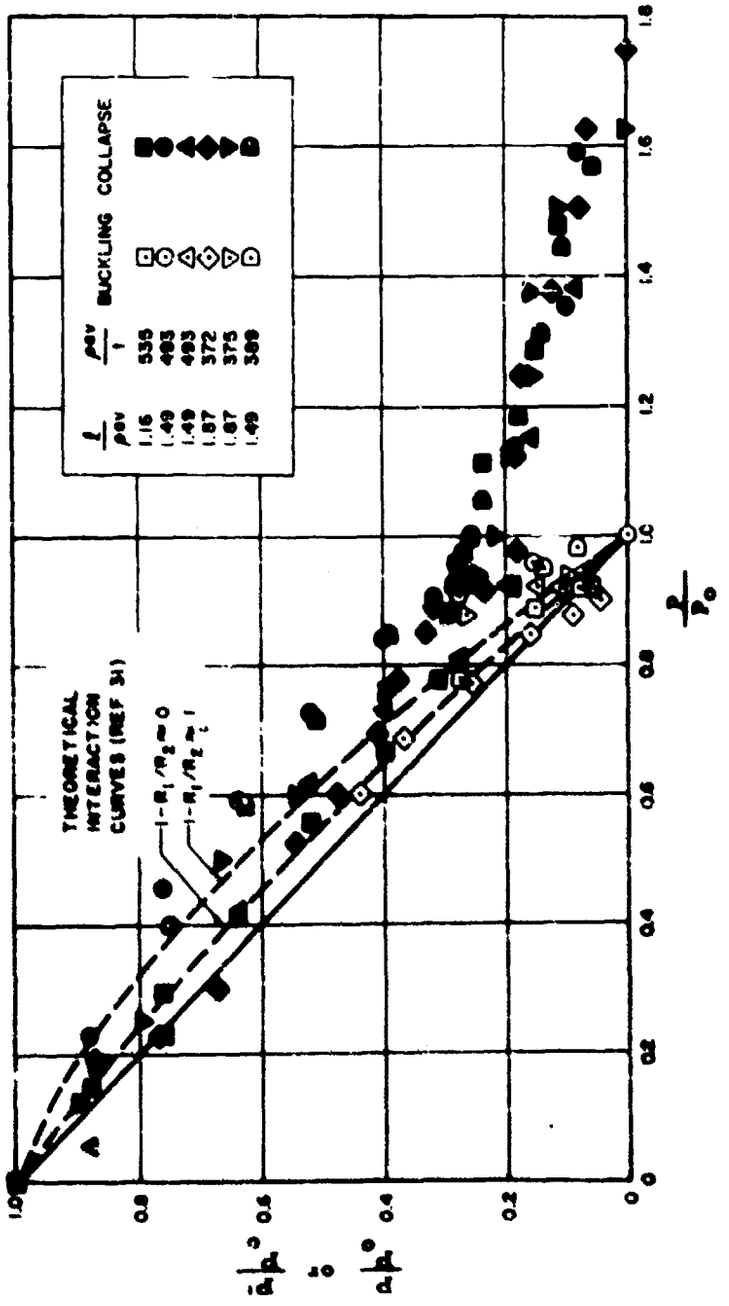

Figure 47. Interaction Curves for 30° Cones Under Axial Compression and External Uniform Hydrostatic Pressure

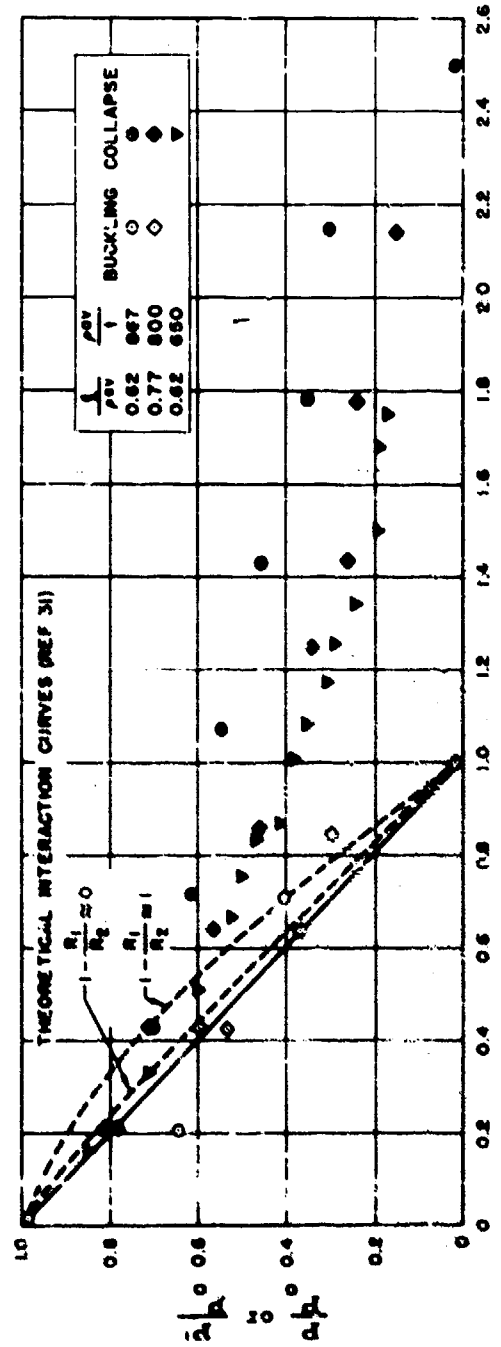

Figure 48. Interaction Curves for 60° Cones Under Axial Compression and External Uniform Hydrostatic Pressure

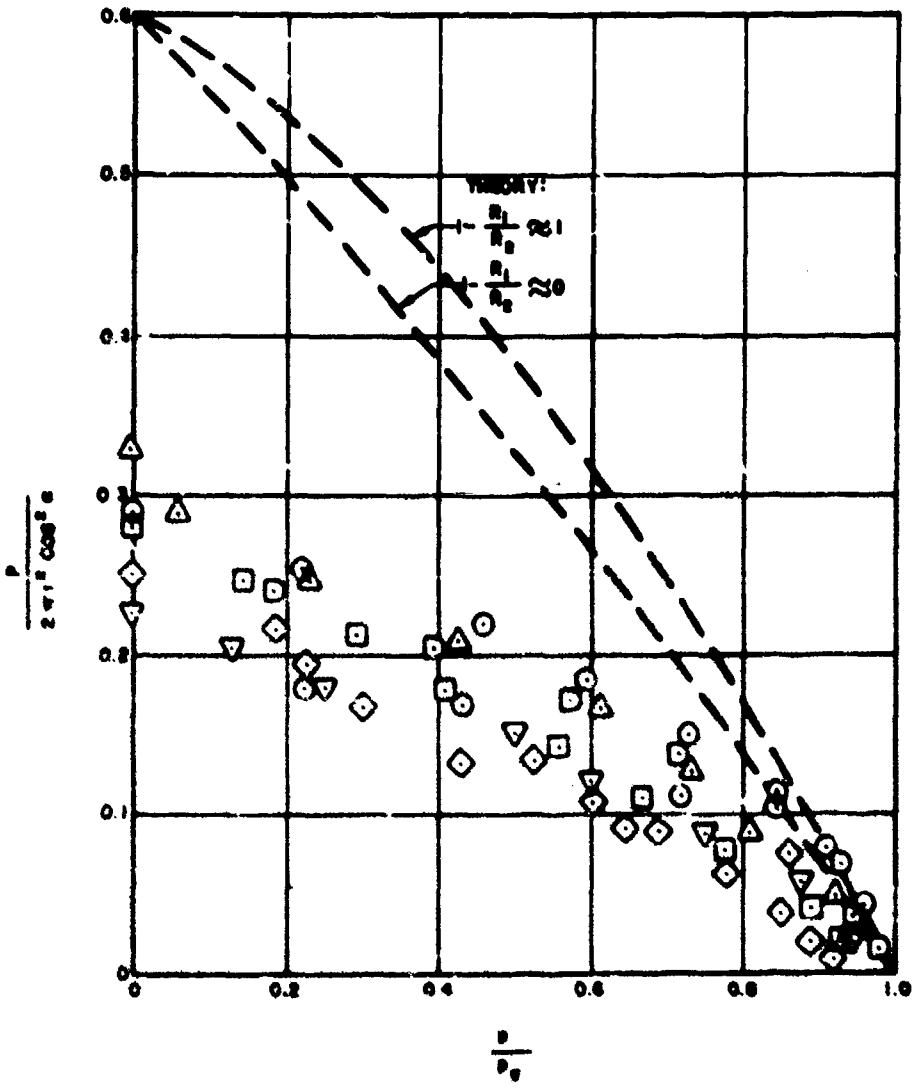

Figure 49. Variation of Axial Compression Coefficient with External Pressure Ratio for 30° and 60° Cones

XII. CYLINDERS AND TRUNCATED CONES IN TORSION

The stability of cylindrical shells under torsion has been comprehensively reviewed in References 55 and 56, which summarize the voluminous literature on this problem. In essence, experimental results are, on the average, about 16 percent below those predicted by the small-deflection theory for simply supported cylinders, while individual tests are as much as 40 percent below. Large-deflection theory indicates that initial imperfections should have some effect, although not nearly so much as for axial compression; but no attempts appear to have been made to correlate the data with radius-thickness ratio and length-radius ratio. For moderate length cylinders, critical torsion loads are given approximately by the equation

$$\frac{T}{\pi D} = 1.70\, \pi^2 \left(\frac{R}{L}\right)^2 Z^{3/4} \quad . \tag{21}$$

It is generally recommended that design values be taken as about 75 percent of the values given by Equation (21).

Truncated conical shells under torsion have only recently been treated, as in Reference 57. The analysis presented therein indicates that the critical torsion load is very closely equal to that for an equivalent cylinder having the same wall thickness, a length equal to the axial length of the conical frustum, and a radius given by the relation

$$\rho^* = \left\{ \left[1 + \frac{1}{2}\left(1 + \frac{R_2}{R_1}\right) \right]^{1/2} \cdot \left[\frac{1}{2}\left(1 + \frac{R_2}{R_1}\right) \right]^{-1/2} \right\} R_1 \cos\alpha \quad . \tag{22}$$

Thus Equation (22) may be used for moderate length cones, provided that R is replaced by ρ^* in the parameter Z and wherever else it explicity appears.

No experimental data have been available for the verification of the theory in Reference 57, other than the few, somewhat inconclusive tests

reported in Reference 58. Therefore, exploratory tests with steel cylinders and cones were made to provide some preliminary data for the assessment of the theory. The material used for the specimens was 0.010 inch thick 1020 steel and 0.020 inch thick 4130 steel with a compressive yield stress of 39,000 psi and 77,000 psi respectively, and an average Young's modulus of 30,000,000 psi.

Experimental critical shear stresses are given in Table 18 and are there compared with analytical predictions. These were obtained from the torque by the relation

$$\tau_{max} = \frac{T}{2\pi R_1^2 t} \tag{23}$$

For the conical shells, this gives the maximum shear stress which occurs at the smallest cross-section. The analytical predictions were obtained from Equations (21), (22), and (23). The results for the cylindrical shells are similar to those obtained by other investigators. The results for the conical shells are in about as good agreement with conical shell theory as those for the cylinders are with cylindrical shell theory. We may therefore conclude that the theory of Reference 57 is adequate for the design of conical shells, provided that the theoretical results are reduced by the factor used for the design of cylindrical shells.

An additional factor of some interest is the buckled shape of cylinders and cones in torsion. In Table 18, the observed number of circumferential buckles is compared with the number predicted by interpolation and extrapolation of the results of Reference 57. The observed number of buckles appears to be always less than the predicted number, but the agreement is fairly good. The experimental buckle patterns are illustrated in Figure 50. It is interesting to note that while the buckles occur over the entire length of the cylinders, they appear to concentrate near the small radius of the cones as the cone length increases, although the derived critical torsion load depends on the length of the specimen.

Table 18. Experimental Data for Steel Cylinders and Cones in Torsion

t (in.)	R_1 (in.)	R_2 (in.)	L (in.)	τ_{max} (experimental) psi	τ_{max} (computed) psi	$\frac{\tau_{exp}}{\tau_{comp}}$	n (observed)	n (predicted)
$\alpha = 0^\circ$								
0.010	8	8	8	4820	5220	0.93	--	19
0.010	8	8	8	5730	5220	1.10	16	19
0.020	8	8	8	10750	12340	0.87	13	15
0.020	8	8	8	10200	12340	0.82	13	15
0.010	8	8	16	4180	3820	1.10	13	14
0.010	8	8	16	3650	3820	0.95	13	14
0.020	8	8	16	8070	8870	0.91	10	11
0.020	8	8	16	8980	8870	1.02	10	11
$\alpha = 30^\circ$								
0.010	4	10	10.39	11650	11100	1.05	12	13
0.010	4	10	10.39	11490	11100	1.03	12	13
0.020	4	10	10.39	32400	26570	1.22	9	10
0.020	4	10	10.39	23400	26570	0.88	9	10
$\alpha = 60^\circ$								
0.010	2	10	4.62	14300	21030	0.68	9	9
0.010	2	10	4.62	14300	21030	0.68	8	9
0.010	3	10	4.04	10800	12460	0.87	9	11
0.010	3	10	4.04	13600	12460	1.09	9	11
0.010	5	10	2.89	8390	7850	1.07	13	15
0.010	5	10	2.89	6900	7850	0.88	12	15

(a) $\frac{L}{R} = 1$ $\alpha = 0^\circ$ (b) $\frac{L}{R} = 2$

$\alpha = 30^\circ$

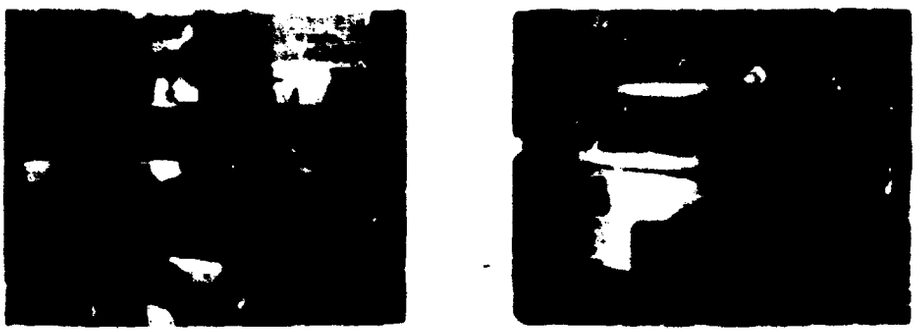

(a) $R_1 = 2$ in $\alpha = 60^\circ$ (b) $R_1 = 5$ in

Figure 50. Buckle Patterns for Thin Cylindrical and Conical Shells in Torsion

XIII. SUMMARY AND RECOMMENDATIONS

As a result of this program, a number of concepts concerning cylindrical and conical shell buckling have been clarified and some new problems requiring further investigation have been uncovered. As in many complex problems, a satisfactory solution depends upon a close association of careful experimentation and sound theoretical studies. Theory is useful in establishing the significant parameters and experiment is required to check the accuracy of the theoretical approach and to point out phenomena which have either been ignored or not sufficiently well considered in the analytical approach. The nature of the shell buckling problem seems to be such that while the theory correctly predicts the important parameters involved, design buckling loads must be found by experimental methods since the current theories are not sufficient to determine exact numerical values of the parametric coefficients.

In the subsections which follow, the state of knowledge concerning each loading condition is summarized with the object of pointing out what is known and where there are areas requiring additional theoretical and experimental studies.

A. Axial Compression

Although the monocoque circular cylinder under a uniform axial load is one of the simplest of shell configurations, and is one which has been studied by many investigators, a completely satisfactory solution to the problem is not yet available. It has been found that many factors combine to determine the buckling load of a particular cylinder. These include the care in fabrication, the patience and experience of the investigator, end conditions of the test specimen, initial deformations, plastic strain nuclei, etc. Fortunately, it appears that there exists a fairly definite lower bound to the buckling stress for cylinders which buckle at stresses in the elastic region. This lower bound can therefore be used for design purposes with a reasonable assurance that the structure will be safe. A discriminating comparison of available data

indicates that the lower bound for the variation of the buckling load with the radius-thickness ratio of the circular cylinder is reasonably well described by the relation

$$\frac{P}{2\pi Et^2} = 9\left(\frac{t}{R}\right)^{0.6} \tag{24}$$

for R/t greater than 500 and for L/R's less than approximately 5 but greater than 0.5. A relation that yields a better representation of the lower bound curve for the entire range of test data,

$$100 < \frac{R}{t} < 4000\ , \tag{25}$$

has been found to be given by

$$\frac{P}{2\pi Et^2} = 0.606 - 0.546\left(1 - e^{-\frac{1}{16}\sqrt{\frac{R}{t}}}\right). \tag{26}$$

The effect of the cylinder length is only vaguely known at the present time, since the number of tests investigating this factor are very few in number. The correction suggested by Kanemitsu and Nojima in Reference 15, on the basis of their tests, consists of the addition of the term

$$0.16\left(\frac{t}{L}\right)^{0.3} \tag{27}$$

to Equation (24). There is some data, however, that tend to indicate that experimental results for cylinders with values of L/R greater than 5 would yield results less than those given by Equations (24) or (26), whereas the combination of Equations (24) and (27) would not predict any such effect. It would also be of interest to know whether the observed increase in buckling load for low values of L/R bear any consistent relation to the increased theoretical buckling load for short clamped cylinders.

For design purposes, then, the situation is as follows. There appears to be no real reason to radically depart from past design methods provided that the range of cylinder parameters does not exceed those tested. The basic Kanemitsu-Nojima formula, giving the radius-thickness ratio effect, might be replaced by Equation (26), which would extend the lower limit of applicability of these design methods.

In order to answer some of the questions raised, it may be necessary to undertake an extensive experimental program, under relatively constant conditions, to determine a statistical design criterion which better describes the effects of radius-thickness ratio and length-radius ratio. This program should involve many identical specimens to give a reasonable statistical sample for each combination of values of L/R and R/t. Care should also be taken to eliminate the possibilities of yielding at the cylinder ends or overall plastic buckling and the separate determinations of these effects made with many different materials. Future theoretical work should include a better large-defection analysis, including the effects of finite length, end conditions, and plasticity.

For conical shells in axial compression the same arguments apply. The data of the present report indicate that for design purpose it is adequate to modify Equations (24) or (26), and (27) in accordance with the theoretical result of Reference 24, and, by use of the small radius of curvature and the slant length of the cone in place of the cylinder radius and length, to obtain

$$\frac{P}{2\pi \bar{\rho}^2 t^2 \cos^2 \alpha} = \left\{ \begin{array}{l} 9\left(\frac{t}{\rho_1}\right)^{0.6} \\ \text{or} \\ 0.606 - 0.546 \left(1 - e^{-\frac{1}{16}\sqrt{\frac{\rho_1}{t}}}\right) \end{array} \right\} + 0.16 \left(\frac{t}{l}\right)^{0.3} \qquad (28)$$

The loads calculated by this formula bear about the same relation to experimental loads for cones as for cylinders. It would be advisable however to investigate the effects of the various geometric parameters in much more detail, in order to determine differences in behavior not brought out by the present set of experiments. In this respect it would be of great interest to have large-deflection studies of the post-buckling behavior, including initial imperfections, to guide the experiments if any great difference in behavior actually exists.

B. Axial Compression and Internal Pressure

The results of the present program qualitatively verify the behavior of elastic, pressurized cylinders under axial compression predicted in References 19 and 28, in that the load carried by the cylinder in addition to that carried by internal pressure increases to the value given by small-deflection theory for unpressurized cylinders. The variation of the net load with internal pressure has been found to depend on the radius-thickness ratio of the cylinder, and curves suitable for design have been obtained.

The predicted load-pressure variation of Reference 19, based on a transfer of energy concept due to Tsien and calculated for an infinitely rigid testing machine, overestimates the effect of pressure. It is interesting to note that the results of most of the investigators, obtained from specimens of different materials and with different testing machines, are similar. The results show that the conclusion reached in Reference 19 and perpetuated in References 20 and 21 (that the buckling stress of a pressurized cylinder is equal to the sum of the buckling load of the unpressurized cylinder and an increment due solely to pressure) is coincidental and that this concept should be abandoned.

For sufficiently high pressures the behavior of the cylinders prior to buckling is in good quantitative agreement with calculations based on linearized axisymmetric large-deflection theory (the beam-column on an elastic foundation), although some unexplained anomalies have been found for the thicker cylinders tested. At some critical value of strain, dependent on the pressure and the radius-thickness ratio, the cylinder snaps into a diamond-shaped buckle mode and the load decreases. Measured load deflection curves show that the presently accepted solution of the large-deflection equations for diamond-shaped deformations is inaccurate. Whether this is due to limitations of the equations or to limitations of their solution is uncertain. It is also uncertain whether or not it would be necessary to solve the large-deflection equations for a finite cylinder to obtain good agreement between theory and experiment.

Experimental buckling loads for conical shells are in relatively good agreement with those based on small-deflection theory for sufficiently high pressures but indicate that the end support condition may be more important than for cylinders. Insuficient data is available to enable design curves to be recommended for the region of low pressure parameter.

One problem for future experimental investigations is the effect of length on the results for cylinders (all results were obtained for cylinders having a constant length and radius). Much additional data is needed for cones for varying values of small radius-thickness ratio, semivertex angle, and length. Finally, the effects of plasticity need to be explored since this factor places limits on the applicability of the present results to metal structures.

C. Bending, Axial Load, and Internal Pressure

The investigation of the stability of cylinders and cones under bending, with or without additional loads, has raised some rather puzzling questions and leads to the conclusion that this is an area not well understood at the present time.

It has been found that a good representation of the lower bound of most experimental data for pure bending of cylinder and cones can be represented by an equation similar to Equation (26), neglecting length effects, as

$$\frac{M}{\pi E t^2 R_1 \cos^2 \alpha} = 0.606 - 0.443 \left(1 - e^{-\frac{1}{16}\sqrt{\frac{R_1}{t}}}\right) \qquad (29)$$

This gives results quite different from those obtained by multiplying the coefficients for axial compression by a constant factor (such as 1.3, commonly used) for which there is no actual justification. The fact that the lower bound for bending is higher than that for axial compression casts doubt on the common assumption that post-buckling characteristics for bending are the same as those for axial compression. The question involved is this: even is a preferred buckling location will, on the average,

yield higher buckling stress coefficients, why are not some of the test results for bending as low as those for axial compression? The answer to this question might be related to the longitudinal seam location. It would be interesting to know if similar results would be obtained if the seam were arbitrarily located, rather than at the neutral axis of the cylinder. Additional indications that further investigation into the behavior of cylinders or cones in bending is necessary are that the effects of pressure for the two cases are different, and that tension and bending produce unexpected phenomena. The addition of pressure, with the axial pressure stress component counterbalanced by axial compression, raises the maximum compressive stress at collapse to values which are above those predicted by small-deflection theory and which increase linearly with pressure. The load-deformation curve, however, always exhibits a behavior characteristic of the snap-through type of buckling: rising to a sharp peak and decreasing suddenly. If, now, the axial compression is removed, the nominal maximum compressive stress for the same pressure is considerably larger than that for lateral pressure alone, and the load-deformation curve becomes more gently curved as for axial compression and internal pressure. However, for large values of the internal pressure, the load-deformation curve continues to rise indefinitely and exhibits no collapse moment. A similar result is obtained for unpressurized cylinders when tension is applied as well as bending moment.

A possible explanation of this phenomenon is that large deformations in the compression region of the cylinder or cone cause a redistribution of stress and a shift of the neutral axis toward the tension side of the shell. The tensile load would then produce an opposing moment which would increase with increasing deformation of the shell to produce the rising load-deformation curve obtained experimentally. It is evident, however, that large-deflection studies are necessary to clarify the situation and to determine whether we can even define a collapse load for these loading conditions. On the other hand, small-deflection theory does appear to satisfactorily predict the moment required for the onset of large deformations.

D. External Pressure and Axial Compression

For external pressure alone the experimental results indicate that for conservative design the critical pressure for cylinders and cones should be taken as

$$P_{cr} = \frac{0.74E}{\frac{l}{\rho_{av}} \left(\frac{\rho_{av}}{t}\right)^{5/2}} \tag{30}$$

which is about 80 percent of the theoretical value for cylinders and from 66 to 80 percent of the theoretical value for cones. An average value for the test data is obtained by increasing the factor of 0.74 in Equation (30) to a value of 0.92. Future study in areas of interest indicated by these results call for a complete explanation of the rather wide scatter band and the discrepancy between theory and experiment that is larger for conical shells than for cylinders.

Interaction curves between external pressure and axial compression indicate that for cylinders the results depend on the radius-thickness ratio and possibly the length-radius ratio. A straight line interaction curve is conservative. For conical shells we have the unexplained phenomenon of a differentiation between buckling and collapse loads. The buckling interaction curves appear to follow an almost straight line, indicating an unexpected uniform percentage decrease in the axial compressive load from the theoretical value, while the collapse interaction curve appears to depend on the semivertex angle of the cone. Additional tests and theoretical investigations are needed for a definitive description of these phenomena.

E. Torsion

Tests on torsion indicate that the agreement between theory and experiment for conical shells is about the same as that for cylinders. It is recommended that design torques for cones and cylinders be taken as about 75 percent of the theoretical value

$$T = 1.70\pi^3 \; D \left(\frac{\rho^*}{L}\right)^2 \left[(1-\nu^2)^{1/2} \frac{L^2}{\rho^* t}\right]^{3/4}, \tag{31}$$

where L is the height of the conical frustum and

$$\rho^* = \left\{1 + \left[\frac{1}{2}\left(1 + \frac{R_2}{R_1}\right)\right]^{1/2} - \left[\frac{1}{2}\left(1 + \frac{R_2}{R_1}\right)\right]^{-1/2}\right\} R_1 \cos\alpha . \tag{32}$$

REFERENCES

1. Barton, M.V. "Vibration of Rectangular and Skew Cantilever Plates," Journal of Applied Mechanics. vol. 18, No. 2. June 1951. pp. 129-134.

2. von Karman. T., and H.S. Tsien. "The Buckling of Thin Cylindrical Shells under Axial Compression, "Journal of the Aeronautical Sciences. vol. 8, No. 6. June 1941. pp. 303-312.

3. Koiter, W.T. Over de Stabiliteit van het Elastisch Evenwicht. Ph.D. Thesis, Technological University of Delft. 1945.

4. Donnell, L.H., and C.C. Wan. "Effect of Imperfections on Buckling of Thin Cylinders and Columns under Axial Compression," Journal of Applied Mechanics. vol. 17, No. 1. March 1950. pp. 73-88.

5. Dow, M.B., and J.P. Peterson. "Bending and Compression Tests of Pressurized Ring-Stiffened Cylinders," NASA TN D-360. April 1960.

6. Brown, J.K., and R.H. Rea. The Elastic Stability of Thin-Walled Pressurized Conical Shells under Compression and Compression-Bending Interaction, M.S. Thesis, Institute of Technology (Air University) Wright-Patterson Air Force Base. August 1960.

7. Timoshenko, S. Theory of Elastic Stability. McGraw-Hill Book Co. 1936. pp. 439-443.

8. Robertson, A. "The Strength of Tubular Struts," Proceedings of the Royal Society of London, Series A. vol. 121. 1928. pp. 558-585.

9. Flügge, W. "Die Stabilitat der Kreiszylinderschale," Ingenieur-Archiv. vol. 3. 1932. pp. 436-506.

10. Lundquist, E.E. "Strength Tests of Thin-Walled Duralumin Cylinders in Compression," NACA Report 473. 1933.

11. Wilson, W.M., and N.M. Newmark. "The Strength of Thin Cylindrical Shells as Columns," Engineering Experiment Station University of Illinois, Bulletin. No. 225, 1933.

REFERENCES (Continued)

12. Bridget, F.J., C.C. Jerome, and A.S. Vosseller. "Some New Experiments on Buckling of Thin-Walled Construction," Transactions of the A.S.M.E. vol. 56, No. 8. August 1934. pp. 569-578.

13. Donnell, L.H. "A New Theory for the Buckling of Thin Cylinders under Axial Compression and Bending," Transactions of the A.S.M.E. vol. 56, No. 11. November 1934. pp. 795-806.

14. Ballerstedt, W., and H. Wagner. "Versuche Über die Festigkeit dünner Unversteifter Zylinder under Schub-und Langskräften," Luftfahrtforschung. vol. 13. 1936. pp. 309-312.

15. Kanemitsu, S., and N.M. Nojima. Axial Compression Tests of Thin Circular Cylinders. M.S. Thesis, California Institute of Technology. 1939.

16. Anonymous. "Some Investigations of the General Instability of Stiffened Metal Cylinders, I - Review of Theory and Bibliography," Guggenheim Aeronautical Laboratory, California Institute of Technology. NACA TN 905. 1943.

17. Bruhn, E.F. "Tests on Thin-Walled Celluloid Cylinders to Determine the Interaction Curves under Combined Bending, Torsion, and Compression or Tension Loads," NACA TN 951. 1945.

18. Clark, J.W., and M. Holt. "Discussion on 'Effect of Imperfections on Buckling of Thin Cylinders and Columns under Axial Compression,'" Journal of Applied Mechanics. vol. 17, No. 3. September 1950. pp. 340-341.

19. Lo, H., H. Crate, and E.B. Schwartz. "Buckling of Thin-Walled Cylinders under Axial Compression and Internal Pressure," NACA Report 1027. 1951.

20. Fung, Y.C., and E.E. Sechler. "Buckling of Thin-Walled Circular Cylinders under Axial Compression and Internal Pressure," Journal of the Aeronautical Sciences. vol. 24, No. 5. May 1957. pp. 351-356.

21. Harris, L.A., H.S. Suer, W.T. Skene, and R.J. Benjamin. "The Stability of Thin-Walled Unstiffened Circular Cylinders under Axial Compression Including the Effects of Internal Pressure," Journal of the Aeronautical Sciences. vol. 24, No. 8. August 1957. pp. 587-596.

REFERENCES (Continued)

22. Kachman, D. R. "Test Report on Buckling of Propellant Cylinders under Compressive Loads," Space Technology Laboratories, Memorandum No. GM 59-7520.6-24. 30 November 1959.

23. Fitzgibbon, D. P. "Preliminary Results of Sub-scale Tests on Cylinders Filled with an Elastic Core," Space Technology Laboratories, Memorandum No. GM 60-7520.6-11. 25 April 1960.

24. Seide, P. "Axisymmetrical Buckling of Circular Cones under Axial Compression," Journal of Applied Mechanics. vol. 23, No. 4. December 1956. pp. 625-628.

25. Morgan, E. J., P. Seide, and V. I. Weingarten. "Semiannual Report on Development of Design Criteria for Elastic Stability of Thin Shell Structures, 1 July - 31 December 1959," Space Technology Laboratories, Report No. STL/TR-59-0000-09959 (AFBMD-TR-60-48).

26. Seide, P., and V. I. Weingarten. "Semiannual Report on Development of Design Criteria for Elastic Stability of Thin Shell Structures, 1 January - 30 June 1960," Space Technology Laboratories, Report No. STL/TR-60-0000-09194 (AFBMD - TR-60-110).

27. Lackman, L., and J. Pensien. "Buckling of Circular Cones under Axial Compression," Journal of Applied Mechanics. vol. 27, No. 3. September 1960. pp. 458-460.

28. Schnell, W. "Zur Stabilitat Dunnwandiger Langsgedruckter Kreiszylinderschalen bei Zusatzlichem Innendruck," Proceedings of the I. U. T. A. M. Symposium on the Theory of Thin Elastic Shells. Delft. August 1959.

29. Peterson, J. P. "Bending Tests of Ring-Stiffened Circular Cylinders," NACA TN 3735. 1956.

30. Peterson, J. P., and M. B. Dow. "Structural Behavior of Pressurized Ring-Stiffened, Thin-Wall Cylinder Subjected to Axial Compression," NASA TN D-506. 1960.

31. Seide, P. "The Stability of Thin Conical Frustums Subjected to Axial Compression and Internal or External Pressure," (in preparation).

REFERENCES (Concluded)

32. Lofblad, R. P. "Stability of Thin-Walled Cylinders and Cones with Internal Pressure under Axial Compression," Massachusetts Institute of Technology, Technical Report No. 25-29, on Office of Naval Research Contract No. Nonr-1841 (22). May 1959.

33. Seide, P., and V. I. Weingarten. "On the Bending of Circular Cylindrical Shells under Pure Bending," Journal of Applied Mechanics. vol. 28, No. 1, March 1961, pp. 112-116.

34. Mossman, R. W., and R. G. Robinson. "Bending Tests of Metal Monocoque Fuselage Construction," NACA TN 357. 1930.

35. Suer, H. S., L. A. Harris, W. T. Skene, and R. J. Benjamin. "The Bending Stability of Thin-Walled Unstiffened Circular Cylinders Including the Effects of Internal Pressure," Journal of the Aeronautical Sciences. vol. 25, No. 5. May 1958.

36. Lundquist, E. E. "Strength Tests of Thin-Walled Duralumin Cylinders in Pure Bending," NACA TN 478. 1933.

37. Weingarten, V. I. "On the Buckling of Circular Cylindrical Shells under Bending, Axial Load, and Internal Pressure," (in preparation).

38. Brazier, L. G. "On the Flexure of Thin Cylindrical Shells and Other Thin Sections," Proceedings of the Royal Society, Series A. vol. 116. 1927. pp. 104-114

39. Wood, J. D. "The Flexure of a Uniformly Pressurized, Circular, Cylindrical Shell," Journal of Applied Mechanics. vol. 25, No. 4. December 1959. pp. 453-458.

40. Reissner, E. "On Finite Bending of Pressurized Tubes," Journal of Applied Mechanics. vol. 26, No. 3. September 1959. pp. 386-392.

41. Seide, P. "On the Buckling of Truncated Conical Shells under Uniform Hydrostatic Pressure," Proceedings of the I. U. T. A.M. Symposium on the Theory of Thin Elastic Shells. Delft, 24-25 August 1959. North-Holland Publishing Co., Amsterdam, 1960. pp. 363-388.

REFERENCES (Continued)

42. Niordson, F.I.N. "Buckling of Conical Shells Subjected to Uniform External Lateral Pressure," Transactions of the Royal Institute of Technology. Stockholm, Sweden. No. 10. 1947.

43. Bijlaard, P.P. "Critical External Pressure of Conical Shells that Are Simply Supported at the Edges," Bell Aircraft Corp., Technical Report No. 02-941-027. February 1953.

44. Batdorf, S.B. "A Simplified Method of Elastic-Stability Analysis for Thin Cylindrical Shells, I-Donnell's Equation," NACA TN 1341. June 1947.

45. Windenberg, D.F., and C. Trilling. "Collapse by Instability of Thin Cylindrical Shells under External Pressure," Transactions A.S.M.E. vol. 56, No. 11. November 1934. pp 819-825.

46. Sturm, R.G. "A Study of the Collapsing Pressure of Thin-Walled Cylinders," Engineering Experiment Station, University of Illinois. Bulletin. No. 329. 1941.

47. Tokugana, T. "Experiments on the Elastic Stability of a Thin-Wall Cone under Uniform Normal Pressure on All Sides, and an approximate Method for Computing its Collapsing Pressure," Congress of Applied Mechanics League, Shipbuilding Association (Zosen Kyokai). Miscellaneous Publication. No. 125. 1932. pp. 151-169.

48. Harris, W.F., and J. Leyland. "The Strength of Conical Vessels Subject to External Pressue," Transactions of the Institute of Chemical Engineers. vol. 30. 1952.

49. Magula, A.W. "Structural Test-Conical Head Assembly, Test No. 815," North American Aviation, Inc., Downey Missile Test Lab. Report MTL-531. 1954.

50. Westmoreland, R.T. "Model Test of Conical Bulkhead, Test No. 1098," North American Aviation, Inc., Downey. Missile Test Lab. Report MTL-652. 1955.

51. Jordan, W.D. "Buckling of Thin Conical Shells under Uniform External Pressure," Technical Report. Bureau of Engineering Research, College of Engineering, University of Alabama. February 1955.